Chemical and isotopic variations in plagioclase from the Upper and Main Zones, Northern Limb, Bushveld Complex.

Mpho Mangwegape

Dissertation submitted in accordance with the requirements for the degree:

Master of Science

In

Geology

Faculty of Natural and Agricultural Sciences

University of the Free State

UNIVERSITY OF THE FREE STATE
UNIVERSITEIT VAN DIE VRYSTAAT
YUNIVESITHI YA FREISTATA

UFS·UV
NATURAL AND AGRICULTURAL SCIENCES
NATUUR- EN LANDBOUWETENSKAPPE
GEOLOGY
GEOLOGIE

Declaration

I Mpho Mangwegape, declare that this dissertation, hereby handed in for the qualification M.Sc in the faculty of Natural and Agricultural Sciences, Department of Geology, University of the Free State, is my own, unaided work, as supervised by my mentor, and that no part of it has been copied or duplicated. It has not been submitted for any degree or examination at any other University or institution. I futhermore renounce copyright in favour of the University of the Free State.

Signed on: Wednesday, 27 January 2016

M MANGWEGAPE

Dedication

To my mother Seipati, and brother Thato.

Acknowledgements

This work wouldn't have been possible if it wasn't for the direct or otherwise indirect involvement of so many people, who, knowingly or blindly, gladly or perhaps forced, contributed to this dissertation. First and foremost I would like to acknowledge, with utmost genuineness, Dr Frederick Roelofse, who suggested, supervised, and assisted this project to its completion. I would like to thank him for the overwhelming academic and social guidance he has given me throughout the duration of this work, and for the invaluable knowledge and experience he has shared with me, both in science and in life. His involvement in this project has been paramount, and for that I am grateful. Secondly, I would like to thank Mr Radikgomo for preparing all materials used in this study (thin sections and epoxy mounts), and for the much appreciated parental guidance he has offered me over the years. Gelu Costin, and his two interns, Lethabo and Thato, are thanked for their assistance with the use of the Jeol JXA 8230 Superprobe, instrument sponsored by NRF/NEP grant 40113 (UID 74464), housed at the Department of Geology, Rhodes University, and for making my stay there enjoyable. Richard Carlson and Timothy Mock of the Carnegie Institution for Science are thanked for their help with Laser Ablation work conducted there, and for a memorable stay in Washington. Christel Tinguely of the Department of Geoscience, University of Cape Town is also thanked for her assistance in Laser Ablation work for trace element determination conducted at the department. Much appreciation is conveyed to Prof Gauert and Prof Tredoux for their helpful academic advices and all the constructive scientific discussions they engaged me in. I also acknowledge, with gratitude, the funds granted to me by the National Research Fund (NRF) under a Thuthuka grant to my supervisor (TTK13053018360), without which it would have been near impossible to complete this momentous task. With all the earnestness I can

master, I would like to thank my mother for the unconditional love she has showered me with, for the vast support she has given me throughout my years of study, for all the sacrifices she has made for me, and for allowing me to pursue my interests without question. I would also like to acknowledge the three queens of the Mangwegape family: Leatso, Mmamotho, and Maletele, the following princesses: Lerato, Mantele, Motlalepule, and Gotshegwang, the following princes: Bareng and Bakang, and all the teletubbies: Thato, Neo, Reo, Onalerona, Owethu, Tshwanelo, and Thandolwethu. Much appreciation is conveyed to the following Heads: Adv. Mathaelira Mopeli, kgosigadi Gaongalelwe Moroka: I would also like to acknowledge the following friends, compatriots, and commanders: Masethabela, Modiri, Tshepi, and Goitsinna.

Ad Maiorom Dei Gloriam-Tua Luce Dirige

Abstract

The *in-situ* major element, trace element, and Sr-isotopic compositions of plagioclase in the broadly gabbroic cumulates from the Upper and Main Zones of the Northern Limb of the Bushveld Complex, as obtained from the Bellevue (BV-1) and Moordkopje (MO-1) drill cores have been determined by means of electron microprobe and Laser Ablation Inductively Coupled Plasma Mass Spectrometry (LA-ICPMS). The results show the existence of inter and intra-crystal initial $^{87}Sr/^{86}Sr$ disequilibrium of coexisting plagioclase, a phenomenon which has received rather rudimentary attention not only in the Bushveld Complex, but in other layered intrusions as well.

This disequilibrium is particularly striking in samples from the Lower Main Zone, an interval which also records a lack of differentiation, as exemplified by the An% of plagioclase. In the rest of the stratigraphy, up to the top of the Rustenburg Layered Suite, there is less, if any, inter and intra-crystal initial $^{87}Sr/^{86}Sr$ disequilibrium of plagioclase coupled to more prominent differentiation trends. These results are in support of a model for the petrogenesis of this part of the Bushveld Complex, which involves the Lower Main Zone forming through the repeated intrusion of crystal mushes derived from a deeper seated, sub-compartmentalized staging chamber, into the Bushveld main magma chamber, with fractionation processes being key in the formation of the Upper Main and Upper Zones.

Based on the initial $^{87}Sr/^{86}Sr$ composition of plagioclase, the Northern Limb of the Bushveld Complex can also be divided into a putative integration and differentiation stages, similar to the Western Limb of the Bushveld Complex. The integration stage in the Western Limb included the Lower, Critical, and Lower Main Zones, whereas the differentiation stage included the Upper Main and Upper Zones. The integration stage

in this study incorporates the lower reaches of the Lower Main Zone, with the rest of the stratigraphy up to the top of the Upper Zone covering the differentiation stage.

Furthermore, the Lower Main Zone of the Northern Limb of the Bushveld Complex has very consistent concentrations of most trace elements investigated, and these concentrations tend to increase upwards into the Upper Main and Upper Zones. This also suggests repeated intrusion for the Lower Main Zone with differentiation processes dominating in the upper parts of the Rustenburg Layered Suite.

Table of contents

List of figures

List of tables

1. Introduction

The Bushveld Complex in South Africa contains the world's largest layered mafic to ultramafic intrusion, the Rustenburg Layered Suite. Within this immense layered intrusion (areal extent of ~65 000 km^2, and a thickness of about 7-9 km), lithologies range between the extremes of dunite and pyroxenite, to anorthosite and oxide layers (chromitite and magnetitite respectively), with almost all imaginable intermediate rock types (Eales & Cawthorn, 1996).

This layered intrusion of mafic to ultramafic cumulates also hosts three of the world's largest platinum-bearing ore bodies, the Merensky reef and the Upper Group 2 (UG2) chromitite in the Eastern and Western Limbs, as well as the Platreef in the Northern Limb (Kruger, 2005). Since the discovery of platinum group elements (PGEs), copper (Cu), and nickel (Ni) in these layers, chromium (Cr) in both the UG2 and in the Lower Group chromitites, iron (Fe), vanadium (V), and titanium (Ti) in magnetitites, especially in the main magnetitite layer, which is deemed the world's largest vanadium resource, the Bushveld Complex has become a hub of scientific research. In addition, the complex is also associated with two other groups of mineral deposits. Firstly, tin and fluorine mineralisation occur in the acid roof rocks of the complex, and secondly, andalusite mineralisation occurs associated with the metamorphic contact aureole produced as a result of emplacement of the complex (Eriksson *et al*., 1995).

The cumulate hosted PGE, Ni & Cu deposits are the most economically significant. A widely accepted model for their formation is that of sulphide immiscibility induced by mixing of different magmas (Irvine, 1977; Campbell *et al*., 1983; see also Li & Ripley, 2005).

The development of this model was supported by the observation of abrupt changes in initial strontium (Sr_i) isotopic ratios across the stratigraphy (Figure 1) (Sharpe, 1981; Sharpe *et al*., 1986; Eales *et al*., 1990b; Kruger, 1990). This variation was interpreted by some authors as indicative of influxes of new magmas, with an isotope composition different from that of the fractionating magma already present in the magma chamber (Kruger & Marsh, 1982; 1985; Sharpe *et al*., 1986). Since the fundamental work by Kruger & Marsh, (1982;1985) and Sharpe *et al*. (1986) among others, more researchers have studied whole rock Sr-isotopic variation across the Complex (e.g., Lee & Butcher, 1990; Kruger, 1994)

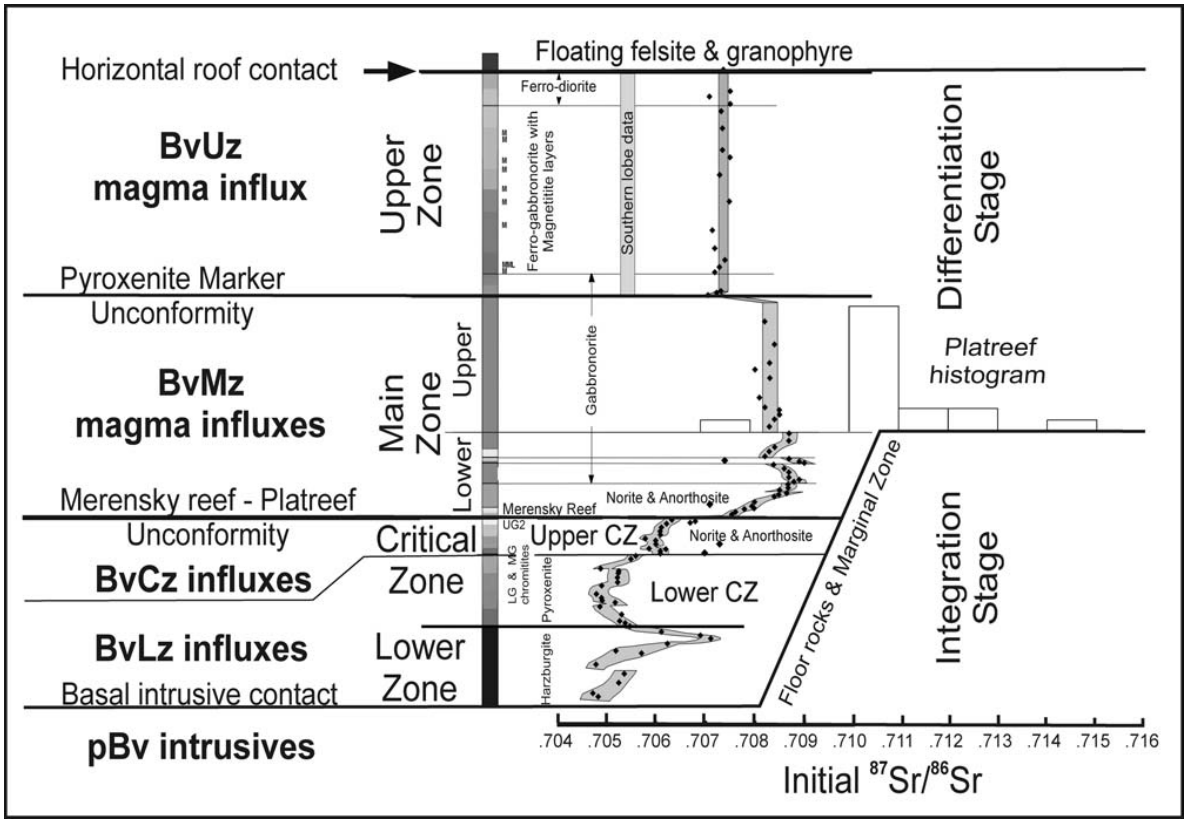

Figure 1: Discontinuities in the initial Sr isotopic ratio across the Rustenburg Layered Suite stratigraphy, showing lithological variations, and the location of major unconformities. Figure from Kruger (2005).

Furthermore, Eales *et al.* (1990a) identified Sr isotopic disequilibrium between coexisting orthopyroxene and feldspar in rocks of the Upper Critical Zone, Western Bushveld Complex. Mathez & Waight (2003) and Mathez & Kent (2007) reported disequlibrium of initial Pb isotope ratios between coexisting plagioclase and sulfide, and between different plagioclase populations in the Upper Critical Zone. Seabrook *et al*. (2005) measured Sr-isotopic ratios of plagioclase and Cr/MgO ratios of coexisting orthopyxoxene across the Merensky and Bastard units in the Eastern Limb, and then argued, based on the results obtained, that these two minerals are not in equlibrium. Sr isotopic disequlibrium between coexisting plagioclase and orthopyroxene was also reported in the Lower Main Zone of the Northern Limb (Roelofse & Ashwal, 2012).

In the present study, rocks from the Bellevue (BV-1) and Moordkopje (MO-1) drill cores in the Northern limb of the Bushveld Complex were investigated, with the aim of determining whether or not plagioclase within these rocks are in isotopic equilibrium, both from an inter- and intra-crystalline perspective.

Isotopic disequilibrium studies are important in layered intrusions for they provide the necessary level of detail required to thoroughly investigate processes occurring during the formation of these intrusions. Whole rock isotopic studies obscure some important petrogenetic aspects, and it is for this reason that isotopic disequilibrium studies are key. The existence of isotopic disequilibrium between coexisting minerals allows one to glance into the the crystallisation history of such minerals, to investigate the magmas from which they formed, as well as in understanding processes occuring in magma chambers.

An overview of the geology and general stratigraphy of the Bushveld Complex, and a review of existing petrogenetic models based on isotopic evidence will be followed by a detailed petrographic characterisation of all the samples used in this study. Results from three sets of analyses, starting with electron microprobe analysis for determination of the major element chemistry of plagioclase, followed by separate Laser Ablation Inductively Coupled Plasma Mass Spectrometry analyses to determine both the Sr-isotopic and trace element composition of plagioclase, are then used to discuss possible models relating to the petrogenesis of the Northern Limb of the Bushveld Complex. Additionally, I shall compare the Sr-isotopic stratigraphy of the Northern Limb to that of the Eastern and Western Limbs of the complex, and comment on the geochemical behaviour of certain trace elements in plagioclase across the studied stratigraphic profile.

1.2 Geological overview and stratigraphy of the Bushveld Complex

1.2.1 Geological setting of the Bushveld Complex

The Rustenburg Layered Suite of the Bushveld Complex, is the oldest and largest preserved layered mafic intrusion on Earth, and is host to the world's largest repository of orthomagmatic metal deposits (Lee, 1996; Cawthorn *et al*., 2005; Clarke *et al*., 2009). Not only is it the mineral wealth of the complex that makes it so spectacular and worthy of our attention. The complex is also very large, comprising of layered mafic rocks that cover an area of about 65 000 km^2, having an estimated vertical thickness of about 9 km (Tankard *et al.*, 1982; Sharman-Harris *et al*., 2005). According to Kruger (2005), this makes the Bushveld Complex the largest mafic magma chamber from which products of magma intrusion and fractional crystallisation can be seen, and from which large-scale processes responsible for the formation of layered rocks may be inferred. These two particulars, the mineralisation and the academic value of the Bushveld Complex surely makes it one of the geological wonders of the world.

The complex is comprised of three main units, a mafic to ultramafic portion known as the Rustenburg Layered Suite, the Lebowa granite suite, and the Rashoop Granophyre Suite (Eriksson *et al*., 1995). The Rustenburg Layered Suite, which forms the base of the complex, was intruded at the boundary between the Rooiberg felsites and the underlying Pretoria Group at 2054.4 ± 1.3 Ma (Scoates & Friedman, 2008), with the subsequent Lebowa and Rashoop Suites intruding the upper Rustenburg rocks and the uplifted Rooiberg felsites which now form the roof to the complex (Eriksson *et al*., 1995; Buchanan *et al*., 2002; Buchanan *et al*., 2004). The host rocks of the Bushveld Complex are rocks of the Late Archaean-Early Proterozoic Transvaal

Supergroup, which is preserved within three structural basins within the Kaapvaal craton of Southern Africa, the Transvaal, Kanye, and Griqualand West structural basins (Eriksson *et al*., 1995; Errikson *et al*., 2001). The Transvaal Supergroup consists of four lithostratigraphic subdivisions, and these are, from bottom to top, the protobasinal rocks, the Blackreef Formation, the Chuniespoort Group, and the Pretoria Group (Figure 3, page 8). The lowermost protobasinal rocks consist of siliciclastic and bimodal volcanic rocks. The Blackreef Formation is composed of quartzite that has lenses of grit, conglomerate, and shale. The overlying Chuniespoort Group is composed of chemical sedimentary rocks (carbonate-banded iron formation), with the uppermost Pretoria Group consisting mainly of clastic sedimentary rocks (shales and quartz arenites) (Eriksson & Reczko, 1995; Pecher, 2011). The Supergroup has an estimated thickness of about 12 km within the Transvaal Basin. The sedimentary strata of the Witwatersrand Supergroup, the Ventersdorp lavas, as well as Archaean granites, gneisses, and greenstones all form the basement rocks of the Transvaal Supergroup (Sharman-Harris *et al*., 2005).

However, the larger Bushveld Magmatic Province as a whole consists of other magmatic suites, and thus, in addition to the three units that make up the Bushveld Complex (i.e Rustenburg Layerd Suite, Lebowa Granite Suite, and Rashoop Granophyre Suite), are: (I) the bimodal Rooiberg volcanic suite, which has also been mentioned (the Rooiberg Group is stratigraphically linked with the Transvaal Supergroup, but is petrogenetically related to the larger Bushveld magmatic province); (II) a suite of marginal pre- and syn- Bushveld sills, (III) and lastly, the outer satellite intrusions of the complex, including the Uitkomst, Molopo, and Mashaneng satellite intrusions (Kinnaird *et al*., 2004; Kruger, 2005). A discussion of these various

components of the Bushveld Large Igneous Province is however beyond the scope of this study. Figure 2 is a symplified geological map that shows the distribution and location of these various components within the Transvaal basin of Southern Africa. All these components were emplaced in a very short space of time (Table 1), and probably from a single magmatic event (Kruger, 2005).

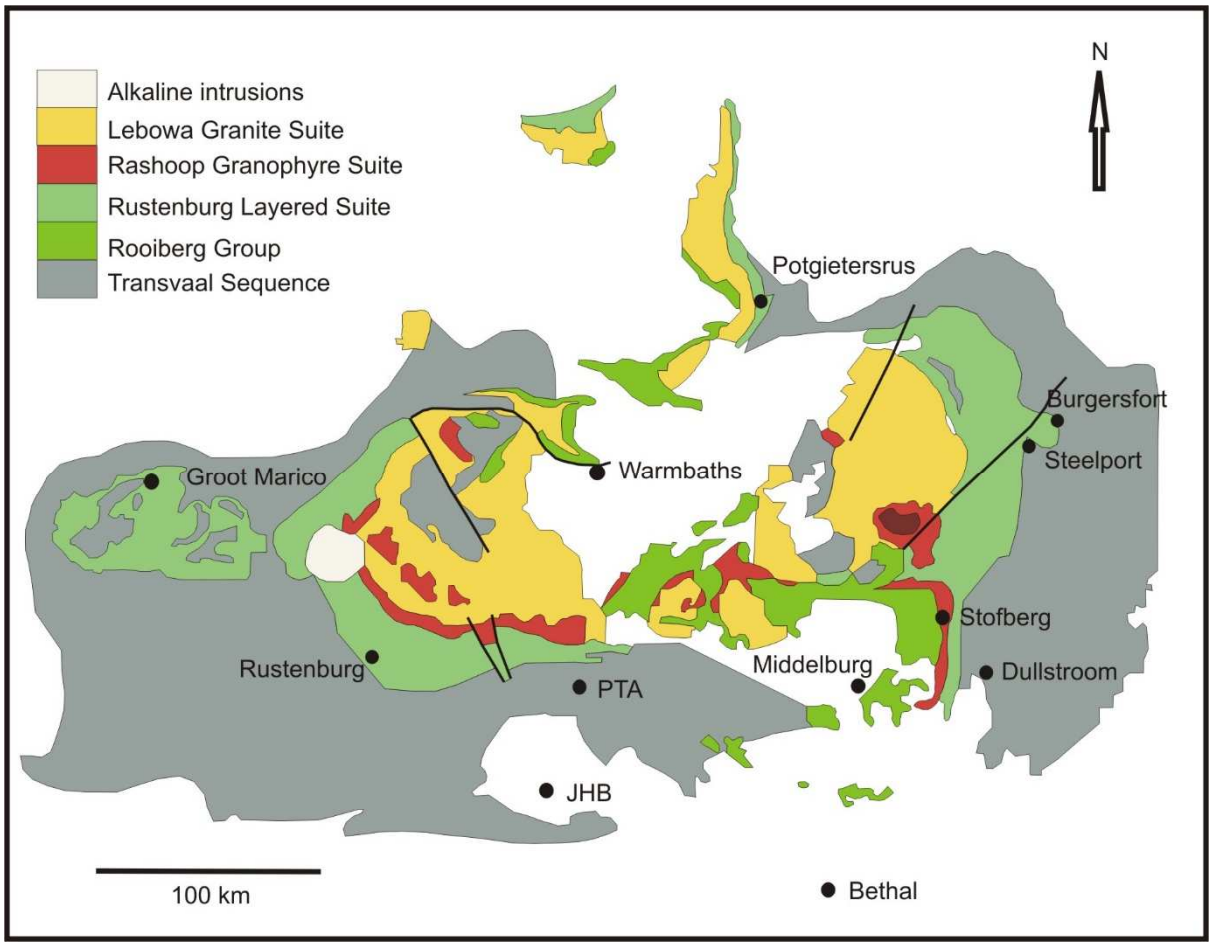

Figure 2: Simplified geological map of the Transvaal Supergroup and the various components of the larger Bushveld magmatic province, which comprises the Rustenburg Layered Suite, Lebowa Granite Suite, Rashoop Granophyre Suite, and the Rooiberg Group. Diagram adapted and modified after Kinnaird *et al.* (2005).

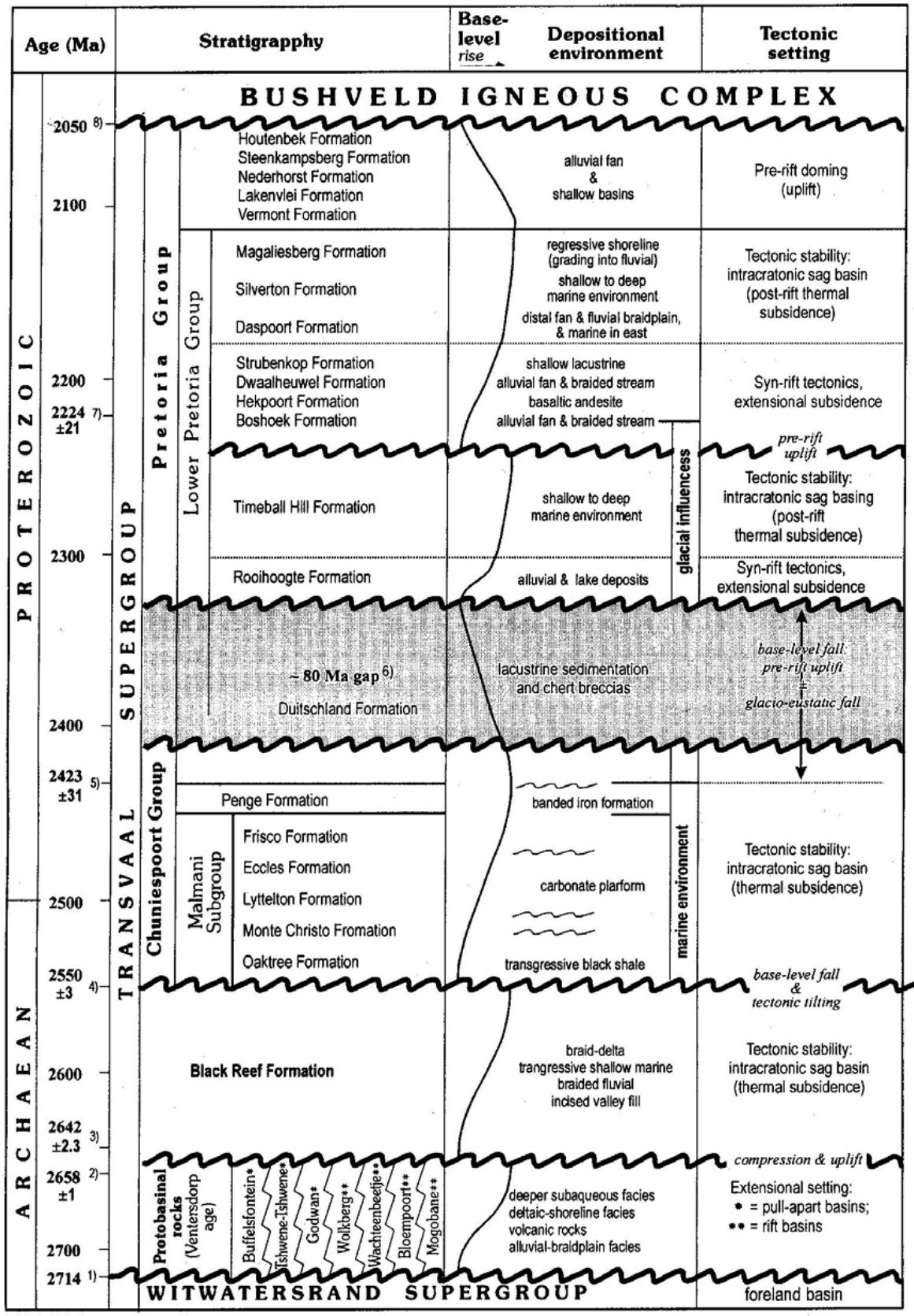

Figure 3: Age, depositional environment, and tectonic setting of the various components of the Transvaal Supergroup, the tectonic setting of the underlying Witwatersrand Supergroup, and emplacement of the Bushveld Complex into the uppermost part of the Pretoria Group. Figure from Eriksson *et a*l. (1995).

Table 1: Age dates of the various components of the larger Bushveld magmatic province. Ages were obtained from different authors: [1]Harmer & Armstrong (2000) cited in Yudovskaya et al. (2013); [2]Kruger (1989) cited in Prendergast (2012); [3]Mapeo *et al*. (2004); [4]de Waal *et al.* (2001), and [5]Zeh *et al*. (2015).

Lithostratigraphic unit		Age (Ma ± 95%)
Loskop Formation	Rhyolite	2057.2 ± 3.8[1]
Lebowa Granite Suite	Makhutso Granite	2053.4 ± 3.9[1]
	Nebo Granite	2054.2 ± 2.8[1]
	Steelpoort park Granite	2057.5 ± 4.2[1]
Rustenburg Layered Suite	Critical Zone (SHRIMP)	2054.4 ± 2.8[1]
	Critical Zone (IDTIMS)	2054.5 ± 1.5[1]
	Centre of RLS (CA-ID-TIMS)	2054.89 ± 0.37[5]
Rashoop Granophyre Suite	Rooikoppies Porphyry	2061.8 ± 5.5[1]
Rooiberg Group	Kwaggasnek Formation	2057.3 ± 2.8[1]
Satellite intrusions	Molopo Farms	2044 ± 24[2]
	Mashaneng Complex	2054 ± 2[3]
	Uitkomst Complex	2044± 8[4]
		(2055 ± 45/-17)[4]

1.2.2 The Rustenburg Layered Suite

The mafic to ultra-mafic portion of the Bushveld Complex, formally known as the Rustenburg Layered Suite (SACS, 1980), occurs in five separate parts called limbs or lobes: the Western, Eastern, Northern (also referred to as the Potgietersrus Limb), Far Western, and the Bethal (Southern) limbs (Figure 4) (Eales & Cawthorn, 1996). The 200 km long Western Limb occurs as an arcuate body with an easterly dip. It covers an area from Thabazimbi in the north to north of Pretoria in the south. Although exposure is poor, this limb is very well known, mainly due to extensive mining activities, which have exposed the uppermost parts of the Critical Zone (Eales & Cawthorn, 1996; Eales *et al*., 1990b). The Eastern Limb is 200 km long, has a westerly dip, and covers an area from Chuniespoort in the north to Stoffberg in the south. Owing to good exposures, this limb is also well known. The other three limbs are less well known, as they are either eroded remnants (the Far Western Limb), or have poor outcrops (the Northern Limb). The Bethal (Southern) Limb, forming the southernmost part of the Bushveld Complex is known only from bore-core information, and was identified on the basis of a gravity high (Eales & Cawthorn, 1996).

The Northern Limb, a part of which forms the focus of this study, is located in the Limpopo Province of South Africa. The limb crops out over a strike length of 110 km from the Melinda Fault in the north, where it has a cover of younger Waterberg Supergroup sediments, to the Zebediela Fault in the south, where it is juxtaposed against Karoo Supergroup sediments (Kinnaird *et al*., 2005; Roelofse & Ashwal, 2012). The Zebediela fault forms part of the Thabazimbi-Murchison Lineament (TML) (Good

& de Wit, 1997), which has been active since Meso-archaean times (2960 Ma) to the Cretaceous (~145 Ma).

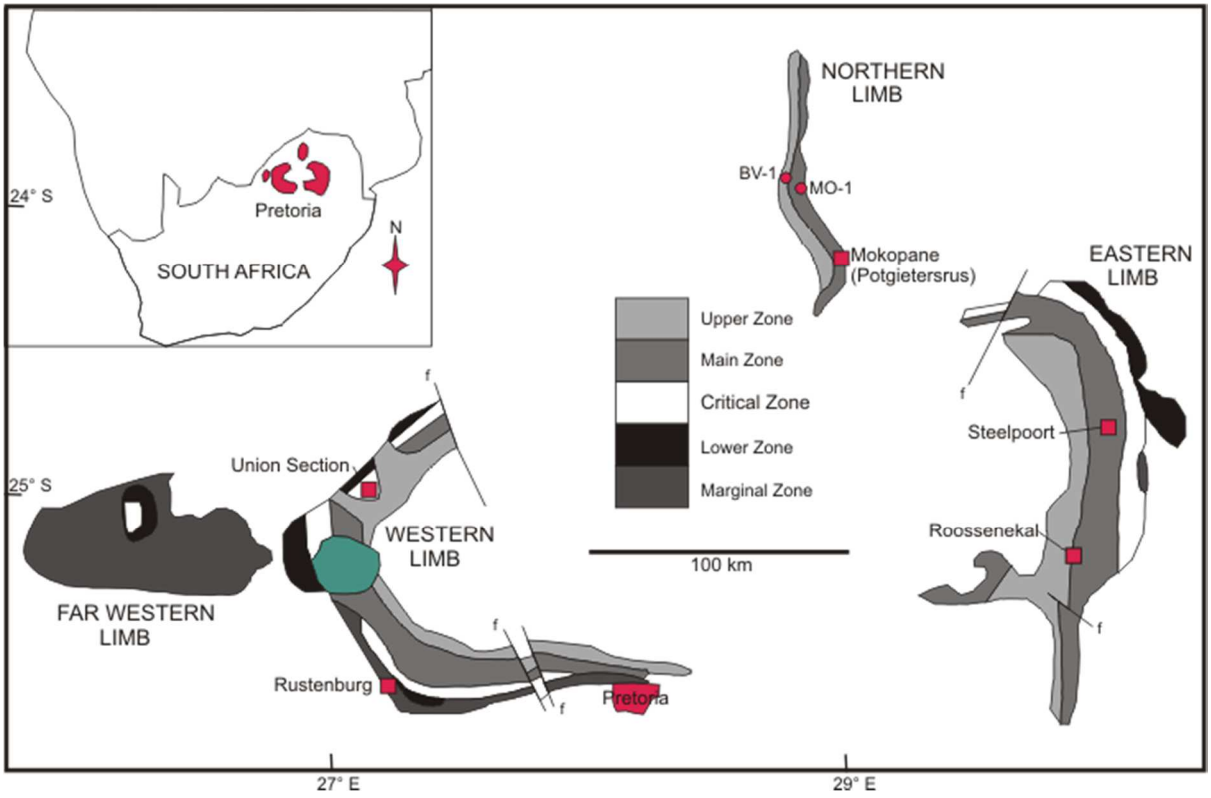

Figure 4: Geological map of the Rustenburg Layered Suite showing the locations of the different limbs and the position of the BV-1 and MO-1 boreholes. The Bethal Limb which is covered by younger rocks is not shown. Inset shows the location of the layered suite in South Africa. Figure adapted and modified from Roelofse & Ashwal (2012)

Van der Merwe (1976) described the Northern Limb of the Bushveld Complex (shown in Figure 5) as a trough-shaped, north-striking body that occupies a buffalo-horn-shaped area of approximately 2000 km^2. The southern part of the limb (Van der Merwe, 1976) appears to have been concordantly emplaced on a floor of the Magaliesberg Formation, and the northern part transgresses into the Transvaal Supergroup until it rests on a floor of Archaean granite.

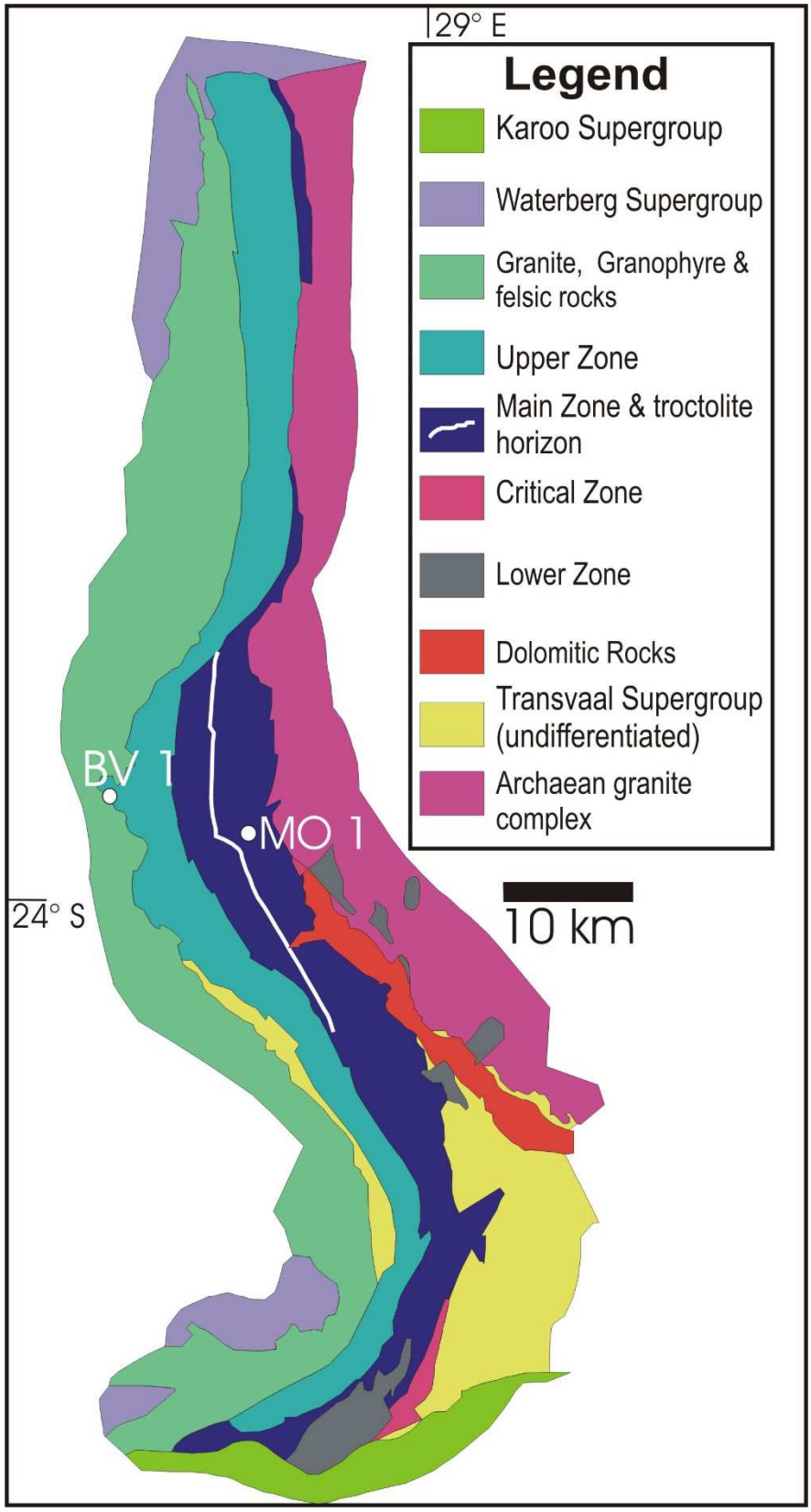

Figure 5: Geological map of the Northern Limb of the Rustenburg Layered Suite showing the localities of the BV-1 and MO-1 boreholes. Figure adapted and modified from Roelofse & Ashwal (2012).

The limb outcrops in three sectors, the northern, central, and southern sectors. The northern sector consists primarily of Upper Zone rocks (with a thin sliver of Main Zone rocks and the Platreef at the base) which lie directly on Archaean basement. The central sector consists of Upper Zone and Main Zone rocks, with Lower Zone rocks occurring as satellite bodies in banded iron formations and dolomites of the Chuniespoort Group which form the footwall rocks (van der Merwe, 2008). In the southern sector, the lower units of both the Upper and Main Zone rocks, as well as the upper units of the Critical Zone, and parts of the Lower Zone are developed (van der Merwe, 2008). Footwall rocks are shales, mudstones, and siltstones of the Proterozoic Pretoria Group.

When contrasted to the better studied Eastern and Western limbs, the Northern limb has a number of unique attributes. Firstly, is the absence of specific marker horizons which are present in both the Eastern and Western limbs (e.g. the Pyroxenite Marker). Secondly, is the occurrence of the Platreef, the main mineralised horizon in the Northern Limb and the origin of which has been the subject of considerable discussion. Thirdly, is the presence of an ~110 m thick troctolitic horizon that occurs about half way through the Main Zone of the Northern Limb, which has been deemed anomalous, because the Main Zone is defined in part by the absence of the mineral olivine (Roelofse & Ashwal, 2012; Tanner *et al*., 2014).

The PGE, Ni, and Cu bearing Platreef in the Northern Limb has been said to possess some petrographic resemblance to the famous Merensky reef of the Eastern and Western limbs (Harris & Chaumba, 2001). The Platreef is situated at the base of the Main Zone, at the contact between the Rustenburg Layered Suite and footwall rocks

(Transvaal Supergroup sediments in the south, dolomite in the centre, and Achaean basement in the north) (Kinnaird *et al*., 2005; Riesberg *et al*., 2011). Its thickness is variable (up to 400 m in places), has a NW or N strike, and dips at 40-45° westwards on surface, becoming shallower and shallower down dip (Kinnaird *et al*., 2005). It is comprised of a series of heterogeneous medium- to coarse crystalline pyroxenites, melanorites, and norites, all with xenoliths of country rocks (e.g. banded ironstone, shales and dolomite). Economic exploitation of the Platreef began in the 1920s, ceased in 1930 because of the platinum price collapse during the Great Depression, and recommenced in 1993 with operations at the Sandsloot Mine situated just outside the town of Potgietersrus/Mokopane (Harris & Chaumba 2001; McDonald *et al.,* 2005). A subsidiary company of Anglo Platinum, Potgietersrus Platinum Ltd is currently operating five open pit mines at Sandsloot, Zwatfontein South, Zwartfontein North, and Overysel, collectively known as Mogalakwena (Kinnaird *et al*., 2005). A few companies, e.g. Ivan plats and Bushveld Minerals have also started exploring the Platreef, whose origin, mineralisation style, and relation to the entire Bushveld Complex are areas of intense scientific dispute, and have been the focus of several studies (e.g. Kinnaird *et al*., 2005; MacDonald *et al*., 2005; Reisberg *et al*., 2011).

1.2.3 Lithostratigraphic units of the Rustenburg Layered Suite

The Rustenburg Layered Suite has been informally divided, from bottom to top, into the Marginal Zone, Lower Zone, Critical Zone, Main Zone, and the Upper Zone. Placement of zone boundaries is derived from mineralogical criteria and the positions of specific marker horizons (Roelofse & Ashwal, 2012), and has been the subject of several studies (e.g. Kruger, 1990).

1.2.3.1 Marginal Zone

The Marginal Zone consists of medium grained, unlayered rocks that underlie most of the complex. There are no upper marginal or border facies as observed in the Skaergaard intrusion (Eales & Cawthorn, 1996). The base is formed of thick sequences of heterogenous noritic rocks. These rocks may represent composite sills, or the distal facies of evolved magmas from within the chamber, but cannot represent parental magmas chilled on the edge of the main chamber (Eales & Cawthorn, 1996). The multi intrusive nature, and the extreme complexity of the Marginal Zone is seen in the Eastern Limb where mafic rocks of different generations interdigitate (Eales & Cawthorn, 1996). However, recent studies (Wilson, 2015) have shown that the Marginal Zone does not represent the oldest rocks of the Bushveld Complex, contrary to what was previously suggested, but that there is a previously unknown Basal Ultramafic Sequence (BUS) beneath this Zone.

1.2.3.2 Lower Zone

The Lower Zone has been poorly studied, mainly as a result of poor exposure and a dearth of economic mineral deposits (chromitites are generally not present) (Eales & Cawthorn, 1996). It is dominated by orthopyroxenites and olivine-rich rocks, with accessory chromite, and variable amounts of intercumulus plagioclase, biotite, and clinopyroxene. The lowermost portion of the Lower Zone is composed of olivine-rich rocks, like dunite and harzburgite, followed by an interval of pyroxene rich rocks. The Lower Zone does not always occur. In areas where it is encountered, its thickness varies from 800-1700 m. Both the distribution and thickness of the Lower Zone are controlled by floor topography and structure (Kinnaird *et al*., 2005).

1.2.3.3 Critical Zone

The Critical Zone is host to two of the world's largest planitiferous ore-bodies, the Merensky reef and the Upper Group 2 (UG2) chromitite in the Eastern and Western Limbs (Barnes *et al*., 2004). In addition, this zone also hosts a number of chromitite layers, the Lower, Middle, and Upper Group chromitite layers labelled from the base upwards LG1-7, MG1-4, and UG1-2 (UG3 only present in the Eastern Bushveld) (Eales & Cawthorn, 1996).

The Critical Zone is also divided into the lower (C_LZ) and Upper (C_UZ) Critical zones, whose transition occurs between the MG2 and MG3 chromitite layers, and is marked by the first appearance of cumulus plagioclase (Eales and Cawthorn, 1996). The Lower Critical Zone is 700-800 m thick and consists predominantly of orthopyroxenite. The Upper Critical Zone is about 500 m thick and it consists of orthopyroxenite, norite, and anorthosite as the main lithologies (Maier *et al*., 2013). A characteristic feature of the Upper Critical Zone is the occurrence of cyclic units (e.g. Cameron, 1982; Eales *et al*., 1986). These units consist of ultra-mafic rocks at their base, overlain by progressively more feldspathic rocks.

1.2.3.4 Main Zone

The 2-3 km thick Main Zone, forming a part of this study, is a succession of gabbroic cumulates lacking the minerals olivine and chromite, as well as the fine scale layering and the extreme lithological diversity observed in the Critical Zone (Eales & Cawthorn, 1996). Cumulus minerals are plagioclase, augite, orthopyroxene and pigeonite (now inverted to orthopyroxene). Pyroxenites are rare, and thick anorthosite layers occur in two short intervals, the main mottled and the upper mottled anorthosites, the latter

occurring only in the Eastern Limb (Eales & Cawthorn, 1996). Further up in the Main Zone is the Pyroxenite Marker. Close to this level there is a reversal in mineral compositions and a break in Sr-isotopic ratio (e.g. Sharpe, 1985). Some authors argue that the transition from the Main Zone to the Upper Zone occurs at this level (e.g. Kruger *et al*., 1987; Kruger, 1990), and not some few hundred metres higher up, where cumulus magnetite first occurs. The Pyroxenite Marker has also been interpreted to represent the level at which the final addition of magma, in the form of a very large single influx, to the Bushveld Complex took place (Kruger, 2005; Mangwegape *et al*., 2016).

1.2.3.5 Upper Zone

The transition from the Main Zone to the Upper Zone is marked by the first appearance of cumulus magnetite (Kruger, 1990). The Upper Zone, a part of which this study is also concerned with, is approximately 2-3 km thick, is well layered, and it contains about 26 layers of magnetitite, including the main magnetitite layer that occurs close to the base, which is mined for its vanadium content (Eales & Cawthorn, 1996). The Upper Zone is also subdivided into three subzones based on cumulus mineralogy. Subzone A contains plagioclase, low-Ca pyroxene, and magnetite. Subzone B is characterised by iron-rich olivine becoming the additional cumulus phase. These two subzones show cyclic units of magnetitite, gabbronorite, and anorthosite. Subzone C is characterised by the presence of apatite and large xenoliths of country rock (Maier *et al*., 2013). A schematic stratigraphic column of the Rustenburg Layered Suite is shown in Figure 6 on the next page. For a summary of the lithostratigraphic units comprising the Rustenburg Layered Suite see Table 2 on page 19.

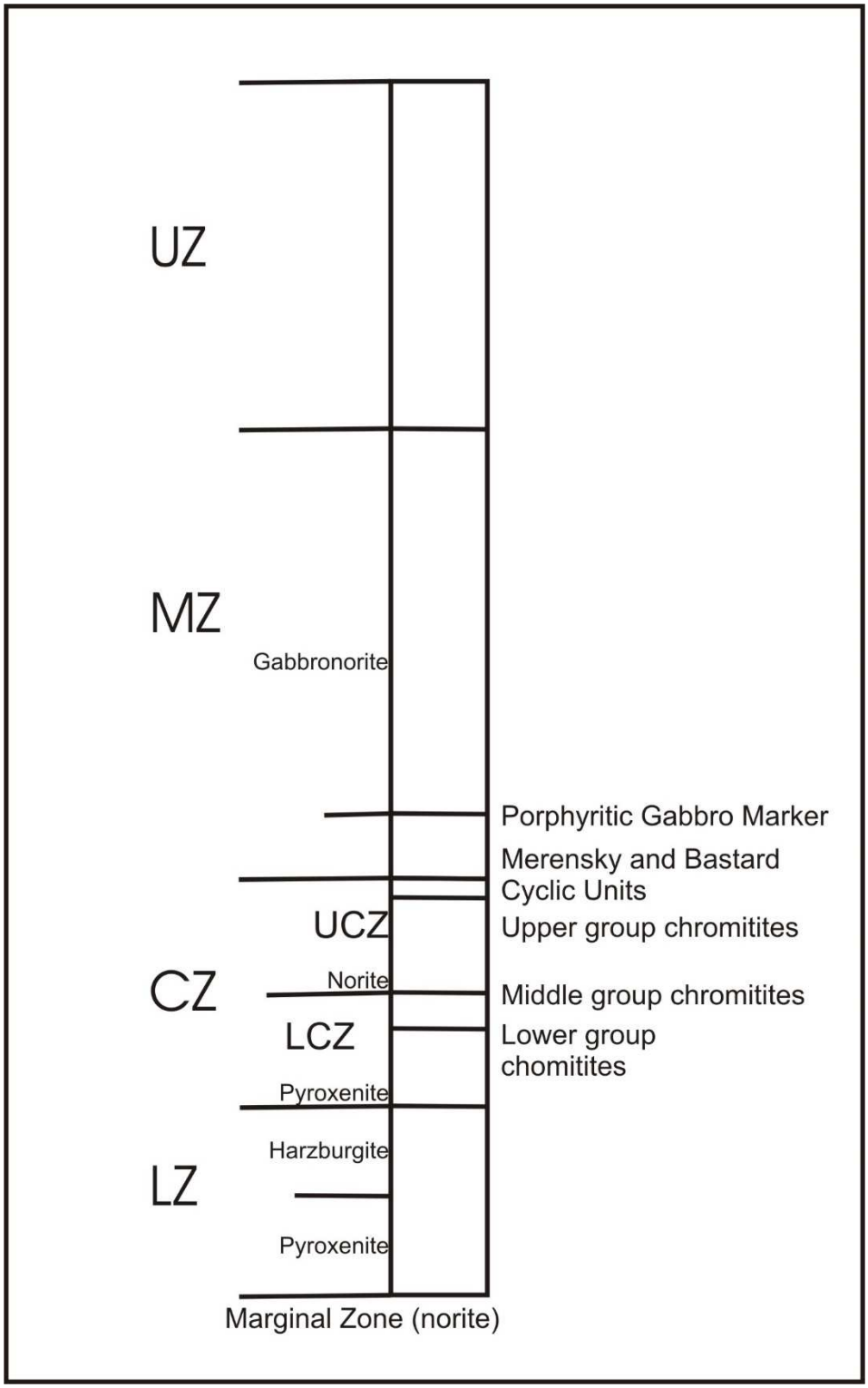

Figure 6: Subdivision of the Rustenburg Layered Suite (Eastern & Western Limbs) into the Upper Zone (UZ) consisting of ferrogabbros and various magnetitite layers, the Main Zone (MZ) composed of gabbronorite, the Critical Zone (CZ), which is in turn divided into the Lower (LCZ) and Upper (UCZ) Critical Zones consisting of pyroxenite and norite respectively, the Lower Zone consisting of pyroxenite and harzburgite, and the Marginal Zone of norite. Figure adapted and modified from Yang *et al*. (2013).

Table 2: Summary of the lithostratigraphic units of the Rustenburg Layered Suite, Bushveld Complex.

Description	Notable features	Relevant references
Upper Zone		
Marked by the first appearance of cumulus magnetite. It is subdivided into three subzones based on cumulus mineralogy. Contains about 26 magnetitite layers.	Some magnetitite horizons are mined for vanadium (V).	Eales & Cawthorn, 1996) (Maier *et al*., 2013)
Main Zone		
The MZ is the thickest unit in the Bushveld Complex. It is comprised of gabbroic cumulates which lack the minerals olivine and Cr-spinel.	No known economic deposits.	(Eales & Cawthorn, 1996) (Sharpe, 1985) (Kruger, 1990)
Upper Critical Zone		
Marked by the onset of cumulus plagioclase. Cyclic units occur, and each grade from ultramafic to more feldspathic rocks upwards.	Merensky and UG-2 (PGE reserves)	(Maier *et al*., 2013)
Lower Critical Zone		
Marked by the first appearance of chromitite. Dominated by orthopyroxenite.	Some chromitite horizons are mined for chromium (Cr).	(Maier *et al*., 2013)
Lower Zone		
Lowermost zone composed of olivine rich rocks, followed by an interval of pyroxene rich rocks.	No known economic deposits.	(Eales & Cawthorn, 1996)
Marginal Zone		
The Marginal Zone is a succession of norites and pyroxenites.	No known economic deposits	(Eales & Cawthorn, 1996)

1.3 Review of previous isotopic work done in the Bushveld Complex

The Bushveld Complex has been at the centre of geological research for decades, and as a result, the three major limbs of the Complex have been studied in a fair amount of detail. Much of these studies have been focused on, but not limited to, whole-rock geochemical variations in stratigraphic context (e.g. Manyeruke *et al*., 2005), determing whether the different limbs of the Complex are connected at depth (e.g. Cawthorn & Webb, 2000), investigating the formation of mineralised horizons and the distribution of PGEs, V, and Cr (e.g. Naldrett *et al*., 1986; Naldrett, 1989; Naldrett & von Gruenewaldt, 1989), determining the nature and intrusion mechanism/s of magmatic influxes (e.g. Cawthorn & Walraven, 1998), and determining the compostion of magmas parental to the Bushveld Complex (e.g. Cawthorn, 2007). However, despite the vast literature that has accumulated, little attention has been given to isotopic disequilibrium in minerals within the Bushveld Complex, and to the implications thereof on the petrogenesis of the Complex.

Hamilton (1977) conducted the first comprehensive Sr isotope study on rocks of the Eastern and Western limbs of the Rustenburg Layered Suite. Results from this study revealed an age of 2095 ± 24 Ma for the Bushveld Complex, and showed abrupt stepwise increases of initial $^{87}Sr/^{86}Sr$ ratios across the entire stratigraphy, and consequently the multiple intrusive nature of the complex.

Following the study by Hamilton (1977), Kruger & Marsh (1982) conducted a detailed Sr-isotope study across the Merensky unit and its immediate hanging and footwall rocks in the Western limb of the Bushveld Complex. The authors found variation of initial Sr-isotope ratios with height, confirming the results of Hamilton (1977).

Sharpe (1985) compiled a Sr-isotope profile across the entire stratigraphy of the Eastern limb of the Bushveld Complex, and Kruger (1994) compiled a comparable profile for the Western Limb. Lee & Butcher (1990) provided evidence for distinct Sr isotopic variations associated with the Merensky reef in the Eastern Limb, and Kruger (1992) provided similar evidence for the Merensky reef in the Western Limb.

All this accumulated work is merely a summary of Sr isotopic work done on whole rocks and/or plagioclase mineral separates in the Bushveld complex. Consequently, researchers of the complex have conducted studies on other isotope systems and these studies include: Nd isotopic studies (Maier *et al*., 2000), Pb isotope studies (Harmer *et al*., 1995; Mathez & Waight, 2003), O-H isotopic studies (Harris & Chaumba, 2001; Harris *et al*., 2005), Os isotopic studies (Hart & Kinloch, 1989; McCandless *et al*., 1999; Schoenberg *et al*., 1999; Curl, 2001; Reisberg *et al*., 2011), and S isotope studies (Liebenberg, 1970; Holwell *et al*., 2007; Penniston-Dorland *et al*., 2007).

Some authors (e.g. Riesberg *et al*., 2011) argue that the results from these studies support conclusions that Bushveld magmas underwent large-scale crustal contamination, whereas others (e.g. Richardson & Shirey, 2008) argue that isotopic features may point not to crustal contamination, but to interaction of Bushveld parental magmas with sub-continental lithospheric mantle (SCLM) prior to emplacement at high crustal levels.

Whatever the case may be, several breaks/reversals in initial Sr-isotopic ratios are observed across the entire stratigraphy of the Rustenburg Layered Suite, and this feature has had a profound influence on Bushveld petrogenetic models.

Prevec *et al*. (2005) argued that the presence of isotopic disequilibrium suggests that isotopic compositions of whole-rock samples in cumulus rocks must be interpreted with caution. These authors studied four lithologies across the Merensky Reef, footwall leuconorite; Merensky Reef pyroxenite; Merensky Reef melanorite; and Merensky Reef norite from the Impala platinum mine, in the Western Limb of the Bushveld Complex, South Africa.

The Sm and Nd isotopic data obtained from this study showed that co-existing orthopyroxene and plagioclase are in isotopic disequilibrium with each other. Based on this evidence, the authors proposed, with regards to the petrogenesis of the Merensky Reef, that orthopyroxene in the Merensky Reef must have been derived from a liquid affected by crustal contamination, and settled into a liquid crystal mush dominated by less contaminated, early formed plagioclase crystals.

This work by Prevec *et al*. (2005) raised concerns on the validity of petrogenetic models developed from data obtained from whole rock, or single mineral separate isotopic analyses.

Additionally, Roelofse & Ashwal (2012) identified disequilibrium in initial Sr isotope ratios between coexisting plagioclase and orthopyroxene in the rocks of the Lower Main Zone (LMZ), northern Bushveld Complex. Based on their data, these authors suggested that the disequilibrium, together with other features of the LMZ (e.g. bulk compositions of LMZ cumulates do not favour the crystallisation of plagioclase and two pyroxenes, decoupling of the differentiation trends of plagioclase and pyroxene over a short vertical interval, non-cotectic proportions of plagioclase and pyroxene,

and poorly developed layering), can be attributed to the repeated intrusion of crystal mushes derived from a deep seated, sub-compartmentalised staging chamber.

Furthermore, Chutas *et al.* (2012) obtained results which show that whole-rock isotopic data cannot solely account for some of the processes involved in the petrogenesis of the Bushveld Complex and layered intrusions at large, as it does not offer the necessary level of detail. Using progressive leaching methods, and microdrilling, these authors identified isotopic disequilibrium in plagioclase, between co-existing plagioclase and orthopyroxene, and in orthopyroxene. The authors argued that the disequilibrium is due to late stage infiltration of a relatively radiogenic magma.

Yang *et al*. (2013) studied rock samples from the Union Section, Western Bushveld Complex, and reported disequilibrium Sr isotopic compositions between cores and rims of plagioclase mineral grains, and between cores of different plagioclase grains across the Merensky interval. From their data, the authors proposed that the rocks formed through slumping of semi-consolidated crystal slurries during subsidence of the centre of the intrusion.

In a more recent study by Roelofse *et al*. (2015), plagioclase was shown to exhibit inter and intra-granular isotopic disequilibrium, and in light of their findings, the authors reiterated the notion that interpretation of isotopic data obtained from whole rocks and/or mineral separates, or interpretation of results obtained by progressive leaching methods should be made with great caution. The authors suggest the use of proper *in-situ* analytical methods, e.g. micro-drilling or LA-ICP-MS. Samples used in their investigation were from the Upper and Main Zones of the Northern Limb, Bushveld Complex.

Isotopic disequilibrium is not only confined to the Bushveld Complex. Isotopic disequilibrium has also been reported from the Skaergaard intrusion, Greenland (McBirney & Creaser, 2003). These authors found variation in isotopic ratios of Nd and Sr in the Layered Sequence. The observed variation occurs on different scales, from the intrusion as a whole, down to co-existing minerals in a single rock. The authors proposed that the observed variation in isotopic ratios can best be explained not by injections of a new magma, but rather as a result of metasomatic alteration after crystallisation of the original magma. The exact nature of this metasomatic process is not known, but is thought to be related to late-stage fluids that permeated the entire intrusion.

Sr isotopic zoning within single plagioclase crystals has also been used to infer events during crystal growth in a magma subjected to contamination (Tepley & Davidson, 2003). These authors investigated rocks from the Rum layered intrusion and found variations in Sr isotopic data between co-existing minerals and between cores and rims of plagioclase mineral grains. The authors proposed that the variation is recorded in crystals growing from a magma undergoing crustal contamination. Through density-driven currents, the isotopically zoned crystals break free from the cooling solidification front, settle onto the floor of the magma reservoir, and are allowed to mix with unzoned crystals.

Wei *et al.* (2014) found Sr-Nd isotopic disequilibrium between coexisting plagioclase and clinopyroxene mineral separates from the Xiaohaizi Wehrlite Intrusion. Based on this evidence, the authors suggested that the formation of the intrusion can be ascribed to fractional crystallisation of a magma contaminated by crustal material.

1.4 Purpose of present investigation

Following the literature review above, it is worthwhile to emphasize that variations in Sr-isotopic ratios between minerals of the same rock, as well as variations within a single mineral (i.e. inter and intra-mineral Sr-isotopic disequilibria) in rocks of the layered sequence of the Bushveld Complex is a subject that has not received adequate attention. This study was conceived to augment this lack of *in-situ* chemical and isotopic data on the Bushveld Complex and to expand the rather small database of *in-situ* Sr-isotopic measurements in the world's largest preserved layered intrusion.

Another rationale of the present investigation is to study disequilibrium phenomena between coexisting minerals from a trace element perspective. Not only isotopic data can harbour information pertaining to disequilibrium between coexisting minerals; trace element data of such minerals can also mirror disequilibrium occurrences, because the trace element composition of such minerals is expected to correlate between minerals that crystallised from the same magma as a function of partition coefficients and melt composition.

With this work, I aim to contribute to the existing studies of the Bellevue and Moordkopje drill cores, and hope that the findings will be of interest to the academic community at large in the context of understanding the genesis of large layered intrusions, magma chamber dynamics of the Bushveld Complex, and the origin of layering.

2. Methodology

2.1 Sampling

2.1.1 Bellevue core

The Bellevue (BV-1) borehole, is a 2950m deep hole that was collared in roof granites on Bellevue farm (23˚55'34.669"S, 28˚45'20.327"E) during the late 1980s to late 1991. BV-1 penetrates the Upper and Main Zones of the Bushveld Complex, and ends in a troctolitic horizon occurring half way through the Main Zone of the Northern Limb. This core is unique as it was drilled for academic purposes. It intersects barren lithologies and thus provides a general view on the evolution of the Bushveld Complex.

Ashwal *et al*. (2005) determined the major and minor elemental compositions of silicate and oxide minerals *in-situ*, and determined differences in density, magnetic susceptibility, and modal abundances along the core. Tanner *et al*. (2014) presented the abundance data for 57 trace elements hosted in the minerals plagioclase, clinopyroxene, low-Ca pyroxene and olivine, obtained by Laser Ablation Inductively Coupled Plasma Mass Spectrometry (LA ICP- MS).

Other work on the Bellevue drill core includes oxygen isotope composition (Harris & Chaumba, 2001), and platinum group-element distribution in the Main and Upper Zones (Barnes *et al*., 2004).

As part of this study, a total of 20 samples from the Bellevue drill core (Figure 7) were used (obtained from Prof LD Ashwal, University of the Witwatersrand). All depths reported here are relative to the Main Zone – Upper Zone boundary, with the depth being the measured depth along the core subtracted from 1575.8 m.

For the reason that the BV-1 intersects the Upper and Main Zones of the Northern Limb, and for the purpose of this work, the Main Zone of the Northern Limb is divided into the Upper and Lower Main Zones, such that the Upper Main Zone is comprised of rocks from the lower end of the BV-1 drillhole, i.e rock samples that are very close to the troctolitic horizon, including samples of the troctolite itself (all samples from the BV-1 drill hole that are below the Upper Zone-Main Zone boundary). The Lower Main Zone is then comprised of all samples from the MO-1 drillhole as it is explained in the Moordkopje core section which follows below.

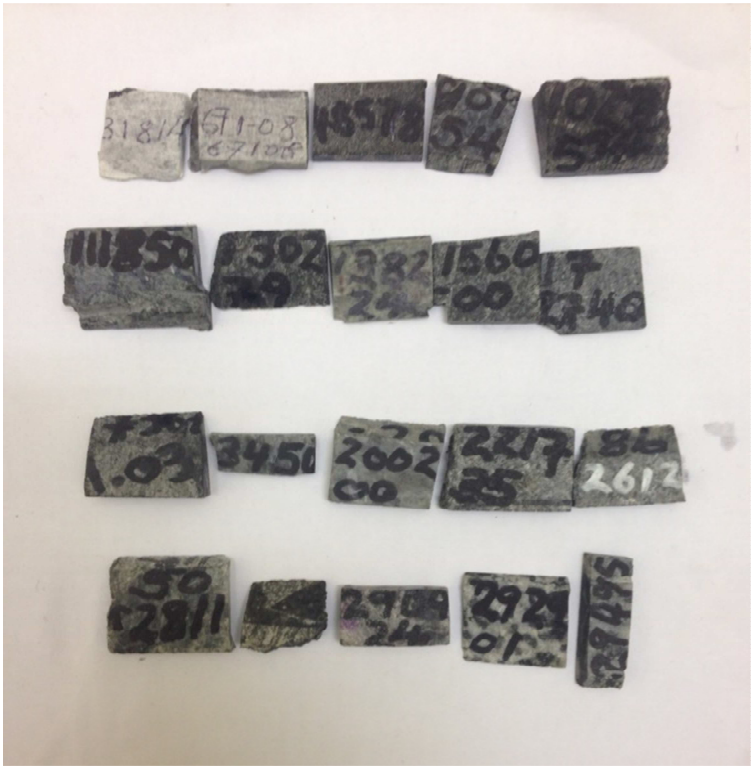

Figure 7: Samples from the Bellevue (BV-1) drill core obtained from Prof L D Ashwal of the University of Witwatersrand.

2.1.2 Moordkopje core

The Moordkopje (MO-1) borehole is a 1563.02 m deep hole drilled on the farm Moordkopje (23.9490° S, 28.86486° E, elevation1075.2 m) during late 1979 to early 1980. It is situated on the eastern border of the farm, ~11.3 km at a bearing of 103° from borehole BV-1. The MO-1 drill core covers the stratigraphy below that covered by the BV-1 drill core (Figure 8). Importantly, MO-1 does not intersect the anomalous troctolitic horizon occurring at the bottom of BV-1. The MO-1 drill core intersects ~ 1350 m of lower Main Zone rocks, followed by ~200 m of Platreef rocks, ending in pinkish granite that forms the footwall to the Platreef (Figure 8).

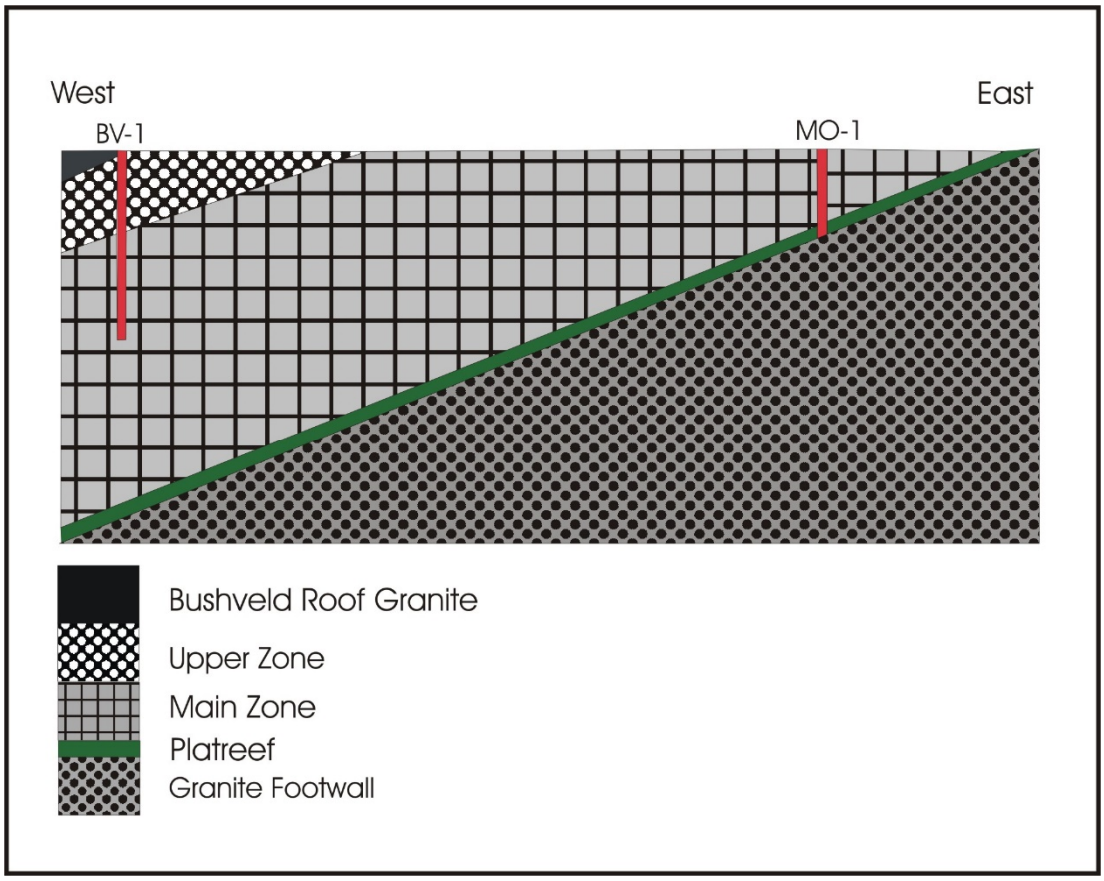

Figure 8: Diagrammatic west to east cross section showing the penetration of Bellevue (BV-1) and Moordkopje (MO-1) boreholes into rocks of the Bushveld Complex. Figure adapted and modified from Roelofse (2010).

A total of 20 samples, previously analysed by Roelofse & Ashwal (2012) were collected from the Moordkopje drill core as part of this study (Figure 9). All depths reported here are relative to the Main Zone-Upper Zone boundary, with the depth relative to this boundary being the measured depth in the hole plus 1863.7 m.

Figure 9: Samples from the Moordkopje (MO-1) drill core.

2.2 Petrography

Polished thin sections were produced from all samples collected and studied using transmitted light microscopy (Figure 10). The modal mineralogy of the samples was determined by visual estimation, using an Olympus BX51 petrographic microscope (Figure 11) coupled with an Olympus SC20 camera used to obtain photomicrographs of the different samples.

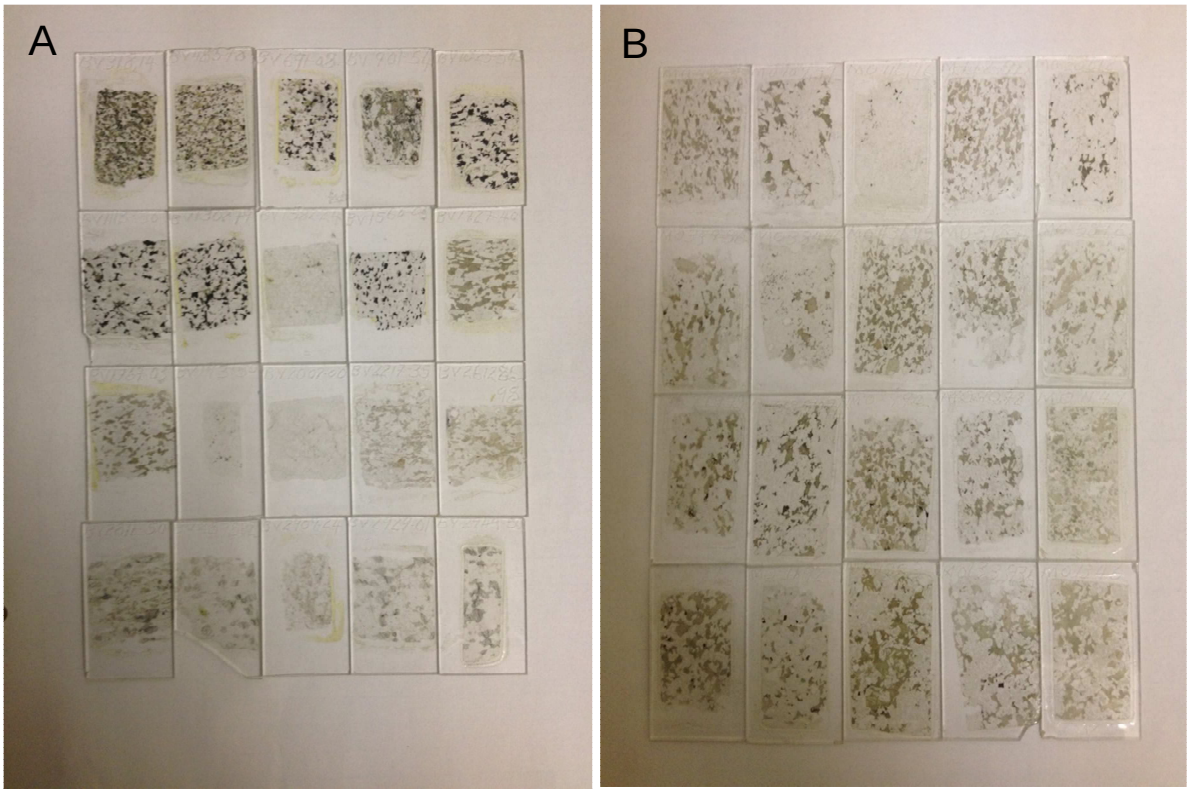

Figure 10: A total of 40 thin sections, 20 prepared from samples obtained from Prof LD Ashwal (A), and the other 20 prepared from samples obtained from the Moordkopje drill core (B).

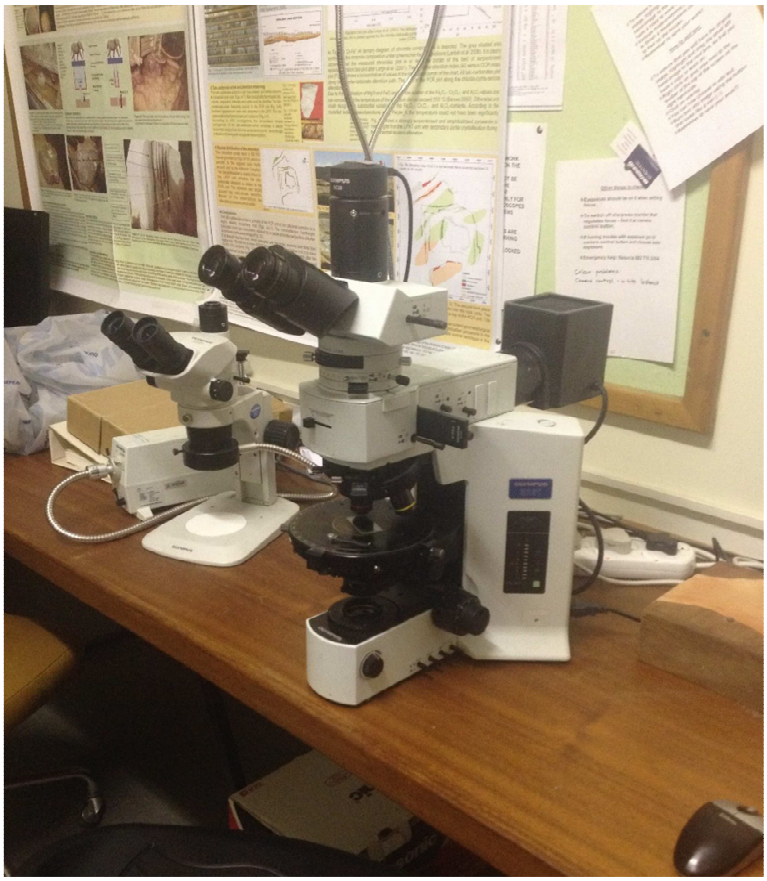

Figure 11: An Olympus BX51 petrographic microscope housed at the Department of Geology, University of the Free State.

The nomenclature used for the classification of the rocks was as far as possible that of the IUGS system, e.g. Streckeisen (1976) (Figure12). The term intergranular was used to describe the occurrence of mafic silicate crystals occurring within a framework formed by lath-shaped plagioclase crystals. Ophitic and sub-ophitic were used to describe the texture in which plagioclase laths are entirely or partially enveloped by mafic silicate crystals, respectively. The term poikilitic was used to describe a texture in which one mafic silicate crystal is enveloped by another and the term poikilophitic to describe the texture in which plagioclase laths and other mafic silicate crystals are enveloped by another mafic silicate crystal.

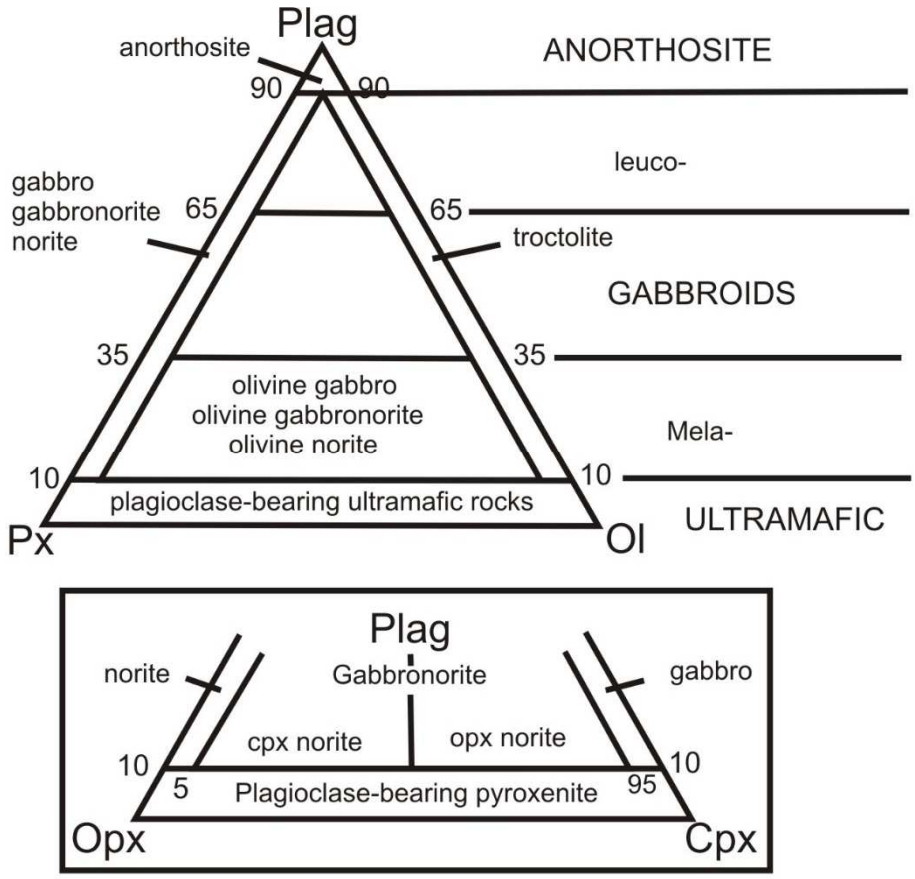

Figure 12: Classification and nomenclature of mafic and ultramafic rocks based on the modal abundance of the minerals plagioclase (Plag), ortho & clinopyroxene (Opx & Cpx), and olivine (Ol), modified after Streckeisen (1976).

2.3 Major element mineral chemistry

Polished blocks were also prepared from all 40 rocks sample obtained from the two drill holes (Figure 13 & 14) and these were used for microprobe and Laser Ablation Inductively Coupled Plasma Mass Spectrometry work. These polished blocks were prepared from exactly the same material as the thin sections.

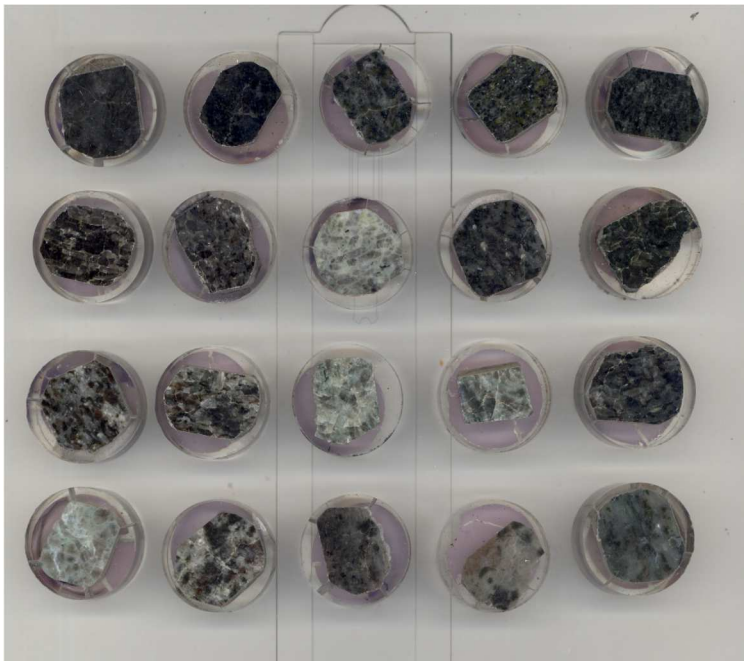

Figure 13: 20 polished blocks prepared from samples from the BV-1 drill core obtained from Prof LD Ashwal. Thick sections are arranged from left to right in order of increasing depth.

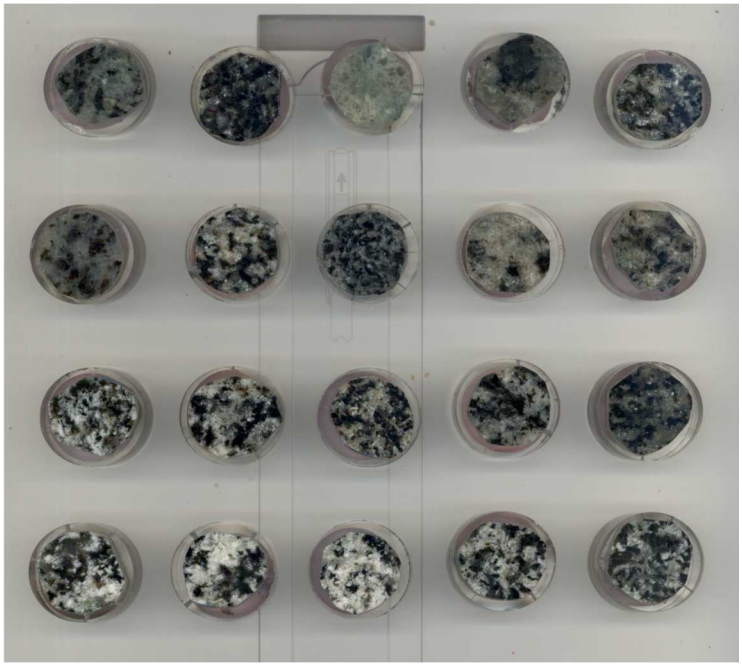

Figure 14: Polished blocks prepared from samples from the MO-1 drill core, arranged from left to right in order of increasing depth.

For major element analysis, a minimum of five euhedral plagioclase grains, with clear discernible grain boundaries were selected per sample (Figure 15A) using reflected light microscopy. For each grain, a total of eight spots were to be analysed, five across the length of the grain, and three across the width (Figure 15B).

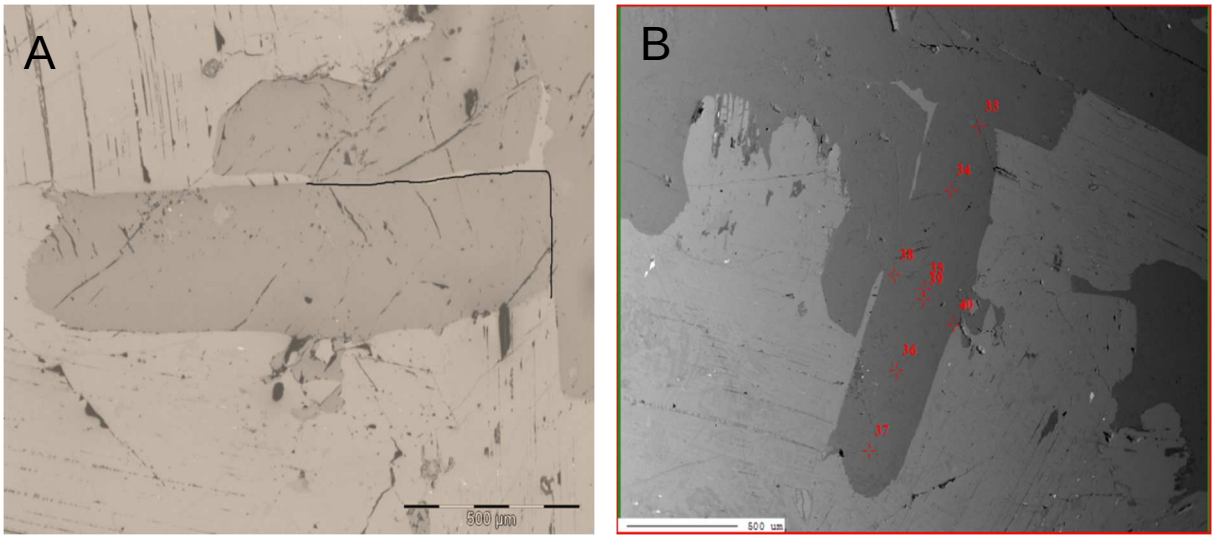

Figure 15: (A) Reflected light photomicrograph of a plagioclase grain selected for analyses. (B) Back Scattered Electron (BSE) image of the grain in (A) showing the positions of electron microprobe spots. The plagioclase grain is of a sample from a depth of -1910.2 m.

The *in-situ* major element composition of these different plagioclase mineral grains in carbon-coated polished blocks was determined by wavelength-dispersive methods using a JEOL JXA 8230 superprobe housed at the Department of Geology, Rhodes University (Figure 16). Analytical conditions used were as follows: acceleration voltage 15 kV, probe current 20 nA, beam size < 1 micron, and on peak counting time was 10 s and 5 s on background. For Sr and Ba, on peak counting time was 30 s and 15 s on background in order to lower the detection limit. Natural standards were used for calibration (in brackets is given the average detection limit): KαSi – olivine (83 ppm); KαAl – almandine (81 ppm); KαTi – rutile (128 ppm); KαFe - almandine (396 ppm);

KαMn – rhodonite (111 ppm); KαMg – olivine (55 ppm); KαCa Plagioclase-An65 (76 ppm); KαNa – albite (74 ppm); KαK – biotite (34 ppm); LαBa – barite (170 ppm); LαSr – celestite (161 ppm). Sr and Ba were measured using a large diffracting crystal (PETL) for higher sensitivity. The ZAF matrix correction method was employed for quantification.

Figure 16: Electron microprobe facility at the Department of Geology, Rhodes University.

2.4 Isotopic determination

Polished blocks were prepared of 13 samples from the BV-1 and of 14 from the MO-1 drill cores, with samples selected to provide good stratigraphic coverage. Two to three plagioclase crystals were identified in each sample for subsequent ablation, with ~2-3 spots analysed per plagioclase crystal. Sr-isotopic determinations of plagioclase were performed using a Nu Plasma HR MC-ICPMS coupled to an Atlex SI laser system employing a 193 nm excimer laser sampler at the Department of Terrestrial

Magnetism, Carnegie Institution for Science (Figure 17). Samples were ablated in He gas at a pulse frequency of 10 Hz and spot diameters of between 95 µm and 120 µm. Measured isotope ratios were corrected for instrument fractionation according to an exponential law and an $^{86}Sr/^{88}Sr$ value of 0.1194. Subtraction of the background was used to correct for the isobaric interference of ^{86}Kr on ^{86}Sr. The BHVO-2 standard was analysed before and after every 9th unknown (Figure 18) and the $^{87}Sr/^{86}Sr$ ratio for unknowns was corrected for the isobaric interference of ^{87}Rb on ^{87}Sr through monitoring of the ^{85}Rb ion signal by assigning a value to the $^{87}Rb/^{85}Rb$ ratio such that BHVO-2 gave $^{87}Sr/^{86}Sr = 0.703469 \pm 0.000014$ (Elburg *et al.,* 2005). Initial $^{87}Sr/^{86}Sr$ ratios were calculated for an age of 2054.4 Ma (Scoates & Friedman, 2008) using a decay constant of 1.393×10^{-11} y^{-1} (Nebel *et al.,* 2011).

Figure 17: LA-ICPMS laboratory at the Department of Terrestrial Magnetism, Carnegie Institution for Science.

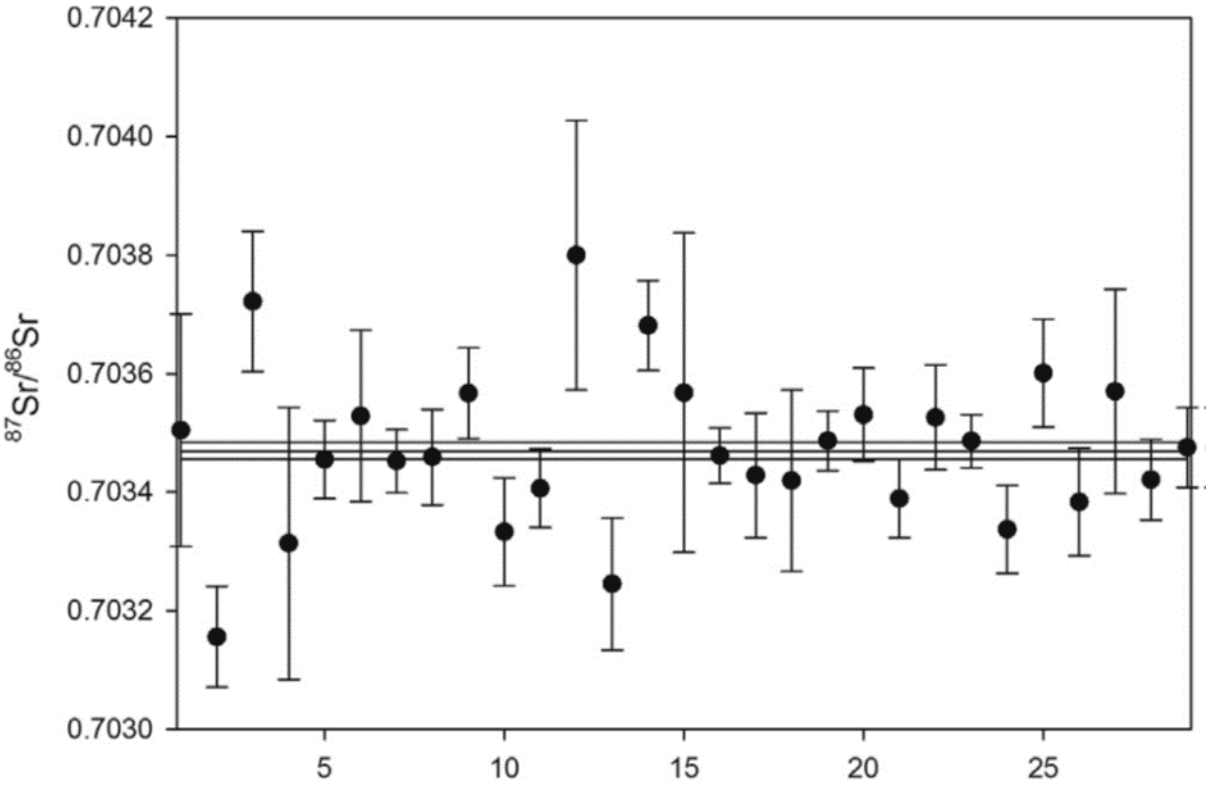

Figure 18: Variation in the $^{87}Sr/^{86}Sr$ ratio (with 2SE error bars) of the BHVO-2 standard over the course of the study. Central horizontal lines represent accepted $^{87}Sr/^{86}Sr$ ratio for BHVO-2 as per Elburg *et al*. (2005) with upper and lower horizontal lines representing 2SE limits.

2.5 Trace element mineral chemistry

Samples for *in-situ* trace element study were the same samples used for Sr isotopic analysis. The trace element composition of plagioclase was determined using a Thermo Fischer XSeries2 ICPMS, coupled to a UP213 laser system at the Department of Geosciences, University of Cape Town (Figure 19). Spot analyses were performed next to the pits generated during the course of isotopic analysis (Figure 20). Analytical parameters were as follows:

- ✓ Pulse frequency 10 Hz
- ✓ Spot diameter 110 µm

For calibration, NIST 610 and 612 international standards were used. Analytical parameters remained constant during measurement of both the samples and the standards.

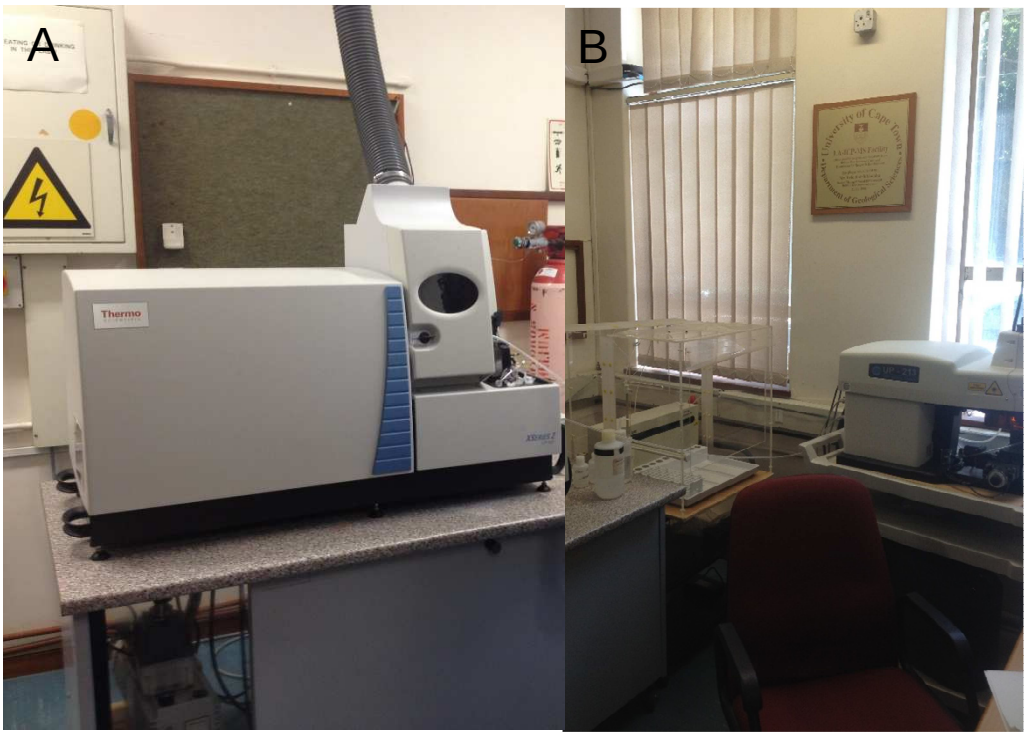

Figure 19: Thermo Fischer Xseries2 ICPMS (left) and UP213 laser system (right) used for trace element analysis at the Department of Geosciences, University of Cape Town.

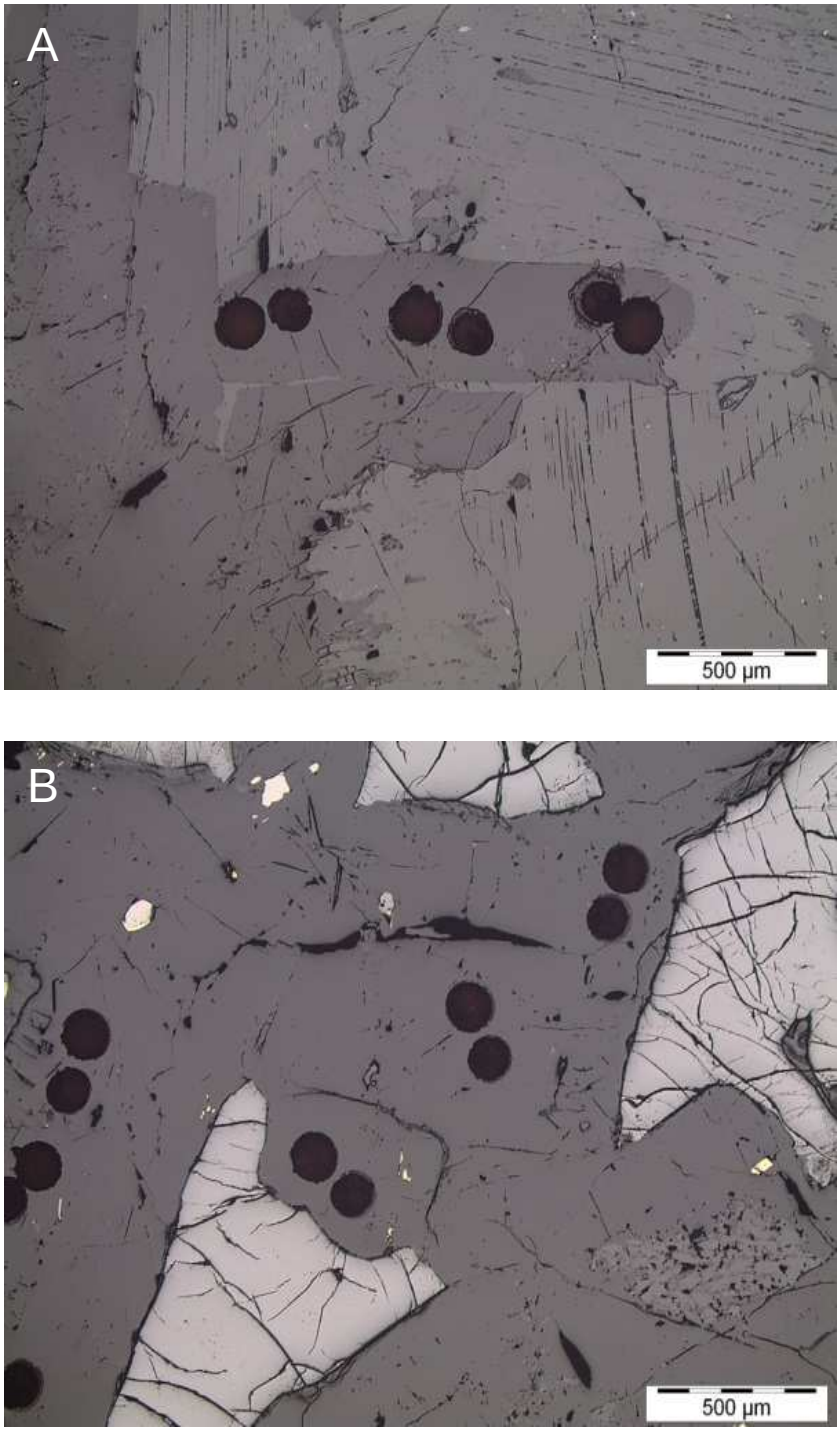

Figure 20: (A) and (B) Reflected light photomicrograph of plagioclase from depth -1910.2 and 273.01 m showing craters formed as a result of laser ablation. Note the difference in size between the craters (smaller ones were formed during trace element determinations).

3. Results

3.1 Petrography

A summary of all the petrographic observations made, including observations such as modal mineralogy, textural information, and grain sizes is given in the Electronic Appendix. Out of the 40 rock samples studied, 32% were gabbronorites, and leucogabbronorites made up a further 28% of all studied samples. Anorthosites constitute about 13%, and olivine gabbros ~ 10%. Leucogabbros constitute 7% of all samples, with troctolites and olivine norite accounting for 5% of all studied samples respectively.

Intergranular texture is the dominant texture. It accounts for 55% of all samples studied, and is most common in rocks from just above and below the Upper Zone-Main Zone boundary, and in most samples from the Lower Main Zone (most samples from the MO-1 drillhole). Poikilophitic texture constitutes about 18% of all samples studied. It occurs in olivine rich rocks found at the top of the Upper Zone, and in rocks found close to the troctolitic layer, which occurs about half way through the Main Zone. Ophitic texture accounts for 20% of all samples, and was observed in the troctolites. Subophitic texture accounts for a further 7% off all 40 rock samples.

Plagioclase is a prevalent phase in the rocks of the Upper and Main Zones of the Bushveld Complex. It occurs as a combination of multiply (polysynthetic) twinned, euhedral to subhedral lath shaped, tabular shaped, and elongated crystals. Its alignment defines the igneous layering present in many of the samples studied (Figure 21-A). In some of the samples, plagioclase is heavily altered to a fine- grained material

thought to be sericite. The alteration occurs in the core of the plagioclase grains and in some cases along the rims (Figure 21-B). Bent and wedged-shaped plagioclase twin lamellae were observed in some of the samples investigated (Figure 21-C). This attribute of plagioclase has been interpreted by some authors, e.g. Von Gruenewaldt (1971) to show deformation after deposition. Pinch and swell textures were also observed in plagioclase (Figure 21-D). Zoned plagioclase was also encountered in some of the samples studied.

Clinopyroxene occurs as subhedral to anhedral grains in the samples studied. It occurs as discrete crystals intergranular to plagioclase (Figure 21-E), and in some cases as oikocrysts enclosing plagioclase laths and/ or orthopyroxene chadacrysts (Figure 21-F). In one instance, clinopyroxene was found enclosing an orthopyroxene grain, which in turn enclosed a plagioclase lath, suggesting the crystallisation sequence plagioclase-orthopyroxene-clinopyroxene (Figure 22-A). Clinopyroxene is characterised by thick exsolution lamellae of orthopyroxene, and twinning is common.

Orthopyroxene is characterised by thin exsolution lamellae of clinopyroxene, and it occurs as subhedral to anhedral grains that are intergranular to plagioclase (Figure 22-B). In other samples orthopyroxene occurs as oikocrysts enclosing both plagioclase laths and very rarely clinopyroxene (Figure 22-C). Inverted pigeonite (orthopyroxene containing thick exsolution lamellae or blebs of clinopyroxene) was encountered in samples from the base of the Upper Zone and the Upper Main Zone from depths 15.8 m, -151.2 m, -192.2 m, and -641.5 m (all gabbronorites), (see Figures 22 D and E).

Biotite is not pervasive in all of the samples studied. It is most common in the rocks of the Upper Zone. Its modal abundance decreases towards the bottom of the studied stratigraphic profile, becoming subordinate in the rocks of the Lower Main Zone. It occurs as lath shaped grains containing pleochroic haloes (Figure 23-A). It occupies the interstitial space between plagioclase grains, and in some instances occurs as patches on rims of plagioclase grains and the pyroxenes. On several occasions, biotite was found to enclose opaque minerals (Figure 22-F).

The occurrence of the mineral quartz is negligible, observed rarely in few of the samples studied. Opaque minerals constitute up to 12% of the Upper Zone rocks, and modally decrease with increasing depth. They occur within interstitial spaces, or within the silicates (Figure 23-A and 23-B). In other instances opaque minerals enclose plagioclase laths, and in some other rare cases ortho and/or clinopyroxene.

The mineral olivine is present in two intervals across the studied profile (see Figure 24 on page 46). It occurs in the uppermost 600 m of the Upper Zone (Figure 23-D), where it is found occupying the interstitial space between plagioclase laths. The mineral was also encountered from depths -1235.7 m, -1322.2 m, and -1333.2 m, and also in two other samples from depths -1353.2 m and -1373.7 m (both troctolites). In this interval olivine occurs as large oikocrysts, enclosing plagioclase in an ophitic to sub-ophitic manner (Figure 23-E and 23F). Olivine is typified by distinctive irregular fracturing.

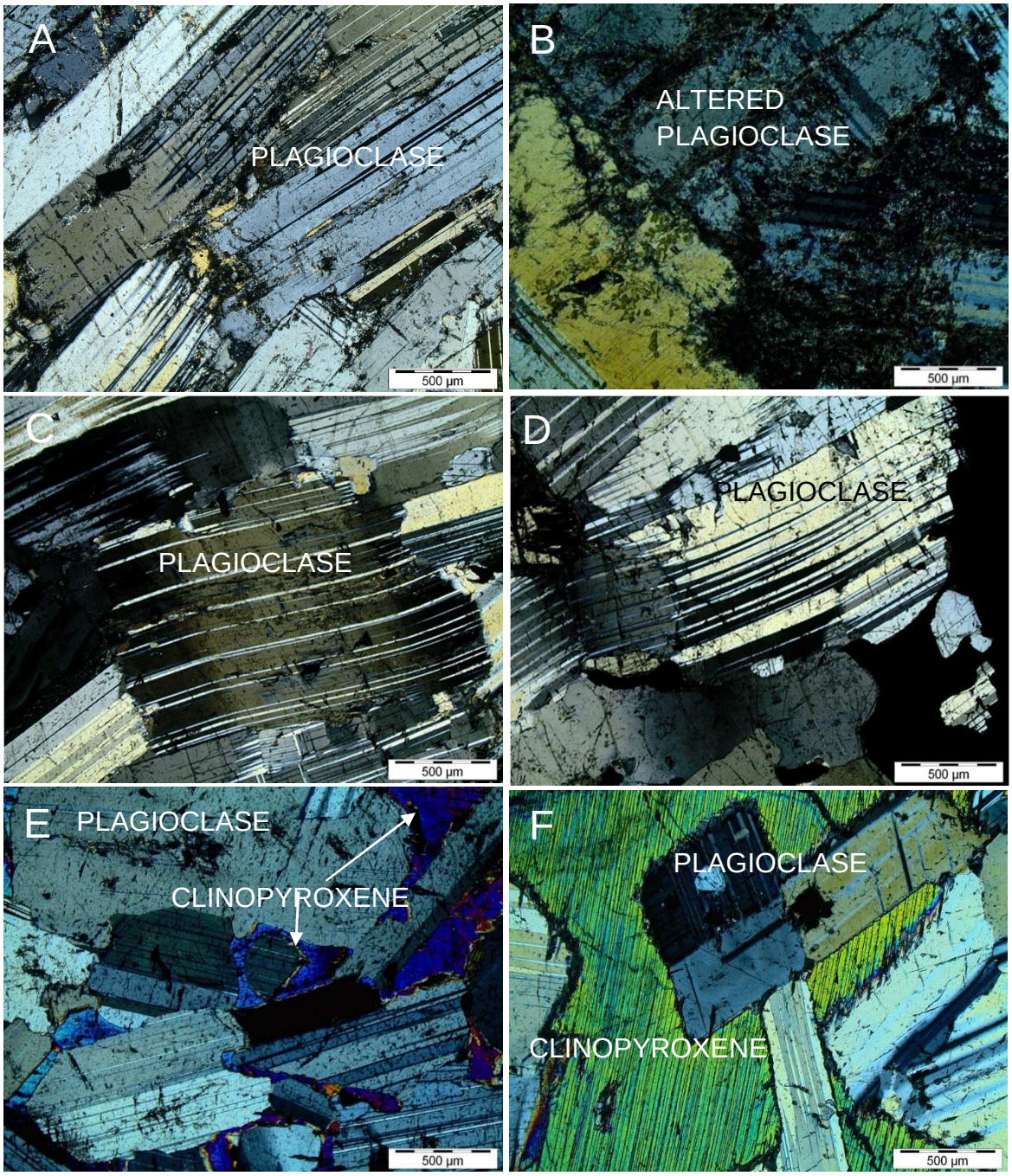

Figure 21: Transmited light photomicrographs of: (A) Plagioclase crystals aligned in a parallel to sub-parallel way, defining the igneous lamination observed in many of the samples studied. Sample from depth -1980.7 m: (B) Plagioclase from a depth of 193.8 m showing extensive sericitization along the rims and within the crystals; (C) Bent and wedged shaped twin lamellae in plagioclase from a depth of -191.2 m; (D) A plagioclase crystal from a depth of -191.2 m exhibiting pinch and swell texture; (E) Clinopyroxene occupying interstitial spaces between plagioclase, and also occuringon rims of plagioclase crystals. Sample froma depth of -2247.7 m; (E) Clinopyroxene oikocryst ophitically enclosing plagioclase crystals of different shapes. Sample from a depth of 3202.7 m. All photomicrographs taken under cross polarized light.

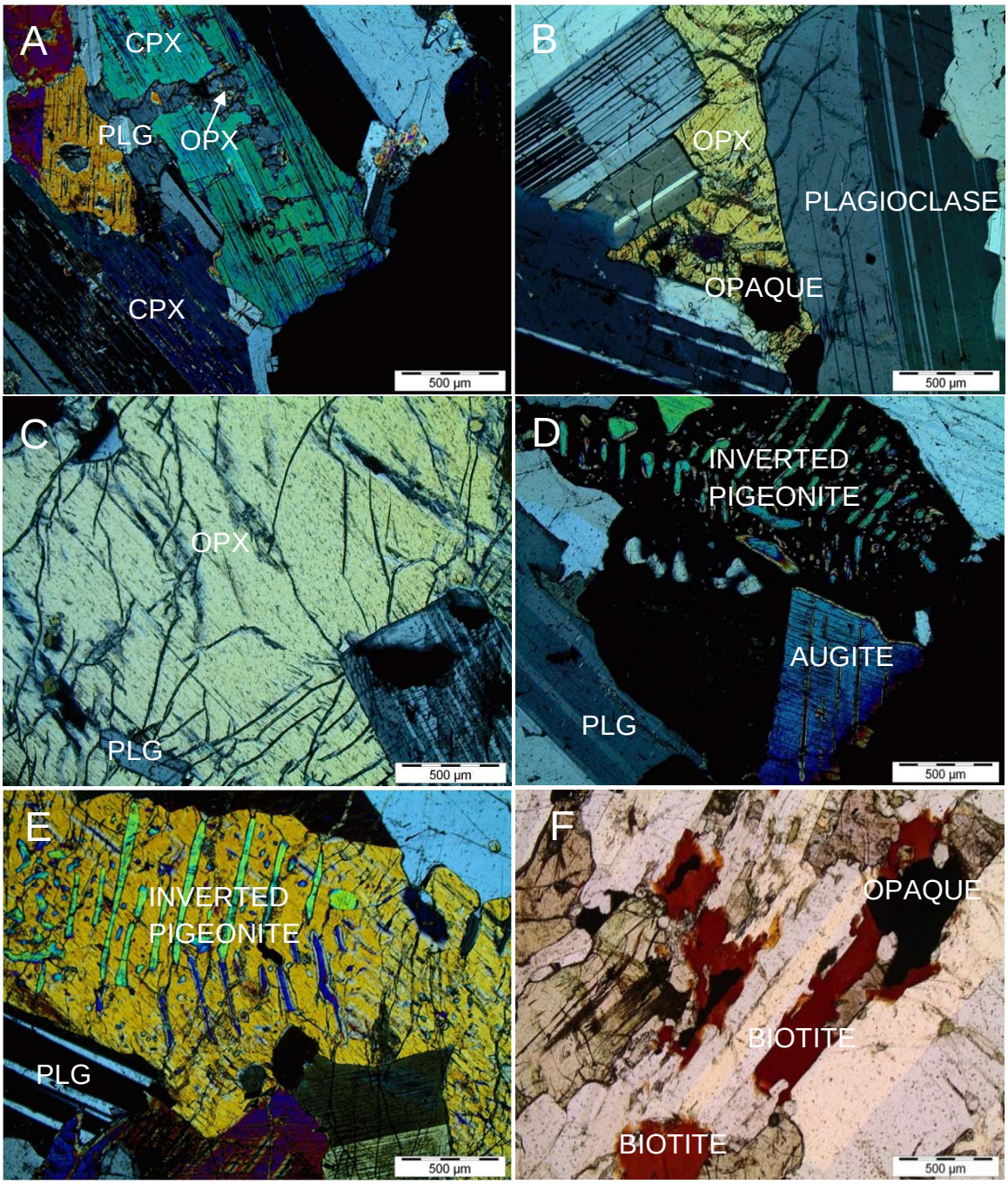

Figure 22: Transmitted light photomicrographs of: (A) Clinopyroxene enclosing an orthopyroxene crystal which in turn partially encloses plagioclase. Sample is from a depth of -641.2 m; (B) An orthopyroxene crystal of intercumulus status from a depth of 273.8 m; (C) An orthopyroxene oikocryst enclosing plagioclase chadacrysts in an ophitic manner. Sample from a depth of -3055.7 m; (D) An inverted pigeonite crystal from depth -152.2 m with the host mineral in extinction. Also note the two generations of exsollution lamellae that are perpendicular to each other, and also the embaying augite crystal occurring at the bottom of the photomicrograph; (E) Inverted pigeonite from depth -151.2 m enclosing a primary orthopyroxene crystal; (F) Biotite from a depth of 1090.2 m occurring both along the rims of plagioclase and pyroxene crystals. Photo under plane polarized light. Photomicrographs A-E were all taken under cross polarized light.

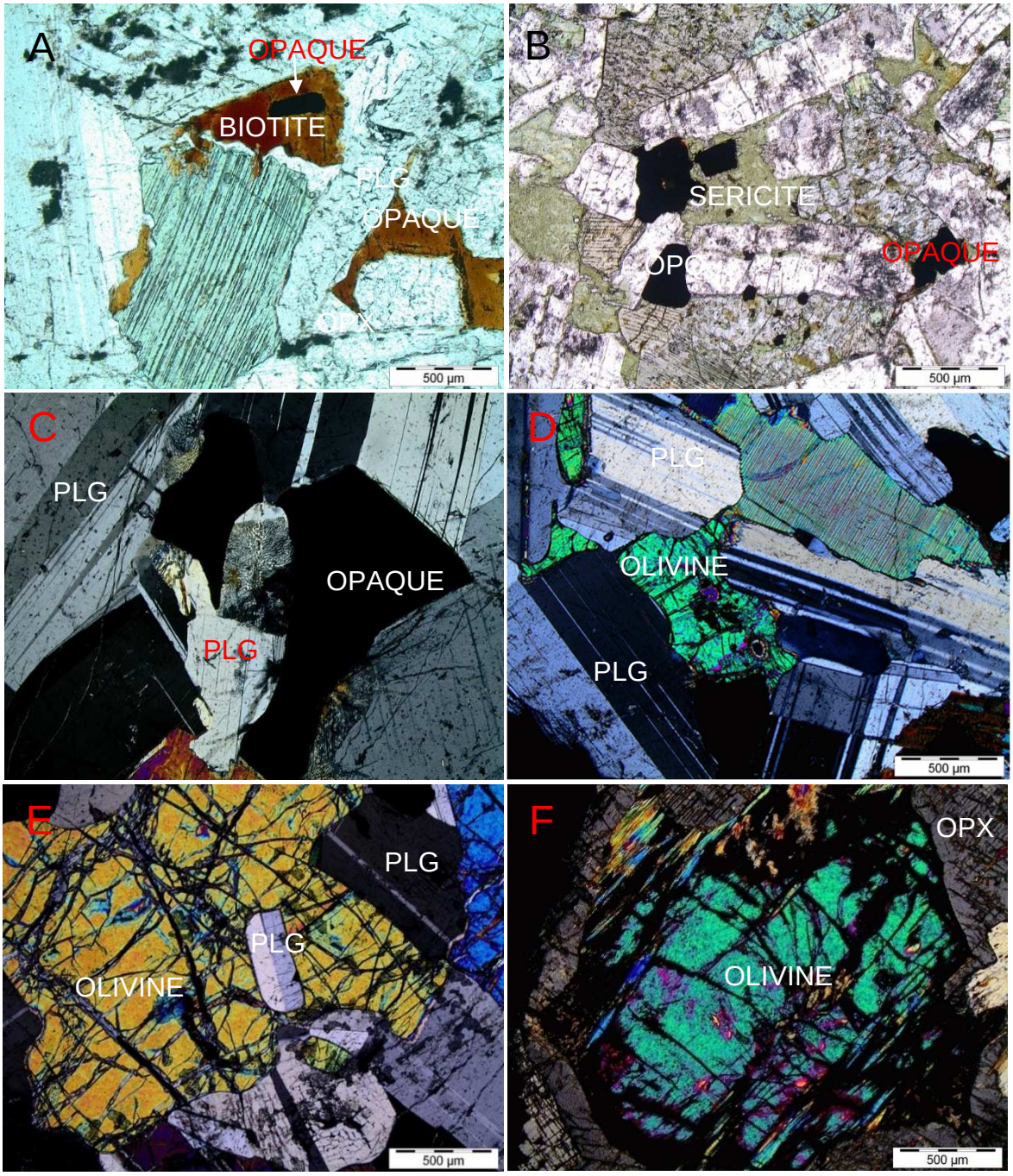

Figure 23: Transmitted light photomicrographs of: (A) Biotite from depth -3055.7 m enclosing an opaque crystal. Also note the thick exsollution lamellae of clinopyroxene occurring just below the biotite crystal. Photomicrograph taken under plane polarized light; (B) Opaque minerals occurring in different ways in a sample from a depth of 1257.8 m. Photomicrograph taken under plane polarized light; (C) Plagioclase-opaque symplectite from depth -191.2 m; (D) Intergranular olivine occurring ata a depth of 1090.02 m; (E) An olivine oikocryst enclosing plagioclase crystals from a depth of -1353.2 m; (F) An olivine crystal from a depth of 674 m occurring within an optically continuous orthopyroxene crystal. Photomicrographs C-F all taken under cross polarized light.

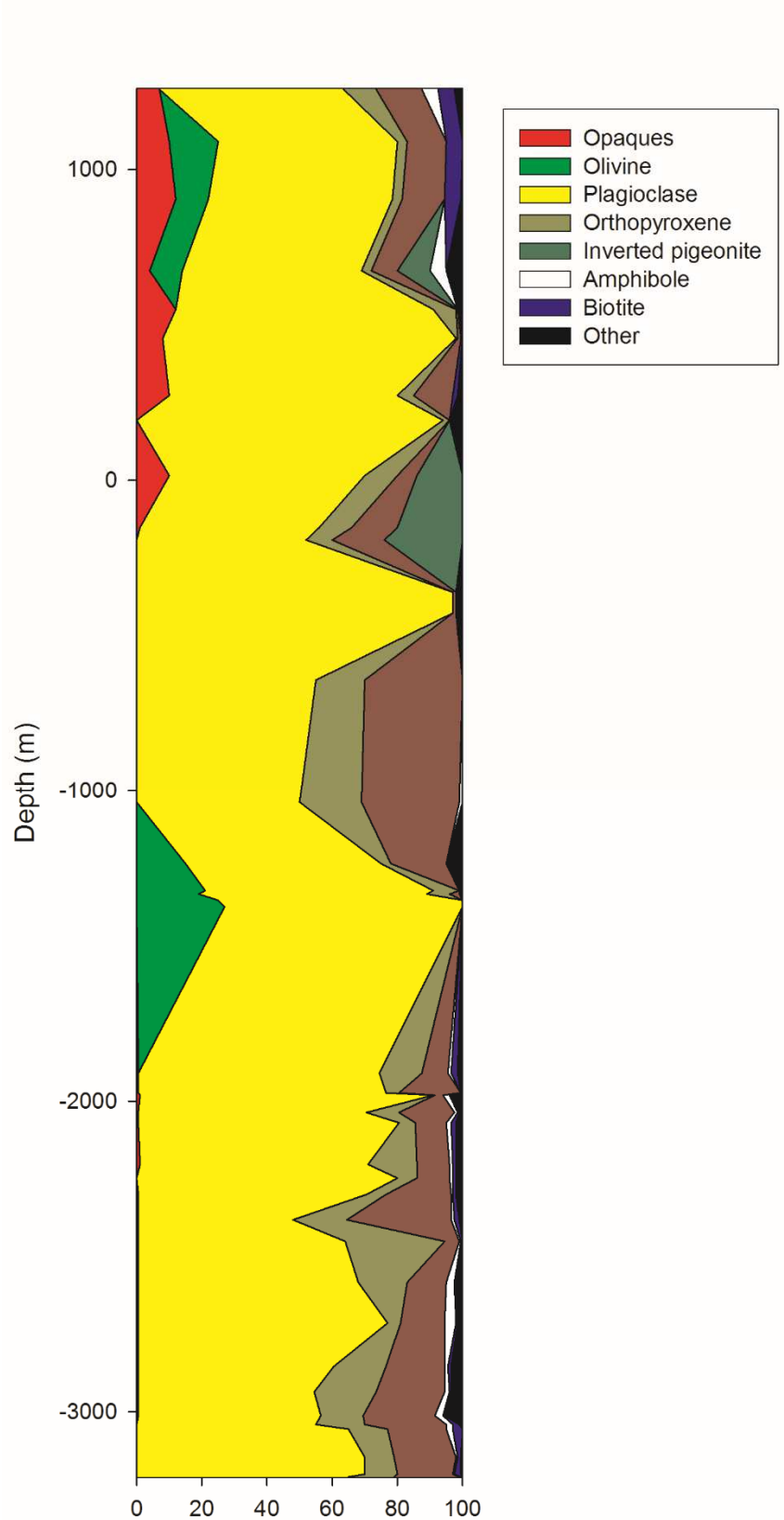

Figure 24: Depth vs. modal mineralogy graph. Plagioclase, ortho- and clinopyroxene are omnipresent phases in the studied stratigraphic profile, the mineral olivine occurs at certain stratigraphic intervals, opaque minerals are mostly encountered in the Upper Zone, whereas biotite and amphibole are inferior phases.

3.2 Major element mineral chemistry

Some of the samples that were investigated under transmitted light microscopy for petrographic features contained plagioclase that was either heavily or slightly altered. Plagioclase crystals that showed heavy alteration were totally ignored and underwent no analysis. Plagioclase crystals that did show some alteration under back scattered electron imagery (BSE) during electron microprobe work were analysed for major element chemistry with the analysis spots selected in such a way as to avoid the altered portions of the crystal. However, such plagioclase crystals were not analysed for *in-situ* trace element chemistry and for *in-situ* Sr isotopic determination. Only crystals that showed very little or no alteration during the initial microprobe work underwent all three sets of analysis (*in-situ* major element, trace element, and Sr isotopic determination). This was done in order to eliminate the possibility of alteration affecting the trace element data as well as the Sr isotopic data. Shown in Figure 25 are back scattered electron images (BSE) of plagioclase crystals that underwent all forms of analysis undertaken in this study (images A, C, and D), as well as crystals that were not further analysed as they either showed significant alteration (images E to H) or contained cracks (image B).

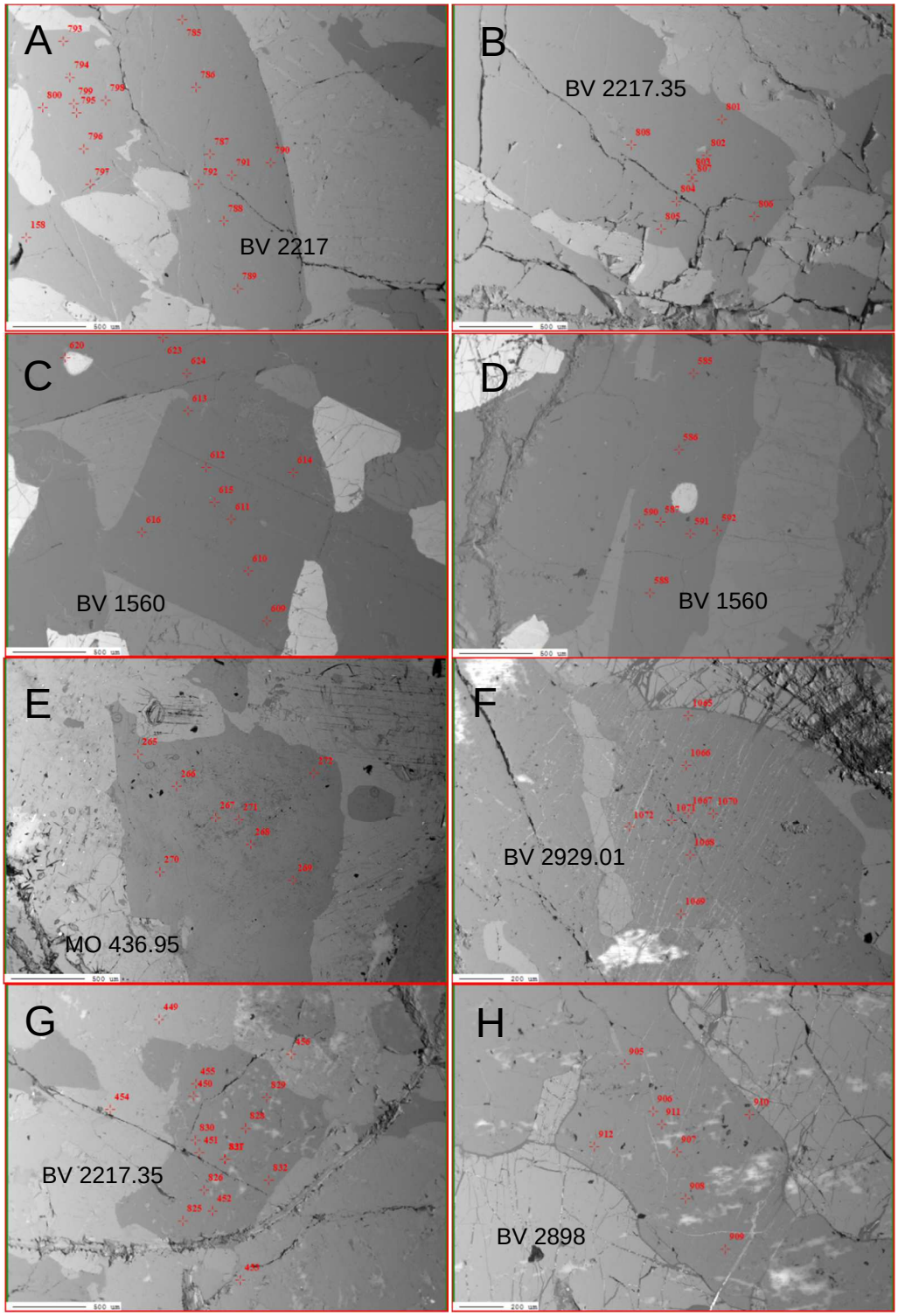

Figure 25: (A), (C) and (D) back scattered electron (BSE) images of unaltered plagioclase crystals that were analysed for *in-situ* major element chemistry, and further analysed for *in-situ* trace element chemistry and Sr isotopic ratios. (B) BSE image of a plagioclase grain that was not further analysed due to cracks. (E) to (H) back scattered electron (BSE) images of altered plagioclase crystals that were analysed for *in-situ* major element chemistry but not analysed for *in-situ* trace element and Sr isotopic ratios as they showed considerable alteration during the initial microprobe work. Samples names in black, red dots and numbers are microprobe spots.

The major element composition of selected unaltered and slightly altered plagioclase crystals is given in Appendix A. The anorthite content (An%) of plagioclase across the studied stratigraphic profile displays strong variation, with an average An% of 61.8 ± 9.5, varying between 41.4% and 77.1%. This variation is shown in Figure 26 where the An% is plotted against depth. The average An% of measured points in rocks of the Upper Zone is 50.9 ± 4.5, with a minimum and maximum An% of 41.4% and 58.6% respectively. The compositional data of these points are shown in Figure 27. Individual points in rocks of the Upper Main Zone have an average An% of 62 ± 9.9, varying between 50.4 and 77.1%, whereas individual points in rocks of the Lower Main Zone average an An% of 68.3% ± 3.9, varying between 60.5% and 75.9%. The compositional data of points analysed in rocks from both the Upper and Lower Main Zones are shown in Figures 28 and 29, respectively. The compositional data for all point analyses are shown in Figure 30.

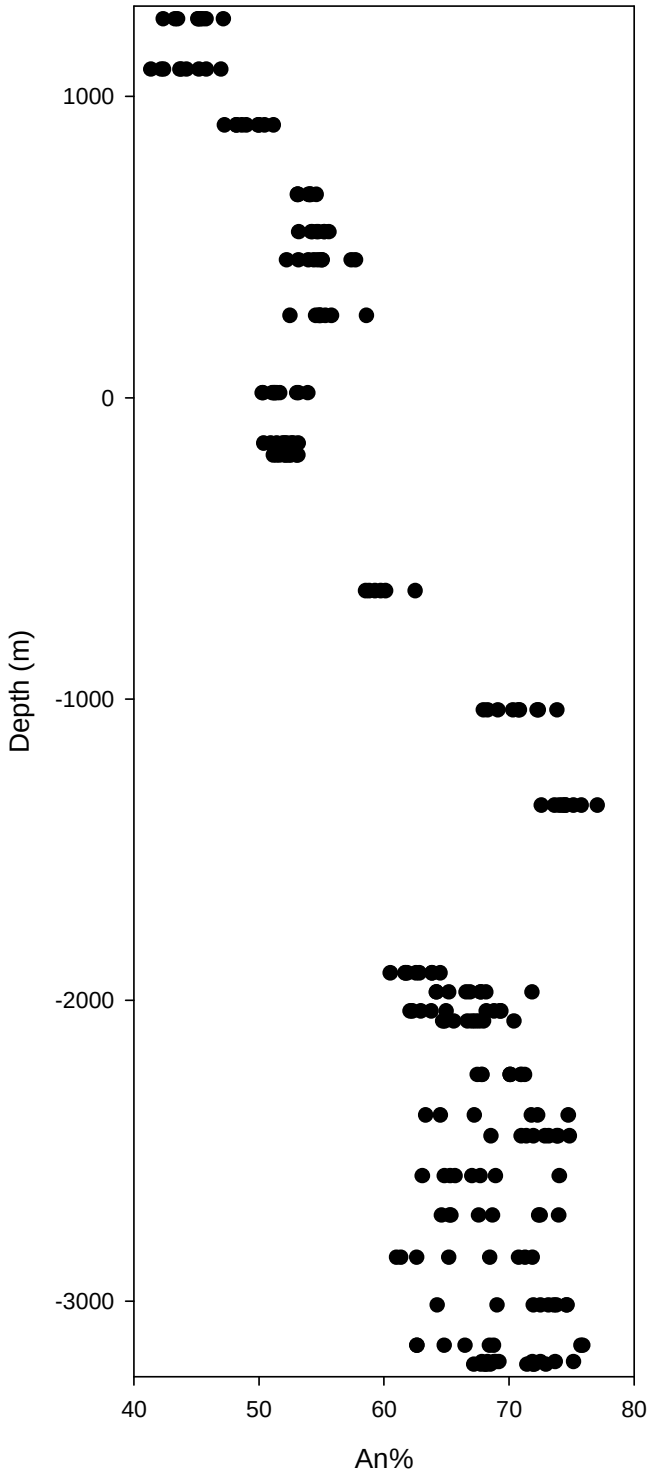

Figure 26: The anorthite content (An%) of plagioclase per analysed spot plotted against depth. Note how varied the An% is across the studied stratigraphic profile. A point of note also is the lack of differentiation in samples from the Lower Main Zone, with the differentiation becoming much more pronounced in samples from high stratigraphic intervals (Upper Main and Upper Zones).

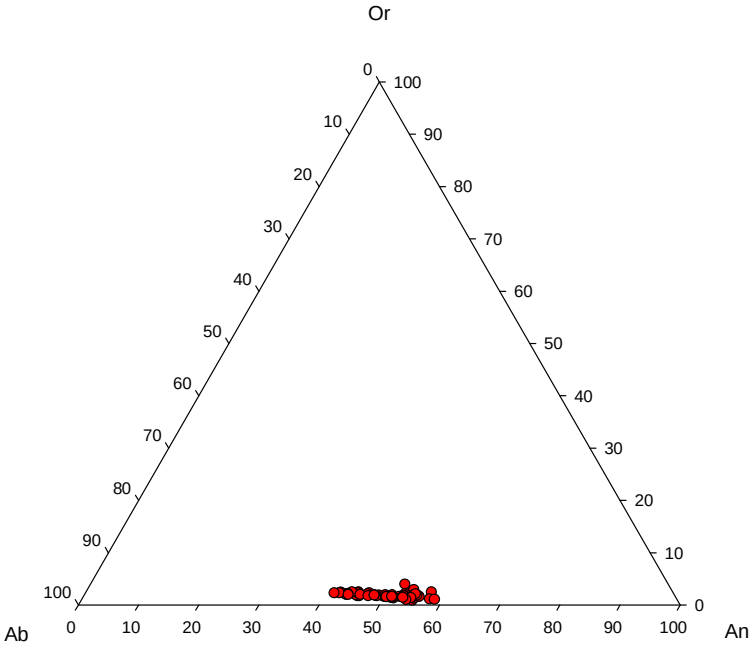

Figure 27: The compositional data of points analysed in rocks from the Upper Zone. Average An% is 50.9% ± 4.5, varying between 41.4% and 58.6%.

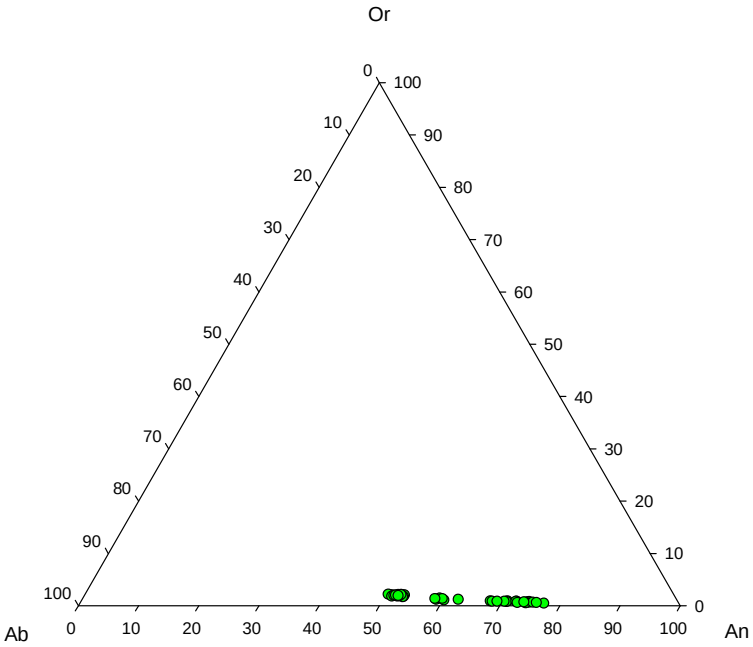

Figure 28: The compositional data of points in rocks from the Upper Main Zone. The average An% for these point analyses is 62% ± 9.9, with the minimum and maximum An% being 50.4% and 77.1% respectively.

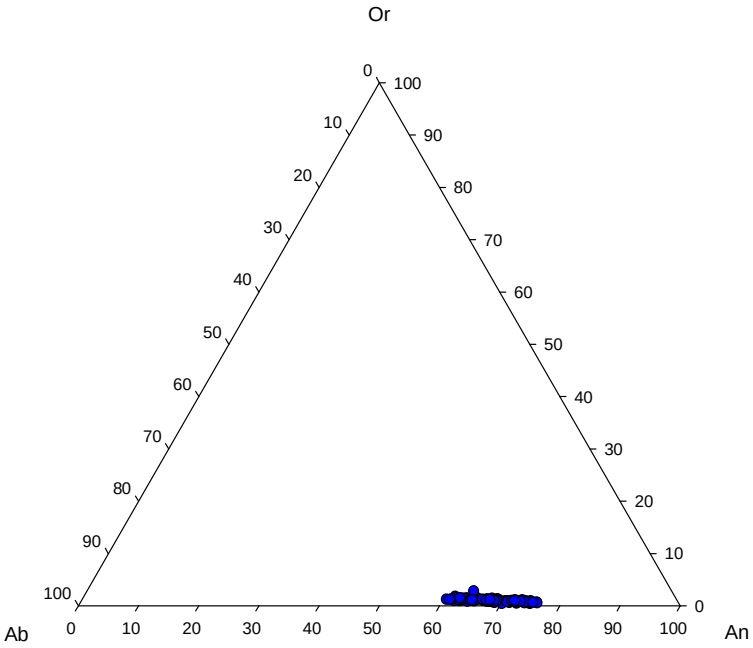

Figure 29: The composition of points analysed in rocks of the Lower Main Zone. Average An% is 68.3% ± 3.9, ranging between 60.5% and 75.9%.

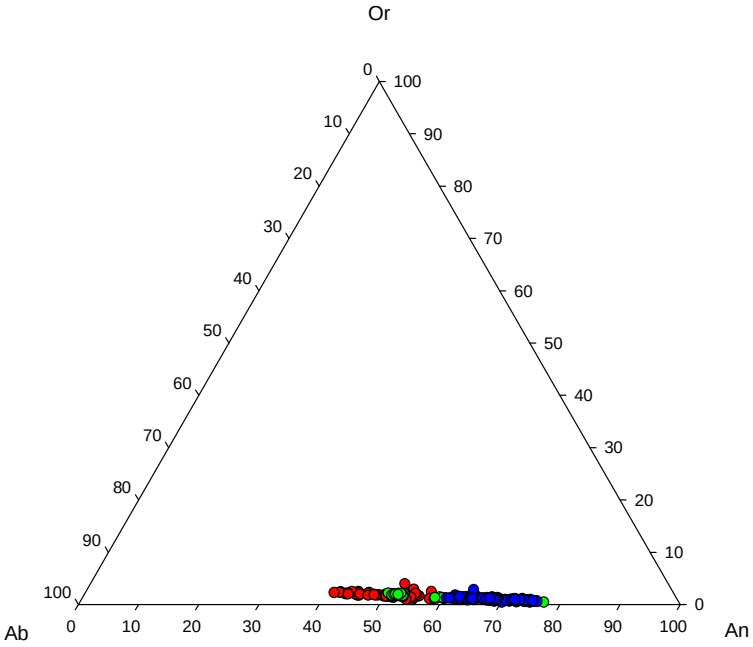

Figure 30: Compositional data of all 236 point analyses in 27 rock sample. The average An% for all point analyses is 61.8% ± 9.5, ranging between 41.4% and 77.1%.

In general, the anorthite content An% of plagioclase decreases from the bottom to the top of the studied stratigraphic profile. This decrease is from a value of 69.7% observed at the bottom of the profile, to a value of 44. 8% at the top of the profile (Figure 31). However, reversals in the An% are observed across the entire stratigraphy. The An% increases from a value of 69.7% at a depth of -3209 m to a value of 71.9% at depth -3012.7 m. From this depth, a decrease to a value of 66.6% is observed at depth -2853.7 m. From this depth, the An% increases again to a value of 72.4% at depth -2451.3 m, from where it once again decreases to a value of 63% at -1910.2 m. From this level, the An% increase again to a value of 74.6%, observed at depth -1353.2, a depth from which the An% decreases to a value of 51.2% at depth -152 m. The An% increases again to a value of 55.2%, only to decrease to a value of 44.8% observed at the top of the studied stratigraphic profile.

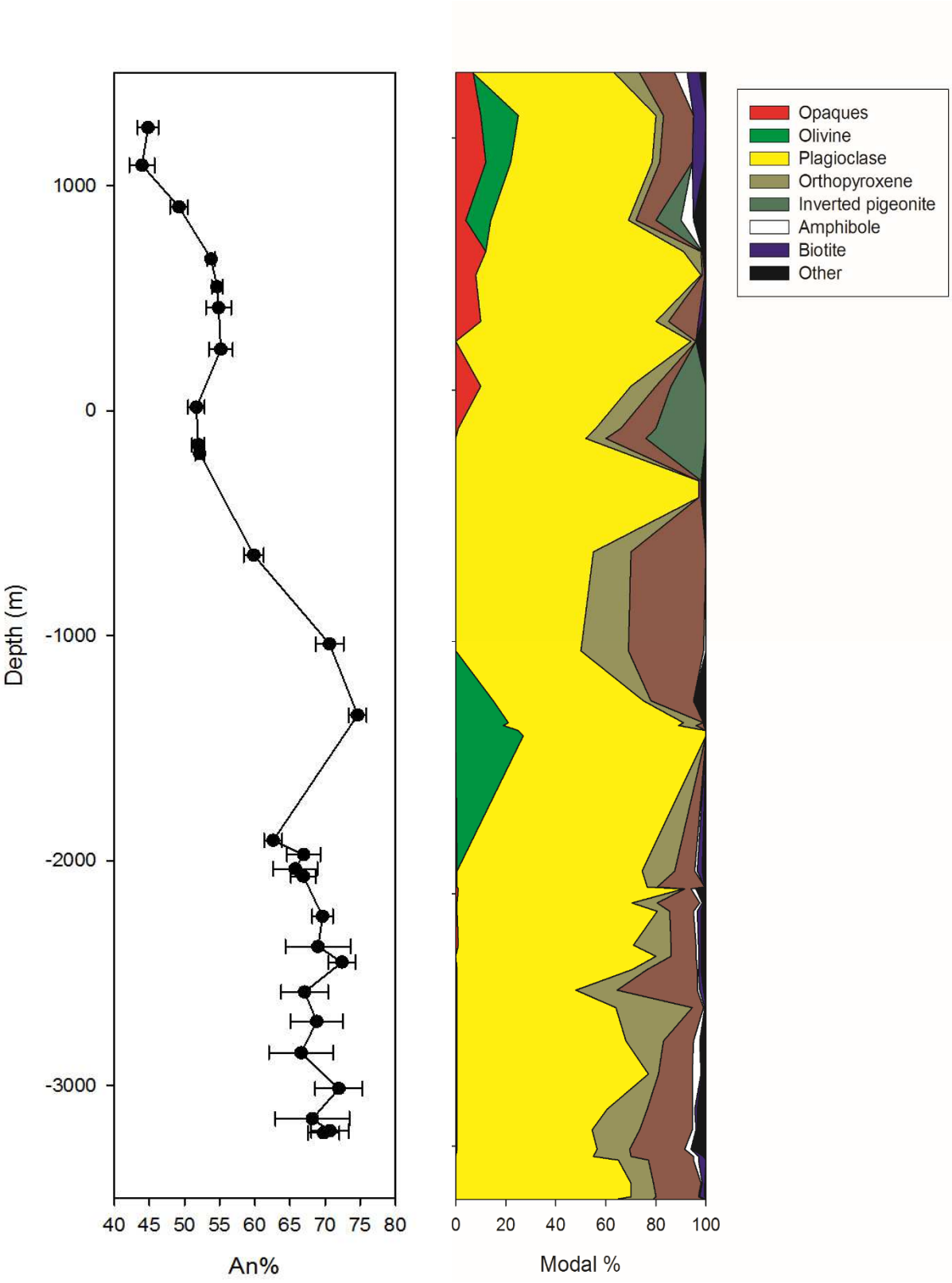

Figure 31: The average An% of samples vs. depth, with error bars representing the standard deviation (1-σ), coupled to changes in modal mineralogy across the studied stratigraphic profile.

3.3 Trace element data

The trace element composition of plagioclase is given in Appendix C. A total of 22 elements, including such elements as Sr, Ba, and Eu were analysed on ~ 235 spots across 26 samples. These trace elements display different stratigraphic trends, in that their concentration in plagioclase, the host mineral, changes differently along the studied stratigraphic profile.

Some of these elements have concentrations that increase linearly from the Lower Main Zone into the lower reaches of the Upper Zone, a point from where the concentration suddenly increases significantly towards the top of the Upper Zone. Some elements however, only increase linearly from the bottom towards the top of the studied profile, with no abrupt significant increase observed in their concentration.

Pb, Sr, Ba, and Eu are the four elements whose concentrations increase sharply in the upper reaches of the Upper Zone. Table 3 below shows how the concentration of each of these elements changes from the Lower Main Zone, through the Upper Main Zone, towards the top of the Upper Zone. Examples of elements whose concentration only linearly changes across the profile are the elements Rb and Gd.

Moreover, the concentration of some elements, like Y, Ho, and U displays no clear pattern across the profile, increasing and decreasing repeatedly from the Lower Main Zone into the Upper Zone, whereas, on the other hand, the concentration of others, like Zr, La, and Th does not vary much throughout the entire stratigraphic profile. All these different stratigraphic trends are illustrated in Figure 32.

Table 3: Table showing how the concentration (in ppm) of the elements Pb, Sr, Ba, and Eu, elements whose concentration increases exponentially in the upper reaches of the Upper Zone, changes from the Lower Main Zone, through the Upper Main, into the Upper Zone. Avg= Average; Std.dev= Standard deviation (1-σ); Min= Minimum; Max= Maximum.

		Pb	Sr	Ba	Eu
Upper Zone					
	Avg	3.7	442.2	175.1	1.0
	Std.dev	2.6	51.8	76.4	0.6
	Min	0.8	367.5	77.5	0.2
	Max	10.7	584.2	396.0	2.2
Upper Main Zone					
	Avg	1.3	350.6	91.7	0.4
	Std.dev	0.3	55.9	29.8	0.1
	Min	0.8	270.1	46.7	0.2
	Max	2.0	433.2	141.6	0.7
Lower Main Zone					
	Avg	3.3	401.4	143.1	0.8
	Std.dev	3.1	232.7	124.8	0.9
	Min	1.2	258.6	49.8	0.3
	Max	15.5	1080.3	532.8	4.3

Another striking feature is that the third lowermost sample and the lowermost sample in the studied stratigraphic profile, samples MO 1283 from a depth of -3146.70 m and MO 1346 from depth -3209.7 m respectively, both contain points that are considerably enriched in all measured trace elements.

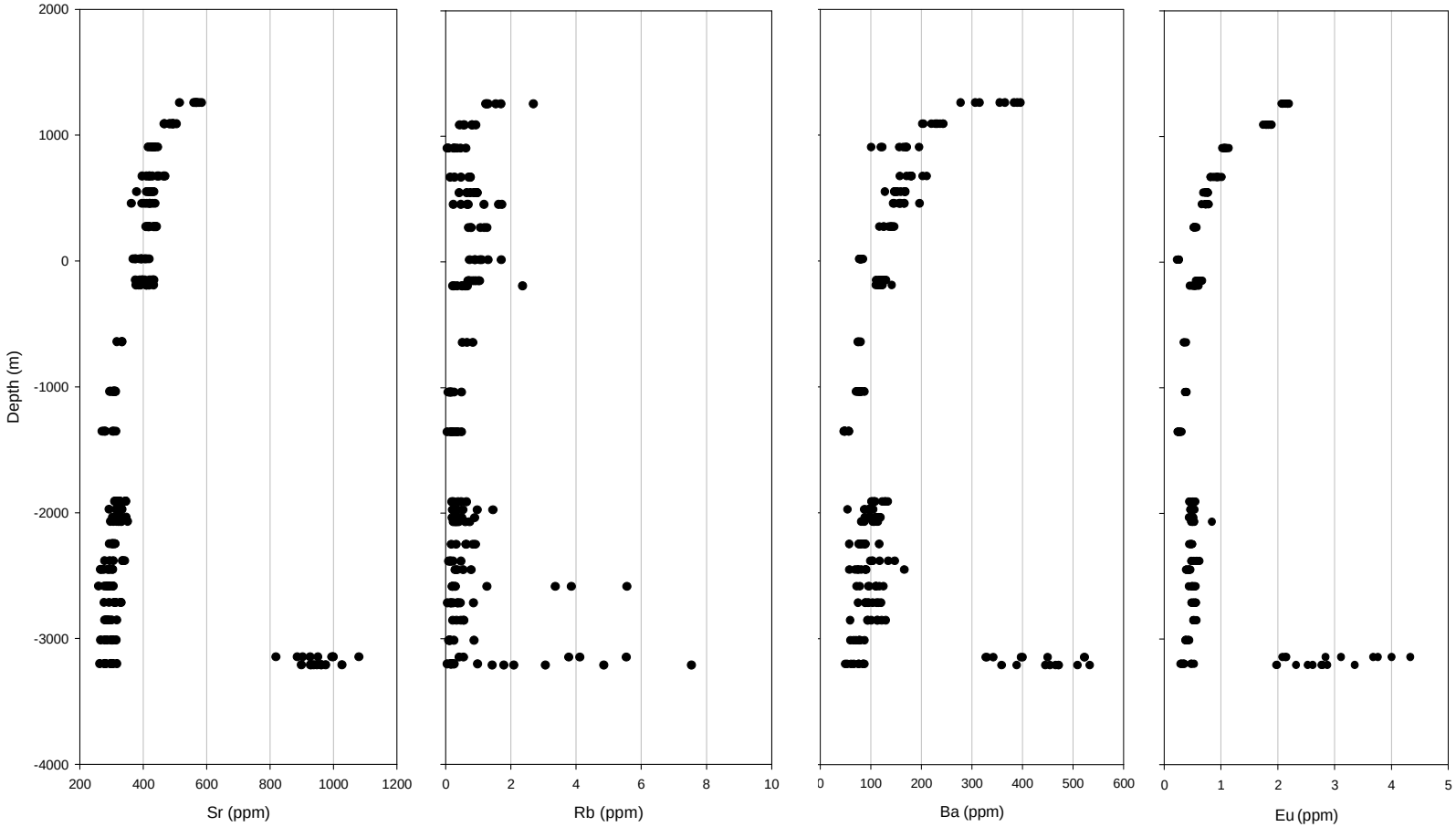

Figure 32: Trace element composition of individual spots plotted against depth.

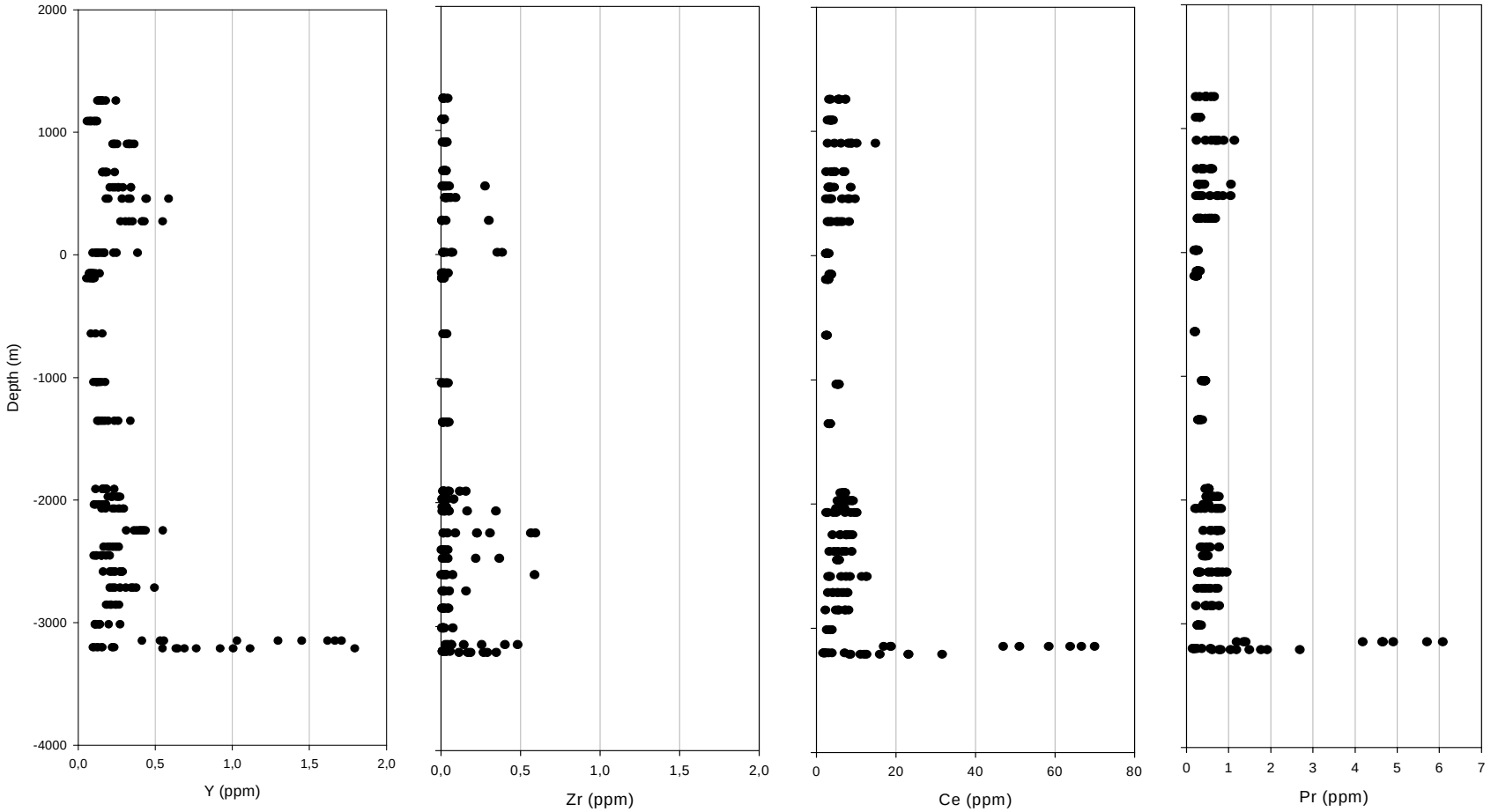

Figure 32 (continued)

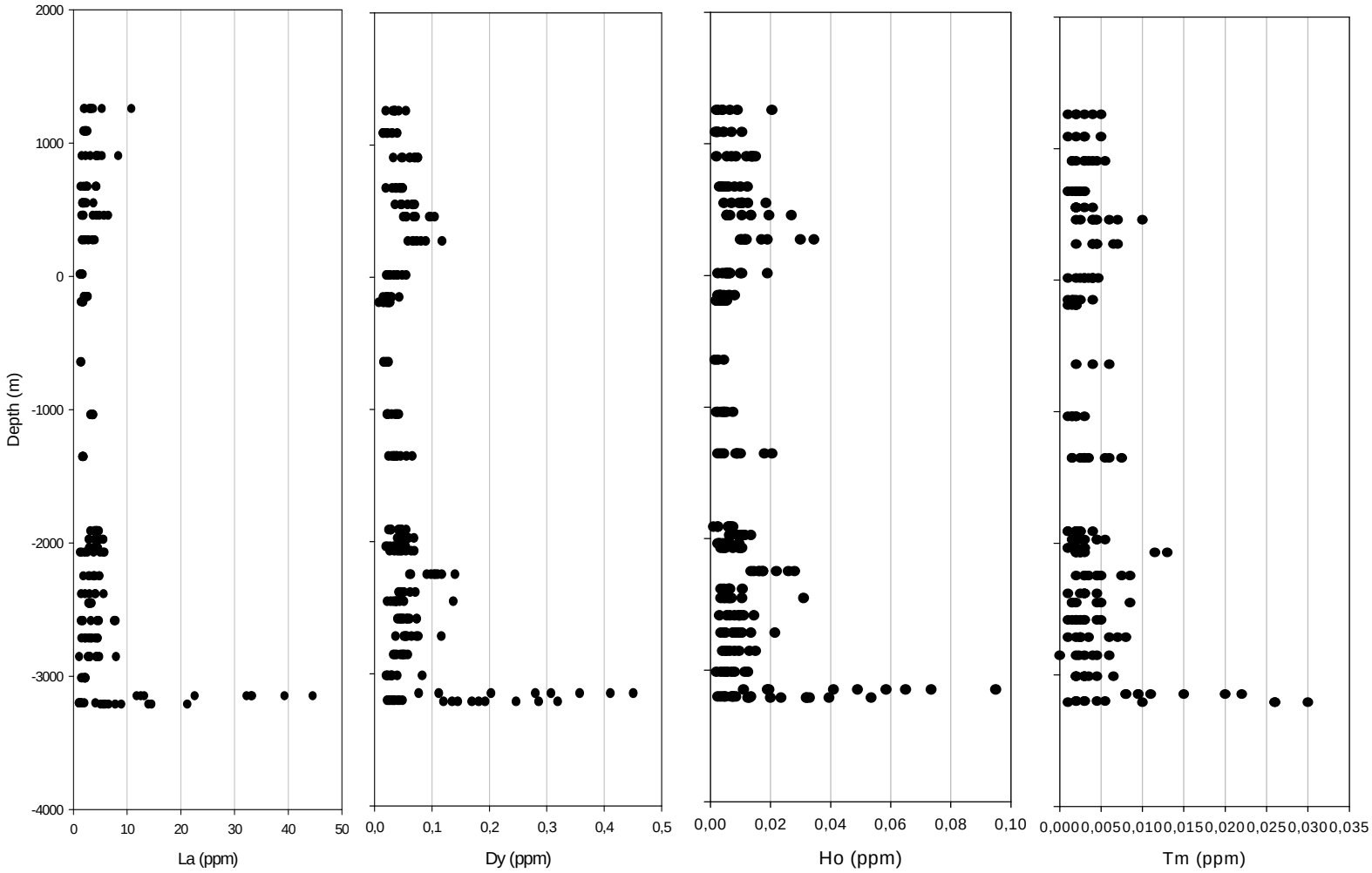

Figure 32 (continued)

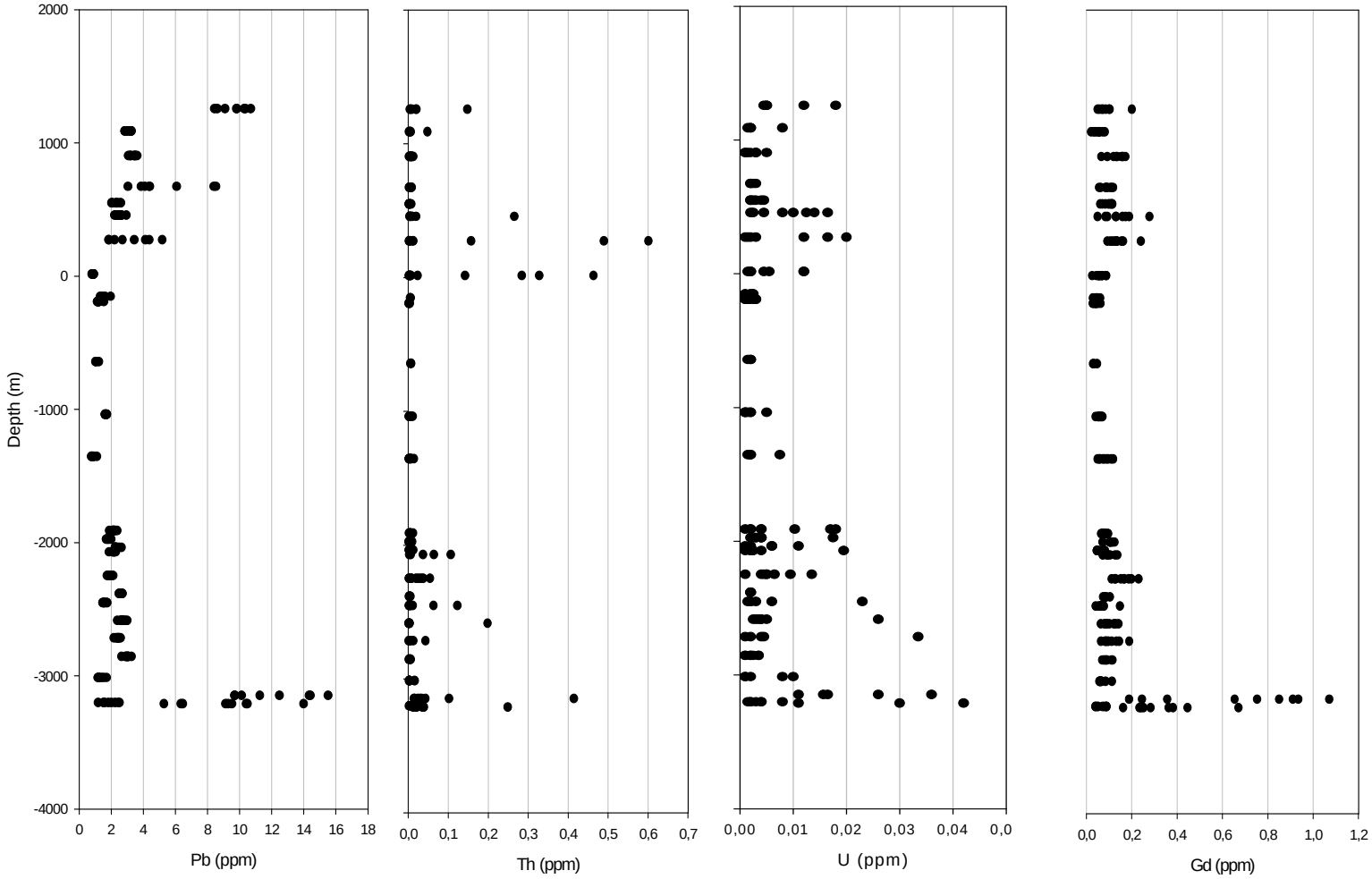

Figure 32 (continued)

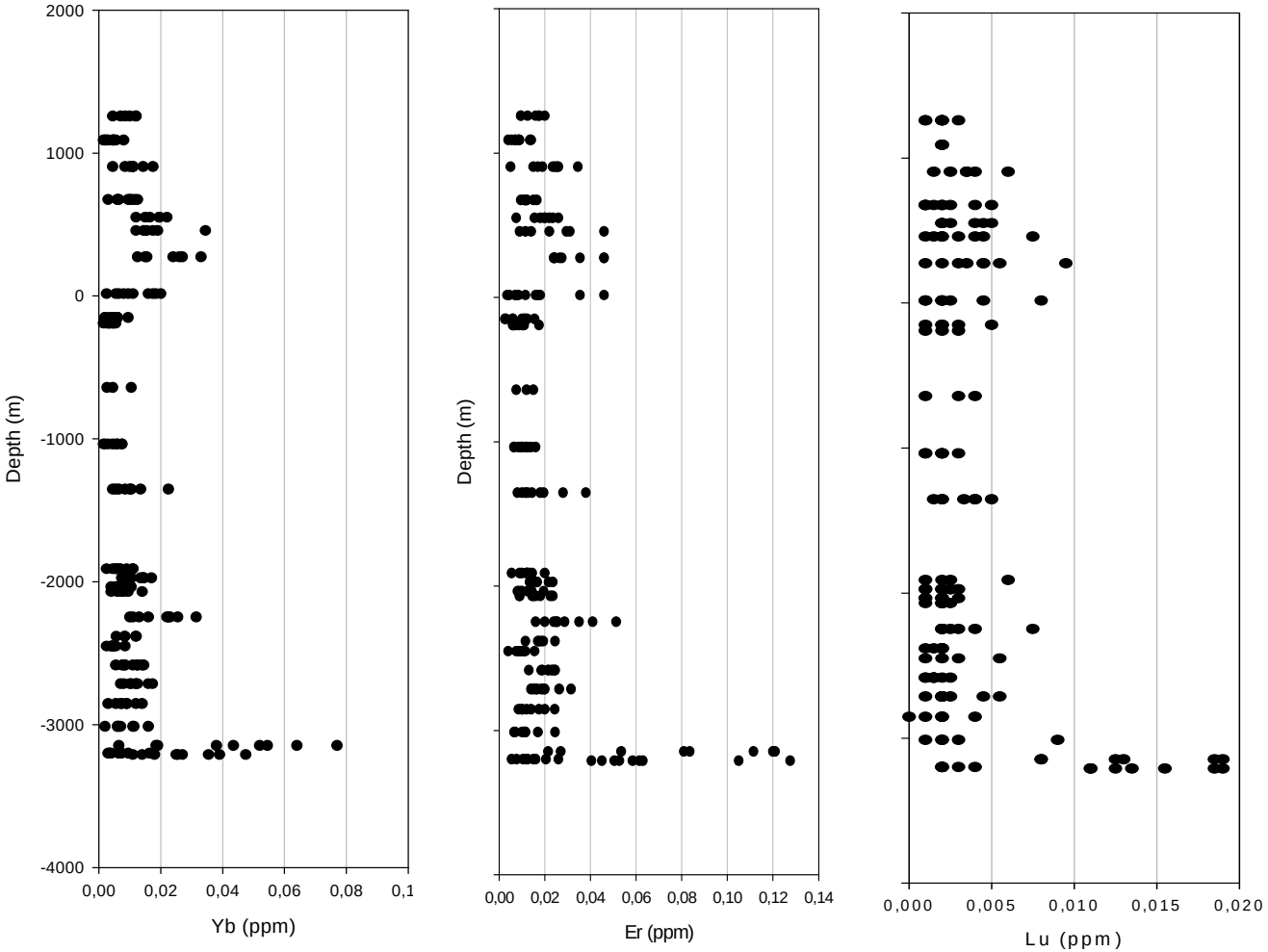

Figure 32 (continued)

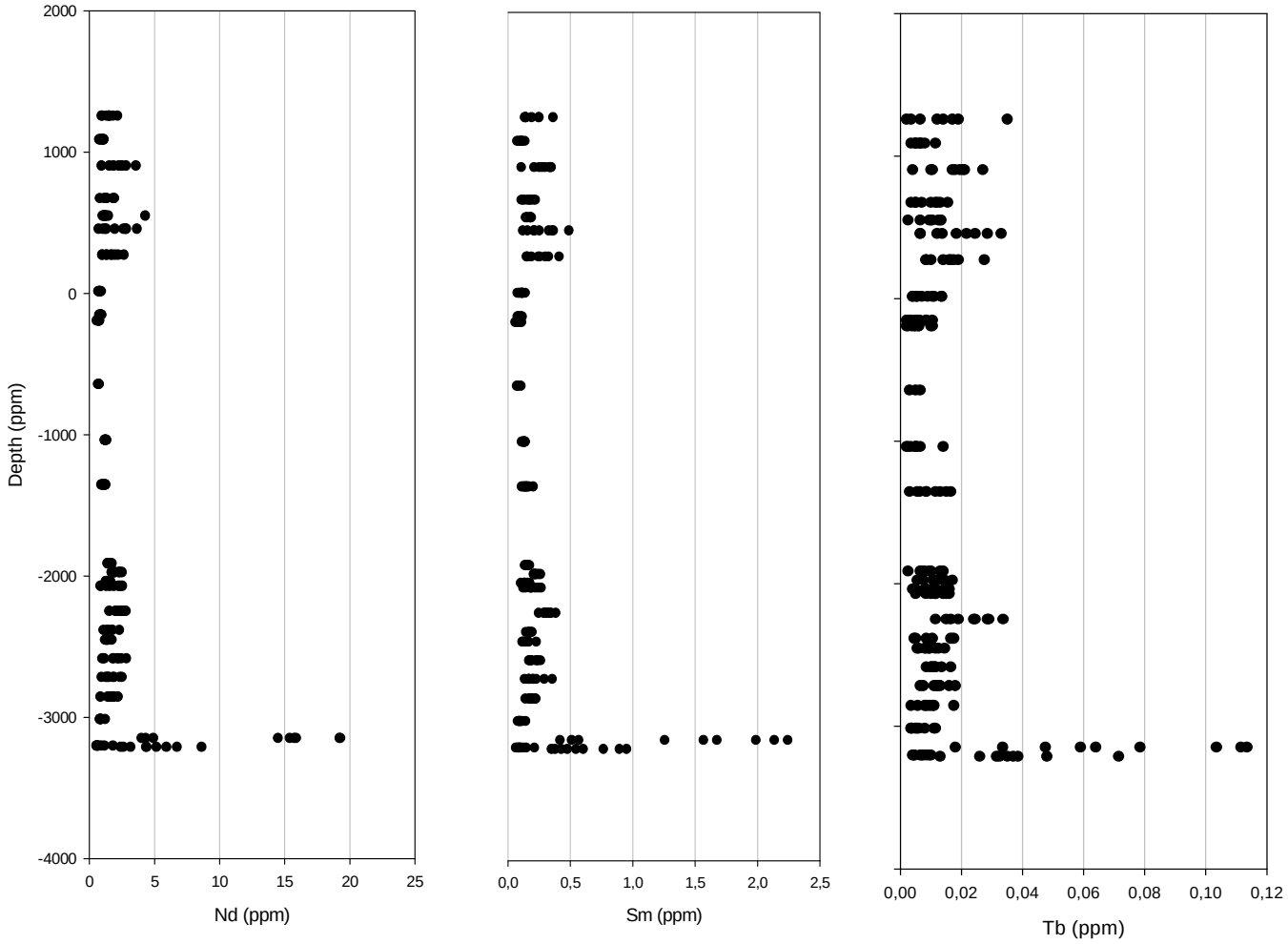

Figure 32 (continued)

3.4 Isotopic data

The Sr isotopic data of plagioclase are given in Appendix B. Across the studied stratigraphic interval, the initial $^{87}Sr/^{86}Sr$ data of plagioclase, recalculated to 2054.4 Ma, is very variable. This variability is depicted in Figure 33, where the initial $^{87}Sr/^{86}Sr$ composition of individual spot analyses is plotted against depth. Samples from the Lower Main Zone are the most varied, with an average initial $^{87}Sr/^{86}Sr$ value of plagioclase being 0.7088, ranging from 0.7075 to 0.7106. Coexisting plagioclase in rocks from the Upper Main Zone shows little variation in initial $^{87}Sr/^{86}Sr$ ratios, with an average value of 0.7078, the minimum and maximum values being 0.7069 and 0.7087 respectively. Upper Zone rocks show very little variation or near constant initial $^{87}Sr/^{86}Sr$ composition of plagioclase, with a minimum and maximum initial $^{87}Sr/^{86}Sr$ value of 0.7063 and 0.7079, respectively. The average initial $^{87}Sr/^{86}Sr$ value for these samples is 0.7072.

A larger variation in initial $^{87}Sr/^{86}Sr$ composition of plagioclase is observed in rocks from the Lower Main Zone, and the occurrence of initial $^{87}Sr/^{86}Sr$ variation between coexisting plagioclase (inter-granular variation) and within individual plagioclase (intra-granular variation) is also widespread in rocks from this interval. To exemplify, a total of six samples from the Lower Main Zone exhibit inter and intra-crystal $^{87}Sr/^{87}Sr$ variation, whereas only a single observed sample from both the Upper and Upper Main Zones exhibit the same variation. In addition, larger ranges of initial $^{87}Sr/^{86}Sr$ are observed both between coexisting plagioclase and within individual plagioclase in samples from the Lower Main Zone than in samples from the other two intervals.

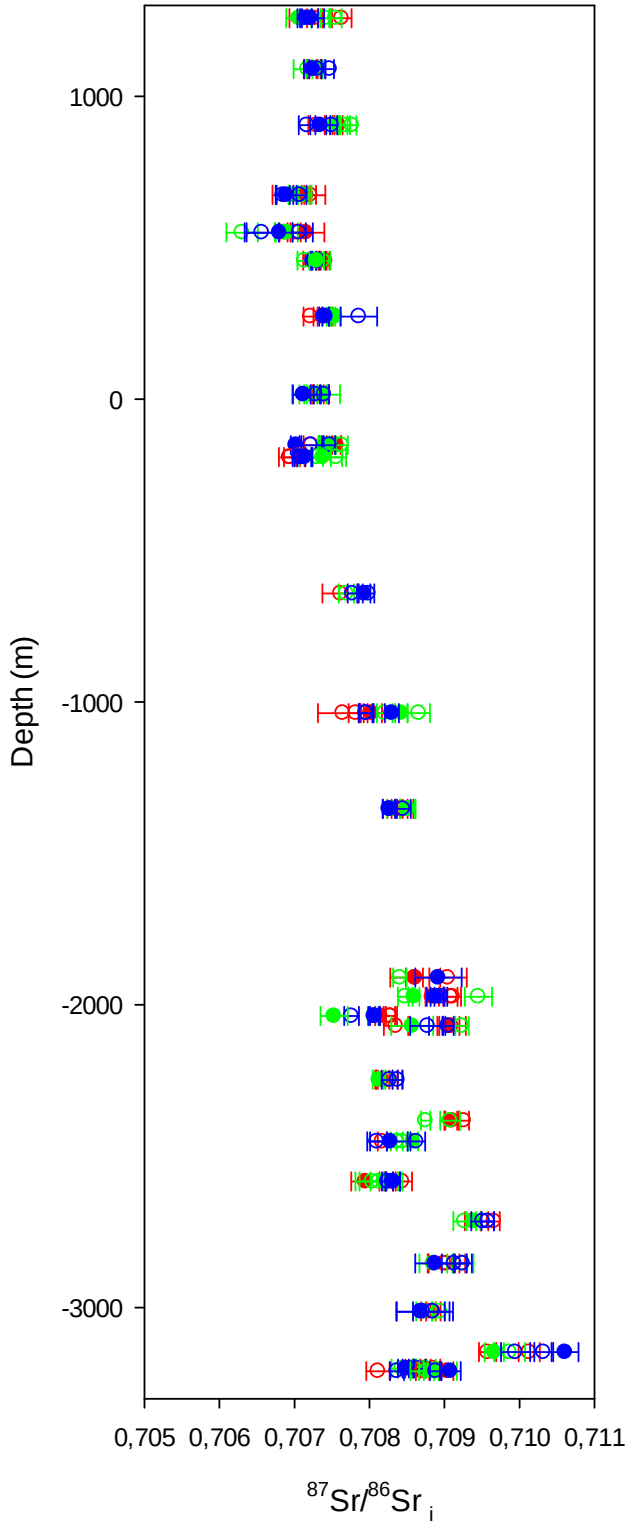

Figure 33: The initial $^{87}Sr/^{86}Sr$ composition of analysed spots plotted against depth. Different colours denote coexisting plagioclase in a single sample. Solid circles represent analysed core domains, whereas open circles represent rims. Error bars indicate 2SE.

Moreover, the variation observed occurs in different forms in different samples. For instance, in some samples, isotopically homogenous plagioclase (plagioclase that does not show isotopic disequilibrium) coexists with isotopically heterogeneous plagioclase in which the core is more radiogenic than the rims, e.g. plagioclase 3 in sample BV 1283.79 at a depth of 273 m; plagioclase 1 from sample MO 1283 at depth -3146.7 m; and plagioclase 3 and 4 in sample MO 1346 from a depth of -3209.7 m. In other samples, homogenous plagioclase coexists with heterogeneous plagioclase in which the rims are more radiogenic than the core, e.g. plagioclase 4 in sample MO 172.91 at a depth of -2036.6 m, as well as in sample MO 206.11 from depth -2069.8 m plagioclase 1.

In other samples however, homogenous plagioclase coexists with heterogeneous plagioclase in which the initial $^{87}Sr/^{86}Sr$ ratio of the heterogeneous plagioclase is the same for one rim domain and the core domain, then it either decreases or increases in the other rim domain. Examples of such samples are plagioclase 6 in sample BV 1025.54 from a depth of 550.3 m; plagioclase 2 in sample BV 1302.79 from depth 273 m; and in plagioclase 7 from sample MO 172.91 at depth -2036.6 m.

In some samples, the initial $^{87}Sr/^{86}Sr$ of the heterogeneous plagioclase increases or decreases from the one rim domain, through the core, to the other rim domain. An example of this form of heterogeneity is plagioclase 4 from sample MO 109.95. The sample is from a depth of -1973.3 m. Table 4 is an illustration of all these different forms of heterogeneity.

Table 4: Samples exhibiting inter and intra-crystal $^{87}Sr/^{86}Sr$ variation.

Depth	Sample	Plg #	Spot	Position	87Sr/86Sr	2SE	Zoned/Unzoned
550.3	BV 1025.54	5	442	RIM	0.7069	7.05E-05	Unzoned
550.3		5	443	CORE	0.7072	2.48E-04	
550.3		5	445	RIM	0.7070	5.67E-05	
550.3		6	449	RIM	0.7069	1.16E-04	Zoned
550.3		6	451	CORE	0.7069	1.47E-04	
550.3		6	453	RIM	0.7063	2.09E-04	
550.3		2	457	RIM	0.7071	8.81E-05	Unzoned
550.3		2	459	CORE	0.7068	4.41E-04	
550.3		2	461	RIM	0.7066	2.26E-04	
273.0	BV 1302.79	3	517	RIM	0.7072	9.22E-05	Zoned
273.0		3	519	CORE	0.7074	1.24E-04	
273.0		5	529	RIM	0.7074	7.22E-05	Unzoned
273.0		5	531	CORE	0.7075	6.78E-05	
273.0		5	533	RIM	0.7075	5.54E-05	
273.0		2	537	RIM	0.7074	6.20E-05	Zoned
273.0		2	541	RIM	0.7079	2.42E-04	
273.0		2	549	CORE	0.7074	4.52E-05	
-1910.2	MO 46.5	5	9	RIM	0.7086	1.14E-04	Unzoned
-1910.2		5	11	CORE	0.7086	3.33E-04	
-1910.2		5	13	RIM	0.7090	2.51E-04	
-1910.2		2	29	RIM	0.7084	8.99E-05	
-1910.2		1	35	CORE	0.7089	3.09E-04	
-1973.3	MO 109.95	3	65	RIM	0.7091	1.09E-04	Unzoned
-1973.3		3	67	CORE	0.7088	8.79E-05	
-1973.3		3	69	RIM	0.7091	9.42E-05	
-1973.3		4	74	RIM	0.7085	9.63E-05	Zoned
-1973.3		4	77	RIM	0.7095	1.82E-04	
-1973.3		4	79	CORE	0.7086	7.27E-05	
-1973.3		2	81	RIM	0.7090	8.54E-05	Unzoned
-1973.3		2	83	CORE	0.7089	1.12E-04	
-1973.3		2	85	RIM	0.7089	8.69E-05	
-2036.6	MO 172.91	8	129	RIM	0.7083	6.38E-05	Unzoned
-2036.6		8	133	RIM	0.7083	9.00E-05	
-2036.6		8	135	CORE	0.7081	7.13E-05	
-2036.6		4	137	RIM	0.7081	6.26E-05	Zoned
-2036.6		4	139	CORE	0.7075	1.82E-04	
-2036.6		7	145	RIM	0.7081	8.04E-05	Zoned
-2036.6		7	149	RIM	0.7078	9.71E-05	
-2036.6		7	151	CORE	0.7081	5.97E-05	
-2069.8	MO 206.11	7	169	RIM	0.7091	1.90E-04	Zoned
-2069.8		7	173	RIM	0.7084	1.61E-04	

Depth	Sample	Plg #	Spot	Position	87Sr/86Sr	2SE	Zoned/Unzoned
-2069.8		1	179	CORE	0.7086	2.78E-04	Zoned
-2069.8		1	181	RIM	0.7092	8.92E-05	
-2069.8		2	185	RIM	0.7088	2.35E-04	Unzoned
-2069.8		2	189	RIM	0.7090	7.45E-05	
-2069.8		2	191	CORE	0.7089	9.20E-05	
-2382.1	MO 518.4	1	290	RIM	0.7091	8.06E-05	Unzoned
-2382.1		1	291	CORE	0.7091	9.94E-05	
-2382.1		1	293	RIM	0.7093	6.69E-05	
-2382.1		4	313	RIM	0.7087	6.23E-05	Zoned
-2382.1		4	316	RIM	0.7091	1.32E-04	
-3146.7	MO 1283	5	1017	RIM	0.7096	1.16E-04	Zoned
-3146.7		5	1020	RIM	0.7101	1.41E-04	
-3146.7		2	1025	RIM	0.7099	2.06E-04	Unzoned
-3146.7		2	1027	CORE	0.7097	1.27E-04	
-3146.7		1	1033	RIM	0.7103	1.26E-04	Zoned
-3146.7		1	1035	CORE	0.7106	1.79E-04	
-3146.7		1	1037	RIM	0.7099	1.95E-04	
-3209.7	MO1346	4	978	RIM	0.7087	8.93E-05	Zoned
-3209.7		4	980	CORE	0.7090	8.28E-05	
-3209.7		4	981	RIM	0.7081	1.55E-04	
-3209.7		1	985	RIM	0.7088	1.01E-04	Unzoned
-3209.7		1	988	RIM	0.7089	3.10E-04	
-3209.7		1	991	CORE	0.7088	9.77E-05	
-3209.7		3	1001	RIM	0.7089	7.75E-05	Zoned
-3209.7		3	1003	CORE	0.7091	1.38E-04	
-3209.7		3	1005	RIM	0.7084	9.33E-05	

Figure 34 below is a graphic representation of inter and intra-crystal $^{87}Sr/^{86}Sr$ variation of plagioclase that is documented in Table 4 above. In Figure 34, the initial $^{87}Sr/^{86}Sr$ ratios of the different plagioclase crystals coexisting in a single sample is plotted relative to a Bushveld aged reference isochron. Figure 35 on page 72 shows reflected light photomicrographs of the samples in Table 3. The initial $^{87}Sr/^{86}Sr$ ratios (in red colour) together with the An% (in black colour) are placed next to the corresponding ablation hole.

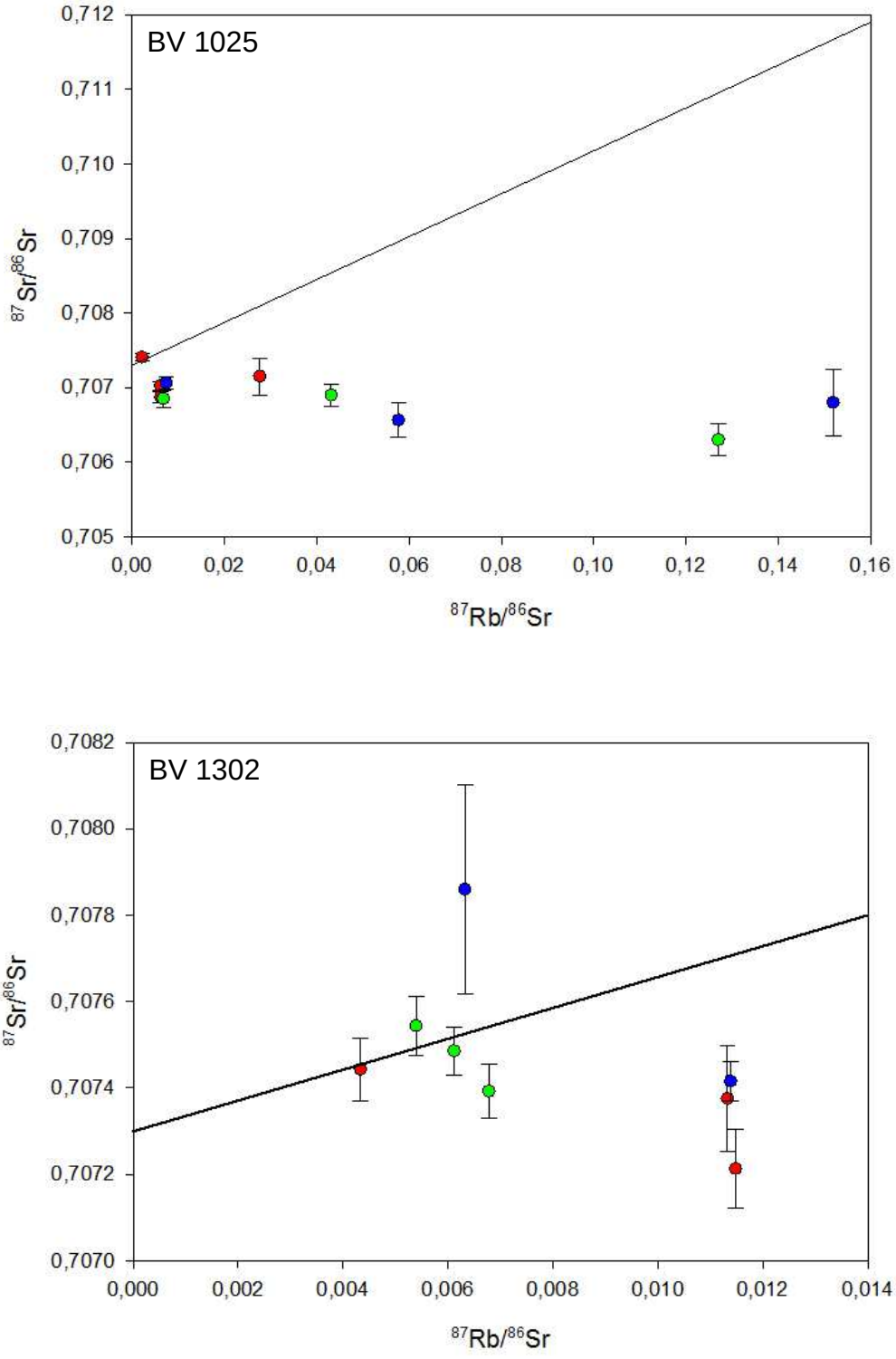

Figure 34: Rb-Sr isochron diagram showing the distribution of *in-situ* analyses in coexisting plagioclase relative to a Bushveld aged (ca. 2054.4 Ma) reference isochron. Plagioclase crystals are from sampe BV 1025 and BV 1302 from the Bellevue core.

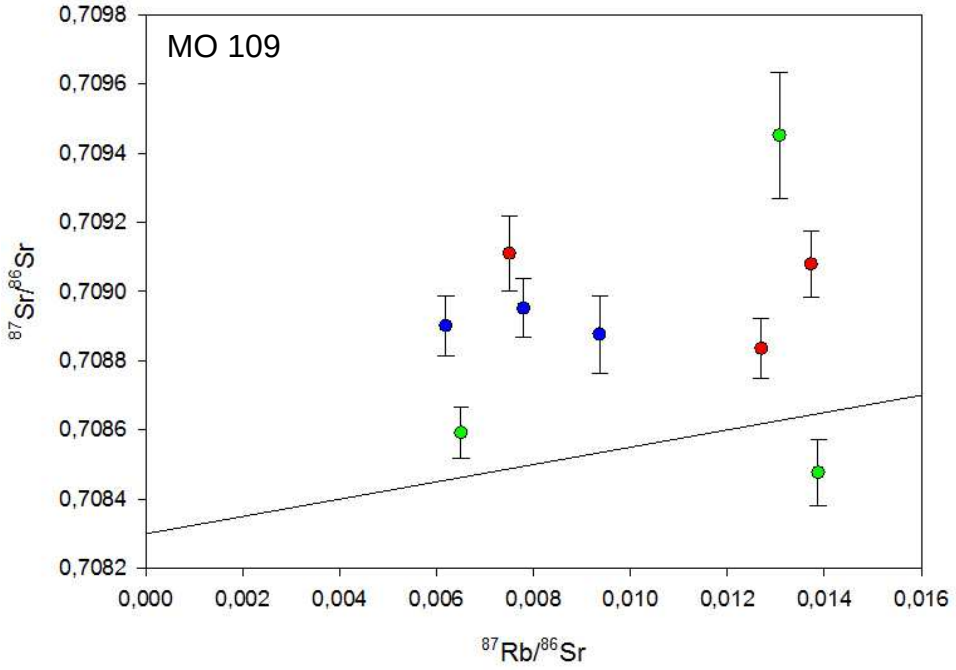

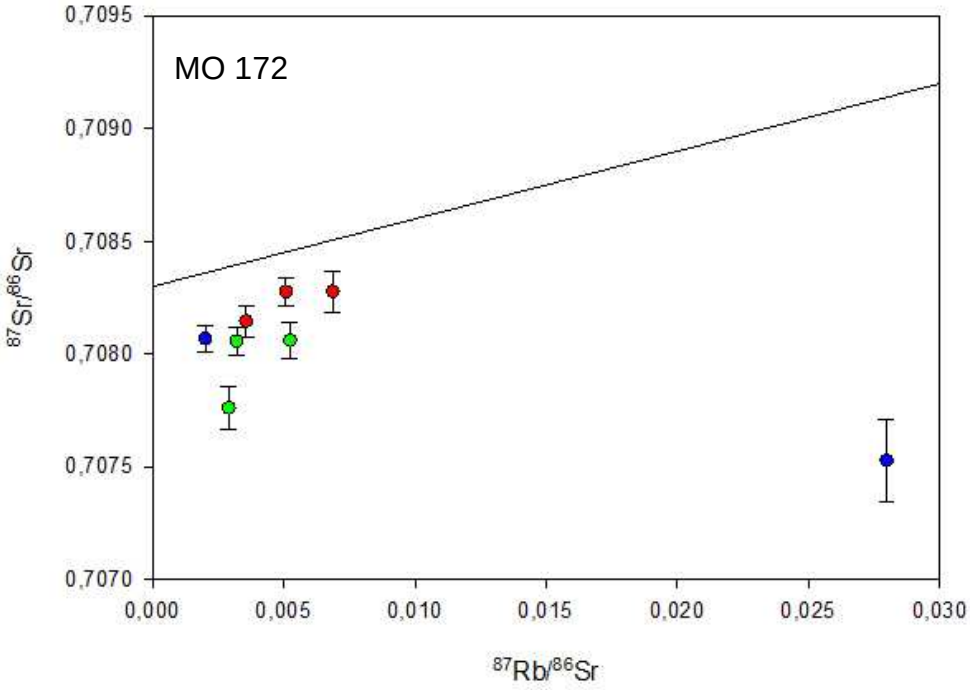

Figure 34: continued with sample MO109 and MO172 from the Moordkopje core.

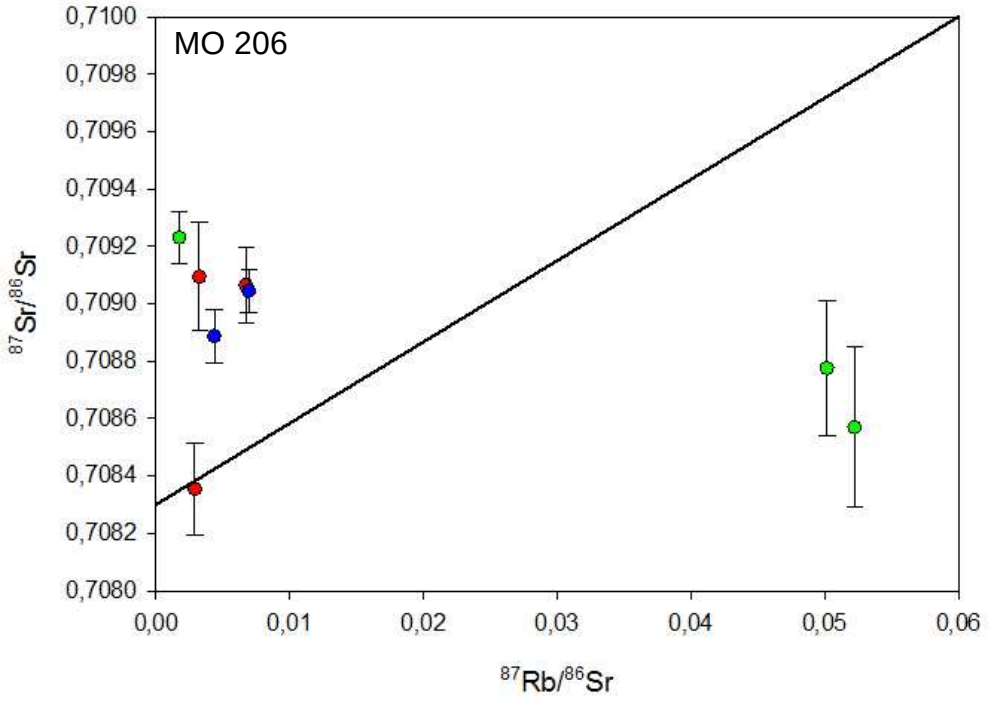

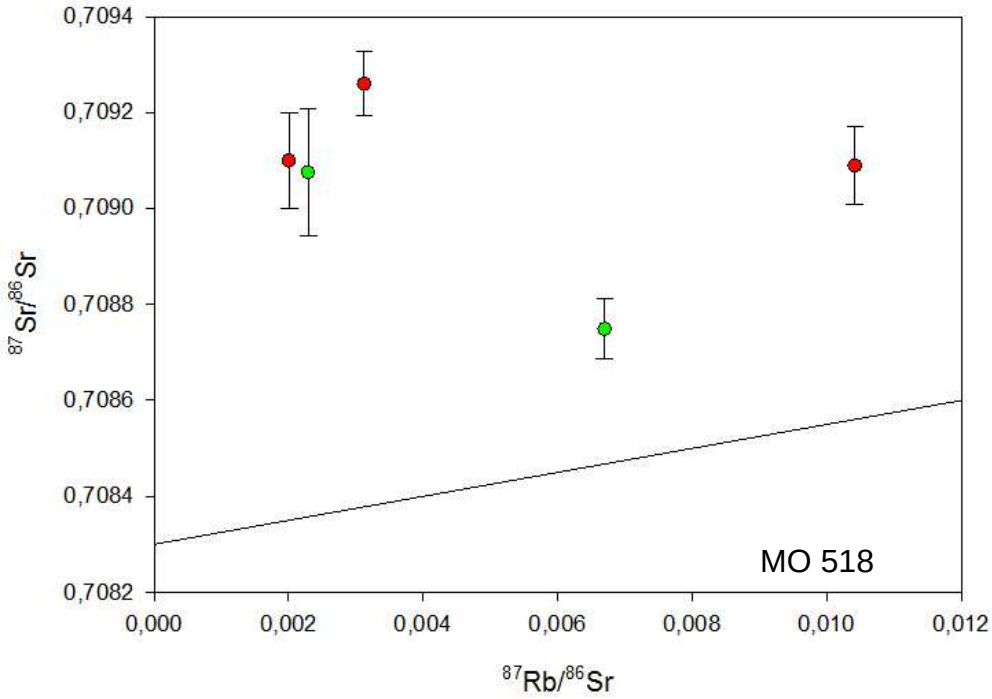

Figure 34: continued with sample MO 206 and MO 518 from the Moordkopje core.

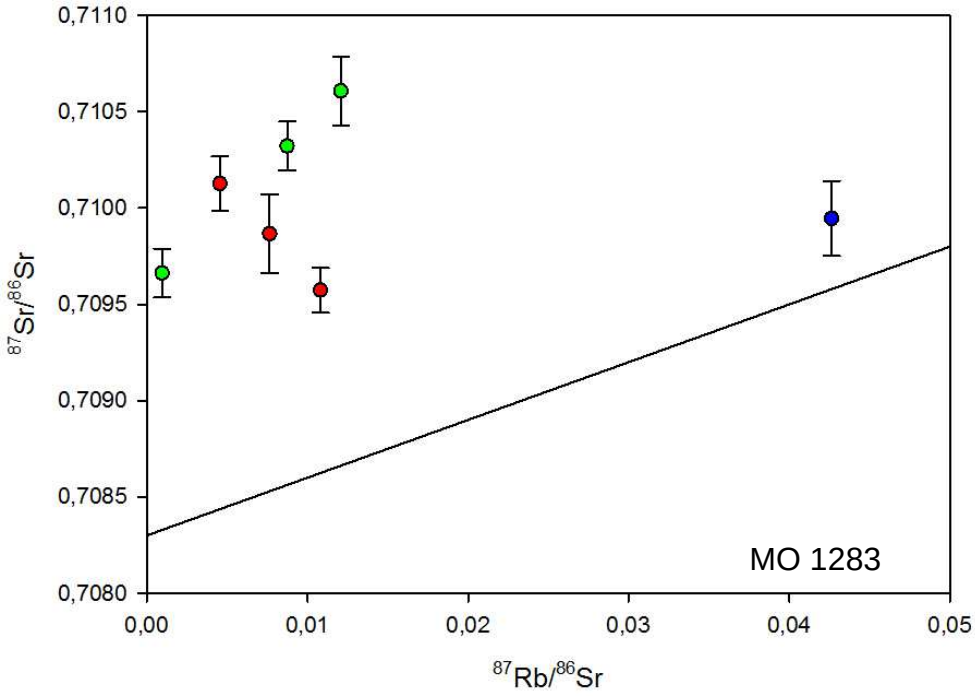

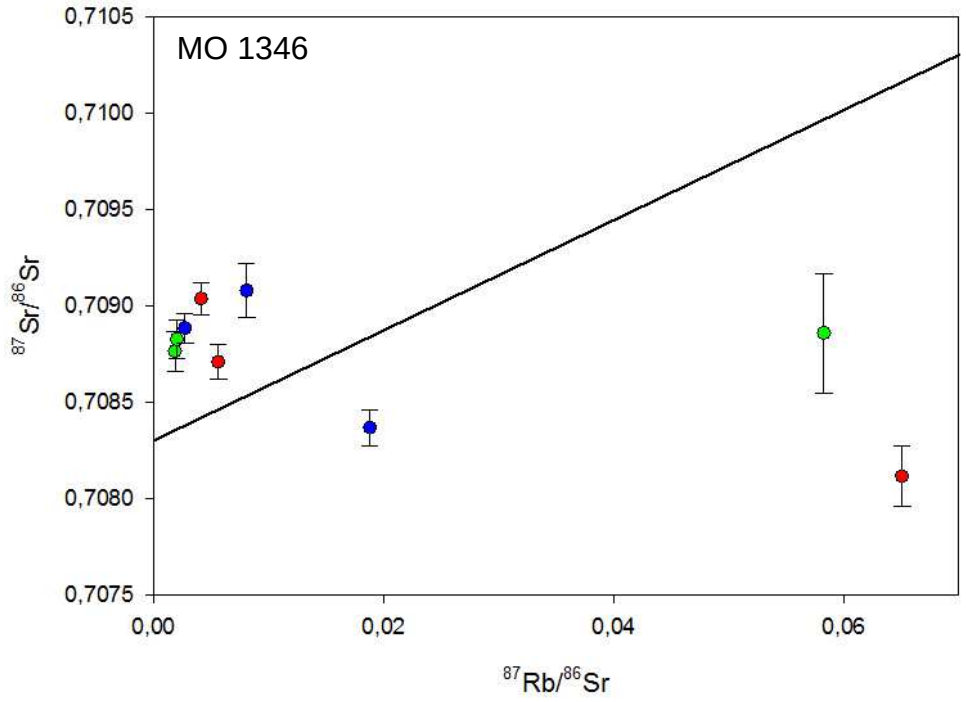

Figure 34: continued with sample MO 1283 and MO 1346 from the Moordkopje core.

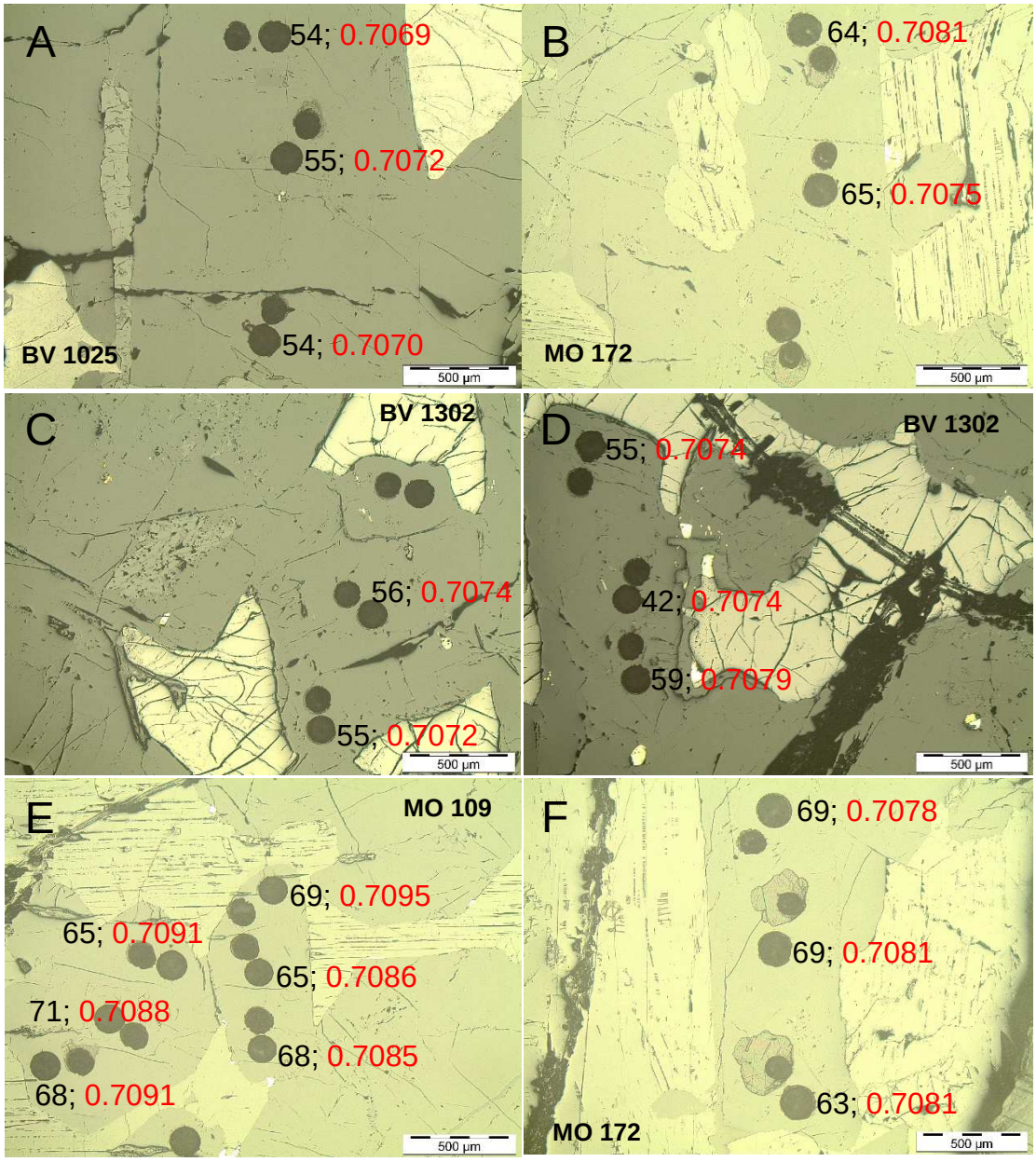

Figure 35: (A) to (F) Reflected light photomicrographs of plagioclase crystals that exhibit inter and intra-crystal initial $^{87}Sr/^{86}Sr$ variation. The numbers in black denote the anorthite content (An%) of the crystal at that spot, whereas the numbers in red are the initial $^{87}Sr/^{86}Sr$ ratios. Sample names are also written in black but in bold.

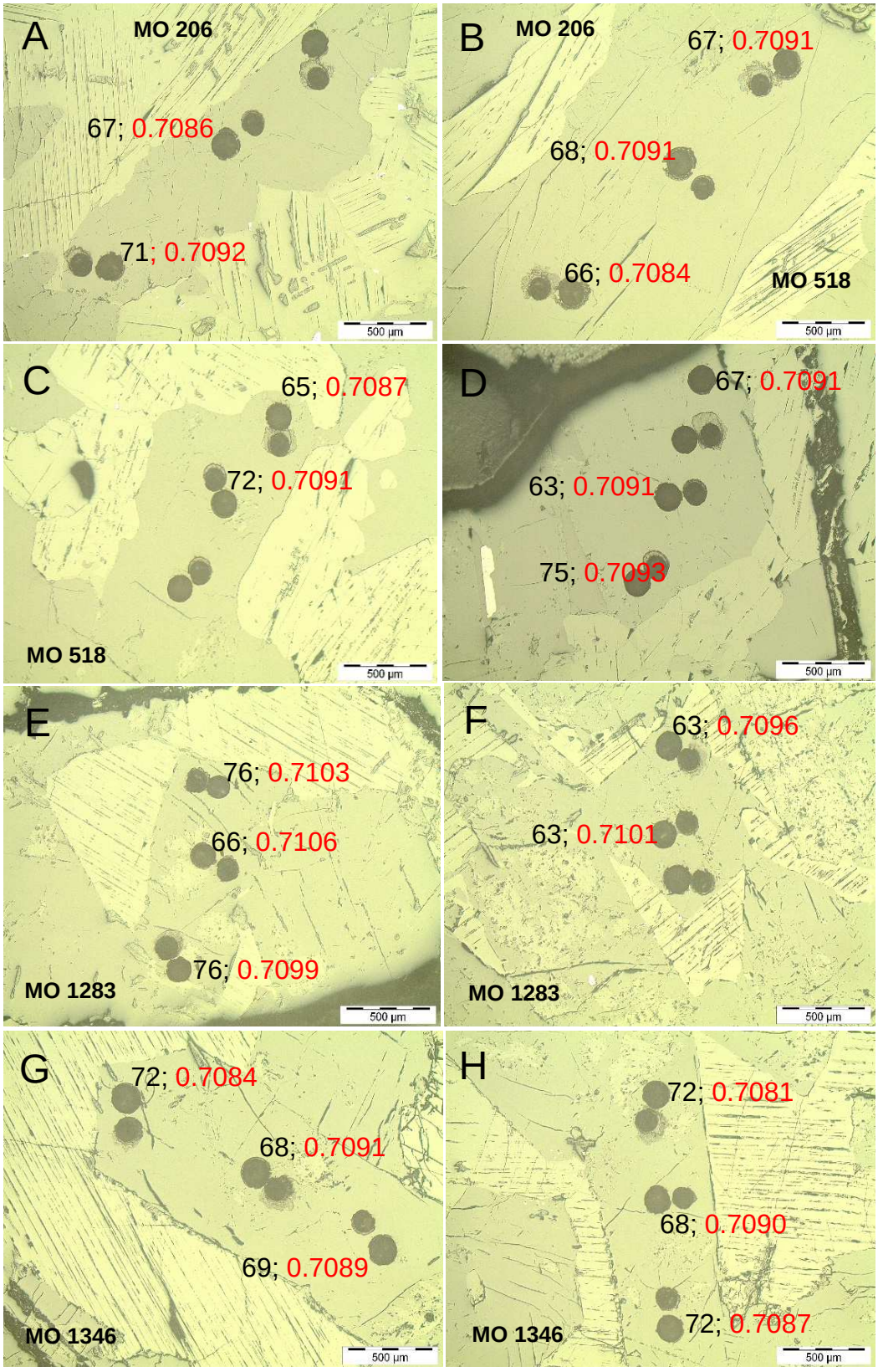

Figure 35: Continued

4. Discussion

4.1 The Sr-isotopic stratigraphy of the Northern Limb of the Bushveld Complex

Based on initial Sr-isotopic ratios of the Western Bushveld Complex, Kruger (1994) divided the Rustenburg Layered Suite into two stages, the Integration and Differentiation stages. The Integration stage comprises the Lower, Critical, and Lower Main Zones, while the Differentiation stage incorporates the Upper Main and Upper Zones of the Layered Sequence. The Integration stage is characterized by an irregular upward increase in initial $^{87}Sr/^{86}Sr$ ratios (Sr_i) from 0.7047 in the Lower Zone to 0.7091 in the Lower Main Zone. Contrary to the Integration stage however, the Differentiation stage is typified by consistent Sr-isotopic ratios, except for a decrease at the Pyroxenite Marker, the boundary between the Main Zone and Upper zone, where Sr-isotopic ratios decrease from 0.7085 to 0.7073. The entire Upper Zone exhibits a uniform Sr-isotopic signature. A similar pattern of Sr-isotopic variation with stratigraphic height can also be seen in the Eastern Limb of the Bushveld Complex (Sharpe, 1985).

According to Kruger (1994), the isotopically heterogeneous integration stage was formed through repeated injections of compositionally distinct magma pulses, with little mixing between the new influxes and the magmas already present in the chamber. Contrary to the integration stage, the isotopically homogenous differentiation stage on the other hand is characterised by no significant introduction of new magma, apart from one major influx that initiated this unit. The differentiation stage is therefore dominated by closed system fractional crystallisation (Kruger, 1994).

The Sr-isotopic data presented in this study for the Northern Limb of the Bushveld Complex show variations that are similar to the ones recognised for the Western Limb of the complex, and therefore the Northern Limb can, on this basis, be divided into the integration and differentiation stages, similar to what Kruger (1994) did for the Western Limb. The integration stage proposed for the Northern Limb comprises the lower reaches of the Lower Main Zone, an interval where significant fluctuations in Sr-isotopic ratios coupled with a lack of differentiation as exemplified by the An% can be observed. This is suggestive of repeated intrusion of magmas during the development of the Lower Main Zone. Furthermore, it can also be argued, based on the fact that coexisting plagioclase from this interval also exhibits inter and intracrystal Sr-isotopic variations, that the influxes were of crystal-charged mushes as opposed to aphyric liquids. The proposed differentiation stage on the other hand comprises of the remainder of the stratigraphy up to the top of the Rustenburg Layered Suite. Here there is less variation in Sr-isotopic ratios of plagioclase, added to a broadly normal differentiation trend as exemplified by the An%. These features are suggestive of magma differentiation as the dominant process during the development of this interval, with no large scale addition of magma, except for small additions that locally resulted in reversed differentiation trends as shown by Ashwal *et al*. (2005).

[1] For further details see Appendix D

[1] Paper by Mangwegape *et al*. (2016) on the Sr-isotopic stratigraphy of the Northern Limb of the Bushveld Complex, South Africa. Published in Journal of African Earth Sciences, Volume 113, pages 95-100.

4.2 The plagioclase trace element stratigraphy of the Northern Limb of the Bushveld Complex

Tanner *et al*. (2014) presented the abundance data for 57 trace elements hosted in plagioclase, clinopyroxene, low-Ca pyroxene, and in olivine along the Bellevue (BV-1) drill core, with all trace elements measured by Laser Ablation Inductively Coupled Plasma Mass Spectrometry (LA-ICPMS). As both plagioclase and pyroxene occur consistently throughout the BV-1 core, Tanner *et al.* (2014) argued that trace elements in both these minerals exhibit systematic geochemical behaviour (i.e. stratigraphic trends). These authors observed three distinct trends displayed by the various trace elements in the different analysed silicate minerals: (i) elements that increase in the host mineral with stratigraphic height, (ii) elements that decrease in the host mineral with stratigraphic height, (iii) elements that show erratic behaviour or that scatter with stratigraphy.

According to Tanner *et al*. (2014), the trace elements Ba, Be, Eu, K, Pb, and Sr in the mineral plagioclase systematically increase with stratigraphic height along the BV-1 core, with a slight decrease to more primitive compositions observed at the Upper Zone-Main Zone boundary. Sr and K display a linear increase, whereas Ba, Be, Eu, and Pb show an exponential increase in the upper third of the core. However, many elements, such as Cs, Rb, Ti, and Y in plagioclase show erratic behaviour or scatter with stratigraphy, whereas some, like Ti, show a limited variation.

The trace element data obtained in this study are in many ways similar to the data obtained by Tanner *et al.* (2014). Some of the trace elements in this study also show a linear increase from the bottom of the Lower Main Zone towards the lower parts of

the Upper Zone. From this interval, an exponential increase in the concentration of the said elements is observed, and this latter trend is retained up to the top of the stratigraphy. Elements behaving in this manner are Ba, Eu, Sr, and Pb.

Other elements, such as Rb and Gd only record a linear increase across the entire stratigraphy with no observed exponential increase, whereas others, like Y, Dy, Ho, U, Yb, Er, Lu, and Tb increase and decrease repeatedly along the profile, i.e. they scatter with stratigraphy. The inconsistent behaviour of these elements can be equated with the erratic behaviour that Tanner *et al*. (2014) described for some of the elements the authors investigated. Elements such as Zr, Ce, Pr, La, Th, Nd, and Sm on the other hand exhibit no variations with stratigraphy, as their concentration in the host mineral remains constant across the entire studied profile.

Moreover, it was also mentioned in the results chapter that the third lowermost and lowermost samples in the studied stratigraphic interval have elevated trace element concentrations. This feature was initially thought to be the result of instrumental error, but because these two samples also record higher initial $^{87}Sr/^{86}Sr$ ratios than any other studied samples, this feature is most likely not attributable to instrumental shortcomings. The Sr-isotopic composition of the lower part of the Northern limb is known to have been affected by floor-rock interaction, and thus the high trace element concentrations observed in these two samples may be due to this interaction. It remains peculiar, however, that all analysed trace elements for these two samples showed increased concentration levels, rather than merely anomalous (i.e. low or high concentrations).

4.3 Petrogenetic aspects

Important constraints on the petrogenesis of the Bushveld Complex were derived from whole rock and/or the mineral separate Sr- isotopic character of the cumulate sequence. This character is defined by a step-wise increase in initial Sr- isotopic ratios from the Lower Zone into the Upper Zone of the Rustenburg Layered Suite. Various authors have interpreted this observation as a result of the repeated injection of magma into the magma chamber of the Bushveld Complex, with the injected magma being different in composition to the magma already present in the chamber, and with all these different magmas having been subjected to crustal contamination (e.g. Maier *et al*., 2000), or perhaps contamination by Sub-Continental Lithospheric Mantle (SCLM) (Richardson & Shirey, 2008). This model of magma addition and mixing has also been associated with the formation of the vast PGE, Ni, Cu, and Cr mineralisation of the complex, and also to other properties of the cumulate sequence, like for instance the layering that is observed across the stratigraphy, which is not solely attributed to magma injection and mixing, but to the interplay between a variety of processes, including such processes as crystal settling, *in-situ* crystallisation at the bottom of the magma chamber, and the effect of density currents to mention but a few. Although the mixing model has been widely accepted, some authors have found evidence that argues against such a model, and this evidence is consistent with PGE, S, and Cu mobilization by migration of metallliferous Cl-rich fluids (Willmore *et al*., 2000). Maier *et al*. (2013) also argued that the sulphur (S) content of Bushveld magmas was too low to allow magma mixing to trigger sulphide saturation.

Despite the success of the magma addition and mixing model in explaining some of the features of the Bushveld Complex, the model is however, not enough to explain some other features of the complex, like the recent identification of isotopic disequilibrium both between and within coexisting minerals in rocks of the Bushveld Complex, a phenomenon which is not only confined to the Bushveld Complex, but occurs in other layered intrusions across the globe. This has compelled researchers to seek new petrogenetic models which will explain and account for the observed isotopic disequilibrium both between and within coexisting minerals. Over the past decade or so, a number of process have been proposed, and the following can be found in the literature: (i) repeated intrusion of variably contaminated crystal mushes derived from a deeper, sub-compartmentalized crustal staging chamber (Roelofse & Ashwal, 2012; Roelofse *et al*., 2015), (ii) density-driven sorting of minerals through slumping of semi-consolidated slurries during subsidence of the centre of the intrusion (Yang *et al*., 2013), (iii) late-stage infiltration of relatively radiogenic contaminants into crystal-liquid mush systems (Chutas *et al*., 2012), (iv) density-driven mixing of minerals crystallised from liquids that underwent different degrees of contamination (Prevec *et al*., 2005), (v) a model involving crystals growing along a cooling solidification front breaking free from the front, and then settling onto the floor of the magma chamber through gravity currents, which then mix isotopically zoned and unzoned crystals as has been proposed by Tepley & Davidson (2003), (vi) McBirney & Creaser (2003) have proposed a model involving metasomatic alteration of crystalline magmas by late-stage fluids that permeated the intrusion.

Results from the present study have identified the presence of isotopic disequilibrium both between and within coexisting plagioclase in rocks of the Upper and Main Zones

of the Northern Limb of the Bushveld Complex. This disequilibrium mainly occurs in rocks from Lower Main Zone, and to a significantly lesser extent in rocks from the Upper Main and Upper Zones of the Northern Limb. These results are in agreement with the results of Roelofse *et al*. (2015) who also identified disequilibrium between and within coexisting plagioclase in the Lower Main Zone of the northern Limb. Additionally, plagioclase from this study also shows a lack of differentiation in the Lower Main Zone, with the differentiation becoming more pronounced as one moves up the stratigraphic interval. A similar observation was also made by Roelofse & Ashwal (2012).

4.3.1 Competing hypothesis

Permeation of an intrusion by late-stage fluids, with the said fluids bringing about isotopic disequilibrium, as proposed by McBirney & Creaser (2003) for the Skaergaard intrusion, seems an unlikely model to account for the observed isotopic disequilibrium in this study. The reason for this is that one would expect the permeating fluids to considerably alter the composition of mineral rims more than mineral cores, as these fluids move through crystalline magmas. Depending on the composition of the supposed fluids, mineral rims should then be more radiogenic or less radiogenic than cores. Results from this study argue against such a model, in that in some of our samples, plagioclase rims are more radiogenic than cores, whereas in others the opposite is true. In a few samples, plagioclase crystals have varying Sr-isotopic ratios across all three domains (from one rim, through the core, onto the opposite rim). Roelofse *et al.* (2015) obtained results which also argue against such a model for the isotopic disequilibrium in the Northern Limb of the Bushveld Complex. The authors

observed that in one of their samples, one plagioclase crystal has rims more radiogenic than the core, and in one crystal from the same sample, the reverse is true.

Present results also discount the model of late-stage infiltration by relatively radiogenic contaminants into a crystal-liquid mush system, as suggested by Chutas *et al*. (2012) for the Lower and Critical Zones of the Eastern Limb of the Bushveld Complex, for the reason that these liquids would affect crystal rims much more than cores, an incidence not observed in the Upper and Main Zones of the Northern Limb. Chutas *et al.* (2012) also proposed that in the presence of these contaminants, larger crystals could grow at the expense of smaller crystals, with larger crystals recording the isotopic signatures of both the infiltrating contaminants and the dissolving smaller crystals. The result would then be pronounced radiogenic ratios in larger crystals than in the smaller ones. No such relationship between crystal size and Sr-isotopic composition was observed in the present study.

The model of crustal contamination along a cooling solidification front, and subsequent mixing of zoned and unzoned crystals due to gravitation (Tepley & Davidson, 2003) is also considered unlikely to have resulted in isotopic heterogeneities observed in the Upper and Main Zones of the Northern Limb of the Bushveld Complex for the reason that the immediate country rocks to the Rustenburg Layered Suite are not suitable contaminants when modelling the isotopic composition of the Main Zone (Roelofse & Ashwal, 2012). Thus it is not feasible that the observed heterogeneities in this study resulted from wall/roof rock contamination, as it was suggested for the Rum layered intrusion. According to Yang *et al*. (2013), the model of Tepley & Davidson (2003) assumes a slower rate of crystallisation than that of wall-rock contamination, but

because the Bushveld Complex is a much larger intrusion than the Rum, Yang *et al.* (2013) argues for slower wall-rock contamination and faster crystallisation for the Bushveld Complex, with wall-rock contamination contributing less to the composition of the Bushveld magma. As a result, Yang *et al*. (2013) are in suggestion that the model of Tepley & Davidson (2003) is unlikely to have resulted in the isotopic heterogeneities the authors observed in the Upper Critical Zone, Western Bushveld Complex. The authors instead propose a model in which plagioclase crystallised from two magmas of distinct composition to account for the observed isotopic disequilibrium between cores of different plagioclase crystals, and that overgrowth of these crystals in a silicate melt of differing composition later occurred, and resulted in core to rim variations observed within individual plagioclase crystals. Plagioclases with unique crystallisation histories were then incorporated into the same rock through density sorting during slumping of semi-consolidated crystal slurries. For isotopic disequilibrium between plagioclase and orthopyroxene in the Merensky interval, Prevec *et al*. (2005) suggested that both these minerals were derived from liquids affected by pre-emplacement crustal contamination and were incorporated into the same rocks through density-driven accumulation.

Roelofse *et al*. (2015) argues that both these models are based on the premise that magmas which entered the Bushveld Complex had different isotopic compositions prior to emplacement, crystallised their respective liquidus phases without mixing because of contrasting densities, and crystallised minerals were then incorporated into the same rocks. These authors suggest that such models are untenable for the Main Zone of the Rustenburg Layered Suite, where compositionally similar magmas would likely have been subjected to mixing.

4.3.2 A petrogenetic model for the Main and Upper Zone in the Northern Limb

Any petrogenetic model envisioned for the Upper and Main Zones of the Northern Limb of the Bushveld Complex has to take into consideration the following key points: (i) the lack of differentiation of the Lower Main Zone, with more pronounced differentiation in the Upper Main and Upper Zones, (ii) the presence of Sr-isotopic disequilibrium both between (inter-crystal) and within (intra-crystal) coexisting plagioclase in the Lower Main Zone, and to a lesser extent in the Upper Main and Upper Zones (Figure 36). The results of the present study broadly supports the model proposed by Roelofse & Ashwal (2012) for the petrogenesis of the Lower Main Zone of the Northern Limb, Bushveld Complex.

To account for the observed isotopic disequilibrium between coexisting plagioclase and orthopyroxene, Roelofse & Ashwal (2012) argued for a model that involves the repeated intrusion of crystal-charged mushes derived form a sub-compartmentalized, deeper staging chamber into the Bushveld main magma chamber. Within these postulated sub chambers, magmas were variably contaminated by different crustal contaminants. These contaminants are the upper and lower crustal rocks of the Vredefort Dome, as represented by the Outer Granite Gneiss (OGG) and Inlandsee Leucogranofels (ILG) respectively. Their choice of crustal contaminants came after the authors showed convincingly that the present country rocks to the Rustenburg Layered Suite cannot be modelled by mixing of mantle-derived melts with melts derived from supracrustal rocks of the Transvaal Supergroup. For their model, these authors assumed that the mantle at 2.06 Ga had εNd = +2.0 and $^{87}Sr/^{86}Sr$ = 0.702 in accordance with the choice of Maier *et al*. (2000).

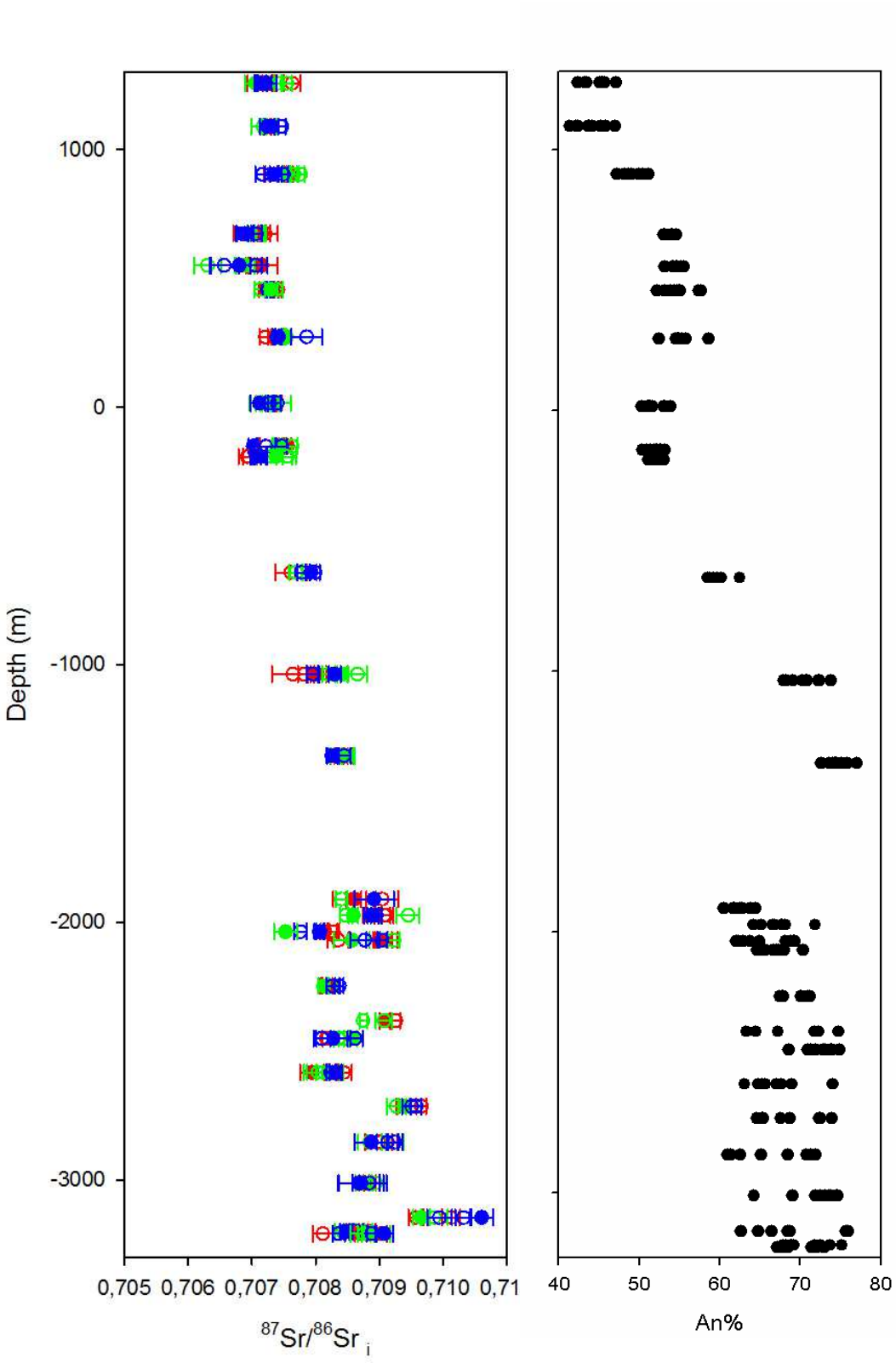

Figure 36: Inter and intra-crystal $^{87}Sr/^{86}Sr$ variation in the Lower Main Zone of the Northern Limb of the Bushveld Complex coupled to a lack of differentiation as shown by the An% of plagioclase. In the Upper Main and Upper Zones of the Northern Limb there is limited $^{87}Sr/^{86}Sr$ variation, and this is coupled to more pronounced differentiation.

To understand the variation of Sr and Nd concentration in a mantle subjected to different degrees of partial melting, modelling was performed by use of the pMELTS software package of Ghiorso *et al.* (2002), with calculations performed using the composition of a spinel peridotite reported by McDonough (1990) as a starting composition. For the calculation of bulk partition coefficients, the mineralogical compositions of the refractory restites were employed using the equations of Shaw (1970) for the case of equilibrium melting and the partition coefficients for Sr and Nd as reported by Arndt *et al*. (1993). Using the Sr and Nd concentrations of primitive mantle from Hofmann (1988), the Sr and Nd concentrations in melts generated by different degrees of partial melting were calculated. The authors then followed the approach of Maier *et al*. (2000) to generate partial melts of the Vredefort crustal end-members. For additional information on this model and on the methods used in its development see Roelofse & Ashwal (2012).

For the model proposed in this study (Figure 37), melts from three end-members were mixed together. These are a mantle melt with an initial $^{87}Sr/^{86}Sr$ value of 0.702 and a Sr content of 320 ppm, a partial melt with an initial $^{87}Sr/^{86}Sr$ value of 0.7417 and a Sr content of 290 ppm derived from the Vredefort OGG, and lastly a Vredefort ILG partial melt having an initial $^{87}Sr/^{86}Sr$ value of 0.718 and a Sr content of 210 ppm. To calculate the Sr content of the hybridised melts from the measured Sr contents of plagioclase as analysed in the present study, a Sr partition coefficient (D_{Sr}) of 1.1 at a temperature (T) of 1400° C and a pressure (P) of 7.5 kb was used, after Vander Auwera (2000).

The isotopic model depicted in Figure 37 shows that the Sr-isotopic composition of plagioclase in rocks from the Lower Main Zone can be explained by the interaction of

a primary mantle melt with partial melts of the Vredefort upper (OGG) and lower (ILG) crust. What is observed from the model is that the Sr-isotopic composition of plagioclase in Lower Main Zone samples coincides with the Sr-isotopic composition of the three end-members, suggesting that all three end-members contributed to the Sr-isotopic composition of these samples. Another observation is that the Sr content of these samples varies less, with an exception of two samples from this interval which show somewhat variable and high Sr contents. This suggests repeated intrusion of magma without significant fractionation for the Lower Main Zone.

However, in the Upper Main and Upper Zones of the Northern Limb, the Sr content of the samples is varied, but the samples on the other hand also record less variations in their Sr-isotopic composition, suggesting that over these two intervals, fractionation processes were dominant, and magma addition was less dominant. The sharp increase in the concentration of elements such as Sr, Rb, Ba, and Eu (Figure 32) in the upper parts of the Upper Zone also shows that in this interval, fractionation was the key petrogenetic process as opposed to repeated intrusion of crystal mushes.

It is therefore proposed, based on what is seen from the model below, and bearing in mind also the presence of inter and intracrystal Sr-isotopic variations for the Lower Main Zone, that rocks from this interval were formed through the repeated intrusion of crystal laden mushes derived from a sub-compartmentalized staging chamber, into the Bushveld main magma chamber. Within these sub chambers, magmas were variably contaminated by the ILG and OGG crustal end-members, and this was followed by blending of crystal mushes from these two sub-compartments prior to final emplacement. The model also suggests that the process defined above was also

partially responsible for the formation of the Upper Main and Upper Zones of the Northern Limb, which also explains the limited inter and intracrystal Sr-isotopic variations observed in samples from these two intervals. However, in the Upper Main and Upper Zones of the Northern Limb fractionation processes were dominant, and it is therefore proposed that these two intervals resulted from the differentiation of magma within the Bushveld Complex, without significant addition of large magma pulses, except for smaller ones which locally resulted in reversed differentiation trends as shown by Ashwal *et al*. (2005).

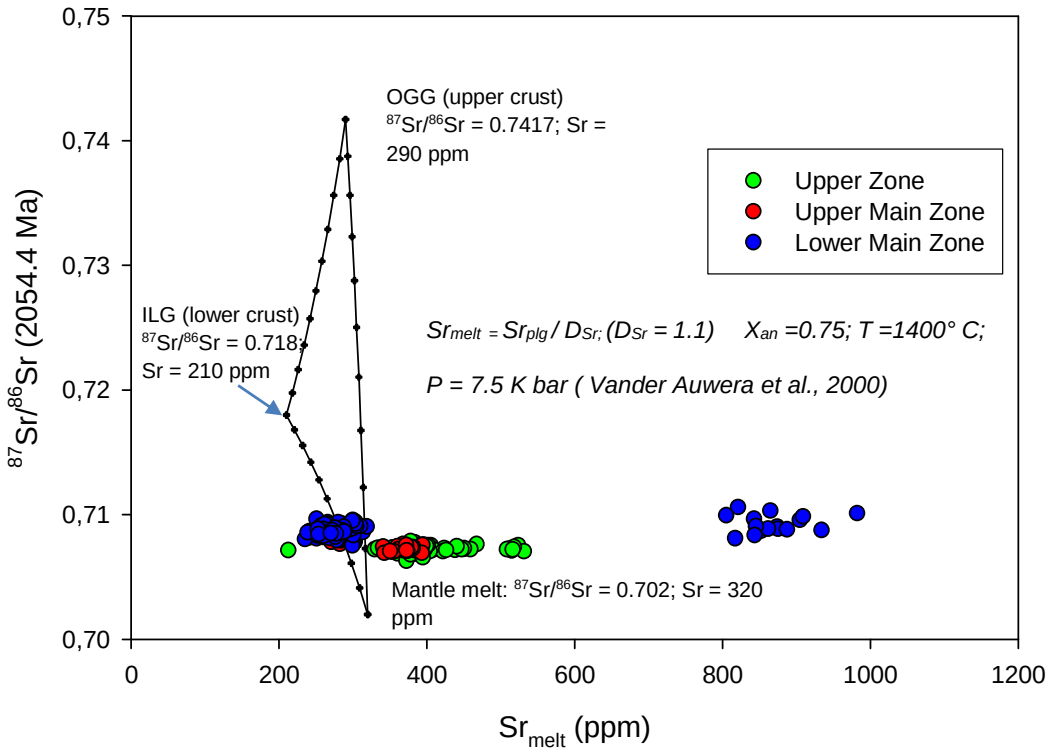

Figure 37: An isotopic mixing model showing how the Sr-isotopic composition of Lower Main Zone plagioclase can be explained by the interaction between a primary mantle melt and melts form the Vredefort ILG and OGG.

Roelofse *et al*. (2015) have also recently identified the presence of multiple, isotopically heterogeneous plagioclase populations coexisting in rocks of the Lower

Main Zone, and these authors have attributed their findings to the repeated injection of crystal mushes derived from a sub-compartmentalized staging chamber.

5. Summary and Conclusion

5.1 Summary of results

All samples investigated in this study are gabbroic cumulates from the Upper and Main Zones of the Northern Limb, Bushveld Complex. Petrographic analysis revealed that plagioclase is the dominant, cumulus mineral in these samples, with clinopyroxene and orthopyroxene both generally assuming intercumulus status. All these minerals exhibit local alteration to secondary minerals such as sericite and amphibole. The minerals olivine and inverted pigeonite occur sporadically in the studied stratigraphic profile. The former occurs interstitial to plagioclase in the upper parts of the Upper Zone, and again as oikocrysts in the troctolitic horizon towards the end of the BV-1 drill core, the latter occurs at the base of the Upper Zone and at the top of the Upper Main Zone. The minerals biotite, quartz, and opaques are all subsidiary in the studied samples and occur as patches or rims on the prominent minerals or sometimes within them. Intergrowth textures are also present.

Electron microprobe analysis of individual spots in multiple plagioclase crystals within the different samples has shown a wide range of plagioclase major element composition in stratigraphic terms. Individual spots in samples from the Upper Zone average at An% of 50.9% ± 4.5, ranging between 41.4% and 58.6%, in the Upper Main Zone, individual spots average at An% of 62% ± 9.9, varying from 50.4% to 77.1%, whereas individual spots in samples from the Lower Main Zone have an average An% of 68.3% ± 3.9, ranging between 60.5% and 75.9%.

In terms of the initial Sr-isotopic composition of plagioclase, analysed spots in samples from the Lower Main Zone are the most varied, with an average initial $^{87}Sr/^{86}Sr$ value

of 0.7088, ranging between 0.7075 and 0.7106. Analysed points in samples from the Upper Main Zone are less varied, and have an average initial $^{87}Sr/^{86}Sr$ value of 0.7078, varying from 0.7069 to 0.7087, whereas individual points in samples from the Upper Zone are the least varied, having an average initial $^{87}Sr/^{86}Sr$ value of 0.7072, ranging between 0.7063 and 0.07079. Additionally, the occurrence of inter and intra-crystal initial Sr-isotopic variation is much more widespread in samples from the Lower Main Zone, compared to samples from the Upper Main Zone and Upper Zone.

The trace element composition of plagioclase on the other hand has shown that different trace elements exhibit different geochemical behaviours (i.e. different stratigraphic trends). Some elements increase linearly with stratigraphy, and some increase sharply in the upper extents of the Upper Zone. Some display erratic behaviours in that they decrease and increase repeatedly across the stratigraphy (their behaviour is inconsistent), whereas others exhibit no variation with stratigraphy.

5.2 Summary of discussion

The present study has identified the presence of inter and intra-crystal initial $^{87}Sr/^{86}Sr$ disequilibrium of plagioclase in the Lower Main Zone, coupled with a lack of differentiation as exemplified by the An% of plagioclase. The rest of the stratigraphy exhibits limited initial $^{87}Sr/^{86}Sr$ variation, coupled to more pronounced differentiation trends. With regards to the petrogenesis of the Northern Limb of the Bushveld Complex, these results are best explained by the repeated intrusion of crystal mushes derived from a deeper seated, sub-compartmentalized staging chamber, into the Bushveld main magma chamber, for the Lower Main Zone, with fractionation

processes being central in the formation of the Upper Main and Upper Zones of the Bushveld Complex.

Furthermore, the initial $^{87}Sr/^{86}Sr$ composition of plagioclase across the studied stratigraphic profile enables then Northern Limb of the complex to be divided into the integration and differentiation stages as it was done by Kruger (1994) for the Western Limb of the complex. This author's integration stage incorporated the Lower, Critical, and Lower Main Zone of the complex, where an increase in initial $^{87}Sr/^{86}Sr$ ratios is observed. Contrary to the integration stage, Kruger's differentiation stage incorporated the Upper Main and Upper Zones, an interval characterised by uniform initial $^{87}Sr/^{86}Sr$ ratios, except for a slight decrease observed at the Pyroxenite Marker.The integration stage proposed in this study incorporates the lower reaches of the Lower Main Zone, an interval where there is significant variations in the initial $^{87}Sr/^{86}Sr$ composition of plagioclase. The differentiation stage includes the rest of the stratigraphy up to the top of the Rustenburg Layered Suite, an interval characterised by limited variation in initial $^{87}Sr/^{86}Sr$ ratios of plagioclase.

Moreover, a total of 22 trace elements were analysed in the different plagioclase crystals across the entire stratigraphy of the Northern Limb. These trace elements can be separated into four different categories: (i) elements like Eu, Sr, and Pb which increase sharply in the Upper reaches of the Upper Zone, (ii) elements like Rb and Gd which exhibit a linear increase with stratigraphy, (iii) Y, U, and Lu scatter with stratigraphy, (iv) whereas Zr, Ce, and La show a limited variation with stratigraphy. Elements like Sr, Eu, and Pb which increase sharply in the Upper Zone show that in

this interval, magma fractionation was the key petrogenetic process, and that repeated magma intrusion was insignificant.

5.3 Conclusion

In view of the results obtained in this study, the presence of isotopic disequilibrium both between and within coexisting minerals in rocks of the Bushveld Complex might be a more common phenomenon than what has already been documented to date, and the same can be said with confidence to other layered intrusions across the globe. The present results have also echoed views shared by many authors with regards to the petrogenesis of these intrusions, particularly the notion that important petrogenetic information is lost during isotopic analysis of whole rocks and/or mineral separates or that derivation of petrogenetic models based on interpretation of data obtained through progressive leaching experiments should be done with caution, as such results may lead to flawed interpretations or interpretations that may only be partially correct. The data set presented here has also succeeded in both expanding the database of *in-situ* Sr-isotopic analysis done on the Bushveld Complex, as well as in constraining the evolution of the Upper and Main Zones of the Northern Limb of the complex. What remains clear is that the Bushveld Complex continues to be a bountiful hunting ground for scientific research, and that advances in technology and new methodologies should only increase the research bounty.

6. References

Arndt, N. T., Czamanske, G. K., Wooden, J. L., & Fedorenko, V. A. (1993) Mantle and crustal contributions to continental flood volcanism. *Tectonophysics, 223*, 39-52.

Ashwal, L. D., Webb, S. J., & Knoper, M. W. (2005) Magmatic stratigraphy in the Bushveld Northern Lobe: continuous geophysical and mineralogical data from the 2950 m Bellevue drillcore. *South African Journal of Geology, 108*, 199-232.

Barnes, S-J., Maier, W. D., & Ashwal, L. D. (2004) Platinum-group element distribution in the Main Zone and Upper Zone of the Bushveld Complex, South Africa. *Chemical Geology, 208*, 293-317.

Buchanan, P. C., Reimold, W. U., Koeberl, C., & Kruger, F. J. (2002) Geochemistry of intermediate to siliceous volcanic rocks of the Rooiberg Group, Bushveld Magmatic Province, South Africa. *Contributions to Mineralogy and Petrology, 144*, 131-143.

Buchanan, P. C., Reimold, W. U., Koeberl, C., & Kruger, F. J. (2004) Rb-Sr and Sm-Nd isotopic compositions of the Rooibeg Group, South Africa: early Bushveld-related volcanism. *Lithos, 29*, 373-388.

Cameron, E. N. (1982) The Upper Critical Zone of the Eastern Bushveld Complex-Precursor of the Merensky Reef. *Economic Geology, 77*, 1307-1327.

Campbell, I. H., Naldrett, A. J., & Barnes, S. J. (1983) A model for the origin of the platinum-rich sulfide horizons in the Bushveld and Stillwater Complexes. *Journal of Petrology, 24*, 133-165.

Cawthorn, R. G. (2005) Contrasting sulphide contents of the Bushveld and Sudbury Igneous Complexes. *Mineralium Deposita, 40*, 1-12.

Cawthorn, R. G. (2007) Cr and Sr: keys to parental magmas and processes in the Bushveld Complex, South Africa. *Lithos, 95*, 381-398.

Cawthorn, R. G., & Walraven, F. (1998) Emplacement and crystallisation time for the Bushveld Complex. *Journal of Petrology, 39*(9), 1669-1687.

Cawthorn, R. G., & Webb, S. J. (2000) Connectivity between the western and eastern limbs of the Bushveld Complex. *Tectonophysics, 330*, 195-209.

Cawthorn, R. G., Barnes, S. J., Ballhaus, C., & Malitch, K. N. (2005) Platinum-group element, chromium and vanadium deposits in mafic and ultramafic rocks. *Economic Geology, 100th Anniversary volume*, 215-249.

Chutas, N. I., Bates, E., Prevec, S. A., Coleman, D. S., & Boudreau, A. E. (2012) Sr and Pb isotopic disequilibrium between coexisting plagioclase and orthopyroxene in the Bushveld Complex, South Africa: microdrilling and progressive leaching evidence for sub-liquidus contamination within a crystal mush. *Contributions to Mineralogy and Petrology, 163*(4), 653-668.

Clarke, B., Uken, R., & Reinhardt, J.N. (2009) Structural and compositional constraints on the emplacement of the Bushveld Complex, South Africa. *Lithos, 111*, 21-36.

Curl, E. A. (2001) *Parental magmas of the Bushveld Complex, South Africa. Ph.D. thesis,* Monash Univerity, Australia, p 140.

de Waal, S. A., Maier, W. D., Armstrong, R. A., & Gauert, C. D. (2001) Parental magma and emplacement of the stratiform Uitkomst Complex, South Africa. *Canadian Mineralogist, 39*(2), 557-571.

Eales, H. V., Marsh, J. S., Mitchell, A. A., De Klerk, W. J., Kruger, F. J., & Field, M. (1986) Some geochemical constraints upon models for the crystallization of the Upper Critical Zone-Main Zone interval, northwestern Bushveld Complex. *Mineralogical Magazine, 50*, 567-582.

Eales, H. V., & Cawthorn, R. G. (1996) The Bushveld Complex. In: Cawthorn R.G (ed) *Layered Intrusions.* Elsevier, Amsterdam, pp. 181-229.

Eales, H. V., de Klerk, W. J., Butcher, A. R., & Kruger, F. J. (1990a) The cyclic unit beneath the UG1/chromitite (UG1FW unit) at R.P.M Union Section Mine, Rosetta Stone of the Bushveld Upper Critical Zone. *Mineralogical Magazine, 54*, 23-43.

Eales, H. V., de Klerk, W. J., & Teigler, B (1990b) Evidence for magma mixing processes within the Critical and Lower Zones of the northwestern Bushveld Complex, South Africa. *Chemical Geology, 88*, 261-278.

Elburg, M., Vroon, P., van der Wagt, B., & Tchalikian, A. (2005) Sr and Pb isotopic composition of five USGS glasses (BHVO-2G,BIR-1G,BCR-2G, TB-1G, NKT-1G). *Chemical Geology, 223*, 196-207.

Eriksson, P. G., & Reczko, B. F.F. (1995) The sedimentary and tectonic setting of the Transvaal Supergroup floor rocks the Bushveld complex. *Journal of African Earth Sciences, 21*, 487-504.

Eriksson, P. G., Hattingh, P. J., & Altermann, W. (1995) An overview of the geology of the Tranvaal Sequence and Bushveld Complex, South Africa. *Mineralium Deposita, 30*, 98-11.

Errikson, P. G., Altermaan, W., Catuneanu, O., van der Merwe, R. & Bumby, A.J. (2001) Major influences on the evolution of the 2.67-2.1 Ga Transvaal basin, Kaapvaal craton. *Sedimentary Geology, 141-142*, 205-231.

Ghiorso, M. S., Hirschmann, M. M., Reiners, P. W., & Kress, V. C. (2002) The pMELTS: An revision of metls aimed at improving calculation of phase relations and major element partitioning involved in partial melting of the mantle at presssures up to 3 GPa. *Geochemistry, Geophysics, Geosystems, 3*, 5.

Good, N., & de Wit, M. J. (1997) The Thabazimbi-Murchison Lineament of the Kaapvaal Craton, South Africa: 2700 Ma of episodic deformation. *Journal of the Geological Society of London, 154*, 93-97.

Hamilton, P. J. (1977) Sr isotope and trace element studies of the Great Dyke and Bushveld mafic phase and their relation to early Proterozoic magma genesis in southern Africa. *Journal of Geology, 18*, 24-52.

Harmer, R. E., Auret, J. M., & Eglington, B. M. (1995) Lead isotope variations within the Bushveld Complex, Southern Africa : a reconnaissance study. *Journal of African Earth Sciences, 21*, 595-606.

Harris, C., & Chaumba, J. B. (2001) Crustal Contamination and Fluid–Rock Interaction During The Formation of the Platreef, Northern Limb of the Bushveld Complex, South Africa. *Journal of Petrology, 42*(7), 1321-1347.

Harris, c., Pronost, J. J. M., Ashwal, L. D., & Cawthorn, R. G. (2005) Oxygen and hydrogen isotope stratigraphy of the Rustenburg Layered Suite Bushveld Complex: Contraints crustal contamination. *Journal of Petrology, 46*, 579-601.

Hart, S. R., & Kinloch, E. D. (1989) Osmium isotope systematics in Witwatersrand and Bushveld magmatism. *Economic Geology, 84*, 1651-1655.

Hofmann, A. W. (1988) Chemical differentiation of the Earth: the relationship between mantle, continental crust and oceanic crust. *Earth and Planetary Science Letters, 90*, 297-314.

Holwell, D. A., Boyce, A. J., & McDonald, I. (2007) Sulfur isotope variations within the platreef Ni-Cu-PGE deposit: genetic implications for the origin of sulfide mineralisation. *Economic Geology, 102*, 1091-1110.

Irvine, T. N. (1977) Origin of chromitite layers in the Muskox Intrusion and other stratiform intrusion; a new interpretation. *Geology, 5*, 273-277.

Kinnaird, J. A., Kruger, F. J., & Cawthorn, R. G. (2004) Rb-Sr and Nd-Sm isotopes in fluorite related to the granites of the Bushveld Complex. *South African Journal of Geology, 107*, 413-430.

Kinnaird, J. A., Hutchinson, D., Schurmann, L., Nex, P. A. M., & De Lange, R. (2005) Petrology and mineralisation of the southern Platreef: northern limb of the Bushveld Complex, South Africa. *Mineralium Deposita, 40*, 576-597.

Kruger, F. J. (1990) The stratigraphy of the Bushveld Complex: a re-appraisal and the relocation of the Main Zone boundaries. *South African Journal of Geology, 93*, 376-381.

Kruger, F. J. (1992) The origin of the Merensky cyclic unit: Sr isotopic and mineralogical evidence for an alternative orthomagmatic model. *Australian Journal of Earth Sciences, 39*, 255-261.

Kruger, F. J. (1994) The Sr-isotopic stratigraphy of the western Bushveld Complex. *South African Journal of Geology, 97*, 393-398.

Kruger, F. J. (2005) Filling the Bushveld Complex magma chamber: lateral expansion, roof and floor interaction, magmatic unconformities, and the formation of giant chromitite, PGE and Ti-V-magnetitite deposits. *Mineralium Deposita, 40*, 451-472.

Kruger, F. J., & Marsh, J. S. (1982) Significance of $^{87}Sr/^{86}$ Sr ratios in the Merensky cyclic unit of the Bushveld Complex. *Nature, 298*, 53-55.

Kruger, F. J., & Marsh, S. J. (1985) The mineralogy, petrology and origin of the Merensky Cyclic Unit of the Bushveld Complex. *Economic Geology, 80*, 958-974.

Kruger, F. J., Cawthorn, R. G., & Walsh, K. L. (1987) Strontium isotopic evidence against magma addition in the Upper Zone of the Bushveld Complex. *Earth and Planetary Science Letters, 84*(1), 51-58.

Lee, C. A. (1996) A review of mineralisation in the Bushveld Complex and some other layered intrusions. In: Cawthorn, R.G.(ed.) *Layered Intrusions. Developments in Petrology 15,* 103-145.

Lee, C. A., & Butcher, A. R. (1990) Cyclicity in the Sr isotope stratigraphy through the Merensky and Bastard Reefs, Atok Section, eastern Bushveld Complex. *Economic Geology, 85*, 877-883.

Li, C., & Ripley, E. M. (2005) Emperical equations to predict the sulfur content of mafic magmas at sulfide saturation and applications to magmatic sulfide deposits. *Mineralium Deposita, 40*, 218-230.

Liebenberg, L. (1970) The sulfides in the layered sequence of the Bushveld Igneous Complex. *Geological Society of South Africa, 1*, 108-208.

Maier, W. D., Arndt, N. T., & Curl, E. A. (2000) Progressive crustal contamination of the Bushveld Complex: evidence from Nd isotopic analyses of the cumulate rocks. *Contributions to Mineralogy and Petrology, 140*, 316-327.

Maier, W. D., Barnes, S. -J., & Groves, D. I. (2013) The Bushveld Complex, South Africa: formation of platinum– palladium, chrome and vanadium-rich layers via hydrodynamic sorting of a mobilized cumulate slurry in a large, relatively slowly cooling, subsiding magma chamber. *Mineralium Deposita, 48*, 1-56.

Manyeruke, T. D., Maeir, W. D., & Barnes, S. -J. (2005) Major and trace element geochemistry of the platreef on the farm Townlands, northern Bushveld Complex. *South African Journal of Geology, 108*(3), 381-396.

Mangwegape, M., Roelofse, F., Mock, T., & Carlson, R. W. (2016) The Sr-isotopic stratigraphy ofthe Northern Limb of the Bushveld Complex, South Africa. *Journal of African Earth Sciences, 113*, 95-100.

Mapeo, R. B., Kampuznu, A. B., Ramokate, L. V., Corfu, F., & Key, R. M. (2004) Bushveld-age magmatism in southeastern Botswana: evidence from U-Pb zircon and titanite geochronology of the Moshaneng Complex. *South African Journal of Geology, 107*, 219-232.

Mathez, E. A., & Kent, A. R. (2007) Variable initial Pb isotopic compositions of rocks associated with the UG2 chromitite, eastern Bushveld Complex. *Geochimica et Cosmochima Acta*, 71, 5514-5527.

Mathez, E. A., & Waight, T. E. (2003) Lead isotopic disequlibrium between sulfide and plagioclase in the Bushveld Complex and the chemical evolution of large layered intrusions. *Geochima et Cosmochima Acta, 67*, 1875-1888.

McBirney, A. R., & Creaser, R. A. (2003) The Skaaergaard Layered Series, Part VII. Sr and Nd isotopes. *Journal of Petrology, 4*(4), 757-771.

McCandless, T. E., Ruiz, J., Adair, B. I., & Freydier, C. (1999) Re-Os isotope and Pd/Ru variations in chromitites from the Critical Zone, Bushveld Complex, South Africa. *Geochemica et Cosmochimica Acta, 63*, 911-923.

McCarthy, T., & Rubidge, B. (2005) *The story of EARTH & LIFE: A southern African perspective on a 4.6-billion-year journey.* Cape Town: Struik Nature.

McDonald, I., David, A., Holwell, P. E., & Armitage, B. (2005) Geochemistry and mineralogy of the Platreef and "Critical Zone" of the northern lobe of the

Bushveld Complex, South Africa: implications for Bushveld stratigraphy and the development of PGE mineralisation. *Mineralium Deposita, 40*, 523-549.

McDonough, W. F. (1990) Constraints on the composition of the continental lithospheric mantle. *Earth and Planetary Science Letters, 101*, 1-18.

Naldrett, A. J. (1989) Stratiform PGE deposits in layered intrusions. *Economic Geology, 4*, 135-165.

Naldrett, A. J., & von Gruenewaldt, G. (1989) Association of PGE with chromitite in the layered intrusions and ophiolite complexes. *Economic Geology, 84*(1), 180-187.

Naldrett, A. J., Gasparrini, E. C., Barnes, S. J., von Gruenewaldt, G., & Sharpe, M. R. (1986) The upper critical zone of the Bushveld Complex and the origin of Merensky-type ore. *Economic Geology, 81*(5), 1105-1117.

Nebel, O., Scherer, E. E., & Mezger, K. (2011) Evaluation of the ^{87}Rb decay constant by age comparison against the U-Pb system. *Earth and Planetary Science Letters, 301*, 1-8.

Pecher, M.-L. (2011) Field relationship and petro-chemical investigation of mafic sills and dykes in the vicinity of the Uitkomst Complex, Mpumalanga, South Africa. M.Sc. Dissertation. University of the Free State.

Penniston-Dorland, S. C., Wing, B. A., Nex, P. M., Kinnaird, J. A., Farquhar, J., & Sharman, E. R. (2007) Multiple Sulfur isotopes reveal a magmatic origin for the platreef platinum group element deposit, Bushveld Complex, South Africa. *Geology, 36*, 979-982.

Prendergast, M. D. (2012) The Molopo Farms Complex, Southern Botswana- A reconsideration of structure, evolution, and the Bushveld connection. *South African Journal of Geology, 115*(1), 77-90.

Prevec, S. A., Ashwal, L. D., & Mkaza, M. S. (2005) Mineral disequilibrium in the Merensky reef, western Bushveld Complex, South Africa: new Sm-Nd isotope evidence. *Contributions to Mineralogy and Petrology, 149*, 306-315.

Ramos, F. C., Wolff, J. A., & Tollstrup, D. L. (2004) Measuring $^{87}Sr/^{86}Sr$ variations in minerals and groundmass from basalts using LA-MC-ICPMS. *Chemical geology, 211*, 135-158.

Reisberg, L., Tredoux, M., Harris, C., Coftier, A., & Chuamba, J. (2011) Re and Os distribution and Os isotope composition of the Platreef at the Sandsloot-Mogolakwena mine, Bushveld Complex, South Africa. *Chemical Geology, 281*, 352-363.

Richardson, S. H., & Shirey, S. B. (2008) Continental mantle signature of Bushveld magmas and coeval diamonds. *Nature, 453*, 910-913.

Roelofse, F. (2010) Constraints on the magmaitc evolution of the lower Main Zone and Platreef on the Northern Limb of the Bushveld Complex as inferred from the Moordkopje drill core. Ph.D. Thesis. University of the Witwatersrand.

Roelofse, F., & Ashwal, L. D. (2012) The lower Main Zone in the Northern Limb of the Bushveld Complex- a >1.3km Thick sequence of intruded and variably contaminated crystal mushes. *Journal of Petrology, 53*, 1449-1476.

Roelofse, F., Ashwal, L. D., & Romer, R. L. (2015) Multiple, isotopically, heterogeneous plagioclase populations in the Bushveld Complex suggest mush intrusion. *Chemier der Erde-Geochemistry*. 75, 465-471.

Schoenberg, R., Kruger, F. J., Nagler, T. F., Meisel, T., & Kramers, J. D. (1999) PGE enrichment in chromitite layers and the merensky reef of the western Bushveld Complex; a Re-Os and Rb-Sr isotope study. *Earth and Planetary Science Letters, 172*, 49-64.

Scoates, J. S., & Friedman, R. M. (2008) Precise age of the planitiferous Merensky Reef, Bushveld Complex, South Africa, by the U-Pb zircon chemical abrasion ID-TIMS technique. *Economic Geology, 103*, 465-471.

Seabrook, C. L., Cawthorn , R. G., & Kruger, F. J. (2005) The Merensky reef, Bushveld Complex: mixing of minerals not mixing of magmas. *Economic Geology, 100*, 1191-1206.

Sharman-Harris, E. R., Kinnaird, J. A., Harris, C., & Horstmann, U. E. (2005) A new look at sulphide mineralisation of the northern limb, Bushveld Complex: a stable isotope study. *Applied Earth Science (Trans. Inst. Min. Metall. B), 114*, 252-263.

Sharpe, M. R. (1981) The chronology of magma influxes to the eastern compartment of the Bushveld Complex as exemplified by its marginal border groups. *Journal of the Geological Society of London, 138*, 307-326.

Sharpe, M. R. (1985) Strontium isotope evidence for preserved density stratification in the main zone of the Bushveld Complex, South Africa. *Nature, 316*, 119-126.

Sharpe, M. R., Evensen, N. M., & Naldrett, A. J. (1986) Sm/Nd and Rb/Sr isotopic evidence for liquid mixing, magma generation and contamination in the eastern Bushveld Complex. *Geological Society of Southern Africa*, 622-624.

Shaw, D. M. (1970) Trace element fractionation during anatexis. *Geochimica et Cosmochimica Acta*, 237-243.

Smith , J., Holwell, D., & McDonald, I. (2014) Precious and base metal geochemistry and mineralogy of the Gravally Norite-Pyroxenite-Anorthosite (GNPA) member, northern Bushveld Complex, South Africa: implications for a multistage emplacement. *Mineralium Deposita, 49*(6), 667-692.

South African Committee of Stratigraphy (SACS) (1980) *Stratigraphy of Southern Africa Part 1: Lithostratigraphy of the Republic of South Africa, Southwest Africa/Namibia and the Republics of Bophutatswana, Transkei and Venda.(*Kent, L.E., Compiler): Handbook of the Geological survey of South Africa. Government Printer, Pretoria.

Streckeisen, A. (1976) To each plutonic rock its proper name. *Earth Science Reviews, 12*, 1-33.

Tankard, A. J., Jackson, M., Eriksson, K. A., Hobday, D. K., Hunter, D. R., & Minter, W. (1982) *Crustal evolution of Southern Africa: 3,8 billion years of Earth history.* Berlin Heidelberg New york: Springer.

Tanner, D., Mavrogenes, J. A., Arculus, R. A., & Jenner, F. E. (2014) Trace element Stratigraphy of the Bellevue Core, Northern Bushveld: Multiple Magma

Injections Obscured By Diffusive Processes. *Journal of Petrology, 55*(5), 859-882.

Tepley, F. J., & Davidson, J. P. (2003) Mineral-scale Sr-isotope constraints on magma evolution and chamber dynamics in the Rum layered intrusion, Scotland. *Contributions to Mineralogy and Petrology, 145*, 628-641.

Van der Merwe, M. J. (1976) The Layered Sequence of the Potgietersrus Limb of the Bushveld Complex. *Economic Geology, 71*, 1337-1351.

Van der Merwe, M. J. (2008) The geology and structure of the Rustenburg Layered Suite in the Potgietersrus/Mokopane area of the Bushveld Complex, South Africa. *Mineralium Deposita, 43*, 405-419.

Vander Auwera, J., Longhi, J., & Clair Duchesne, J. (2000) The effect of pressure on DSr (plag/melt) and DCr (opx/melt): implications for anorthosite petrogenesis. *Earth and Planetary Science Letters, 178*, 303-314.

Walraven, F., Armstrong, R. A., & Kruger, F. J. (1990) A chronostratigraphic framework for the north-central Kaapvaal craton, the Bushveld Complex and the Vredefort Structure. *Tectonophysics, 171*, 23-48.

Wei, X., Xu, Y. G., Zhang, C. L., Zhao, J. X., & Feng, Y. X. (2014) Petrology and Sr-Nd Isotopic Disequilibrium of the Xiaohaizi Intrusion, NW China: Genesis of Layered Intrusions in the Tarim Large Igneous Province. *Journal of Petrology, 55,* 2567-2598.

Willmore, C. C., Boudreau, A. E., & Kruger, F. J. (2000) The Halogen Geochemistry of the Bushveld Complex, Republic of South Africa: Implications for Chalcophile Distribution in Lower and Critical Zones. *Journal of Petrology*, 1517-1539.

Wilson, A. H. (2015) The Earliest Stages of Emplacement of the Eastern Bushveld Complex: Development of the Lower Zone, Marginal Zone and Basal Ultramafic Sequence. *Journal of Petrology , 56*(2), 347-388.

Yang, S.-H., Maier, W. D., Lahaye, Y., & O'Brien, H. (2013) Strontium isotope disequilibrium of plagioclase in the Upper Critical Zone of the Bushveld Complex: evidence for mixing of crystal slurries. *Contributions to Mineralogy and Petrology, 166*, 959-974.

Yudovskaya, M., Kinnaird, J., Naldrett, A. J., Rodionov, N., Antonov, A., Simakin , S., & Kuzmin, D. (2013) Trace-element study and age dating of zircon from chromitites of the Bushveld Complex (South Africa). *Mineralogy and Petrology, 107*, 915-942.

Zeh, A., Ovtcharova, M., Wilson, A. H., & Schaltegger, U. (2015) The Bushveld Complex was emplaced and cooled in less than one million years-results of zirconology, and geotectonic implications. *Earth and Planetary Science Letters, 418*, 103-114.

7. Appendices

Appendix A

Table A-1: The major element composition of plagioclase per analysed spot in weight%, including the anorthite content An% of plagioclase. Depths are reported relative to the Upper Zone-Main Zone boundary in metres (m).

Depth	Sample	Plg number	POINT	SiO_2	Al_2O_3	TiO_2	MnO	FeO	MgO	CaO	Na_2O	K_2O	BaO	SrO	Total	An%
1257.7	BV 318.8	6	264	57.6	26.7	0.1	n.d.	0.3	n.d.	9.6	6.2	0.4	0.1	n.d.	101.0	45.2
1257.7		6	266	57.8	26.7	n.d.	n.d.	0.3	n.d.	9.5	6.6	0.4	n.d.	n.d.	101.2	43.5
1257.7		6	268	58.2	26.9	n.d.	n.d.	0.3	n.d.	9.6	6.7	0.4	n.d.	n.d.	102.1	43.3
1257.7		4	280	57.2	26.8	n.d.	n.d.	0.3	n.d.	9.7	6.2	0.4	n.d.	n.d.	100.6	45.3
1257.7		4	282	58.4	26.2	n.d.	n.d.	0.3	n.d.	9.2	6.7	0.4	n.d.	n.d.	101.3	42.3
1257.7		4	284	57.2	26.9	0.1	n.d.	0.2	n.d.	9.9	6.3	0.3	n.d.	n.d.	100.9	45.8
1257.7		1	288	56.8	27.0	n.d.	n.d.	0.2	n.d.	9.7	6.2	0.3	0.1	n.d.	100.3	45.5
1257.7		1	290	56.7	26.7	n.d.	n.d.	0.2	n.d.	9.7	6.3	0.4	n.d.	n.d.	100.1	45.1
1257.7		1	292	57.5	26.8	n.d.	n.d.	0.2	n.d.	9.8	5.8	0.4	n.d.	n.d.	100.6	47.2

Depth	Sample	Plg number	POINT	SiO_2	Al_2O_3	TiO_2	MnO	FeO	MgO	CaO	Na_2O	K_2O	BaO	SrO	Total	An%
1090	BV 485.8	2	304	56.8	26.9	0.1	n.d.	0.2	n.d.	9.9	5.9	0.4	n.d.	n.d.	100.1	47.0
1090		2	306	57.2	26.6	n.d.	n.d.	0.3	n.d.	9.9	6.3	0.4	0.1	n.d.	100.7	45.2
1090		2	307	57.5	26.6	n.d.	n.d.	0.2	n.d.	9.5	6.3	0.4	n.d.	n.d.	100.6	44.2
1090		1	312	57.1	26.8	n.d.	n.d.	0.2	n.d.	9.9	6.2	0.4	n.d.	n.d.	100.5	45.8
1090		1	314	57.5	26.3	0.1	n.d.	0.1	n.d.	9.3	6.7	0.4	n.d.	n.d.	100.5	42.4
1090		1	315	57.5	26.5	n.d.	n.d.	0.2	n.d.	9.5	6.5	0.4	n.d.	n.d.	100.6	43.7
1090		7	320	58.4	25.9	0.1	n.d.	0.2	n.d.	9.1	6.6	0.4	n.d.	n.d.	100.6	42.2
1090		7	322	57.9	26.4	0.1	n.d.	0.0	n.d.	9.2	6.3	0.4	n.d.	n.d.	100.2	43.8
1090		7	323	58.2	25.9	0.1	n.d.	0.2	n.d.	9.0	6.8	0.4	0.1	n.d.	100.6	41.4
904.7	BV 671.1	8	352	55.6	27.4	n.d.	n.d.	0.3	n.d.	10.6	5.7	0.3	n.d.	n.d.	99.8	49.9
904.7		8	354	55.9	27.3	0.1	n.d.	0.2	n.d.	10.5	5.8	0.3	n.d.	n.d.	100.1	49.0
904.7		8	356	56.6	27.2	n.d.	n.d.	0.2	n.d.	10.2	6.1	0.3	0.1	n.d.	100.8	47.2
904.7		4	360	56.4	27.3	0.1	n.d.	0.2	n.d.	10.4	5.9	0.3	0.1	n.d.	100.6	48.6
904.7		4	362	55.9	27.5	0.1	n.d.	0.3	n.d.	10.7	5.5	0.3	n.d.	n.d.	100.3	51.2

Depth	Sample	Plg number	POINT	SiO_2	Al_2O_3	TiO_2	MnO	FeO	MgO	CaO	Na_2O	K_2O	BaO	SrO	Total	An%
904.7		4	364	55.4	27.5	0.1	n.d.	0.1	n.d.	10.8	5.7	0.3	n.d.	n.d.	99.9	50.5
904.7		5	376	56.1	27.5	0.1	n.d.	0.3	n.d.	10.5	5.6	0.3	n.d.	n.d.	100.5	50.0
904.7		5	378	55.6	27.2	0.1	n.d.	0.2	n.d.	10.4	5.9	0.3	n.d.	n.d.	99.9	48.2
904.7		5	380	56.3	27.1	0.1	n.d.	0.4	n.d.	10.4	6.0	0.3	n.d.	n.d.	100.7	48.2
674.3	BV 901.5	1	392	54.8	28.0	0.1	n.d.	0.4	n.d.	11.2	5.3	0.3	n.d.	n.d.	100.0	53.1
674.3		1	396	54.5	28.3	0.1	n.d.	0.1	n.d.	11.8	5.3	0.2	0.1	n.d.	100.3	54.6
674.3		1	399	55.1	28.2	n.d.	n.d.	0.2	n.d.	11.4	5.2	0.3	0.1	n.d.	100.4	54.1
674.3		6	400	54.9	28.0	n.d.	n.d.	0.2	n.d.	11.2	5.2	0.4	n.d.	n.d.	100.1	53.1
674.3		6	402	55.1	28.1	n.d.	n.d.	0.3	n.d.	11.5	5.2	0.4	n.d.	n.d.	100.7	54.0
674.3		6	404	55.1	27.9	n.d.	n.d.	0.3	n.d.	11.5	5.2	0.3	n.d.	n.d.	100.5	54.1
674.3		7	416	51.4	30.2	n.d.	n.d.	0.5	n.d.	14.3	3.5	0.2	n.d.	n.d.	100.0	68.8
674.3		7	420	54.1	28.1	0.1	n.d.	0.4	n.d.	11.4	5.4	0.3	n.d.	n.d.	99.8	53.1
674.3		7	422	55.0	28.0	0.1	n.d.	0.4	n.d.	11.5	5.2	0.3	n.d.	n.d.	100.5	54.2
550.3	BV 1025	5	442	54.5	28.4	n.d.	n.d.	0.3	n.d.	11.7	5.0	0.3	n.d.	n.d.	100.1	55.6

Depth	Sample	Plg number	POINT	SiO_2	Al_2O_3	TiO_2	MnO	FeO	MgO	CaO	Na_2O	K_2O	BaO	SrO	Total	An%
550.3		5	445	54.3	27.7	0.1	n.d.	0.7	0.1	11.1	4.8	0.5	n.d.	n.d.	99.4	54.3
550.3		6	449	54.4	28.2	n.d.	n.d.	0.3	n.d.	11.6	5.1	0.3	0.1	n.d.	100.1	54.6
550.3		6	451	54.9	28.0	n.d.	n.d.	0.4	n.d.	11.5	5.0	0.3	n.d.	n.d.	100.2	54.8
550.3		6	453	55.1	27.9	0.1	n.d.	0.3	n.d.	11.3	5.1	0.2	n.d.	n.d.	100.0	54.2
550.3		2	457	54.9	27.8	0.1	n.d.	0.1	n.d.	11.7	5.0	0.4	n.d.	n.d.	100.0	55.2
550.3		2	459	55.4	27.9	n.d.	n.d.	0.3	n.d.	11.2	5.3	0.3	n.d.	n.d.	100.4	53.2
550.3		2	461	55.2	28.0	0.1	n.d.	0.2	n.d.	11.7	5.0	0.3	0.1	n.d.	100.5	55.2
457.3	BV 1118	2	469	55.0	27.9	n.d.	n.d.	0.2	n.d.	11.3	5.2	0.3	0.1	n.d.	100.0	54.0
457.3		2	470	55.4	27.9	0.1	n.d.	0.2	n.d.	11.2	5.3	0.3	n.d.	n.d.	100.4	53.2
457.3		2	472	55.1	28.0	n.d.	n.d.	0.3	n.d.	11.5	5.2	0.3	n.d.	n.d.	100.3	54.4
457.3		1	476	53.3	28.5	0.1	n.d.	0.6	0.1	12.0	4.6	0.4	n.d.	n.d.	99.7	57.4
457.3		1	474	54.3	27.5	0.1	n.d.	0.6	n.d.	10.9	5.1	0.7	n.d.	n.d.	99.3	52.2
457.3		3	497	54.2	28.3	n.d.	n.d.	0.2	n.d.	11.6	5.1	0.2	n.d.	n.d.	99.7	55.0

Depth	Sample	Plg number	POINT	SiO_2	Al_2O_3	TiO_2	MnO	FeO	MgO	CaO	Na_2O	K_2O	BaO	SrO	Total	An%
457.3		3	499	53.8	28.3	n.d.	n.d.	0.4	n.d.	12.0	4.7	0.2	n.d.	n.d.	99.5	57.7
457.3		3	501	54.0	28.6	n.d.	n.d.	0.3	n.d.	11.5	5.0	0.2	n.d.	n.d.	99.7	55.1
457.3		1	479	55.2	28.0	n.d.	n.d.	0.3	n.d.	11.5	5.1	0.3	n.d.	n.d.	100.4	54.7
273	BV 1302	3	513	54.8	28.3	0.1	n.d.	0.2	n.d.	11.8	5.2	0.3	n.d.	n.d.	100.6	54.9
273		3	517	54.6	28.3	n.d.	n.d.	0.3	n.d.	11.6	5.1	0.3	n.d.	n.d.	100.3	54.8
273		3	519	54.6	28.4	n.d.	n.d.	0.3	n.d.	11.8	5.0	0.3	n.d.	n.d.	100.5	55.8
273		5	529	54.7	28.4	0.1	n.d.	0.5	n.d.	11.8	5.1	0.3	n.d.	n.d.	100.9	55.3
273		5	531	55.5	28.3	0.1	n.d.	0.3	n.d.	11.6	5.0	0.4	n.d.	n.d.	101.2	54.9
273		5	533	55.3	27.7	0.1	n.d.	0.3	n.d.	11.0	5.3	0.3	n.d.	n.d.	100.0	52.5
273		2	537	55.3	28.1	0.1	n.d.	0.2	n.d.	11.5	5.2	0.3	n.d.	n.d.	100.6	54.5
273		2	541	54.3	29.0	0.1	n.d.	0.4	n.d.	12.5	4.8	0.2	n.d.	n.d.	101.4	58.6
15.8	BV 1560	4	585	55.5	27.8	0.1	n.d.	0.3	n.d.	11.1	5.7	0.3	n.d.	n.d.	100.8	51.2
15.8		4	588	55.9	27.4	n.d.	n.d.	0.2	n.d.	10.7	5.7	0.3	n.d.	n.d.	100.3	50.3

Depth	Sample	Plg number	POINT	SiO_2	Al_2O_3	TiO_2	MnO	FeO	MgO	CaO	Na_2O	K_2O	BaO	SrO	Total	An%
15.8		4	591	55.4	27.6	n.d.	n.d.	0.2	n.d.	10.9	5.6	0.3	n.d.	n.d.	100.1	51.1
15.8		2	609	55.0	27.9	n.d.	n.d.	0.2	n.d.	11.3	5.2	0.2	n.d.	n.d.	99.8	53.9
15.8		2	610	55.2	27.7	n.d.	n.d.	0.4	n.d.	10.9	5.5	0.2	n.d.	n.d.	99.9	51.7
15.8		2	611	55.3	27.3	n.d.	n.d.	0.2	n.d.	10.7	5.6	0.3	0.1	n.d.	99.4	50.3
15.8		2	612	55.4	27.6	n.d.	n.d.	0.2	n.d.	10.9	5.5	0.3	n.d.	n.d.	100.0	51.3
15.8		2	613	54.7	27.8	0.1	n.d.	0.3	n.d.	11.2	5.3	0.3	n.d.	n.d.	99.8	53.0
15.8		1	618	55.4	27.7	n.d.	n.d.	0.3	n.d.	10.9	5.5	0.3	n.d.	n.d.	100.2	51.5
15.8		1	621	55.2	27.7	n.d.	n.d.	0.3	n.d.	11.3	5.3	0.3	0.1	n.d.	100.3	53.2
15.8		1	623	55.1	27.4	n.d.	n.d.	0.4	n.d.	10.9	5.5	0.3	n.d.	n.d.	99.7	51.2
-151.2	BV 1727	9	625	56.5	27.6	n.d.	n.d.	0.4	n.d.	10.9	5.6	0.4	n.d.	n.d.	101.4	50.9
-151.2		9	628	54.8	27.8	0.1	n.d.	0.2	n.d.	11.2	5.4	0.4	n.d.	n.d.	99.8	52.2
-151.2		9	631	55.3	27.1	0.1	n.d.	0.3	n.d.	11.3	5.3	0.4	n.d.	n.d.	99.8	53.1
-151.2		8	641	55.5	27.7	n.d.	n.d.	0.4	n.d.	11.2	5.3	0.4	n.d.	n.d.	100.6	52.7
-151.2		8	644	55.5	27.6	0.1	n.d.	0.4	n.d.	10.8	5.6	0.4	n.d.	n.d.	100.5	50.4

Depth	Sample	Plg number	POINT	SiO_2	Al_2O_3	TiO_2	MnO	FeO	MgO	CaO	Na_2O	K_2O	BaO	SrO	Total	An%
-151.2		8	647	56.5	27.4	0.1	n.d.	0.3	n.d.	10.9	5.4	0.4	n.d.	n.d.	101.0	51.4
-151.2		7	657	55.0	27.8	n.d.	n.d.	0.5	n.d.	11.1	5.3	0.4	n.d.	n.d.	100.0	52.6
-151.2		7	661	55.4	28.0	0.1	n.d.	0.4	n.d.	10.9	5.4	0.4	n.d.	n.d.	100.6	51.9
-151.2		7	663	55.2	27.1	n.d.	n.d.	0.5	n.d.	10.9	5.3	0.4	n.d.	n.d.	99.5	52.1
-191.2	BV 1767	6	665	55.0	27.9	0.1	n.d.	0.3	n.d.	11.2	5.5	0.3	n.d.	n.d.	100.3	52.1
-191.2		6	667	54.4	27.9	0.1	n.d.	0.2	n.d.	11.3	5.3	0.3	n.d.	n.d.	99.5	53.1
-191.2		6	669	55.7	28.2	n.d.	n.d.	0.3	n.d.	11.3	5.3	0.3	n.d.	n.d.	101.2	53.0
-191.2		3	673	55.4	27.4	n.d.	n.d.	0.3	n.d.	11.2	5.4	0.3	n.d.	n.d.	100.1	52.4
-191.2		3	675	55.7	27.9	n.d.	n.d.	0.3	n.d.	11.1	5.6	0.3	n.d.	n.d.	101.0	51.2
-191.2		3	677	55.0	27.6	n.d.	n.d.	0.4	n.d.	10.9	5.5	0.3	n.d.	n.d.	99.8	51.4
-191.2		4	697	55.4	27.9	n.d.	n.d.	0.3	n.d.	11.1	5.5	0.4	n.d.	n.d.	100.6	51.7
-191.2		4	699	55.2	27.3	n.d.	n.d.	0.4	n.d.	11.1	5.3	0.4	0.1	n.d.	99.7	52.5
-191.2		4	701	55.3	27.9	0.1	n.d.	0.3	n.d.	11.0	5.4	0.3	n.d.	n.d.	100.3	52.2
-641.6	BV 2217	1	785	53.1	28.8	n.d.	n.d.	0.2	n.d.	12.5	4.5	0.2	n.d.	n.d.	99.3	60.1

Depth	Sample	Plg number	POINT	SiO_2	Al_2O_3	TiO_2	MnO	FeO	MgO	CaO	Na_2O	K_2O	BaO	SrO	Total	An%
-641.6		1	787	52.9	29.2	n.d.	n.d.	0.3	n.d.	13.1	4.2	0.2	n.d.	n.d.	100.0	62.5
-641.6		1b	797	53.5	28.7	n.d.	n.d.	0.3	n.d.	12.3	4.6	0.2	n.d.	n.d.	99.6	58.8
-641.6		7	809	54.1	28.8	n.d.	n.d.	0.3	n.d.	12.6	4.6	0.3	n.d.	n.d.	100.7	59.3
-641.6		7	811	53.5	29.1	n.d.	n.d.	0.1	n.d.	12.6	4.5	0.2	0.1	n.d.	100.2	59.8
-641.6		7	813	53.5	28.9	n.d.	n.d.	0.3	n.d.	12.4	4.7	0.2	n.d.	n.d.	100.2	58.5
-1037	BV 2612	7	833	50.9	31.1	n.d.	n.d.	0.2	n.d.	14.9	3.3	0.2	n.d.	n.d.	100.6	70.8
-1037		7	837	51.1	31.0	n.d.	n.d.	0.2	n.d.	14.6	3.2	0.1	n.d.	n.d.	100.2	70.8
-1037		7	839	50.6	30.4	0.1	n.d.	0.2	n.d.	14.4	3.3	0.1	n.d.	n.d.	99.0	70.3
-1037		6	841	51.8	30.7	0.1	n.d.	0.3	n.d.	14.2	3.6	0.2	n.d.	n.d.	100.9	67.9
-1037		6	845	49.7	31.3	0.1	n.d.	0.1	n.d.	15.3	2.9	0.1	n.d.	n.d.	99.5	73.9
-1037		6	847+843	50.4	31.0	n.d.	n.d.	0.1	n.d.	15.1	3.1	0.1	n.d.	n.d.	99.9	72.4
-1037		1	851	50.8	31.0	n.d.	n.d.	0.1	n.d.	14.8	3.0	0.1	n.d.	n.d.	99.9	72.3
-1037		1	853	51.9	30.5	0.1	n.d.	0.1	n.d.	14.4	3.6	0.1	n.d.	n.d.	100.8	68.3
-1037		1	857	51.4	30.9	n.d.	n.d.	0.2	n.d.	14.3	3.4	0.1	n.d.	n.d.	100.4	69.1

Depth	Sample	Plg number	POINT	SiO_2	Al_2O_3	TiO_2	MnO	FeO	MgO	CaO	Na_2O	K_2O	BaO	SrO	Total	An%
-1353	BV 2929	4	1057	50.1	31.1	n.d.	n.d.	0.4	n.d.	15.4	2.9	0.1	n.d.	n.d.	100.1	74.3
-1353		4	1061	50.2	31.6	n.d.	n.d.	0.3	n.d.	15.4	2.8	0.1	n.d.	n.d.	100.6	74.5
-1353		4	1063	49.5	31.5	n.d.	n.d.	0.5	n.d.	15.3	2.8	0.1	n.d.	n.d.	99.8	74.6
-1353		1	1073	50.2	31.6	0.1	n.d.	0.3	n.d.	15.4	2.9	0.1	0.1	n.d.	100.7	74.0
-1353		1	1077	49.9	31.7	0.1	n.d.	0.6	n.d.	15.7	2.5	0.1	n.d.	n.d.	100.6	77.1
-1353		1	1079	50.5	31.2	n.d.	n.d.	0.2	n.d.	15.3	3.1	0.1	n.d.	n.d.	100.6	72.6
-1353		6	1082	50.4	31.8	n.d.	n.d.	0.3	n.d.	15.6	2.8	0.1	n.d.	n.d.	101.0	75.2
-1353		6	1083	50.4	31.5	n.d.	n.d.	0.4	n.d.	15.3	2.9	0.1	n.d.	n.d.	100.8	73.6
-1353		6	1085	50.1	31.7	n.d.	n.d.	0.4	n.d.	15.4	2.7	0.1	n.d.	n.d.	100.5	75.8
-1910	MO 46.5	5	9	52.8	29.1	n.d.	n.d.	0.2	n.d.	12.9	4.3	0.2	n.d.	n.d.	99.6	61.9
-1910		5	11	52.7	29.7	0.1	n.d.	0.4	n.d.	12.9	3.9	0.2	n.d.	n.d.	99.9	63.9
-1910		5	13	52.3	29.1	n.d.	n.d.	0.4	n.d.	12.8	4.1	0.2	n.d.	n.d.	99.0	62.6
-1910		2	25	52.9	29.1	0.1	n.d.	0.3	n.d.	13.1	4.2	0.2	n.d.	n.d.	99.8	62.8
-1910		2	27	52.6	29.3	0.1	n.d.	0.4	n.d.	12.7	4.2	0.3	n.d.	n.d.	99.4	61.7

Depth	Sample	Plg number	POINT	SiO_2	Al_2O_3	TiO_2	MnO	FeO	MgO	CaO	Na_2O	K_2O	BaO	SrO	Total	An%
-1910		2	29	52.2	29.3	0.1	n.d.	0.2	n.d.	13.3	4.0	0.2	n.d.	n.d.	99.3	63.9
-1910		1	33	53.3	28.9	0.1	n.d.	0.6	n.d.	12.7	4.4	0.2	n.d.	n.d.	100.2	60.5
-1910		1	35	52.7	29.1	0.1	n.d.	0.4	n.d.	12.8	4.2	0.3	n.d.	n.d.	99.6	61.7
-1910		1	37	52.3	29.6	0.1	n.d.	0.3	n.d.	13.3	3.9	0.2	n.d.	n.d.	99.8	64.5
-1973	MO 109	3	65	52.1	29.5	n.d.	n.d.	0.3	n.d.	13.4	4.0	0.2	n.d.	n.d.	99.4	64.2
-1973		3	67	51.3	30.8	n.d.	n.d.	0.6	n.d.	14.8	3.1	0.2	n.d.	n.d.	100.9	71.8
-1973		3	69	52.5	30.4	n.d.	n.d.	0.4	n.d.	14.0	3.6	0.2	n.d.	n.d.	101.1	67.8
-1973		4	74	52.2	30.3	n.d.	n.d.	0.6	n.d.	14.3	3.7	0.2	0.1	n.d.	101.4	67.7
-1973		4	77	52.1	30.1	0.2	n.d.	0.6	n.d.	13.6	3.6	0.2	n.d.	n.d.	100.4	66.9
-1973		4	79	52.5	30.0	n.d.	n.d.	0.3	n.d.	13.9	4.0	0.2	n.d.	n.d.	100.9	65.2
-1973		2	81	52.8	29.8	n.d.	n.d.	0.4	n.d.	13.4	4.0	0.1	n.d.	n.d.	100.6	64.2
-1973		2	83	51.0	29.8	n.d.	n.d.	0.5	n.d.	14.1	3.5	0.2	n.d.	n.d.	99.1	68.2
-1973		2	85	52.1	30.2	n.d.	n.d.	0.4	n.d.	13.9	3.7	0.2	n.d.	n.d.	100.6	66.6
-2037	MO 172	8	129	52.9	29.5	n.d.	n.d.	0.4	n.d.	13.2	4.3	0.2	n.d.	n.d.	100.5	62.3

Depth	Sample	Plg number	POINT	SiO_2	Al_2O_3	TiO_2	n.d.	FeO	MgO	CaO	Na_2O	K_2O	BaO	SrO	Total	An%
-2037		8	133	51.7	30.5	n.d.	n.d.	0.4	n.d.	14.3	3.6	0.2	n.d.	n.d.	100.7	68.2
-2037		8	135	53.0	29.4	0.1	n.d.	0.3	n.d.	13.0	4.2	0.3	n.d.	n.d.	100.4	62.1
-2037		4	137	52.9	29.5	0.1	n.d.	0.4	n.d.	13.3	4.0	0.3	n.d.	n.d.	100.6	63.8
-2037		4	141	51.7	30.3	n.d.	n.d.	0.3	n.d.	14.1	3.4	0.2	n.d.	n.d.	100.2	68.8
-2037		7	145	52.3	29.5	0.1	n.d.	0.4	n.d.	12.9	4.0	0.2	n.d.	n.d.	99.5	63.0
-2037		7	149	51.8	30.9	n.d.	n.d.	0.3	n.d.	14.5	3.4	0.2	n.d.	n.d.	101.2	69.3
-2037		7	151	51.0	30.8	n.d.	n.d.	0.2	n.d.	14.5	3.4	0.2	n.d.	n.d.	100.2	69.4
-2037		4	139	53.2	30.2	n.d.	n.d.	0.4	n.d.	13.6	3.9	0.3	n.d.	n.d.	101.6	65.0
-2070	MO 206	7	169	51.4	29.8	n.d.	n.d.	0.3	n.d.	13.7	3.6	0.2	n.d.	n.d.	99.0	67.0
-2070		7	173	51.4	29.5	n.d.	n.d.	0.5	n.d.	13.6	3.8	0.2	0.1	n.d.	99.2	65.6
-2070		7	175	51.4	29.6	n.d.	n.d.	0.5	n.d.	13.8	3.4	0.2	n.d.	n.d.	99.1	68.0
-2070		1	177	50.6	28.3	n.d.	n.d.	2.3	1.5	12.1	3.4	0.3	n.d.	n.d.	98.5	64.9
-2070		1	179	51.5	29.6	n.d.	n.d.	0.2	n.d.	13.8	3.7	0.2	n.d.	n.d.	99.0	66.7
-2070		1	181	50.2	30.0	0.1	n.d.	0.4	n.d.	14.3	3.2	0.2	n.d.	n.d.	98.4	70.4

Depth	Sample	Plg number	POINT	SiO_2	Al_2O_3	TiO_2	MnO	FeO	MgO	CaO	Na_2O	K_2O	BaO	SrO	Total	An%
-2070		2	185	51.1	29.7	0.1	n.d.	0.3	n.d.	13.8	3.6	0.1	n.d.	n.d.	98.8	67.3
-2070		2	189	51.0	29.9	n.d.	n.d.	0.4	n.d.	13.8	3.5	0.2	n.d.	n.d.	98.9	67.6
-2070		2	191	51.7	29.2	n.d.	n.d.	0.4	n.d.	13.2	3.8	0.3	n.d.	n.d.	98.5	64.7
-2248	MO 384	4	209	52.0	30.1	n.d.	n.d.	0.5	n.d.	13.9	3.6	0.2	n.d.	n.d.	100.4	67.5
-2248		4	213	50.9	30.8	n.d.	n.d.	0.5	n.d.	14.6	3.2	0.1	n.d.	n.d.	100.2	71.0
-2248		4	215	50.7	30.9	0.1	n.d.	0.3	n.d.	14.7	3.2	0.2	n.d.	n.d.	100.1	71.0
-2248		2	217	51.2	30.5	n.d.	n.d.	0.3	n.d.	14.2	3.6	0.1	n.d.	n.d.	100.0	67.9
-2248		2	219	50.7	30.4	n.d.	n.d.	0.3	n.d.	14.5	3.3	0.1	n.d.	n.d.	99.4	70.1
-2248		2	221	50.9	30.6	n.d.	n.d.	0.5	n.d.	14.7	3.4	0.1	n.d.	n.d.	100.3	70.1
-2248		1	225	51.7	30.7	0.1	n.d.	0.3	n.d.	14.2	3.6	0.2	n.d.	n.d.	100.8	67.8
-2248		1	227	51.2	31.0	n.d.	n.d.	0.3	n.d.	14.4	3.4	0.1	0.1	n.d.	100.4	70.1
-2248		1	229	50.9	30.9	n.d.	n.d.	0.4	n.d.	14.6	3.2	0.1	0.1	n.d.	100.2	71.3
-2382		1	290	51.3	29.9	n.d.	n.d.	0.4	n.d.	13.7	3.5	0.2	n.d.	n.d.	99.1	67.2

Depth	Sample	Plg number	POINT	SiO_2	Al_2O_3	TiO_2	MnO	FeO	MgO	CaO	Na_2O	K_2O	BaO	SrO	Total	An%
-2382		1	291	52.7	29.2	n.d.	n.d.	0.3	n.d.	13.0	4.0	0.3	0.1	n.d.	99.6	63.3
-2382		1	293	49.8	31.1	n.d.	n.d.	0.4	n.d.	15.1	2.8	0.1	n.d.	n.d.	99.3	74.8
-2382		4	313	51.4	29.4	0.1	n.d.	0.3	n.d.	13.3	3.9	0.2	n.d.	n.d.	98.7	64.5
-2382		4	315	49.9	30.5	n.d.	n.d.	0.3	n.d.	14.8	3.1	0.1	n.d.	n.d.	98.8	72.3
-2382		4	316	49.9	30.3	n.d.	n.d.	0.4	n.d.	14.5	3.1	0.2	n.d.	n.d.	98.5	71.8
-2451	MO 587	4	9	51.1	31.1	0.1	n.d.	0.4	n.d.	15.0	2.9	0.1	n.d.	n.d.	100.7	73.8
-2451		4	11	51.4	30.2	n.d.	n.d.	0.2	n.d.	14.2	3.5	0.2	n.d.	n.d.	99.6	68.6
-2451		4	13	51.1	31.1	n.d.	n.d.	0.2	n.d.	15.1	3.0	0.1	n.d.	n.d.	100.7	72.9
-2451		8	25	51.5	31.0	n.d.	n.d.	0.2	n.d.	14.7	3.2	0.1	0.1	n.d.	100.8	71.4
-2451		8	29	50.2	31.4	n.d.	n.d.	0.3	n.d.	15.5	2.8	0.1	n.d.	n.d.	100.3	74.8
-2451		8	31	51.4	30.9	0.1	n.d.	0.2	n.d.	14.8	3.1	0.2	n.d.	n.d.	100.6	72.0
-2451		1	34	51.1	30.5	n.d.	n.d.	0.2	n.d.	14.8	3.3	0.2	n.d.	n.d.	100.2	71.0
-2451		1	36	50.8	31.3	n.d.	n.d.	0.2	n.d.	15.0	2.9	0.2	n.d.	n.d.	100.4	73.2
-2451		1	37	50.9	31.0	n.d.	n.d.	0.2	n.d.	15.1	2.9	0.1	n.d.	n.d.	100.3	73.9

Depth	Sample	Plg number	POINT	SiO_2	Al_2O_3	TiO_2	MnO	FeO	MgO	CaO	Na_2O	K_2O	BaO	SrO	Total	An%
-2583	MO 719	4	49	52.7	29.6	n.d.	n.d.	0.3	n.d.	13.1	4.1	0.2	n.d.	n.d.	100.0	63.1
-2583		4	51	49.8	31.1	n.d.	n.d.	0.4	n.d.	15.2	2.9	0.1	n.d.	n.d.	99.6	74.0
-2583		4	53	52.1	29.9	n.d.	n.d.	0.3	n.d.	13.5	3.9	0.3	n.d.	n.d.	100.1	64.8
-2583		7	57	52.2	30.1	n.d.	n.d.	0.4	n.d.	13.6	3.9	0.2	0.1	n.d.	100.5	65.3
-2583		7	59	50.6	25.3	0.1	n.d.	0.2	n.d.	10.0	4.4	0.1	n.d.	n.d.	90.7	55.2
-2583		7	61	51.6	30.5	0.1	n.d.	0.3	n.d.	14.0	3.7	0.2	n.d.	n.d.	100.3	67.0
-2583		6	70	51.3	30.2	n.d.	n.d.	0.4	n.d.	14.2	3.4	0.2	n.d.	n.d.	99.7	68.9
-2583		6	71	52.5	30.1	0.1	n.d.	0.3	n.d.	13.6	3.8	0.2	0.1	n.d.	100.7	65.7
-2583		6	72	51.7	30.4	n.d.	n.d.	0.2	n.d.	13.8	3.6	0.1	n.d.	n.d.	99.9	67.7
-2714	MO 850	2	81	52.9	30.0	n.d.	n.d.	0.4	n.d.	13.8	4.0	0.2	n.d.	n.d.	101.4	65.3
-2714		2	85	52.3	29.7	n.d.	n.d.	0.2	n.d.	13.5	3.8	0.2	n.d.	n.d.	99.6	65.4
-2714		2	87	54.9	27.9	n.d.	n.d.	0.3	n.d.	10.9	5.3	0.2	n.d.	n.d.	99.5	52.7
-2714		5	97	50.2	31.2	0.1	n.d.	0.4	n.d.	14.9	3.1	0.1	n.d.	n.d.	100.0	72.5
-2714		5	101	52.4	29.7	0.1	n.d.	0.3	n.d.	13.6	4.0	0.2	n.d.	n.d.	100.2	64.6

Depth	Sample	Plg number	POINT	SiO_2	Al_2O_3	TiO_2	MnO	FeO	MgO	CaO	Na_2O	K_2O	BaO	SrO	Total	An%
-2714		5	103	50.0	30.9	n.d.	n.d.	0.3	n.d.	15.3	2.9	0.1	n.d.	n.d.	99.5	74.0
-2714		8	105	50.1	30.6	n.d.	n.d.	0.4	n.d.	14.9	3.1	0.1	n.d.	n.d.	99.2	72.4
-2714		8	106.5	51.3	30.1	n.d.	n.d.	0.3	n.d.	14.1	3.5	0.2	0.1	n.d.	99.5	68.7
-2714		8	108	51.2	29.6	n.d.	n.d.	0.4	n.d.	14.2	3.6	0.2	0.1	n.d.	99.3	67.6
-2854	MO 990	6	129	51.6	30.5	n.d.	n.d.	0.3	n.d.	14.4	3.5	0.2	n.d.	n.d.	100.5	68.5
-2854		6	133	51.3	31.0	n.d.	n.d.	0.3	n.d.	14.8	3.2	0.2	0.1	n.d.	100.8	71.3
-2854		6	135	51.4	31.6	n.d.	n.d.	0.3	n.d.	15.0	3.1	0.2	n.d.	n.d.	101.5	71.9
-2854		7	137	53.7	29.7	0.1	n.d.	0.3	n.d.	13.3	4.3	0.2	n.d.	n.d.	101.5	62.6
-2854		7	141	53.0	29.3	0.1	n.d.	0.3	n.d.	13.1	4.4	0.2	n.d.	n.d.	100.5	61.3
-2854		3	147	52.1	30.3	n.d.	n.d.	0.2	n.d.	13.6	3.9	0.2	n.d.	n.d.	100.4	65.2
-2854		3	149	53.1	29.2	n.d.	n.d.	0.4	n.d.	12.8	4.4	0.2	n.d.	n.d.	100.2	61.0
-2854		3	145	51.5	31.2	n.d.	n.d.	0.1	n.d.	14.9	3.3	0.1	n.d.	n.d.	101.2	70.8
-3013	MO 1149	4	193	50.8	30.0	n.d.	n.d.	0.4	n.d.	14.2	3.4	0.2	n.d.	n.d.	99.1	69.0
-3013		4	195	50.0	30.6	n.d.	n.d.	0.3	n.d.	14.8	3.0	0.2	n.d.	n.d.	99.0	72.0

Depth	Sample	Plg number	POINT	SiO_2	Al_2O_3	TiO_2	MnO	FeO	MgO	CaO	Na_2O	K_2O	BaO	SrO	Total	An%
-3013		4	197	50.0	30.6	n.d.	n.d.	0.3	n.d.	15.0	2.9	0.1	n.d.	n.d.	99.0	73.6
-3013		2	200	49.1	30.5	n.d.	n.d.	0.4	n.d.	14.7	2.7	0.2	n.d.	n.d.	97.5	74.6
-3013		2	202	50.2	30.3	n.d.	n.d.	0.3	n.d.	14.9	2.9	0.2	n.d.	n.d.	98.8	73.2
-3013		2	204	49.6	30.4	n.d.	n.d.	0.4	n.d.	15.0	2.9	0.1	n.d.	n.d.	98.5	73.8
-3013		7	224	51.3	29.7	n.d.	n.d.	0.5	n.d.	13.2	3.7	0.5	n.d.	n.d.	99.0	64.3
-3013		7	226	49.2	30.5	n.d.	n.d.	0.3	n.d.	14.8	3.0	0.2	n.d.	n.d.	98.0	72.5
-3013		7	228	49.4	30.3	n.d.	n.d.	0.4	n.d.	14.9	2.7	0.1	n.d.	n.d.	97.9	74.6
-3147	MO 1283	5	1017	52.7	29.0	n.d.	n.d.	0.4	n.d.	13.0	4.1	0.3	n.d.	n.d.	99.5	62.6
-3147		5	1020	52.8	29.2	n.d.	n.d.	0.2	n.d.	13.1	4.1	0.3	n.d.	n.d.	99.8	62.6
-3147		2	1025	51.5	30.4	n.d.	n.d.	0.3	n.d.	14.1	3.5	0.1	n.d.	n.d.	99.9	68.8
-3147		2	1027	51.9	30.5	n.d.	n.d.	0.2	n.d.	14.3	3.6	0.2	n.d.	n.d.	100.7	68.4
-3147		2	1029	52.5	29.6	n.d.	n.d.	0.3	n.d.	13.3	3.9	0.2	n.d.	n.d.	99.7	64.8
-3147		1	1033	49.7	31.1	n.d.	n.d.	0.3	n.d.	15.5	2.7	0.1	n.d.	n.d.	99.5	75.8

Depth	Sample	Plg number	POINT	SiO_2	Al_2O_3	TiO_2	MnO	FeO	MgO	CaO	Na_2O	K_2O	BaO	SrO	Total	An%
-3147		1	1035	51.8	29.8	n.d.	n.d.	0.4	n.d.	13.9	3.7	0.2	n.d.	n.d.	99.8	66.5
-3147		1	1037	49.6	31.0	n.d.	n.d.	0.3	n.d.	15.4	2.6	0.1	0.1	n.d.	99.0	75.9
-3201	MO 1337	4	945	52.0	30.1	n.d.	n.d.	0.4	n.d.	14.3	3.6	0.1	n.d.	n.d.	100.7	67.8
-3201		4	947.5	52.3	29.9	n.d.	n.d.	0.3	n.d.	14.3	3.5	0.2	n.d.	n.d.	100.6	68.8
-3201		4	949	51.9	30.3	n.d.	n.d.	0.3	n.d.	14.4	3.4	0.2	n.d.	n.d.	100.6	69.2
-3201		1	953	50.7	30.9	n.d.	n.d.	0.4	n.d.	15.0	3.0	0.1	n.d.	n.d.	100.2	72.5
-3201		1	955	50.9	30.9	n.d.	n.d.	0.4	n.d.	14.8	3.1	0.2	n.d.	n.d.	100.3	71.9
-3201		1	957	51.5	30.4	n.d.	0.1	0.3	n.d.	14.2	3.6	0.1	n.d.	n.d.	100.1	68.3
-3201		6	969	51.7	30.5	n.d.	n.d.	0.4	n.d.	14.4	3.5	0.2	n.d.	n.d.	100.7	68.9
-3201		6	971	50.7	31.2	n.d.	n.d.	0.4	n.d.	15.4	3.0	0.1	n.d.	n.d.	100.9	73.7
-3201		6	972	50.3	31.4	n.d.	n.d.	0.5	n.d.	15.4	2.7	0.1	n.d.	n.d.	100.5	75.2
-3210	MO 1346	4	978	50.6	30.6	n.d.	n.d.	0.3	n.d.	14.5	3.1	0.2	n.d.	n.d.	99.3	71.4
-3210		4	980	51.6	30.2	n.d.	n.d.	0.2	n.d.	14.3	3.6	0.2	n.d.	n.d.	100.2	68.1
-3210		4	981	50.8	31.0	n.d.	n.d.	0.4	n.d.	14.8	3.1	0.2	n.d.	n.d.	100.5	71.9

Depth	Sample	Plg number	POINT	SiO_2	Al_2O_3	TiO_2	MnO	FeO	MgO	CaO	Na_2O	K_2O	BaO	SrO	Total	An%
-3210		1	985	51.9	30.4	n.d.	n.d.	0.3	n.d.	14.0	3.7	0.2	n.d.	n.d.	100.4	67.2
-3210		1	988	50.5	31.0	n.d.	n.d.	0.3	n.d.	14.9	3.0	0.2	n.d.	n.d.	99.8	73.0
-3210		1	991	51.7	30.2	n.d.	n.d.	0.2	n.d.	14.2	3.5	0.2	n.d.	n.d.	100.1	68.2
-3210		3	1001	51.0	30.4	n.d.	n.d.	0.4	n.d.	14.0	3.5	0.2	n.d.	n.d.	99.5	68.5
-3210		3	1003	52.0	30.3	n.d.	n.d.	0.2	n.d.	14.1	3.6	0.2	n.d.	n.d.	100.4	67.8
-3210		3	1005	50.7	30.7	0.1	n.d.	0.4	n.d.	14.8	3.1	0.2	n.d.	n.d.	99.8	72.0

Appendix B

Table B-1: The Sr-isotopic composition of plagioclase per analysed spot. Depths are reported relative to the Upper Zone-Main Zone boundary in metres (m). Initial $^{87}Sr/^{86}Sr$ ratios calculated using the decay constant of Nebel *et al*. (2011) at an age 2054.4 Ma (Scoates & Friedman, 2008).

Depth	Sample	Plg number	Point	Texture	Interval	Core/Rim	$^{87}Sr/^{86}Sr$	$^{87}Rb/^{86}Sr$	$^{87}Sr/^{86}Sr$ i	2SE
1257.7	BV 318.84	6	264	Eu	UZ	RIM	0.70808	0.01553	0.70763	1.31E-04
1257.7		6	266	Eu	UZ	CORE	0.70795	0.02857	0.70713	1.94E-04
1257.7		6	268	Eu	UZ	RIM	0.70756	0.00998	0.70727	1.02E-04
1257.7		4	280	Eu	UZ	RIM	0.70788	0.01161	0.70755	8.16E-05
1257.7		4	282	Eu	UZ	CORE	0.70782	0.02610	0.70706	1.66E-04
1257.7		4	284	Eu	UZ	RIM	0.70765	0.00808	0.70741	6.66E-05
1257.7		1	288	Eu	UZ	RIM	0.70770	0.01878	0.70715	7.90E-05
1257.7		1	290	Eu	UZ	CORE	0.70747	0.00882	0.70722	1.76E-04
1257.7		1	292	Eu	UZ	RIM	0.70738	0.00589	0.70720	1.07E-04
1090.0	BV 485.78	2	304	Eu	UZ	RIM	0.70758	0.01214	0.70723	5.93E-05

Depth	Sample	Plg number	Point	Texture	Interval	Core/Rim	$^{87}Sr/^{86}Sr$	$^{87}Rb/^{86}Sr$	$^{87}Sr/^{86}Sr$ i	2SE
1090		2	306	Eu	UZ	CORE	0.70739	0.00519	0.70724	6.44E-05
1090		2	307	Eu	UZ	RIM	0.70760	0.01243	0.70724	1.06E-04
1090		1	314	Eu	UZ	CORE	0.70755	0.00830	0.70731	7.14E-05
1090		1	315	Eu	UZ	RIM	0.70811	0.02902	0.70726	1.04E-04
1090		7	320	Eu	UZ	RIM	0.70767	0.01253	0.70730	1.06E-04
1090		7	322	Eu	UZ	CORE	0.70756	0.01094	0.70724	1.16E-04
1090		7	323	Eu	UZ	RIM	0.70754	0.00254	0.70747	5.83E-05
904.7	BV 671.08	8	352	Eu	UZ	RIM	0.70733	0.00135	0.70729	1.09E-04
904.7		8	354	Eu	UZ	CORE	0.70758	0.00105	0.70755	3.76E-05
904.7		8	356	Eu	UZ	RIM	0.70766	0.00240	0.70759	5.45E-05
904.7		4	360	S-eu	UZ	RIM	0.70782	0.00189	0.70776	5.91E-05
904.7		4	362	S-eu	UZ	CORE	0.70759	0.00143	0.70755	6.27E-05
904.7		4	364	S-eu	UZ	RIM	0.70777	0.00368	0.70766	7.36E-05
904.7		5	376	Eu	UZ	RIM	0.70720	0.00106	0.70717	1.13E-04
904.7		5	378	Eu	UZ	CORE	0.70748	0.00488	0.70734	1.32E-04

Depth	Sample	Plg number	Point	Texture	Interval	Core/Rim	$^{87}Sr/^{86}Sr$	$^{87}Rb/^{86}Sr$	$^{87}Sr/^{86}Sr$ i	2SE
904.7		5	380	Eu	UZ	RIM	0.70753	0.00139	0.70749	7.33E-05
674.3	BV 901.54	1	392	Eu	UZ	RIM	0.70725	0.00158	0.70721	7.91E-05
674.3		1	396	Eu	UZ	RIM	0.70785	0.02720	0.70706	3.51E-04
674.3		1	399	Eu	UZ	CORE	0.70719	0.00094	0.70716	6.28E-05
674.3		6	400	S-eu	UZ	RIM	0.70747	0.01365	0.70708	1.50E-04
674.3		6	402	S-eu	UZ	CORE	0.70714	0.00538	0.70698	6.05E-05
674.3		6	404	S-eu	UZ	RIM	0.70730	0.00623	0.70712	7.80E-05
674.3		7	416	Eu	UZ	RIM	0.70745	0.02069	0.70685	8.81E-05
674.3		7	420	Eu	UZ	RIM	0.70719	0.00408	0.70707	8.60E-05
674.3		7	422	Eu	UZ	CORE	0.70786	0.03337	0.70689	1.37E-04
550.3	BV 1025.5	5	442	S-eu	UZ	RIM	0.70705	0.00616	0.70687	7.05E-05
550.3		5	443	S-eu	UZ	CORE	0.70795	0.02764	0.70715	2.48E-04
550.3		5	445	S-eu	UZ	RIM	0.70720	0.00607	0.70703	5.67E-05
550.3		6	449	Eu	UZ	RIM	0.70705	0.00677	0.70685	1.16E-04
550.3		6	451	Eu	UZ	CORE	0.70815	0.04311	0.70690	1.47E-04

Depth	Sample	Plg number	Point	Texture	Interval	Core/Rim	$^{87}Sr/^{86}Sr$	$^{87}Rb/^{86}Sr$	$^{87}Sr/^{86}Sr$ i	2SE
550.3		6	453	Eu	UZ	RIM	0.70999	0.12702	0.70630	2.09E-04
550.3		2	457	S-eu	UZ	RIM	0.70728	0.00736	0.70706	8.81E-05
550.3		2	459	S-eu	UZ	CORE	0.71121	0.15194	0.70680	4.41E-04
550.3		2	461	S-eu	UZ	RIM	0.70824	0.05773	0.70656	2.26E-04
457.3	BV 1118.5	2	469	Eu	UZ	RIM	0.70747	0.00212	0.70741	5.58E-05
457.3		2	470	Eu	UZ	CORE	0.70746	0.00337	0.70736	6.41E-05
457.3		2	472	Eu	UZ	RIM	0.70727	0.00179	0.70722	1.04E-04
457.3		1	476	Eu	UZ	RIM	0.70771	0.01137	0.70738	9.86E-05
457.3		1	479	Eu	UZ	RIM	0.70781	0.02320	0.70713	9.71E-05
457.3		3	497	Eu	UZ	RIM	0.70735	0.00215	0.70729	4.65E-05
457.3		3	499	Eu	UZ	CORE	0.70741	0.00563	0.70725	4.19E-05
457.3		3	501	Eu	UZ	RIM	0.70745	0.00477	0.70731	9.37E-05
457.3		1	479R	Eu	UZ	CORE	0.70807	0.02649	0.70730	9.77E-05
273	BV 1302.8	3	517	S-eu	UZ	RIM	0.70755	0.01148	0.70721	9.22E-05
273		3	519	S-eu	UZ	CORE	0.70770	0.01133	0.70738	1.24E-04

Depth	Sample	Plg number	Point	Texture	Interval	Core/Rim	$^{87}Sr/^{86}Sr$	$^{87}Rb/^{86}Sr$	$^{87}Sr/^{86}Sr$ i	2SE
273		5	529	Eu	UZ	RIM	0.70757	0.00433	0.70744	7.22E-05
273		5	531	Eu	UZ	CORE	0.70770	0.00539	0.70754	6.78E-05
273		5	533	Eu	UZ	RIM	0.70766	0.00611	0.70749	5.54E-05
273		2	537	Eu	UZ	RIM	0.70759	0.00678	0.70739	6.20E-05
273		2	541	Eu	UZ	RIM	0.70804	0.00632	0.70786	2.42E-04
273		2	549	Eu	UZ	CORE	0.70775	0.01139	0.70742	4.52E-05
15.8	BV 1560	4	585	Eu	UZ	RIM	0.70766	0.01102	0.70734	1.08E-04
15.8		4	588	Eu	UZ	CORE	0.70806	0.02462	0.70734	1.21E-04
15.8		4	591	Eu	UZ	RIM	0.70746	0.00490	0.70732	6.52E-05
15.8		2	609	Eu	UZ	RIM	0.70761	0.00821	0.70737	6.62E-05
15.8		2	610	Eu	UZ	RIM	0.70836	0.04022	0.70720	2.28E-04
15.8		2	611	Eu	UZ	CORE	0.70873	0.04684	0.70737	2.38E-04
15.8		2	612	Eu	UZ	RIM	0.70770	0.01916	0.70714	7.83E-05
15.8		2	613	Eu	UZ	RIM	0.70737	0.00468	0.70723	6.92E-05
15.8		1	618	S-eu	UZ	RIM	0.70755	0.00528	0.70740	5.90E-05

Depth	Sample	Plg number	Point	Texture	Interval	Core/Rim	$^{87}Sr/^{86}Sr$	$^{87}Rb/^{86}Sr$	$^{87}Sr/^{86}Sr$ i	2SE
15.8		1	621	S-eu	UZ	RIM	0.70742	0.00457	0.70728	6.89E-05
15.8		1	623	S-eu	UZ	CORE	0.70794	0.02821	0.70712	1.36E-04
-151.2	BV 1727	9	625	Eu	UMZ	RIM	0.70748	0.00868	0.70723	1.08E-04
-151.2		9	628	Eu	UMZ	RIM	0.70768	0.00539	0.70752	9.38E-05
-151.2		9	631	Eu	UMZ	CORE	0.70772	0.00542	0.70756	6.02E-05
-151.2		8	641	Eu	UMZ	RIM	0.70783	0.00675	0.70763	8.00E-05
-151.2		8	644	Eu	UMZ	RIM	0.70758	0.00661	0.70739	7.35E-05
-151.2		8	647	Eu	UMZ	CORE	0.70777	0.01132	0.70744	9.16E-05
-151.2		7	657	Eu	UMZ	RIM	0.70767	0.00709	0.70747	7.67E-05
-151.2		7	661	Eu	UMZ	RIM	0.70748	0.00908	0.70722	1.52E-04
-151.2		7	663	Eu	UMZ	CORE	0.70726	0.00819	0.70702	6.93E-05
-191.2	BV 1767.0	6	665	S-eu	UMZ	RIM	0.70716	0.00737	0.70694	8.28E-05
-191.2		6	667	S-eu	UMZ	CORE	0.70724	0.00593	0.70707	6.74E-05
-191.2		6	669	S-eu	UMZ	RIM	0.70822	0.04433	0.70693	1.42E-04
-191.2		3	673	Eu	UMZ	RIM	0.70741	0.00374	0.70730	7.83E-05

Depth	Sample	Plg number	Point	Texture	Interval	Core/Rim	$^{87}Sr/^{86}Sr$	$^{87}Rb/^{86}Sr$	$^{87}Sr/^{86}Sr$ i	2SE
-191.2		3	675	Eu	UMZ	CORE	0.70752	0.00485	0.70738	3.13E-04
-191.2		3	677	Eu	UMZ	RIM	0.70762	0.00211	0.70756	7.61E-05
-191.2		4	697	S-eu	UMZ	RIM	0.70729	0.00646	0.70710	1.23E-04
-191.2		4	699	S-eu	UMZ	CORE	0.70731	0.00610	0.70714	1.01E-04
-191.2		4	701	S-eu	UMZ	RIM	0.70732	0.00837	0.70707	7.28E-05
-641.6	BV 2217.4	1	785	Eu	UMZ	RIM	0.70814	0.01816	0.70761	2.42E-04
-641.6		2	797	Eu	UMZ	RIM	0.70808	0.01328	0.70769	1.02E-04
-641.6		7	809	S-eu	UMZ	RIM	0.70811	0.00431	0.70799	7.72E-05
-641.6		7	811	S-eu	UMZ	CORE	0.70803	0.00362	0.70793	8.45E-05
-641.6		7	813	S-eu	UMZ	RIM	0.70790	0.00444	0.70777	6.31E-05
-1037.1	BV 2612.9	7	833	S-eu	UMZ	RIM	0.70791	0.00324	0.70782	9.96E-05
-1037.1		7	837	S-eu	UMZ	RIM	0.70930	0.05691	0.70765	3.30E-04
-1037.1		7	839	S-eu	UMZ	CORE	0.70814	0.00404	0.70803	1.41E-04
-1037.1		6	841	Eu	UMZ	RIM	0.70824	0.00140	0.70820	1.04E-04
-1037.1		6	845	Eu	UMZ	RIM	0.70875	0.00323	0.70866	1.48E-04

Depth	Sample	Plg number	Point	Texture	Interval	Core/Rim	$^{87}Sr/^{86}Sr$	$^{87}Rb/^{86}Sr$	$^{87}Sr/^{86}Sr$ i	2SE
-1037.1		6	847	Eu	UMZ	CORE	0.70847	0.00166	0.70842	8.23E-05
-1037.1		1	851	S-eu	UMZ	CORE	0.70835	0.00164	0.70830	9.40E-05
-1037.1		1	853	S-eu	UMZ	RIM	0.70798	0.00086	0.70795	8.55E-05
-1037.1		1	857	S-eu	UMZ	RIM	0.70797	0.00052	0.70796	1.00E-04
-1353.2	BV 2929.0	4	1057	S-eu	UMZ	RIM	0.70858	0.00620	0.70840	1.05E-04
-1353.2		4	1061	S-eu	UMZ	RIM	0.70837	0.00119	0.70834	1.04E-04
-1353.2		4	1063	S-eu	UMZ	CORE	0.70856	0.00216	0.70850	8.76E-05
-1353.2		1	1073	S-eu	UMZ	RIM	0.70854	0.00852	0.70829	5.66E-05
-1353.2		1	1077	S-eu	UMZ	RIM	0.70860	0.00304	0.70851	9.21E-05
-1353.2		1	1079	S-eu	UMZ	CORE	0.70854	0.00090	0.70851	1.03E-04
-1353.2		6	1082	S-eu	UMZ	RIM	0.70849	0.00137	0.70845	1.03E-04
-1353.2		6	1083	S-eu	UMZ	CORE	0.70838	0.00362	0.70827	9.69E-05
-1353.2		6	1085	Eu	UMZ	RIM	0.70859	0.01145	0.70826	7.97E-05
-1910.2	MO 46.5	5	9	Eu	LMZ	RIM	0.70888	0.00964	0.70860	1.14E-04
-1910.2		5	11	Eu	LMZ	CORE	0.70902	0.01415	0.70861	3.33E-04

Depth	Sample	Plg number	Point	Texture	Interval	Core/Rim	$^{87}Sr/^{86}Sr$	$^{87}Rb/^{86}Sr$	$^{87}Sr/^{86}Sr$ i	2SE
-1910.2		5	13	Eu	LMZ	RIM	0.70976	0.02454	0.70905	2.51E-04
-1910.2		2	29	Eu	LMZ	RIM	0.70866	0.00896	0.70840	8.99E-05
-1910.2		1	35	Eu	LMZ	CORE	0.71059	0.05748	0.70892	3.09E-04
-1973.3	MO 109.9	3	65	Eu	LMZ	RIM	0.70933	0.00750	0.70911	1.09E-04
-1973.3		3	67	Eu	LMZ	CORE	0.70920	0.01270	0.70884	8.79E-05
-1973.3		3	69	Eu	LMZ	RIM	0.70948	0.01372	0.70908	9.42E-05
-1973.3		4	74	Eu	LMZ	RIM	0.70888	0.01387	0.70848	9.63E-05
-1973.3		4	77	Eu	LMZ	RIM	0.70983	0.01307	0.70945	1.82E-04
-1973.3		4	79	Eu	LMZ	CORE	0.70878	0.00650	0.70859	7.27E-05
-1973.3		2	81	Eu	LMZ	RIM	0.70918	0.00779	0.70895	8.54E-05
-1973.3		2	83	Eu	LMZ	CORE	0.70915	0.00936	0.70888	1.12E-04
-1973.3		2	85	Eu	LMZ	RIM	0.70908	0.00619	0.70890	8.69E-05
-2036.6	MO 172.9	8	129	Eu	LMZ	RIM	0.70842	0.00509	0.70828	6.38E-05
-2036.6		8	133	Eu	LMZ	RIM	0.70848	0.00686	0.70828	9.00E-05
-2036.6		8	135	Eu	LMZ	CORE	0.70825	0.00356	0.70815	7.13E-05

Depth	Sample	Plg number	Point	Texture	Interval	Core/Rim	$^{87}Sr/^{86}Sr$	$^{87}Rb/^{86}Sr$	$^{87}Sr/^{86}Sr$ i	2SE
-2036.6		4	137	Eu	LMZ	RIM	0.70815	0.00320	0.70806	6.26E-05
-2036.6		7	145	Eu	LMZ	RIM	0.70821	0.00524	0.70806	8.04E-05
-2036.6		7	149	Eu	LMZ	RIM	0.70785	0.00290	0.70776	9.71E-05
-2036.6		7	151	Eu	LMZ	CORE	0.70813	0.00200	0.70807	5.97E-05
-2036.6		4	139	Eu	LMZ	CORE	0.70834	0.02799	0.70753	1.82E-04
-2069.8	MO 206.1	7	169	Eu	LMZ	RIM	0.70919	0.00324	0.70909	1.90E-04
-2069.8		7	173	Eu	LMZ	RIM	0.70844	0.00290	0.70835	1.61E-04
-2069.8		7	175	Eu	LMZ	CORE	0.70926	0.00672	0.70907	1.33E-04
-2069.8		1	179	Eu	LMZ	CORE	0.71009	0.05225	0.70857	2.78E-04
-2069.8		1	181	Eu	LMZ	RIM	0.70928	0.00173	0.70923	8.92E-05
-2069.8		2	185	Eu	LMZ	RIM	0.71023	0.05016	0.70877	2.35E-04
-2069.8		2	189	Eu	LMZ	RIM	0.70925	0.00693	0.70904	7.45E-05
-2069.8		2	191	Eu	LMZ	CORE	0.70901	0.00436	0.70889	9.20E-05
-2247.7	MO 384	4	209	Eu	LMZ	RIM	0.70843	0.00667	0.70824	1.32E-04
-2247.7		4	213	Eu	LMZ	RIM	0.70849	0.00777	0.70827	1.73E-04

Depth	Sample	Plg number	Point	Texture	Interval	Core/Rim	$^{87}Sr/^{86}Sr$	$^{87}Rb/^{86}Sr$	$^{87}Sr/^{86}Sr$ i	2SE
-2247.7		4	215	Eu	LMZ	CORE	0.70855	0.01303	0.70817	9.45E-05
-2247.7		2	219	Eu	LMZ	CORE	0.70828	0.00531	0.70813	8.33E-05
-2247.7		2	221	Eu	LMZ	RIM	0.70833	0.00280	0.70825	5.81E-05
-2247.7		1	225	Eu	LMZ	RIM	0.70850	0.00422	0.70837	6.58E-05
-2247.7		1	229	Eu	LMZ	RIM	0.70839	0.00409	0.70827	1.07E-04
-2382.1	MO 518.4	1	290	Eu	LMZ	RIM	0.70939	0.01042	0.70909	8.06E-05
-2382.1		1	291	Eu	LMZ	CORE	0.70916	0.00200	0.70910	9.94E-05
-2382.1		1	293	Eu	LMZ	RIM	0.70935	0.00312	0.70926	6.69E-05
-2382.1		4	313	Eu	LMZ	RIM	0.70894	0.00670	0.70875	6.23E-05
-2382.1		4	316	Eu	LMZ	RIM	0.70914	0.00229	0.70907	1.32E-04
-2451.3	MO 587.6	4	13	Eu	LMZ	RIM	0.70826	0.00293	0.70817	6.24E-05
-2451.3		8	25	Eu	LMZ	RIM	0.70858	0.00760	0.70836	7.83E-05
-2451.3		8	29	Eu	LMZ	RIM	0.70880	0.01244	0.70844	7.55E-05
-2451.3		8	31	Eu	LMZ	CORE	0.70879	0.00720	0.70858	6.53E-05
-2451.3		1	34	Eu	LMZ	RIM	0.70860	0.01735	0.70810	1.30E-04

Depth	Sample	Plg number	Point	Texture	Interval	Core/Rim	$^{87}Sr/^{86}Sr$	$^{87}Rb/^{86}Sr$	$^{87}Sr/^{86}Sr$ i	2SE
-2451.3		1	36	Eu	LMZ	CORE	0.70953	0.04323	0.70828	2.68E-04
-2451.3		1	37	Eu	LMZ	RIM	0.70914	0.01767	0.70862	1.18E-04
-2583.5	MO 719.8	4	49	Eu	LMZ	RIM	0.70852	0.00857	0.70827	7.72E-05
-2583.5		4	51	Eu	LMZ	CORE	0.70940	0.05011	0.70794	1.88E-04
-2583.5		4	53	Eu	LMZ	RIM	0.70853	0.00314	0.70844	1.29E-04
-2583.5		7	57	Eu	LMZ	RIM	0.70832	0.00965	0.70804	1.72E-04
-2583.5		7	59	Eu	LMZ	CORE	0.70940	0.04156	0.70819	1.84E-04
-2583.5		7	61	Eu	LMZ	RIM	0.70905	0.03167	0.70813	3.13E-04
-2583.5		6	70	Eu	LMZ	RIM	0.70864	0.01119	0.70832	9.13E-05
-2583.5		6	71	Eu	LMZ	CORE	0.70847	0.00561	0.70831	9.40E-05
-2583.5		6	72	Eu	LMZ	RIM	0.70831	0.00219	0.70824	7.45E-05
-2714.4	MO 850.7	2	85	Eu	LMZ	RIM	0.70970	0.00142	0.70966	7.81E-05
-2714.4		2	87	Eu	LMZ	CORE	0.70963	0.00867	0.70938	1.05E-04
-2714.4		5	101	Eu	LMZ	RIM	0.70952	0.00874	0.70927	1.52E-04
-2714.4		5	103	Eu	LMZ	CORE	0.70942	0.00112	0.70939	9.77E-05

Depth	Sample	Plg number	Point	Texture	Interval	Core/Rim	$^{87}Sr/^{86}Sr$	$^{87}Rb/^{86}Sr$	$^{87}Sr/^{86}Sr$ i	2SE
-2714.4		8	105	Eu	LMZ	RIM	0.70967	0.00326	0.70958	8.30E-05
-2714.4		8	108	Eu	LMZ	RIM	0.70980	0.01019	0.70951	1.51E-04
-2853.7	MO 990	6	129	Eu	LMZ	RIM	0.70966	0.02310	0.70899	2.06E-04
-2853.7		6	133	Eu	LMZ	RIM	0.70955	0.01812	0.70902	2.51E-04
-2853.7		7	137	Eu	LMZ	RIM	0.71030	0.05001	0.70885	1.85E-04
-2853.7		7	141	Eu	LMZ	RIM	0.70945	0.00718	0.70925	1.41E-04
-2853.7		3	147	Eu	LMZ	CORE	0.70968	0.02788	0.70887	2.64E-04
-2853.7		3	149	Eu	LMZ	RIM	0.70951	0.01327	0.70913	1.67E-04
-2853.7		3	451	Eu	LMZ	RIM	0.70953	0.00982	0.70924	1.22E-04
-3012.7	MO 1149	4	193	Eu	LMZ	RIM	0.70883	0.00141	0.70879	9.87E-05
-3012.7		4	195	Eu	LMZ	CORE	0.70890	0.00182	0.70885	9.78E-05
-3012.7		2	200	Eu	LMZ	RIM	0.70879	0.00291	0.70871	1.28E-04
-3012.7		2	202	Eu	LMZ	CORE	0.70877	0.00120	0.70873	1.09E-04
-3012.7		2	204	Eu	LMZ	RIM	0.70899	0.00156	0.70894	6.01E-05
-3012.7		7	224	Eu	LMZ	RIM	0.71048	0.06078	0.70871	3.55E-04

Depth	Sample	Plg number	Point	Texture	Interval	Core/Rim	$^{87}Sr/^{86}Sr$	$^{87}Rb/^{86}Sr$	$^{87}Sr/^{86}Sr$ i	2SE
-3012.7		7	226	Eu	LMZ	CORE	0.71076	0.07163	0.70868	3.19E-04
-3012.7		7	228	Eu	LMZ	RIM	0.70910	0.00876	0.70885	2.67E-04
-3146.7	MO 1283	5	1017	Eu	LMZ	RIM	0.70989	0.01082	0.70957	1.16E-04
-3146.7		5	1020	Eu	LMZ	RIM	0.71026	0.00455	0.71013	1.41E-04
-3146.7		2	1025	Eu	LMZ	RIM	0.71009	0.00766	0.70987	2.06E-04
-3146.7		2	1027	Eu	LMZ	CORE	0.70969	0.00096	0.70966	1.27E-04
-3146.7		1	1033	Eu	LMZ	RIM	0.71058	0.00874	0.71032	1.26E-04
-3146.7		1	1035	Eu	LMZ	CORE	0.71096	0.01209	0.71061	1.79E-04
-3146.7		1	1037	Eu	LMZ	RIM	0.71118	0.04264	0.70995	1.95E-04
-3200.7	MO 1337	4	945	Eu	LMZ	RIM	0.70861	0.00113	0.70858	9.98E-05
-3200.7		4	947.5	Eu	LMZ	CORE	0.70876	0.00205	0.70870	1.19E-04
-3200.7		4	949	Eu	LMZ	RIM	0.70889	0.00134	0.70885	9.16E-05
-3200.7		1	953	Eu	LMZ	RIM	0.70927	0.02883	0.70843	1.37E-04
-3200.7		1	955	Eu	LMZ	CORE	0.70872	0.00212	0.70866	7.70E-05
-3200.7		1	957	Eu	LMZ	RIM	0.70887	0.00381	0.70875	1.29E-04

Depth	Sample	Plg number	Point	Texture	Interval	Core/Rim	$^{87}Sr/^{86}Sr$	$^{87}Rb/^{86}Sr$	$^{87}Sr/^{86}Sr$ i	2SE
-3200.7		6	969	Eu	LMZ	RIM	0.70907	0.01506	0.70864	1.11E-04
-3200.7		6	971	Eu	LMZ	CORE	0.70902	0.01868	0.70848	1.02E-04
-3200.7		6	972	Eu	LMZ	RIM	0.70862	0.00336	0.70852	8.11E-05
-3209.7	MO 1346	4	978	Eu	LMZ	RIM	0.70887	0.00560	0.70871	8.93E-05
-3209.7		4	980	Eu	LMZ	CORE	0.70915	0.00411	0.70903	8.28E-05
-3209.7		4	981	Eu	LMZ	RIM	0.71000	0.06505	0.70811	1.55E-04
-3209.7		1	985	Eu	LMZ	RIM	0.70882	0.00184	0.70876	1.01E-04
-3209.7		1	988	Eu	LMZ	RIM	0.71055	0.05828	0.70886	3.10E-04
-3209.7		1	991	Eu	LMZ	CORE	0.70888	0.00200	0.70882	9.77E-05
-3209.7		3	1001	Eu	LMZ	RIM	0.70896	0.00270	0.70888	7.75E-05
-3209.7		3	1003	Eu	LMZ	CORE	0.70931	0.00808	0.70908	1.38E-04
-3209.7		3	1005	Eu	LMZ	RIM	0.70891	0.01879	0.70837	9.33E-05

Appendix C

Table C-1: The trace element composition of individual spots analysed in plagioclase. This table includes the following traces elements: Rb, Sr, Y, Zr, Ba, La, Ce, Pr, Nd, Sm, and Eu. Sample depths are reported relative to the Upper Zone-Main Zone boundary in metres (m). All concentrations are reported in parts per million (ppm).

Depth	Plg #	Point	85Rb	88Sr	89Y	90Zr	137Ba	139La	140Ce	141Pr	144Nd	152Sm	153Eu
1257.7	6	264	8.778	514.2	5.256	15.99	396.0	10.79	21.04	2.195	8.176	1.443	2.176
1257.7	6	266	1.541	566.2	0.136	0.021	277.6	5.299	7.354	0.583	1.565	0.144	2.073
1257.7	6	268	1.232	562.4	0.146	0.014	355.0	3.263	5.850	0.452	1.339	0.140	2.087
1257.7	4	280	2.690	576.0	0.127	0.043	389.7	2.105	3.560	0.311	0.999	0.140	2.205
1257.7	4	282	1.261	584.2	0.154	0.015	365.2	1.946	3.217	0.223	0.940	0.134	2.186
1257.7	4	284	1.697	569.8	0.159	0.016	383.1	3.223	5.656	0.452	1.514	0.247	2.141
1257.7	1	288	5.480	233.9	2.601	412.0	134.2	3.647	7.326	0.658	2.161	0.360	1.274
1257.7	1	290	8.111	559.0	0.246	1.774	306.7	3.158	5.662	0.470	1.808	0.249	2.098
1257.7	1	292	1.302	567.8	0.180	1.119	315.1	2.943	5.477	0.474	1.531	0.190	2.177
1090.0	2	304	0.545	467.3	0.106	0.020	219.9	2.206	3.549	0.316	0.943	0.106	1.745
1090.0	2	306	0.573	495.0	0.123	0.017	229.9	2.404	3.642	0.320	1.068	0.112	1.845
1090.0	2	307	1.256	504.9	0.076	0.010	242.7	2.360	3.807	0.322	1.095	0.112	1.901

Depth	Plg #	Point	85Rb	88Sr	89Y	90Zr	137Ba	139La	140Ce	141Pr	144Nd	152Sm	153Eu
1090	1	312	0.428	481.9	0.084	0.010	204.1	2.048	3.301	0.244	0.792	0.098	1.814
1090	1	314	0.810	465.8	0.069	0.020	227.5	2.062	3.452	0.304	0.879	0.085	1.839
1090	1	315	0.813	492.1	0.060	0.013	243.5	2.237	3.864	0.319	1.011	0.112	1.877
1090	7	320	1.175	495.3	0.107	0.008	237.0	2.344	3.765	0.283	1.101	0.103	1.887
1090	7	322	0.926	491.6	0.119	0.009	232.2	2.616	4.217	0.324	1.066	0.135	1.804
1090	7	323	1.814	484.7	0.090	0.654	201.9	1.856	2.871	0.221	0.754	0.072	1.791
904.7	8	352	0.067	436.3	0.347	0.019	123.0	4.238	7.992	0.692	2.255	0.295	1.076
904.7	8	354	0.047	445.7	0.333	0.030	120.0	5.293	10.12	0.882	2.814	0.329	1.098
904.7	8	356	0.092	434.8	0.331	0.031	100.8	8.334	14.88	1.140	3.570	0.340	1.107
904.7	4	360	0.351	421.9	0.224	0.021	195.6	1.546	2.816	0.237	0.936	0.106	1.059
904.7	4	362	0.251	427.8	0.364	0.010	171.4	4.695	8.847	0.733	2.456	0.347	1.056
904.7	4	364	0.458	415.1	0.240	0.034	170.1	2.253	4.549	0.452	1.531	0.209	1.026
904.7	5	376	0.249	435.5	0.318	0.017	164.4	4.315	8.932	0.756	2.500	0.341	1.146
904.7	5	378	0.623	432.5	0.254	0.027	156.6	3.140	6.193	0.594	1.851	0.250	1.063
904.7	5	380	0.283	428.9	0.234	0.038	168.9	4.286	8.365	0.683	2.353	0.273	1.075
674.3	1	392	0.273	449.4	0.183	0.030	202.5	4.249	6.786	0.583	1.916	0.220	0.932
674.3	1	396	3.700	463.9	0.160	0.015	177.3	4.130	6.855	0.552	1.811	0.177	0.945
674.3	1	399	0.139	468.7	0.176	0.032	210.6	4.268	7.137	0.614	1.908	0.206	0.936
674.3	6	400	0.710	418.5	0.172	0.023	180.0	2.477	4.586	0.377	1.331	0.131	0.864

Depth	Plg #	Point	85Rb	88Sr	89Y	90Zr	137Ba	139La	140Ce	141Pr	144Nd	152Sm	153Eu
674.3	6	402	1.219	419.5	0.189	0.016	180.2	2.629	4.676	0.366	1.276	0.119	0.903
674.3	6	404	4.445	428.4	0.238	0.014	180.7	2.288	4.142	0.378	1.152	0.185	0.976
674.3	7	416	0.474	410.1	0.182	0.027	170.7	2.459	4.453	0.418	1.328	0.155	0.823
674.3	7	420	0.756	444.3	0.159	0.026	180.8	1.897	3.708	0.353	1.177	0.168	1.019
674.3	7	422	0.758	396.2	0.159	0.024	157.4	1.354	2.506	0.246	0.802	0.107	0.822
550.3	5	442	0.942	422.6	0.261	0.036	168.7	2.128	3.715	0.378	1.272	0.141	0.774
550.3	5	443	0.964	427.2	0.241	0.014	167.9	2.087	3.506	0.301	1.250	0.181	0.773
550.3	5	445	0.864	429.8	0.343	0.029	166.7	1.659	3.022	0.279	1.086	0.153	0.778
550.3	6	449	0.648	418.0	0.205	0.022	146.4	1.701	3.036	0.277	1.013	0.153	0.726
550.3	6	451	0.417	419.4	0.344	0.012	153.0	2.391	4.462	0.429	1.457	0.182	0.757
550.3	6	453	6.000	409.6	0.291	0.278	159.6	1.696	3.189	0.306	1.158	0.175	0.725
550.3	2	457	21.61	379.0	6.679	43.33	128.0	3.727	8.666	1.054	4.284	0.918	0.690
550.3	2	459	0.751	415.7	0.263	0.051	147.4	1.854	3.377	0.323	1.233	0.187	0.738
550.3	2	461	0.967	433.8	0.226	0.009	150.5	1.825	3.356	0.308	1.123	0.178	0.774
457.3	2	469	0.467	395.4	0.285	0.028	166.3	1.900	3.807	0.372	1.302	0.207	0.731
457.3	2	470	3.400	411.2	0.339	0.092	196.6	1.696	3.505	0.328	1.193	0.211	0.781
457.3	2	472	33.50	362.3	0.960	29.24	263.9	6.482	11.48	1.048	3.653	0.488	0.664
457.3	1	476	1.627	420.3	0.182	0.033	159.4	1.496	2.397	0.231	0.709	0.118	0.728
457.3	1	479	1.728	421.7	0.326	0.035	166.5	3.609	6.470	0.559	1.963	0.250	0.768

Depth	Plg #	Point	85Rb	88Sr	89Y	90Zr	137Ba	139La	140Ce	141Pr	144Nd	152Sm	153Eu
457.3	3	497	0.655	403.7	0.444	0.061	144.4	4.787	8.299	0.754	2.826	0.363	0.741
457.3	3	499	0.238	437.3	0.440	0.029	146.6	5.682	9.740	0.865	2.806	0.325	0.793
457.3	3	501	0.698	418.3	0.588	0.044	155.9	4.306	7.944	0.723	2.631	0.354	0.735
457.3	1	REAL479	1.178	429.3	0.197	0.025	157.6	1.805	3.054	0.293	1.043	0.156	0.739
273	3	513	5.309	408.3	0.419	10.28	125.3	3.556	6.071	0.572	1.747	0.243	0.581
273	3	517	1.186	414.2	0.415	0.031	139.2	2.719	5.044	0.449	1.660	0.254	0.545
273	3	519	0.704	419.2	0.331	0.008	141.2	1.966	3.546	0.321	1.298	0.147	0.529
273	5	529	1.067	434.9	0.353	0.008	146.5	2.220	3.745	0.339	1.340	0.187	0.562
273	5	531	0.770	441.6	0.276	0.007	144.2	1.665	2.945	0.278	0.993	0.157	0.542
273	5	533	0.783	439.0	0.307	0.007	140.3	1.606	2.851	0.258	0.980	0.153	0.524
273	2	537	1.266	417.6	0.550	0.301	117.2	2.830	5.422	0.523	1.980	0.300	0.527
273	2	541	3.262	416.0	0.431	0.927	135.4	3.630	6.634	0.608	2.211	0.324	0.543
273	2	549	5.769	432.2	0.987	2.646	126.1	3.953	8.215	0.678	2.658	0.409	0.535
15.8	4	585	1.301	374.3	0.229	0.355	79.96	1.723	3.094	0.249	0.815	0.107	0.248
15.8	4	588	9.845	367.5	0.124	2.269	77.53	1.414	2.822	0.211	0.836	0.111	0.258
15.8	4	591	2.115	393.7	0.172	0.072	84.77	1.592	2.965	0.256	0.853	0.109	0.258
15.8	2	609	0.907	411.6	0.134	0.015	79.60	1.545	2.622	0.209	0.687	0.075	0.251
15.8	2	610	1.109	395.0	0.116	0.014	79.44	1.359	2.482	0.238	0.723	0.090	0.252
15.8	2	611	2.298	388.6	0.169	0.016	81.22	1.398	2.634	0.232	0.749	0.137	0.256

Depth	Plg #	Point	85Rb	88Sr	89Y	90Zr	137Ba	139La	140Ce	141Pr	144Nd	152Sm	153Eu
15.8	2	612	1.710	394.4	0.118	0.014	81.54	1.333	2.437	0.214	0.767	0.106	0.254
15.8	2	613	3.563	376.0	0.386	0.384	78.02	1.554	2.915	0.272	0.904	0.115	0.231
15.8	1	618	1.050	404.2	0.151	0.063	80.91	1.498	2.530	0.243	0.784	0.087	0.272
15.8	1	621	0.735	418.7	0.094	< d.l.	78.96	1.513	2.664	0.185	0.784	0.118	0.252
15.8	1	623	0.887	406.5	0.250	0.033	81.34	1.175	2.385	0.214	0.767	0.120	0.253
-151.2	9	625	0.686	426.8	0.073	0.021	127.5	2.514	3.606	0.293	0.809	0.075	0.647
-151.2	9	628	0.717	432.2	0.082	0.045	130.4	2.554	3.511	0.243	0.737	0.086	0.615
-151.2	9	631	0.702	433.2	0.074	0.005	126.3	2.357	3.646	0.323	0.864	0.082	0.601
-151.2	8	641	0.882	404.5	0.095	< d.l.	116.7	2.655	3.700	0.263	0.926	0.080	0.648
-151.2	8	644	0.822	419.7	0.090	< d.l.	122.6	2.628	3.695	0.272	0.896	0.088	0.604
-151.2	8	647	0.760	375.0	0.140	0.026	110.7	2.177	3.453	0.260	0.854	0.105	0.561
-151.2	7	657	1.007	396.1	0.113	0.019	122.0	2.072	3.404	0.263	0.894	0.110	0.602
-151.2	7	661	0.938	397.6	0.101	0.009	118.6	1.935	3.748	0.276	0.934	0.114	0.676
-151.2	7	663	1.039	388.8	0.086	0.011	117.6	1.989	3.233	0.265	0.881	0.087	0.603
-191.2	6	665	0.220	432.7	0.096	0.006	121.6	1.709	3.075	0.250	0.740	0.108	0.614
-191.2	6	667	0.259	391.4	0.080	< d.l.	109.9	1.768	2.682	0.238	0.660	0.068	0.520
-191.2	6	669	0.355	376.9	0.068	0.018	113.7	1.624	2.470	0.186	0.562	0.058	0.455
-191.2	3	673	0.671	419.2	0.098	0.009	120.2	1.720	2.928	0.254	0.778	0.072	0.552
-191.2	3	675	0.620	416.9	0.096	0.019	121.6	1.764	2.943	0.252	0.704	0.086	0.579

Depth	Plg #	Point	85Rb	88Sr	89Y	90Zr	137Ba	139La	140Ce	141Pr	144Nd	152Sm	153Eu
-191.2	3	677	0.524	409.4	0.083	0.014	116.6	1.854	3.003	0.237	0.749	0.077	0.540
-191.2	4	697	2.361	411.0	0.055	0.007	141.6	1.856	3.029	0.204	0.767	0.082	0.533
-191.2	4	699	0.500	409.5	0.107	0.011	115.3	1.388	2.385	0.214	0.691	0.081	0.552
-191.2	4	701	0.588	385.4	0.095	0.006	123.5	1.591	2.820	0.219	0.690	0.081	0.498
-641.6	7	809	0.513	316.6	0.157	0.028	74.54	1.441	2.584	0.201	0.664	0.070	0.349
-641.6	7	811	0.834	333.0	0.083	0.014	80.14	1.464	2.681	0.208	0.735	0.081	0.392
-641.6	7	813	0.655	332.6	0.114	0.036	76.40	1.279	2.453	0.197	0.732	0.103	0.362
-1037.2	7	833	2.933	297.8	0.123	< d.l.	87.37	3.563	5.443	0.449	1.297	0.130	0.387
-1037.2	7	837	0.181	310.5	0.175	< d.l.	79.75	3.536	5.618	0.443	1.272	0.120	0.402
-1037.2	7	839	0.488	305.3	0.139	0.015	79.15	3.473	5.408	0.435	1.218	0.108	0.391
-1037.2	6	841	0.126	293.7	0.123	0.037	76.14	3.140	4.999	0.398	1.188	0.126	0.373
-1037.2	6	845	0.121	305.9	0.150	< d.l.	74.49	3.419	5.237	0.424	1.179	0.135	0.390
-1037.2	6	847	0.080	307.9	0.134	0.010	78.08	3.280	5.262	0.426	1.311	0.137	0.370
-1037.2	1	851	0.183	307.4	0.117	0.045	71.14	3.615	5.352	0.377	1.189	0.133	0.392
-1037.2	1	853	0.148	313.0	0.120	0.030	81.54	3.701	5.595	0.359	1.190	0.117	0.401
-1037.2	1	857	0.260	311.0	0.101	0.006	80.10	3.655	5.699	0.433	1.266	0.131	0.385
-1353.2	4	1057	0.149	302.5	0.175	0.037	56.73	1.667	3.464	0.330	1.182	0.151	0.298
-1353.2	4	1061	0.048	313.9	0.260	0.040	56.94	1.870	3.405	0.372	1.249	0.153	0.313
-1353.2	4	1063	0.266	307.8	0.237	0.050	55.81	1.834	3.232	0.320	1.230	0.167	0.281

Depth	Plg #	Point	85Rb	88Sr	89Y	90Zr	137Ba	139La	140Ce	141Pr	144Nd	152Sm	153Eu
-1353.2	1	1073	0.187	280.5	0.159	0.013	48.54	1.824	3.261	0.321	1.125	0.145	0.284
-1353.2	1	1077	0.337	279.8	0.144	0.012	48.88	1.675	3.304	0.276	1.021	0.132	0.241
-1353.2	1	1079	1.502	305.0	0.195	0.017	49.25	1.868	3.499	0.315	1.099	0.133	0.250
-1353.2	6	1082	0.380	277.2	0.131	0.012	46.69	1.796	3.240	0.287	0.993	0.108	0.247
-1353.2	6	1083	0.486	270.1	0.339	0.880	49.13	1.680	3.385	0.290	1.108	0.202	0.263
-1353.2	6	1085	0.202	274.0	0.126	0.015	47.39	1.644	3.035	0.299	0.916	0.120	0.252
-1910.2	5	9	0.641	317.1	0.235	0.118	101.8	4.366	6.872	0.528	1.408	0.138	0.443
-1910.2	5	11	0.192	344.6	0.185	0.015	102.0	4.358	7.262	0.504	1.719	0.133	0.507
-1910.2	5	13	11.79	313.0	0.164	0.023	133.9	4.299	6.846	0.526	1.534	0.145	0.452
-1910.2	2	25	0.476	343.7	0.158	0.019	123.1	3.994	6.616	0.531	1.608	0.173	0.557
-1910.2	2	27	0.235	324.6	0.179	0.045	106.7	3.135	6.022	0.450	1.583	0.145	0.505
-1910.2	2	29	0.382	324.4	0.164	0.051	108.9	4.536	7.164	0.525	1.603	0.162	0.528
-1910.2	1	33	1.203	344.6	0.186	0.157	128.1	4.743	7.248	0.511	1.628	0.163	0.538
-1910.2	1	35	1.604	326.5	0.159	0.014	129.2	3.941	6.536	0.495	1.388	0.161	0.511
-1910.2	1	37	1.860	309.4	0.114	0.014	106.7	4.172	6.977	0.514	1.440	0.151	0.459
-1973.3	3	65	0.237	328.5	0.263	0.013	88.80	3.879	6.904	0.625	1.943	0.260	0.509
-1973.3	3	67	0.526	322.6	0.260	0.032	101.0	2.872	5.333	0.474	1.722	0.213	0.505
-1973.3	3	69	0.215	331.2	0.222	0.024	95.44	2.860	5.589	0.478	1.712	0.210	0.545
-1973.3	4	74	1.451	325.4	0.247	0.023	97.81	5.013	8.957	0.732	2.404	0.235	0.519

Depth	Plg #	Point	85Rb	88Sr	89Y	90Zr	137Ba	139La	140Ce	141Pr	144Nd	152Sm	153Eu
-1973.3	4	77	0.296	333.2	0.273	0.009	87.23	5.510	9.213	0.743	2.261	0.250	0.509
-1973.3	4	79	0.327	326.2	0.222	0.009	96.88	4.881	8.555	0.705	2.283	0.214	0.522
-1973.3	2	81	0.355	291.9	0.195	0.080	54.22	5.565	9.042	0.770	2.513	0.226	0.466
-1973.3	2	83	0.969	313.7	0.218	0.031	96.59	4.592	7.984	0.637	1.921	0.218	0.489
-1973.3	2	85	1.552	318.0	0.215	0.039	105.1	4.966	8.148	0.642	1.930	0.203	0.467
-2036.6	8	129	0.351	315.6	0.104	0.017	115.8	4.423	6.949	0.498	1.361	0.132	0.501
-2036.6	8	133	2.262	316.7	0.162	0.012	112.4	4.602	6.700	0.502	1.390	0.130	0.456
-2036.6	8	135	0.492	302.8	0.114	0.016	88.35	4.543	7.071	0.465	1.326	0.102	0.440
-2036.6	4	137	0.377	312.8	0.170	0.022	109.4	3.746	6.002	0.453	1.293	0.131	0.494
-2036.6	4	141	0.399	346.2	0.177	0.025	109.9	3.070	5.233	0.423	1.377	0.135	0.516
-2036.6	7	145	0.198	313.6	0.182	0.013	97.59	4.067	6.601	0.524	1.620	0.165	0.498
-2036.6	7	149	0.891	330.8	0.151	0.026	95.13	4.370	6.660	0.518	1.578	0.175	0.521
-2036.6	7	151	0.297	311.4	0.173	0.009	101.0	3.872	6.201	0.492	1.531	0.155	0.452
-2036.6	4	139	0.447	329.2	0.133	0.034	119.1	2.907	4.981	0.403	1.251	0.151	0.487
-2069.8	7	169	0.400	331.0	0.270	0.009	107.1	2.118	4.262	0.343	1.316	0.184	0.533
-2069.8	7	173	0.335	330.8	0.264	0.016	103.6	1.240	2.487	0.208	0.856	0.140	0.503
-2069.8	7	175	0.607	322.6	0.154	0.050	105.9	1.520	2.873	0.243	0.897	0.121	0.509
-2069.8	1	177	0.301	296.0	0.236	0.049	87.39	3.754	7.216	0.596	1.881	0.219	0.481
-2069.8	1	179	1.413	305.7	0.179	0.166	85.16	4.977	8.643	0.699	2.248	0.178	0.483

Depth	Plg #	Point	85Rb	88Sr	89Y	90Zr	137Ba	139La	140Ce	141Pr	144Nd	152Sm	153Eu
-2069.8	1	181	0.231	315.7	0.225	0.022	81.60	5.542	9.532	0.758	2.391	0.244	0.510
-2069.8	2	185	33.55	322.2	0.292	0.346	111.8	5.783	10.14	0.821	2.536	0.266	0.504
-2069.8	2	189	0.737	350.6	0.840	0.753	106.8	17.27	30.99	2.596	8.160	0.989	0.848
-2069.8	2	191	1.726	329.4	0.297	0.028	114.4	2.597	5.040	0.438	1.576	0.189	0.537
-2247.7	4	209	9.138	303.7	0.312	0.308	116.7	4.806	8.515	0.753	2.505	0.301	0.460
-2247.7	4	213	0.322	299.4	0.380	0.042	77.80	3.702	7.570	0.729	2.475	0.320	0.443
-2247.7	4	215	0.631	304.2	0.363	0.091	88.17	3.967	7.534	0.700	2.357	0.291	0.476
-2247.7	2	217	2.529	292.7	0.437	0.228	75.93	3.866	7.986	0.731	2.609	0.346	0.487
-2247.7	2	219	0.178	307.8	0.425	0.016	87.29	2.987	5.951	0.584	2.123	0.287	0.500
-2247.7	2	221	0.912	311.0	0.416	0.595	89.96	4.846	9.113	0.807	2.804	0.382	0.500
-2247.7	1	225	0.626	301.0	0.551	0.227	57.74	2.831	6.042	0.573	2.002	0.303	0.474
-2247.7	1	227	0.840	303.1	0.398	0.015	82.11	1.842	4.054	0.399	1.530	0.245	0.483
-2247.7	1	229	1.104	310.5	0.405	0.567	80.38	3.840	7.509	0.741	2.498	0.333	0.455
-2382.1	1	290	1.256	341.0	0.265	0.012	134.8	4.009	6.597	0.542	1.741	0.193	0.584
-2382.1	1	291	0.473	335.1	0.226	0.042	147.5	2.984	5.398	0.475	1.457	0.143	0.574
-2382.1	1	293	0.157	334.0	0.193	0.003	117.6	5.614	8.906	0.772	2.297	0.189	0.627
-2382.1	4	313	0.092	277.6	0.166	0.013	99.18	4.143	7.383	0.560	1.774	0.171	0.484
-2382.1	4	315	0.228	293.9	0.247	0.023	103.2	2.183	4.466	0.377	1.367	0.166	0.482
-2382.1	4	316	0.143	305.3	0.207	0.014	103.8	1.448	3.255	0.337	1.079	0.166	0.528

Depth	Plg #	Point	85Rb	88Sr	89Y	90Zr	137Ba	139La	140Ce	141Pr	144Nd	152Sm	153Eu
-2451.3	4	9	2.639	270.9	0.115	0.010	74.54	2.862	5.548	0.402	1.308	0.129	0.399
-2451.3	4	11	1.628	265.3	0.122	< d.l.	57.80	2.776	5.172	0.389	1.204	0.113	0.389
-2451.3	4	13	0.536	265.3	0.688	1.059	69.13	2.947	5.513	0.477	1.719	0.227	0.397
-2451.3	8	25	0.784	302.3	0.206	0.015	91.23	3.235	5.505	0.447	1.393	0.142	0.458
-2451.3	8	29	0.352	287.9	0.151	0.043	81.07	2.904	5.354	0.452	1.321	0.160	0.436
-2451.3	8	31	0.291	303.5	0.151	< d.l.	89.35	3.309	5.596	0.436	1.442	0.162	0.471
-2451.3	1	34	1.836	275.7	0.103	0.368	75.48	2.903	5.320	0.422	1.302	0.121	0.430
-2451.3	1	36	9.349	291.3	0.154	0.219	166.4	3.390	5.757	0.465	1.357	0.146	0.448
-2451.3	1	37	3.110	295.0	0.181	0.024	89.98	3.057	5.512	0.505	1.456	0.166	0.445
-2583.5	4	49	1.269	292.2	0.289	0.002	117.1	4.766	8.445	0.717	2.165	0.240	0.516
-2583.5	4	51	0.212	305.7	0.275	0.026	110.5	3.246	6.260	0.523	1.819	0.233	0.544
-2583.5	4	53	0.292	285.3	0.242	0.030	125.2	4.392	7.474	0.600	1.846	0.183	0.503
-2583.5	7	57	3.861	258.6	0.215	0.074	78.50	7.854	11.39	0.772	2.227	0.192	0.437
-2583.5	7	59	5.565	286.3	0.162	0.589	72.33	7.594	12.47	0.853	2.455	0.222	0.504
-2583.5	7	61	3.366	295.2	0.230	0.013	95.03	7.648	12.69	0.954	2.838	0.260	0.492
-2583.5	6	70	0.221	277.2	0.206	0.025	97.48	1.392	2.959	0.276	0.995	0.169	0.488
-2583.5	6	71	0.294	286.4	0.283	0.035	109.9	1.643	3.322	0.296	1.058	0.168	0.538
-2583.5	6	72	0.200	303.8	0.272	0.013	110.3	1.796	3.512	0.331	1.156	0.180	0.561
-2714.4	2	81	0.362	309.4	0.239	0.009	115.6	3.212	5.455	0.441	1.472	0.169	0.514

Depth	Plg #	Point	85Rb	88Sr	89Y	90Zr	137Ba	139La	140Ce	141Pr	144Nd	152Sm	153Eu
-2714.4	2	85	0.056	275.8	0.205	< d.l.	89.53	4.062	6.959	0.542	1.809	0.199	0.485
-2714.4	2	87	0.153	292.3	0.310	0.158	74.85	2.831	5.270	0.444	1.496	0.169	0.488
-2714.4	5	97	3.227	311.2	0.272	0.011	111.7	2.164	4.116	0.372	1.242	0.166	0.510
-2714.4	5	101	0.166	313.3	0.345	0.024	93.88	3.409	6.341	0.566	1.895	0.225	0.538
-2714.4	5	103	0.853	308.1	0.222	< d.l.	96.29	1.509	2.894	0.262	0.938	0.133	0.538
-2714.4	8	105	0.385	329.9	0.496	0.016	103.9	4.428	7.879	0.692	2.496	0.354	0.566
-2714.4	8	106.5	0.447	328.3	0.377	0.052	89.50	4.539	7.708	0.739	2.356	0.290	0.564
-2714.4	8	108	0.227	329.2	0.357	0.019	120.5	2.234	4.140	0.401	1.358	0.202	0.554
-2853.7	6	129	5.024	282.8	0.215	0.010	94.84	4.223	7.256	0.566	1.636	0.183	0.520
-2853.7	6	133	0.563	316.5	0.267	0.008	121.5	3.068	5.668	0.475	1.769	0.217	0.578
-2853.7	6	135	0.466	300.2	0.205	< d.l.	112.7	4.371	7.266	0.608	1.809	0.173	0.551
-2853.7	7	137	3.116	278.2	0.183	0.043	59.39	7.937	11.22	0.773	2.196	0.191	0.514
-2853.7	7	141	1.803	292.6	0.248	0.009	113.9	4.825	8.112	0.625	1.882	0.223	0.524
-2853.7	3	147	0.553	285.7	0.244	0.020	93.58	1.080	2.260	0.228	0.863	0.139	0.536
-2853.7	3	149	0.333	283.7	0.213	0.048	130.0	2.692	4.856	0.453	1.424	0.168	0.538
-2853.7	3	451	0.221	288.2	0.188	0.024	101.1	2.914	5.539	0.457	1.587	0.198	0.521
-3012.7	4	193	0.101	298.7	0.111	0.075	77.41	2.086	3.455	0.262	0.830	0.086	0.429
-3012.7	4	195	0.151	300.9	0.111	0.012	70.92	2.264	3.592	0.327	0.891	0.078	0.432
-3012.7	4	197	2.636	303.8	0.132	0.022	88.03	1.903	3.290	0.278	0.897	0.088	0.423

Depth	Plg #	Point	85Rb	88Sr	89Y	90Zr	137Ba	139La	140Ce	141Pr	144Nd	152Sm	153Eu
-3012.7	2	200	0.129	300.1	0.11	0.007	77.68	2.153	3.604	0.272	0.812	0.091	0.389
-3012.7	2	202	0.107	314.2	0.143	0.014	79.61	2.210	3.604	0.287	0.903	0.106	0.450
-3012.7	2	204	0.105	303.2	0.120	0.018	76.81	2.171	3.530	0.285	0.841	0.100	0.396
-3012.7	7	224	29.53	278.0	0.139	0.007	241.8	1.659	2.975	0.281	0.850	0.097	0.380
-3012.7	7	226	0.869	265.5	0.198	0.009	65.94	1.447	2.607	0.257	0.799	0.117	0.379
-3012.7	7	228	0.255	286.1	0.272	0.018	59.69	2.246	3.922	0.349	1.212	0.140	0.382
-3146.7	5	1017	5.544	994.8	1.031	0.256	449.7	39.31	63.82	4.909	15.73	1.567	3.769
-3146.7	5	1020	3.779	1080	1.709	0.403	523.1	44.57	69.98	5.709	19.27	2.136	4.010
-3146.7	5	1023	106.9	998.6	1.451	0.144	961.2	33.27	51.09	4.183	14.49	1.256	3.120
-3146.7	2	1025	4.117	999.6	1.619	1.250	327.5	32.25	66.66	6.085	19.20	2.243	4.340
-3146.7	2	1027	0.546	926.7	1.666	0.483	329.9	22.58	47.01	4.648	15.40	1.987	3.687
-3146.7	2	1029	58.95	818.5	1.297	0.029	522.1	33.08	58.46	4.661	15.88	1.674	2.846
-3146.7	1	1033	0.414	951.1	0.556	0.065	342.2	12.56	18.59	1.402	4.912	0.511	2.157
-3146.7	1	1035	14.15	903.1	0.415	0.044	400.5	13.17	18.82	1.353	3.993	0.567	2.139
-3146.7	1	1037	24.76	885.6	0.533	0.065	397.0	11.77	16.92	1.193	4.332	0.416	2.088
-3200.7	4	945	0.158	262.2	0.224	0.012	61.15	1.025	1.918	0.166	0.602	0.076	0.290
-3200.7	4	947.5	0.196	281.7	0.234	0.01	53.43	1.151	1.905	0.176	0.709	0.101	0.309
-3200.7	4	949	0.266	277.8	0.131	0.057	49.75	1.163	1.898	0.174	0.563	0.084	0.309
-3200.7	1	953	0.172	279.0	0.102	0.010	75.96	1.380	2.324	0.210	0.623	0.088	0.363

Depth	Plg #	Point	85Rb	88Sr	89Y	90Zr	137Ba	139La	140Ce	141Pr	144Nd	152Sm	153Eu
-3200.7	1	955	0.242	298.8	0.122	0.014	76.55	1.015	1.697	0.144	0.539	0.062	0.339
-3200.7	1	957	0.044	299.5	0.098	0.011	66.59	1.434	2.289	0.182	0.635	0.098	0.350
-3200.7	6	969	0.162	316.7	0.222	0.035	84.92	4.091	7.108	0.573	1.812	0.212	0.534
-3200.7	6	971	0.982	304.9	0.154	0.032	87.45	2.021	3.931	0.362	1.166	0.145	0.489
-3200.7	6	972	0.140	297.1	0.157	< d.l.	85.31	1.475	3.077	0.249	0.932	0.122	0.478
-3209.7	4	978	4.853	937.6	0.647	0.349	445.1	14.55	23.10	1.768	5.913	0.602	2.621
-3209.7	4	980	1.784	961.0	0.922	< d.l.	454.2	13.96	23.19	1.916	6.727	0.893	2.877
-3209.7	4	981	23.56	898.9	1.116	0.115	388.5	21.22	31.61	2.692	8.621	0.951	2.531
-3209.7	1	985	3.063	1027	1.796	0.291	532.8	8.914	15.97	1.491	5.142	0.765	3.362
-3209.7	1	988	7.539	962.3	1.007	0.268	471.6	6.548	12.62	1.049	4.348	0.476	2.774
-3209.7	1	991	1.428	975.8	0.690	0.187	471.3	5.554	11.08	1.185	4.401	0.544	2.796
-3209.7	3	1001	2.094	947.8	0.635	< d.l.	358.7	5.092	8.628	0.817	2.613	0.349	2.329
-3209.7	3	1003	81.66	929.7	0.767	0.169	465.5	5.908	8.283	0.611	2.405	0.377	1.992
-3209.7	3	1005	79.11	927.6	0.549	< d.l.	508.8	7.796	12.04	0.774	3.165	0.427	1.979

Table C-2: Trace element composition of plagioclase. The following trace elements are included in this table: Tb, Gd, Dy, Ho, Er, Tm, Yb, Lu, Pb, Th, and U. Depths reported relative to the Upper Zone-Main Zone boundary in metres (m). All values reported in parts per million (ppm).

Depth	Plg #	Point	159Tb	160Gd	163Dy	165Ho	166Er	169Tm	174Yb	175Lu	208Pb	232Th	238U
1257.7	6	264	0.175	1.130	1.123	0.198	0.538	0.080	0.570	0.085	10.69	0.231	0.320
1257.7	6	266	0.007	0.075	0.020	0.004	0.010	< d.l.	0.012	0.001	10.29	0.019	0.018
1257.7	6	268	0.004	0.069	0.032	0.002	0.010	0.002	0.009	0.003	10.36	< d.l.	0.005
1257.7	4	280	0.012	0.059	0.035	0.004	0.020	0.002	0.005	0.002	9.093	0.009	0.005
1257.7	4	282	0.002	0.050	0.035	0.009	0.018	0.003	0.007	0.002	8.439	0.004	0.005
1257.7	4	284	0.017	0.100	0.042	0.003	0.013	0.005	0.010	0.002	9.799	0.005	0.012
1257.7	1	288	0.035	0.201	0.183	0.096	0.259	0.041	0.103	0.013	5.157	0.906	0.994
1257.7	1	290	0.019	0.104	0.055	0.021	0.016	0.004	0.022	0.002	8.621	0.148	0.112
1257.7	1	292	0.014	0.087	0.036	0.007	0.018	0.001	0.012	0.001	9.829	0.021	0.057
1090	2	304	0.005	0.059	0.023	0.002	0.007	0.002	0.003	< d.l.	2.844	0.004	0.002
1090	2	306	0.007	0.058	0.015	0.004	0.006	0.005	0.008	0.002	2.855	< d.l.	< d.l.
1090	2	307	0.007	0.072	0.031	0.003	0.014	0.001	0.002	0.002	2.980	< d.l.	< d.l.
1090	1	312	0.005	0.032	0.031	0.002	0.009	< d.l.	0.005	0.002	3.230	0.006	0.002
1090	1	314	0.004	0.038	0.015	0.011	0.007	0.003	0.005	< d.l.	3.017	< d.l.	< d.l.
1090	1	315	0.008	0.082	0.022	0.005	0.009	< d.l.	0.006	< d.l.	3.242	< d.l.	0.002
1090	7	320	0.012	0.048	0.040	0.003	0.014	< d.l.	0.005	< d.l.	3.204	< d.l.	< d.l.

Depth	Plg #	Point	159Tb	160Gd	163Dy	165Ho	166Er	169Tm	174Yb	175Lu	208Pb	232Th	238U
1090	7	322	0.007	0.055	0.016	0.007	0.004	< d.l.	0.003	0.002	3.144	0.002	0.008
109	7	323	0.005	0.022	0.022	0.002	0.009	0.003	0.002	0.002	3.273	0.048	0.031
904.7	8	352	0.020	0.161	0.076	0.015	0.035	0.004	0.010	0.004	3.215	0.005	< d.l.
904.7	8	354	0.018	0.161	0.071	0.014	0.024	0.002	0.009	0.002	3.408	0.002	0.005
904.7	8	356	0.027	0.172	0.076	0.014	0.026	0.005	0.005	< d.l.	3.615	0.009	0.003
904.7	4	360	0.004	0.067	0.033	0.002	0.015	0.003	0.011	0.006	3.071	0.004	0.002
904.7	4	362	0.021	0.155	0.061	0.012	0.025	0.004	0.018	0.004	3.149	0.008	0.002
904.7	4	364	0.021	0.092	0.047	0.007	0.005	0.002	0.011	< d.l.	3.240	0.005	0.001
904.7	5	376	0.010	0.121	0.062	0.006	0.026	0.003	0.011	< d.l.	3.465	0.009	0.001
904.7	5	378	0.017	0.136	0.069	0.009	0.019	0.006	0.023	0.003	3.509	0.008	0.003
904.7	5	380	0.011	0.132	0.049	0.014	0.017	0.002	0.014	0.004	3.512	0.013	0.003
674.3	1	392	0.005	0.087	0.046	0.005	0.010	0.002	0.003	0.002	8.391	0.006	< d.l.
674.3	1	396	0.004	0.119	0.036	0.004	0.015	0.002	0.007	0.002	12.06	0.008	< d.l.
674.3	1	399	0.016	0.112	0.044	0.004	0.012	0.003	0.006	0.005	8.521	0.003	0.003
674.3	6	400	0.005	0.064	0.046	0.004	0.017	0.002	0.006	0.002	3.045	0.008	< d.l.
674.3	6	402	0.012	0.105	0.020	0.006	0.012	0.002	0.010	0.001	4.102	0.004	< d.l.
674.3	6	404	0.010	0.057	0.031	0.010	0.012	0.003	0.010	0.001	3.864	0.002	0.002
674.3	7	416	0.007	0.093	0.039	0.003	0.011	0.003	0.012	0.001	4.373	0.006	0.003
674.3	7	420	0.013	0.085	0.049	0.012	0.012	0.002	0.011	0.003	6.078	0.005	< d.l.

Depth	Plg #	Point	159Tb	160Gd	163Dy	165Ho	166Er	169Tm	174Yb	175Lu	208Pb	232Th	238U
674.3	7	422	0.012	0.089	0.049	0.008	0.011	0.001	0.013	0.004	4.404	0.004	0.002
550.3	5	442	0.010	0.097	0.046	0.011	0.024	0.002	0.012	0.005	2.392	0.004	0.002
550.3	5	443	0.011	0.072	0.047	0.013	0.022	0.004	0.022	0.002	2.293	0.002	< d.l.
550.3	5	445	0.003	0.084	0.036	0.011	0.020	0.002	0.017	0.002	2.328	0.002	0.003
550.3	6	449	0.010	0.062	0.058	0.005	0.008	0.003	0.020	< d.l.	2.018	< d.l.	0.003
550.3	6	451	0.013	0.115	0.067	0.010	0.018	0.002	0.015	0.004	2.082	0.004	0.002
550.3	6	453	0.013	0.114	0.070	0.011	0.026	0.002	0.041	0.005	2.051	0.008	0.005
550.3	2	457	0.142	0.889	1.020	0.246	0.749	0.101	0.970	0.116	2.609	2.950	0.695
550.3	2	459	0.013	0.110	0.066	0.019	0.020	0.002	0.022	0.003	2.325	0.002	0.004
550.3	2	461	0.007	0.104	0.067	0.007	0.016	0.002	0.020	0.002	2.552	0.002	< d.l.
457.3	2	469	0.012	0.093	0.056	0.006	0.012	0.003	0.012	0.001	2.351	0.005	0.003
457.3	2	470	0.025	0.130	0.068	0.011	0.069	0.010	0.081	0.012	2.557	0.010	0.014
457.3	2	472	0.033	0.278	0.186	0.027	0.077	0.004	0.091	0.005	2.940	0.266	0.074
457.3	1	476	0.007	0.049	0.050	0.006	0.009	0.002	0.015	0.002	2.319	0.005	0.002
457.3	1	479	0.014	0.132	0.072	0.007	0.022	0.006	0.016	0.002	2.442	0.005	0.013
457.3	3	497	0.029	0.160	0.098	0.014	0.031	0.007	0.035	0.002	2.638	0.020	0.010
457.3	3	499	0.022	0.190	0.096	0.020	0.030	0.005	0.019	0.004	2.628	0.005	0.017
457.3	3	501	0.018	0.174	0.105	0.014	0.046	0.004	0.035	0.008	2.619	0.010	0.008
457.3	1	REAL479	0.007	0.084	0.055	0.006	0.014	0.004	0.018	0.003	2.204	0.003	0.005

Depth	Plg #	Point	159Tb	160Gd	163Dy	165Ho	166Er	169Tm	174Yb	175Lu	208Pb	232Th	238U
273	3	513	0.017	0.136	0.118	0.017	0.046	0.007	0.066	0.010	5.072	0.601	0.017
273	3	517	0.014	0.128	0.089	0.019	0.025	0.005	0.027	0.005	3.439	0.011	0.003
273	3	519	0.009	0.106	0.058	0.012	0.024	0.004	0.013	0.002	5.183	0.003	0.001
273	5	529	0.016	0.118	0.074	0.011	0.027	0.007	0.016	< d.l.	2.209	0.002	0.002
273	5	531	0.010	0.094	0.067	0.010	0.024	0.005	0.015	0.001	1.850	0.005	0.002
273	5	533	0.008	0.134	0.067	0.012	0.028	< d.l.	0.024	0.003	1.846	0.004	< d.l.
273	2	537	0.019	0.162	0.121	0.030	0.036	0.002	0.026	0.004	2.702	0.013	0.012
273	2	541	0.018	0.156	0.081	0.012	0.046	0.004	0.033	0.005	4.134	0.158	0.020
273	2	549	0.028	0.241	0.201	0.035	0.076	0.012	0.072	0.006	4.365	0.490	0.069
15.8	4	585	0.014	0.060	0.040	0.006	0.017	0.004	0.018	0.013	0.889	0.024	0.012
15.8	4	588	0.006	0.057	0.034	0.007	0.018	0.018	0.008	0.002	0.902	0.328	0.002
15.8	4	591	0.006	0.054	0.021	0.007	0.009	0.004	0.007	0.001	0.902	0.464	0.012
15.8	2	609	0.004	0.045	0.025	0.010	0.005	0.003	0.010	0.003	0.871	0.003	0.005
15.8	2	610	0.004	0.055	0.023	0.006	0.012	0.004	0.003	0.002	0.824	0.006	0.002
15.8	2	611	0.011	0.067	0.040	0.011	0.007	0.001	0.011	0.002	0.858	0.007	0.002
15.8	2	612	0.007	0.070	0.027	0.005	0.016	0.003	0.019	0.001	0.862	0.004	0.006
15.8	2	613	0.014	0.088	0.115	0.019	0.046	0.005	0.054	0.008	0.912	0.142	0.053
15.8	1	618	0.005	0.070	0.048	0.004	0.008	0.004	0.020	< d.l.	0.879	0.284	0.068
15.8	1	621	0.011	0.026	0.025	0.006	0.004	0.002	0.006	< d.l.	0.817	0.002	0.002

Depth	Plg #	Point	159Tb	160Gd	163Dy	165Ho	166Er	169Tm	174Yb	175Lu	208Pb	232Th	238U
15.8	1	623	0.009	0.088	0.055	0.003	0.036	0.003	0.016	0.005	0.787	0.002	< d.l.
-151.2	9	625	0.002	0.030	0.015	0.006	0.003	0.002	0.005	< d.l.	1.623	< d.l.	< d.l.
-151.2	9	628	0.003	0.030	0.023	0.007	0.006	0.004	0.002	0.005	1.486	< d.l.	0.003
-151.2	9	631	0.009	0.044	0.043	0.003	0.010	0.003	0.006	0.002	1.401	< d.l.	< d.l.
-151.2	8	641	0.005	0.045	0.022	0.003	0.016	< d.l.	0.005	< d.l.	1.400	< d.l.	< d.l.
-151.2	8	644	0.006	0.042	0.023	0.004	0.006	< d.l.	0.002	< d.l.	1.318	< d.l.	0.002
-151.2	8	647	0.009	0.047	0.030	0.003	0.003	0.002	0.006	0.002	1.450	0.005	0.001
-151.2	7	657	0.004	0.050	0.028	0.005	0.011	0.001	0.010	0.001	1.417	< d.l.	< d.l.
-151.2	7	661	0.006	0.061	0.020	0.003	0.012	< d.l.	0.006	< d.l.	1.963	0.006	< d.l.
-151.2	7	663	0.011	0.053	0.021	0.008	0.012	0.002	0.004	0.003	1.406	< d.l.	< d.l.
-191.2	6	665	0.010	0.043	0.025	0.003	0.007	< d.l.	0.002	< d.l.	1.545	< d.l.	0.002
-191.2	6	667	0.002	0.029	0.026	0.004	0.010	< d.l.	0.004	< d.l.	1.230	< d.l.	0.001
-191.2	6	669	0.003	0.041	0.008	0.005	0.006	0.002	0.003	0.001	1.144	< d.l.	0.003
-191.2	3	673	0.006	0.052	0.022	0.006	0.007	0.002	0.005	0.003	1.223	< d.l.	0.003
-191.2	3	675	0.005	0.036	0.015	0.005	0.011	< d.l.	0.006	< d.l.	1.181	0.002	0.002
-191.2	3	677	0.011	0.063	0.027	0.002	0.011	0.002	0.005	< d.l.	1.245	0.004	< d.l.
-191.2	4	697	0.006	0.030	0.016	0.003	0.006	< d.l.	0.005	< d.l.	1.195	0.002	0.003
-191.2	4	699	0.005	0.048	0.024	0.002	0.018	0.001	0.004	0.002	1.191	0.002	0.002
-191.2	4	701	0.004	0.040	0.021	0.002	0.009	0.002	0.003	< d.l.	1.137	0.001	0.001

Depth	Plg #	Point	159Tb	160Gd	163Dy	165Ho	166Er	169Tm	174Yb	175Lu	208Pb	232Th	238U
-641.6	7	809	0.005	0.034	0.016	0.003	0.015	0.006	0.003	0.003	1.031	0.005	0.002
-641.6	7	811	0.003	0.047	0.020	0.002	0.008	0.004	0.005	0.001	1.228	0.007	0.002
-641.6	7	813	0.007	0.030	0.025	0.005	0.012	0.002	0.011	0.004	1.043	0.007	0.002
-1037.2	7	833	0.003	0.069	0.030	0.005	0.007	0.002	0.003	0.002	1.628	0.002	0.001
-1037.2	7	837	0.004	0.072	0.036	0.003	0.016	< d.l.	0.006	< d.l.	1.639	< d.l.	0.002
-1037.2	7	839	0.005	0.059	0.022	0.002	0.007	0.002	0.008	< d.l.	1.688	0.002	< d.l.
-1037.2	6	841	0.005	0.054	0.043	0.004	0.013	0.003	0.005	0.002	1.609	0.002	0.002
-1037.2	6	845	0.002	0.051	0.023	0.005	0.010	< d.l.	0.004	0.003	1.733	< d.l.	0.001
-1037.2	6	847	0.014	0.053	0.038	0.008	0.010	0.002	0.008	0.002	1.622	< d.l.	< d.l.
-1037.2	1	851	0.007	0.041	0.025	0.005	0.009	0.001	0.002	< d.l.	1.714	0.011	0.001
-1037.2	1	853	0.005	0.064	0.022	0.006	0.012	< d.l.	0.002	0.001	1.672	0.006	0.005
-1037.2	1	857	0.005	0.062	0.040	0.004	0.014	0.002	0.006	0.001	1.680	0.005	0.002
-1353.2	4	1057	0.006	0.079	0.025	0.010	0.028	0.006	0.011	< d.l.	0.901	0.007	< d.l.
-1353.2	4	1061	0.013	0.096	0.034	0.021	0.018	0.006	0.014	0.003	0.909	0.008	< d.l.
-1353.2	4	1063	0.009	0.109	0.046	0.003	0.012	0.003	0.023	0.004	0.761	0.006	0.002
-1353.2	1	1073	0.003	0.073	0.056	0.009	0.020	0.004	0.006	< d.l.	0.829	0.002	< d.l.
-1353.2	1	1077	0.006	0.060	0.030	0.009	0.013	0.002	0.007	0.002	0.820	0.002	< d.l.
-1353.2	1	1079	0.009	0.090	0.039	0.009	0.010	0.003	0.010	0.004	0.790	0.002	< d.l.
-1353.2	6	1082	0.015	0.058	0.035	0.005	0.014	0.002	0.005	0.002	0.792	0.004	0.002

Depth	Plg #	Point	159Tb	160Gd	163Dy	165Ho	166Er	169Tm	174Yb	175Lu	208Pb	232Th	238U
-1353.2	6	1083	0.017	0.119	0.066	0.018	0.038	0.008	0.043	0.005	1.101	0.014	0.008
-1353.2	6	1085	0.012	0.050	0.039	0.004	0.008	0.003	0.009	0.002	0.812	0.002	0.002
-1910.2	5	9	0.010	0.096	0.028	0.007	0.020	0.002	0.009	0.003	2.128	0.007	0.017
-1910.2	5	11	0.014	0.073	0.048	0.001	0.006	0.004	0.005	< d.l.	1.882	0.003	< d.l.
-1910.2	5	13	0.010	0.072	0.025	0.003	0.013	0.003	0.007	0.006	2.107	0.012	0.004
-1910.2	2	25	0.008	0.080	0.044	0.008	0.012	0.001	0.011	< d.l.	2.189	< d.l.	0.002
-1910.2	2	27	0.003	0.085	0.055	0.007	0.013	0.002	0.006	< d.l.	2.163	0.005	0.010
-1910.2	2	29	0.014	0.093	0.047	0.003	0.015	0.003	0.011	< d.l.	2.060	0.006	0.004
-1910.2	1	33	0.013	0.066	0.029	0.006	0.010	0.002	0.007	0.001	2.278	0.006	0.018
-1910.2	1	35	0.008	0.068	0.042	0.007	0.009	0.001	0.003	< d.l.	2.196	< d.l.	0.001
-1910.2	1	37	0.007	0.082	0.028	0.006	0.012	0.002	0.006	0.002	2.368	0.002	0.002
-1973.3	3	65	0.008	0.125	0.060	0.007	0.022	0.005	0.014	0.003	1.805	0.007	0.002
-1973.3	3	67	0.006	0.104	0.057	0.009	0.015	0.006	0.017	0.002	1.711	0.002	0.004
-1973.3	3	69	0.014	0.106	0.057	0.012	0.017	< d.l.	0.015	0.002	1.690	< d.l.	0.003
-1973.3	4	74	0.015	0.104	0.051	0.014	0.016	0.002	0.015	< d.l.	1.947	0.002	0.004
-1973.3	4	77	0.017	0.106	0.069	0.011	0.014	0.003	0.008	0.003	2.010	< d.l.	0.003
-1973.3	4	79	0.011	0.116	0.058	0.011	0.024	0.005	0.011	0.003	1.835	0.002	0.004
-1973.3	2	81	0.011	0.112	0.045	0.007	0.014	0.002	0.010	0.002	1.909	0.010	0.018
-1973.3	2	83	0.012	0.072	0.043	0.006	0.017	0.003	0.008	0.001	1.819	0.001	< d.l.

Depth	Plg #	Point	159Tb	160Gd	163Dy	165Ho	166Er	169Tm	174Yb	175Lu	208Pb	232Th	238U
-1973.3	2	85	0.013	0.074	0.040	0.010	0.014	0.002	0.014	0.001	1.746	0.005	0.033
-2036.6	8	129	0.012	0.048	0.020	0.003	0.014	0.003	0.006	0.001	2.634	0.003	0.006
-2036.6	8	133	0.008	0.056	0.047	0.010	0.009	0.001	0.004	0.003	2.348	0.005	0.006
-2036.6	8	135	0.009	0.047	0.023	0.006	0.013	0.001	0.007	0.002	2.494	0.004	0.011
-2036.6	4	137	0.016	0.046	0.041	0.004	0.008	0.002	0.010	< d.l.	2.261	0.002	< d.l.
-2036.6	4	141	0.005	0.072	0.028	0.005	0.010	0.002	0.010	0.002	2.242	0.002	0.001
-2036.6	7	145	0.004	0.083	0.037	0.005	0.020	0.039	0.011	0.001	2.288	< d.l.	< d.l.
-2036.6	7	149	0.012	0.071	0.055	0.003	0.014	0.002	0.009	0.002	2.271	0.013	0.002
-2036.6	7	151	0.011	0.075	0.036	0.003	0.010	0.002	0.006	< d.l.	2.323	0.002	< d.l.
-2036.6	4	139	0.015	0.076	0.033	0.007	0.014	0.003	0.010	0.002	2.297	0.003	< d.l.
-2069.8	7	169	0.010	0.073	0.064	0.005	0.018	0.003	0.007	< d.l.	2.186	< d.l.	0.002
-2069.8	7	173	0.008	0.090	0.041	0.004	0.009	0.002	0.014	0.002	1.871	< d.l.	0.001
-2069.8	7	175	0.005	0.072	0.027	0.005	0.015	0.003	0.006	0.002	2.063	< d.l.	< d.l.
-2069.8	1	177	0.016	0.097	0.035	0.005	0.016	0.003	0.004	0.002	2.223	0.007	0.002
-2069.8	1	179	0.015	0.106	0.048	0.010	0.009	0.002	0.010	0.001	2.144	0.037	0.020
-2069.8	1	181	0.012	0.127	0.045	0.011	0.015	0.003	0.008	0.002	2.277	0.003	0.004
-2069.8	2	185	0.012	0.137	0.069	0.010	0.024	0.013	0.007	0.014	2.232	0.064	0.052
-2069.8	2	189	0.072	0.493	0.254	0.051	0.071	0.012	0.066	0.003	2.153	0.107	0.472
-2069.8	2	191	0.014	0.096	0.055	0.008	0.023	0.002	0.008	< d.l.	2.122	< d.l.	0.003

Depth	Plg #	Point	159Tb	160Gd	163Dy	165Ho	166Er	169Tm	174Yb	175Lu	208Pb	232Th	238U
-2247.7	4	209	0.017	0.127	0.061	0.014	0.016	0.002	0.013	0.004	1.929	0.038	0.005
-2247.7	4	213	0.019	0.167	0.104	0.015	0.020	0.003	0.011	0.002	1.749	0.007	0.001
-2247.7	4	215	0.012	0.129	0.064	0.018	0.025	0.005	0.010	0.002	1.798	0.009	0.005
-2247.7	2	217	0.029	0.187	0.099	0.026	0.051	0.004	0.022	0.008	2.019	0.055	0.014
-2247.7	2	219	0.025	0.166	0.110	0.016	0.026	0.005	0.016	0.002	1.933	0.002	0.004
-2247.7	2	221	0.015	0.198	0.106	0.022	0.041	0.003	0.023	< d.l.	2.113	0.026	0.005
-2247.7	1	225	0.029	0.153	0.140	0.028	0.035	0.005	0.032	0.002	1.819	0.033	0.007
-2247.7	1	227	0.024	0.112	0.091	0.018	0.029	0.009	0.026	0.003	1.856	0.002	< d.l.
-2247.7	1	229	0.034	0.231	0.117	0.017	0.024	0.008	0.023	0.003	1.907	0.020	0.010
-2382.1	1	290	0.005	0.080	0.062	0.011	0.019	0.005	0.012	0.002	2.602	0.003	< d.l.
-2382.1	1	291	0.018	0.084	0.042	0.004	0.018	0.003	0.008	0.002	2.615	0.003	0.002
-2382.1	1	293	0.009	0.074	0.071	0.006	0.012	0.003	0.012	0.002	2.699	0.006	0.002
-2382.1	4	313	0.011	0.088	0.044	0.005	0.017	0.003	0.009	0.001	2.705	0.002	0.002
-2382.1	4	315	0.017	0.104	0.047	0.006	0.019	0.001	0.006	0.002	2.490	0.004	< d.l.
-2382.1	4	316	0.005	0.086	0.051	0.007	0.025	0.003	0.012	0.002	2.487	< d.l.	< d.l.
-2451.3	4	9	0.010	0.065	0.022	0.006	0.009	0.002	0.005	< d.l.	1.657	< d.l.	< d.l.
-2451.3	4	11	0.012	0.041	0.028	< d.l.	0.012	< d.l.	0.004	< d.l.	1.610	0.002	0.002
-2451.3	4	13	0.009	0.149	0.137	0.031	0.074	0.009	0.068	0.006	1.546	0.011	0.002
-2451.3	8	25	0.015	0.068	0.037	0.007	0.004	0.002	0.005	< d.l.	1.474	0.005	0.002

Depth	Plg #	Point	159Tb	160Gd	163Dy	165Ho	166Er	169Tm	174Yb	175Lu	208Pb	232Th	238U
-2451.3	8	29	0.008	0.053	0.038	0.005	0.011	0.005	0.004	< d.l.	1.750	0.002	0.003
-2451.3	8	31	0.013	0.061	0.051	0.011	0.016	0.005	0.006	0.002	1.528	< d.l.	< d.l.
-2451.3	1	34	0.006	0.078	0.033	0.004	0.008	0.002	0.003	0.001	1.554	0.123	0.044
-2451.3	1	36	0.006	0.063	0.038	0.005	0.009	< d.l.	0.009	0.003	1.737	0.063	0.023
-2451.3	1	37	0.010	0.072	0.044	0.007	0.010	< d.l.	0.005	< d.l.	1.476	0.006	0.006
-2583.5	4	49	0.012	0.130	0.074	0.015	0.023	0.002	0.013	0.002	2.794	< d.l.	0.004
-2583.5	4	51	0.011	0.102	0.061	0.010	0.022	0.002	0.009	< d.l.	2.690	0.002	< d.l.
-2583.5	4	53	0.009	0.089	0.040	0.011	0.019	0.003	0.013	0.002	2.710	0.003	0.004
-2583.5	7	57	0.010	0.064	0.048	0.003	0.013	0.002	0.008	0.002	2.619	0.004	0.003
-2583.5	7	59	0.017	0.142	0.046	0.006	0.025	0.003	0.008	0.001	3.003	0.199	0.026
-2583.5	7	61	0.011	0.122	0.051	0.010	0.022	0.003	0.006	0.003	2.878	0.003	0.004
-2583.5	6	70	0.012	0.091	0.056	0.007	0.024	0.005	0.011	0.002	2.378	0.001	0.003
-2583.5	6	71	0.010	0.082	0.044	0.008	0.019	0.001	0.014	0.001	2.604	0.003	< d.l.
-2583.5	6	72	0.014	0.081	0.058	0.010	0.025	0.005	0.015	0.002	2.599	0.001	0.005
-2714.4	2	81	0.008	0.098	0.057	0.005	0.014	0.004	0.013	0.002	2.484	< d.l.	< d.l.
-2714.4	2	85	0.012	0.084	0.051	0.009	0.015	0.003	0.008	0.001	2.589	0.001	0.001
-2714.4	2	87	0.011	0.085	0.065	0.010	0.019	0.006	0.007	0.002	2.424	0.043	0.034
-2714.4	5	97	0.013	0.092	0.037	0.004	0.016	0.002	0.016	0.002	2.282	0.005	< d.l.
-2714.4	5	101	0.012	0.134	0.054	0.008	0.017	0.003	0.012	0.003	2.500	0.004	0.004

Depth	Plg #	Point	159Tb	160Gd	163Dy	165Ho	166Er	169Tm	174Yb	175Lu	208Pb	232Th	238U
-2714.4	5	103	0.007	0.065	0.054	0.014	0.020	0.001	0.012	0.002	2.164	< d.l.	< d.l.
-2714.4	8	105	0.040	0.189	0.116	0.011	0.032	0.007	0.017	0.006	2.375	< d.l.	< d.l.
-2714.4	8	106.5	0.018	0.145	0.073	0.005	0.026	0.003	0.010	0.005	2.374	0.013	0.005
-2714.4	8	108	0.016	0.112	0.076	0.022	0.020	0.008	0.011	0.002	2.471	< d.l.	0.002
-2853.7	6	129	0.009	0.091	0.035	0.007	0.010	0.005	0.009	0.002	2.645	0.003	0.004
-2853.7	6	133	0.008	0.116	0.039	0.005	0.020	0.002	0.007	0.004	3.054	0.004	0.002
-2853.7	6	135	0.011	0.088	0.053	0.004	0.009	0.002	0.008	< d.l.	3.058	0.005	0.004
-2853.7	7	137	0.006	0.080	0.033	0.006	0.012	< d.l.	0.003	0.001	2.986	0.006	0.001
-2853.7	7	141	0.010	0.111	0.050	0.013	0.010	0.003	0.009	0.002	3.036	0.002	0.001
-2853.7	3	147	0.004	0.078	0.058	0.010	0.018	0.006	0.014	0.002	2.943	0.002	0.002
-2853.7	3	149	0.011	0.088	0.045	0.008	0.014	0.000	0.012	< d.l.	3.268	0.005	0.003
-2853.7	3	451	0.018	0.071	0.049	0.015	0.024	0.004	0.006	0.000	2.887	0.005	< d.l.
-3012.7	4	193	0.011	0.060	0.031	0.006	0.011	0.007	0.042	0.009	1.538	0.003	0.010
-3012.7	4	195	0.006	0.060	0.028	0.007	0.007	0.003	0.002	0.002	1.224	0.003	< d.l.
-3012.7	4	197	0.012	0.065	0.023	0.004	0.007	0.004	0.007	0.003	1.286	< d.l.	0.002
-3012.7	2	200	0.004	0.061	0.030	0.008	0.011	0.003	0.011	< d.l.	1.189	< d.l.	0.001
-3012.7	2	202	0.004	0.064	0.030	0.012	0.010	0.003	0.007	< d.l.	1.232	< d.l.	< d.l.
-3012.7	2	204	0.006	0.068	0.020	0.002	0.012	0.002	0.006	< d.l.	1.167	0.003	< d.l.
-3012.7	7	224	0.004	0.058	0.023	0.006	0.017	0.002	0.006	0.001	1.707	< d.l.	< d.l.

Depth	Plg #	Point	159Tb	160Gd	163Dy	165Ho	166Er	169Tm	174Yb	175Lu	208Pb	232Th	238U
-3012.7	7	226	0.005	0.085	0.040	0.005	0.012	0.005	0.011	0.002	1.426	0.002	0.001
-3012.7	7	228	0.008	0.113	0.083	0.013	0.025	0.002	0.016	< d.l.	1.223	0.016	0.008
-3146.7	5	1017	0.079	0.911	0.280	0.059	0.081	0.022	0.052	0.019	15.51	0.034	0.017
-3146.7	5	1020	0.104	0.850	0.451	0.065	0.112	0.011	0.077	< d.l.	14.41	0.043	0.051
-3146.7	5	1023	0.034	0.753	0.308	0.049	0.084	0.008	0.064	0.029	11.26	0.016	0.016
-3146.7	2	1025	0.112	1.071	0.620	0.095	0.181	0.010	0.044	0.019	20.16	0.415	0.447
-3146.7	2	1027	0.114	0.935	0.411	0.020	0.121	0.015	0.055	0.013	14.33	0.102	0.036
-3146.7	2	1029	0.059	0.654	0.358	0.074	0.120	0.020	0.019	0.008	12.48	0.024	0.026
-3146.7	1	1033	0.064	0.357	0.203	0.041	0.022	< d.l.	0.038	0.013	9.685	0.014	< d.l.
-3146.7	1	1035	0.048	0.188	0.112	0.011	0.054	0.010	0.019	0.008	9.710	0.029	< d.l.
-3146.7	1	1037	0.018	0.245	0.077	0.019	0.027	0.008	0.007	< d.l.	10.12	< d.l.	0.011
-3200.7	4	945	0.007	0.089	0.031	0.014	0.013	0.002	0.010	0.003	1.545	0.003	< d.l.
-3200.7	4	947.5	0.010	0.080	0.049	0.005	0.026	0.006	0.016	0.004	1.192	0.008	0.004
-3200.7	4	949	0.007	0.049	0.022	0.003	0.008	0.003	0.007	< d.l.	1.533	0.006	0.002
-3200.7	1	953	0.004	0.052	0.025	0.008	0.006	0.003	0.007	0.002	2.017	< d.l.	0.003
-3200.7	1	955	0.005	0.040	0.027	0.005	0.011	< d.l.	0.003	0.002	1.593	< d.l.	< d.l.
-3200.7	1	957	0.007	0.041	0.035	0.004	0.015	< d.l.	0.004	0.002	1.823	0.003	0.002
-3200.7	6	969	0.010	0.088	0.044	0.009	0.021	0.005	0.004	0.002	2.518	0.027	0.004
-3200.7	6	971	0.009	0.089	0.041	0.008	0.016	0.002	0.007	0.002	2.447	0.007	0.008

Depth	Plg #	Point	159Tb	160Gd	163Dy	165Ho	166Er	169Tm	174Yb	175Lu	208Pb	232Th	238U
-3200.7	6	972	0.005	0.071	0.033	0.007	0.012	< d.l.	0.007	< d.l.	2.244	0.002	0.002
-3209.7	4	978	0.039	0.253	0.145	0.013	0.128	< d.l.	0.026	0.014	10.41	0.249	0.042
-3209.7	4	980	0.048	0.364	0.247	0.040	0.105	0.010	0.036	0.019	9.284	< d.l.	< d.l.
-3209.7	4	981	0.037	0.446	0.193	0.020	0.063	< d.l.	0.027	0.011	13.99	0.012	1.239
-3209.7	1	985	0.072	0.671	0.286	0.032	0.062	0.026	0.018	0.033	9.517	0.039	< d.l.
-3209.7	1	988	0.033	0.242	0.135	0.024	0.053	0.026	0.025	0.016	10.48	< d.l.	0.030
-3209.7	1	991	0.035	0.383	0.319	0.033	0.059	0.030	0.048	< d.l.	9.130	0.021	< d.l.
-3209.7	3	1001	0.013	0.284	0.170	0.032	0.045	< d.l.	0.039	0.019	6.462	0.019	< d.l.
-3209.7	3	1003	0.032	0.234	0.120	0.054	0.051	0.001	0.014	0.013	5.288	0.035	0.011
-3209.7	3	1005	0.026	0.163	0.182	0.013	0.041	< d.l.	0.011	0.011	6.343	< d.l.	< d.l.

Appendix D

The Sr-isotopic stratigraphy of the Northern Limb of the Bushveld Complex, South Africa.

Mpho Mangwegape[1], Frederick Roelofse[1*], Timothy Mock[2], Richard W. Carlson[2]

1. Department of Geology, University of the Free State, PO Box 339, Bloemfontein, 9300, SOUTH AFRICA

2. Department of Terrestrial Magnetism, Carnegie Institution for Science, 5241 Broad Branch Road, NW Washington, DC 20015-1305

*. Corresponding author (roelofsef@ufs.ac.za)

ABSTRACT

We present a compilation of Sr-isotopic data obtained on plagioclase from 27 samples covering the entire stratigraphy of the Northern Limb of the Bushveld Complex as determined by LA-MC-ICPMS. The lower parts of the Main Zone in the Northern Limb are characterised by significant variations in Sr-isotopic compositions ($^{87}Sr/^{86}Sr$ ~0.7087 ± 0.0005 (1-σ)) coupled with very limited differentiation as exemplified by plagioclase An%, suggesting construction of the lower Main Zone through the repeated influx of magmas. Fairly constant Sr-isotopic compositions of plagioclase within the Upper and upper Main Zones ($^{87}Sr/^{86}Sr$ ~0.7073 ± 0.0003) coupled with a broad normal differentiation trend are suggestive of fractionation processes being the dominant factor in the petrogenesis of these zones. The present results argue against the laterally extensive troctolite horizon of the Northern Limb having a Critical Zone parentage or being the direct equivalent of the Pyroxenite Marker in the Northern Limb. It may, however, be an analogue of the Pyroxenite Marker in that it occurs at the approximate level where the last voluminuous influx of magma into the Northern Limb is inferred to have taken place. The nature of the magmas that gave rise to the lower parts of the Main Zone in

the Northern Limb deserves further investigation in light of the fact that plagioclase here shows considerable variation both within and between individual co-existing plagioclase crystals that may point to the intrusion of crystal mushes as opposed to aphyric liquids.

Keywords:

Bushveld Complex; Sr isotopes; Northern Limb; LA-MC-ICPMS; differentiation; integration

1. Introduction

More than three decades have passed since the first comprehensive account of the Sr-isotopic stratigraphy of the Eastern Limb of the Bushveld Complex was presented by Sharpe (1985) and more than two decades since a similar study was performed for the Western Limb of the Bushveld Complex (Kruger, 1994). Since publication of Sharpe's (1985) and Kruger's (1994) work on the Sr-isotopic stratigraphy of the Eastern and Western limbs of the Bushveld Complex, the focus of research and exploration on the Bushveld Complex has shifted from the well described Eastern and Western limbs of the complex to the relatively less well studied Northern Limb. Despite this shift in Bushveld Complex research, no comprehensive account of the Sr-isotopic stratigraphy of the Northern Limb of the complex has as yet been presented, notwithstanding the realisation that the Northern Limb is distinctly different from the Eastern and Western limbs in a number of important aspects. These include i) the presence of an ~200 m thick troctolite horizon within the Main Zone that is not found in the Eastern and Western limbs, ii) the apparent absence of certain marker horizons known from the Eastern and Western limbs and iii) the fact that much of the known Cu-Ni-PGE mineralisation is confined to the Platreef that occurs as the basal unit of the westerly dipping layered sequence in the Northern limb for which analogues are not known in the Eastern and Western limbs (Roelofse & Ashwal, 2012). Despite numerous studies on the Platreef, there exists little agreement as to its origin and its correlatives (if any) in the Eastern and Western limbs (e.g. Wagner, 1929; Van der Merwe, 1976; White, 1994; McDonald *et al.,* 2005; Pronost *et al.,* 2008, Holwell *et al.,* 2011; Mitchell & Scoon, 2012).

Furthermore, recent work on the Bushveld Complex (and other layered intrusions) has started to cast doubts on the petrological usefulness of considering whole-rock or single mineral separate isotopic data (as performed by Sharpe (1985) and Kruger (1994)) due to the fact that many "cumulate" rocks in layered intrusions show evidence of both inter- and intracrystalline isotopic disequilibrium (e.g. McBirney & Creaser, 2003; Tepley & Davidson, 2003; Prevec *et al.,* 2005; Chutas *et al.,* 2012; Roelofse & Ashwal, 2012; Yang *et al.,* 2013, Wei *et al.,* 2014, Roelofse *et al.,* 2015). Reliance on whole-rock or single mineral separate isotopic data for petrogenetic reconstruction in layered intrusions therefore may lead to flawed interpretations or to interpretations that may be only partially "correct". This realisation has necessitated new methodological approaches for the determination of radiogenic isotope ratios in layered rocks like the isotopic analysis of multiple mineral separates (e.g. Prevec *et al.,* 2005; Roelofse & Ashwal, 2012), isotopic determinations on partial dissolution aliquots (e.g. Chutas *et al.,* 2012) or *in-situ* methods like LA-MC-ICPMS (e.g. Yang *et al.,* 2013).

Here we present the Sr-isotopic stratigraphy of the Northern Limb of the Bushveld Complex as obtained using LA-MC-ICPMS on individual plagioclase crystals from 27 samples covering the entire stratigraphy of the Northern Limb, with the exception of the Platreef, the Sr-isotopic composition of which is known to have been affected by floor rock interaction (Cawthorn *et al.,* 1985; Barton *et al.,* 1986).

2. Geological setting

Excellent reviews of the geology and petrology of the Rustenburg Layered Suite (RLS) of the Bushveld Complex (Figure 1), the world's largest (>65,000 km^2) layered intrusion and the world's largest host of Cr, V and platinum-group elements (Kruger, 2005) are provided by Eales & Cawthorn (1996) and Cawthorn (2015). The sequence of mafic / ultramafic layered rocks comprising the RLS range in thickness between 7 km and 9 km and occurs in five limbs, viz. the Western, Eastern, Far Western, Northern and Southern limbs (Eales & Cawthorn, 1996). Intrusion of the RLS took place into the supracrustal rocks of the Transvaal Supergroup at 2054.4 ± 1.3 Ma (Ashwal *et al.,* 2005; Scoates & Friedman, 2008).

The layered mafic to ultramafic succession comprising the RLS is informally divided into 5 zones, primarily on the basis of the presence or absence of specific cumulus minerals and the positions of specific marker horizons (Hall, 1932; Wager & Brown, 1968; Willemse, 1969). From the base of the RLS upwards these are: i) the Marginal Zone, an up to 800 m thick succession of medium-grained, unlayered noritic rocks, ii) the Lower Zone, a package of pyroxenitic and peridotitic rocks, the distribution of which is strongly controlled by floor topography and structure, iii) the Critical Zone, consisting of a lower pyroxenitic sequence followed by cyclic units with ultramafic bases and anorthositic tops, hosting numerous chromitite layers, iv) the Main Zone, consisting mostly of gabbronoritic rocks with subordinate anorthosite layers and v) the Upper Zone, consisting mostly of gabbronoritic rocks in which magnetite is a cumulus phase (Eales & Cawthorn, 1995).

Samples analysed during the present study originated from the 1563 m deep Moordkopje (MO-1) and the 2950 m deep Bellevue (BV-1) drill holes drilled on the Northern Limb of the Bushveld Complex (Figure 2). The former sampled the lower Main Zone, the Platreef and its granitic footwall, whereas the latter sampled the entire Upper Zone of the Rustenburg Layered Suite and the upper Main Zone. Detailed accounts of the geology of MO-1 and BV-1 were presented by Roelofse & Ashwal (2012) and Ashwal *et al.* (2005), respectively. Boreholes sampling the crucial interval between MO-1 and BV-1 are not available at present. An initiative to sample this interval is underway (Trumbull *et al.,* 2015).

3. Methodology

Polished thick sections were prepared of 13 samples from the BV-1 and 14 from the MO-1 drill cores, with samples selected to provide good stratigraphic coverage. Two to three plagioclase crystals were identified in each sample for subsequent ablation, with ~2-3 spots analysed per plagioclase crystal. Sr-isotopic determinations of plagioclase were performed using a Nu Plasma HR MC-ICPMS coupled to a Photon Machines laser system employing a 193 nm excimer laser sampler at the Department of Terrestrial Magnetism, Carnegie Institution for Science. Samples were ablated in He gas at a pulse frequency of 10 Hz and spot diameters of between 95 µm and 120 µm. Measured isotope ratios were corrected for instrument fractionation according to an exponential law and an $^{86}Sr/^{88}Sr$ value of 0.1194. Laser-off

monitoring of the background was used to correct for the isobaric interference of ^{86}Kr on ^{86}Sr. The average ^{88}Sr signal obtained for plagioclase samples was 0.37 V. The BHVO-2 standard was analysed before and after every 9th unknown. The $^{87}Sr/^{86}Sr$ ratio was corrected for the isobaric interference of ^{87}Rb on ^{87}Sr through monitoring of the ^{85}Rb ion signal by assigning a value to the $^{87}Rb/^{85}Rb$ ratio such that BHVO-2 gave $^{87}Sr/^{86}Sr = 0.703469 \pm 0.000014$ (Elburg *et al.,* 2005). The variation in $^{87}Sr/^{86}Sr$ of BHVO-2 during sequential analyses of the standard over the course of the study are given in Figure 3. Initial $^{87}Sr/^{86}Sr$ ratios were calculated for an age of 2054.4 Ma (Scoates & Friedman, 2008; *cf.* also Zeh *et al.,* 2015 (2054.89 ± 0.37 Ma)) using a decay constant of 1.393×10^{-11} y^{-1} (Nebel *et al.,* 2011).

4. Results

A total of 218 Sr-isotopic determinations were performed, the results of which are contained in Electronic Appendix A. The results are shown graphically in Figure 4 where the Sr-isotope data are compared to variations in modal mineralogy and plagioclase An% over the studied stratigraphic interval. Plagioclase in the lower Main Zone (between the Platreef and the troctrolite horizon) has an average $^{87}Sr/^{86}Sr$ ratio of 0.7088 and displays a wide range of $^{87}Sr/^{86}Sr$ values for individual spots analysed, ranging between 0.7075 and 0.7106. The upper Main Zone (from the bottom of the BV-1 drill core to the UZ-MZ boundary) has plagioclase with an average $^{87}Sr/^{86}Sr$ ratio of 0.7078, with individual spots showing a narrower range of $^{87}Sr/^{86}Sr$ values compared to the lower Main Zone (0.7069-0.7087), whereas the Upper Zone has plagioclase with an average $^{87}Sr/^{86}Sr$ ratio of 0.7073 with individual spots showing values between 0.7063 and 0.7079.

5. Discussion

In the Western Limb of the Bushveld Complex, Kruger (1994) divided the RLS into a so-called integration stage and a differentiation stage on the basis of variations in Sr-isotopic compositions across the layered sequence. Kruger's integration stage covers the Lower Zone, the Critical Zone and the lower Main Zone and is characterised by an irregular upward increase in $^{87}Sr/^{86}Sr$ ratios from ~0.7047-0.7091 (at 2060 Ma). The differentiation stage, which covers the upper Main Zone and Upper Zone, is characterised by a near constant $^{87}Sr/^{86}Sr$

ratio of 0.7085 up to the level of the Pyroxenite Marker, where values abruptly decrease to ~0.7073, a value that is retained all the way to the top of the RLS. Broadly similar patterns of Sr-isotopic variations are seen in the Eastern Limb (Sharpe, 1985).

A broadly similar pattern of Sr-isotopic variations is seen for the Northern Limb, with the lower parts of the Main Zone up to ~1000 m below the UZ-MZ boundary being characterised by significant fluctuations in plagioclase Sr-isotopic compositions (average $^{87}Sr/^{86}Sr$ = 0.7087 ± 0.0005 (1-σ)) and the remainder of the stratigraphy up to the top of the RLS showing much less pronounced variations in plagioclase Sr-isotopic compositions (average $^{87}Sr/^{86}Sr$ = 0.7073 ± 0.0003 (1-σ)). In the Northern Limb, the stratigraphic interval over which significant variations in plagioclase Sr-isotopic compositions are seen (i.e. the lower Main Zone up to ~1000 m below the UZ-MZ boundary) is characterised by extremely little variation in plagioclase An%, whereas the stratigraphic interval showing very little variation in plagioclase Sr-isotopic compositions (from ~1000 m below the UZ-MZ boundary to the top of the RLS) is characterised by and large by a normal differentiation trend as exemplified by decreasing plagioclase An% with stratigraphic height.

5.1 The lower Main Zone in the Northern Limb

The lack of significant differentiation as exemplified by plagioclase An% in the lower parts of the Main Zone in the Northern Limb, coupled with significant variations in the Sr-isotopic compositions of plagioclase is suggestive of the repeated intrusion of magmas that gave rise to the lower Main Zone. A similar conclusion was reached by Roelofse & Ashwal (2012), who argued on the basis of Sr-isotopic disequilibrium between co-existing plagioclase and orthopyroxene in the lower Main Zone of the Northern Limb, that the magmas that gave rise to the lower Main Zone were not aphyric, but instead variably contaminated crystal mushes derived from a deeper, sub-compartmentalized, sub-Bushveld staging chamber. The large variations in plagioclase Sr-isotopic composition observed for the lower Main Zone in the present study, both between and within co-existing plagioclase crystals, may be supportive of such a model and deserves further scrutiny, especially in light of the recent work of Roelofse *et al.* (2015) that also showed the presence of multiple, isotopically heterogeneous populations of plagioclase co-existing within the lower Main Zone of the Northern Limb. The

lower reaches of the RLS in the Northern Limb may therefore, in our opinion, also be regarded as an "integration stage" similar to that of Kruger (1994) in the Western Limb, although the nature of the magma influxes (as aphyric liquids / as crystal mushes) remain contentious.

5.2 The upper Main Zone and Upper Zone in the Northern limb

The narrow range of plagioclase Sr-isotopic compositions for the upper parts of the Main Zone and the Upper Zone in the Northern Limb, coupled with a broadly normal differentiation trend as exemplified by plagioclase An% is suggestive of the fractionation of magmas within the presently exposed parts of the RLS, in a manner analogous to Kruger's (1994) "differentiation stage" as identified for the Western Limb. The upper parts of the Main Zone and the Upper Zone in the Northern Limb is therefore, in our opinion, the product of differentiation of magma within the Bushveld Complex, without significant input of additional magma, apart from smaller influxes that locally result in reversed differentiation trends as shown by Ashwal *et al.* (2005).

5.3 The troctolite horizon in the Northern Limb

Several suggestions have been made to explain the petrogenesis of the laterally extensive (~35 km along strike) troctolite horizon (Van der Merwe, 1976) that occurs about halfway through the Main Zone in the Northern Limb. Ashwal *et al.* (2005) suggested that the troctolite may represent i) a sliver of Critical Zone rocks dismembered by the intrusion of Main Zone magmas, ii) an intrusive sill of syn- or post-Bushveld age or iii) merely a mineralogically unusual horizon in otherwise typical Main Zone rocks. Kruger (2005) suggests on the basis of unpublished isotopic data that the troctolite may be the equivalent of the Pyroxenite Marker within the Northern Limb.

The present results argue against the contention that the troctolite horizon represents either a sliver of dismembered Critical Zone rocks or that it represents a direct equivalent of the Pyroxenite Marker, with plagioclase from this unit having $^{87}Sr/^{86}Sr$ of 0.7084 ± 0.0001 (1-σ), compared to typical CZ values <0.707 and a value of ~0.7072 for the Pyroxenite Marker

(Kruger, 1994). What should be clear is that the troctolite horizon occurs at a level within the stratigraphy where a distinct reversal in mineral compositions is apparent, from plagioclase with An% of 71.7 ± 2.2% (Roelofse & Ashwal, 2012) for the entire underlying Main Zone, to plagioclase with An% of ~78% (Ashwal *et al.,* 2005) in the troctolite package itself. An additional point to note is the fact that the troctolite horizon occurs in the stratigraphy at roughly the level where repeated magma influxes appear to give way to a magma chamber in which fractionation processes dominated. This seems to support the contention of Roelofse & Ashwal (2012) that the troctolite horizon may represent a rejuvenated, primitive crystal mush derived from the base of a sub-Bushveld staging chamber during a "last", voluminous influx of magma into the Northern Limb of the complex. In this regard, the troctolite horizon is therefore an analogue to the Pyroxenite Marker elsewhere in the Bushveld Complex (*cf.* Kruger *et al.,* 1987; Cawthorn *et al.,* 1991).

6. Conclusions

The Sr-isotopic compositions of plagioclase in the Northern Limb of the Bushveld Complex record the same overall sequence of events as has been inferred for the Western Limb by Kruger (1994). Significant variations in the Sr-isotopic compositions of plagioclase within the lower parts of the RLS coupled with very limited differentiation as exemplified by parameters such as the An% of plagioclase are suggestive of construction of the lower Main Zone through the repeated influx of magmas. Fairly constant Sr-isotopic compositions of plagioclase within the Upper and upper Main Zones coupled with a broad normal differentiation trend in plagioclase composition are suggestive of fractionation processes being the dominant factor in the petrogenesis of these zones. The present results argue against the troctolite horizon having a Critical Zone parentage or being the direct equivalent of the Pyroxenite Marker in the Northern Limb. It may, however, be an analogue of the Pyroxenite Marker in that it occurs at the approximate level where the last voluminuous influx of magma into the Northern Limb is inferred to have taken place. The nature of the magmas that gave rise to the lower parts of the Main Zone in the Northern Limb deserves further investigation in light of the fact that plagioclase here shows considerable variation both within and between individual co-existing

plagioclase crystals that may point to the intrusion of crystal mushes as opposed to aphyric liquids.

Acknowledgments

This work is based on research supported in part by the National Research Foundation (NRF) of South Africa through a Thuthuka Grant (#87896) to F.R. Any opinion, finding and conclusion or recommendation expressed in this material is that of the authors and the NRF does not accept any liability in this regard. Lew Ashwal, the Council for Geoscience and Anglo Platinum are thanked for access to the samples analysed as part of this study. Johan Kruger and an anonymous reviewer are thanked for their constructive criticisms on the initial version of this manuscript.

References

Barton, J.M. Cawthorn, R.G., White, J. (1986) The role of contamination in the evolution of the Platreef of the Bushveld Complex. *Economic Geology* 81:1096-1104

Cawthorn, R.G. (2015) The Bushveld Complex, South Africa, in: Charlier, B., Namur, O., Latypov, R., Tegner, C. (eds.) *Layered Intrusions.* Dordrecht, Springer: 517-588

Cawthorn, R.G., Barton, J.M., Viljoen, M.J. (1985) Interaction of floor rocks with the Platreef on Overysel, Potgietersrus, Northern Transvaal. *Economic Geology* 80:988-1006

Cawthorn, R.G., Meyer, P.S., Kruger, F.J. (1991) Major addition of magma at the Pyroxenite Marker in the western Bushveld Complex, South Africa. *Journal of Petrology* 32:739-763

Chutas, N.I., Bates, E., Prevec, S.A., Coleman, D.S., Boudreau, A.E., (2012) Sr and Pb isotopic disequilibrium between coexisting plagioclase and orthopyroxene in the Bushveld Complex, South Africa: microdrilling and progressive leaching evidence for sub-liquidus contamination within a crystal mush. *Contributions to Mineralogy and Petrology* 163:653-668

Eales, H.V., Cawthorn, R.G., (1996) The Bushveld Complex, in: Cawthorn, R.G. (ed.), *Layered Intrusions.* Amsterdam, Elsevier: 181-229

Elburg, M., Vroon, P., Van der Wagt, B., Tchalikian, A. (2005) Sr and Pb isotopic composition of five USGS glasses (BHVO-2G, BIR-1G, BCR-2G, TB-1G, NKT-1G) *Chemical Geology* 223:196-207

Hall, A.L. (1932) *The Bushveld Igneous Complex of the central Transvaal*. Geological Survey Memoir 28. Pretoria, Government Printer

Holwell, D.A., McDonald, I., Butler, I.B., (2011) Precious metal enrichment in the Platreef, Bushveld Complex, South Africa: evidence from homogenized magmatic sulphide melt inclusions. *Contributions to Mineralogy and Petrology* 161:1011-1026

Kruger, F.J. (1994) The Sr-isotopic stratigraphy of the western Bushveld Complex. *South African Journal of Geology* 97:393-398

Kruger, F.J., (2005) Filling the Bushveld Complex magma chamber: lateral expansion, roof and floor interaction, magmatic unconformities, and the formation of giant chromitite, PGE and Ti-V-magnetitite deposits. *Mineralium Deposita* 40:451-472

Kruger, F.J. (2005) The Main Zone of the Bushveld Complex: source of the Merensky Reef and the Platreef. *10th International Platinum Symposium Abstracts Volume.* Oulu, Finland

Kruger, F.J., Cawthorn, R.G., Walsh, K.L. (1987) Strontium isotopic evidence against magma addition in the Upper Zone of the Bushveld Complex. *Earth and Planetary Science Letters* 84:51-58

McBirney, A.R., Creaser, R.A., (2003) The Skaergaard Layered Series, Part VII: Sr and Nd isotopes. *Journal of Petrology* 44:757-771

McDonald, I., Holwell, D.A., Armitage, P.E.B. (2005) Geochemistry and mineralogy of the Platreef and "Critical Zone" of the northern lobe of the Bushveld Complex, South Africa: implications for Bushveld stratigraphy and the development of PGE mineralization. *Mineralium Deposita* 40:526-549

Mitchell, A.A., Scoon, R.N. (2012) The Platreef of the Bushveld Complex, South Africa: a new hypothesis of multiple, non-sequential magma replenishment based on observations at the Akanani project, north-west of Mokopane. *South African Journal of Geology* 115:535-550

Nebel, O., Scherer, E.E., Mezger, K. (2011) Evaluation of the ^{87}Rb decay constant by age comparison against the U-Pb system. *Earth and Planetary Science Letters* 301:1-8

Prevec, S.A., Ashwal, L.D., Mkaza, M.S., (2005) Mineral disequilibrium in the Merensky Reef, western Bushveld Complex, South Africa: new Sm-Nd isotopic evidence. *Contributions to Mineralogy and Petrology* 149:306-315

Pronost, J., Harris, C., Pin, C. (2008) Relationship between footwall composition, crustal contamination, and fluid-rock interaction in the Platreef, Bushveld Complex, South Africa. *Mineralium Deposita* 43:825-848

Roelofse, F., Ashwal, L.D., (2012) The Lower Main Zone in the Northern Limb of the Bushveld Complex – a >1.3 km Thick Sequence of Intruded and Variably Contaminated Crystal Mushes. *Journal of Petrology* 53:1449-1476

Roelofse, F., Ashwal, L.D., Romer, R.L. (2015) Multiple, isotopically hetereogeneous plagioclase populations in the Bushveld Complex suggest mush intrusion. *Chemie der Erde – Geochemistry* 75: 357-364

Scoates, J.S., Friedman, R.M., (2008) Precise age of the platiniferous Merensky Reef, Bushveld Complex, South Africa, by the U-Pb zircon chemical abrasion ID-TIMS technique. *Economic Geology* 103:465-471

Sharpe, M.R. (1985) Strontium isotope evidence for preserved density stratification in the main zone of the Bushveld Complex, South Africa. *Nature* 316:119-126

Tepley, F.J., Davidson, J.P., (2003) Mineral-scale Sr-isotope constraints on magma evolution and chamber dynamics in the Rum layered intrusion, Scotland. *Contributions to Mineralogy and Petrology* 145:628-641

Trumbull, R.B., Ashwal, L.D., Webb, S.J., Veksler, I.V. (2015) Drilling through the largest magma chamber on Earth: Bushveld Igneous Complex Drilling Project (BICDP). *Scientific Drilling* 19: 33-37

Wager, L.R. & Brown, G.M. (1968) *Layered igneous rocks*. Edinburgh, Oliver and Boyd Ltd.

Wagner, P.A. (1929) *Platinum deposits & mines of South Africa* (1973 Reprint). Cape Town: Struik

Wei, X., Xu, Y., Zhang, C., Zhao, J., Feng, Y. (2014) Petrology and Sr-Nd isotopic disequilibrium of the Xiaohaizi Intrusion, NW China: Genesis of layered intrusions in the Tarim Large Igneous Province. *Journal of Petrology* 55:2567-2598

White, J.A. (1994) *The Potgietersrus prospect- Geology and exploration history.* XVth CMMI Congress, Johannesburg, SAIMM Volume 3:173-181

Willemse, J. (1969) The geology of the Bushveld Igneous Complex, the largest repository of magmatic ore deposits in the world. *Economic Geology Monographs* 4:1-22

Van der Merwe, M.J. (1976) The layered sequence of the Potgietersrus Limb of the Bushveld Complex. *Economic Geology* 71:1337-1351

Yang, S-H., Maier, W.D., Lahaye, Y., O'Brien, H., (2013) Strontium isotope disequilibrium of plagioclase in the Upper Critical Zone of the Bushveld Complex: evidence for mixing of crystal slurries. *Contributions to Mineralogy and Petrology* 166:959-974

Zeh, A., Ovtcharova, M., Wilson, A.H., Schaltegger, U. (2015) The Bushveld Complex was emplaced and cooled in less than one million years – results of zirconology, and geotectonic implications. *Earth and Planetary Science Letters* 418: 103-11.

FIGURE CAPTIONS

Figure 1: Geological map of the Bushveld Complex showing the locations of the various limbs and the positions of the BV-1 and MO-1 drill holes. Inset shows the location of the Bushveld Complex within South Africa.

Figure 2: Geology of the Northern Limb of the Bushveld complex showing the locations of the BV-1 and MO-1 bore holes (After Van der Merwe (1976) as modified by Ashwal et al. (2005)).

Figure 3: Variation in the $^{87}Sr/^{86}Sr$ ratio (with 2SE error bars) of the BHVO-2 standard over the course of the study. Central horizontal line shows accepted $^{87}Sr/^{86}Sr$ ratio for BHVO-2 as per Elburg et al. (2005) with upper and lower horizontal lines indicating 2SE limits.

Figure 4: Variation in modal mineralogy, plagioclase An% (Ashwal et al., 2005; Roelofse & Ashwal, 2012) and initial $^{87}Sr/^{86}Sr$ of plagioclase as determined by LA-MC-ICPMS (this study). In the case of the latter, error bars indicate 2SE, and in the case of plagioclase An%, 1-σ errors.

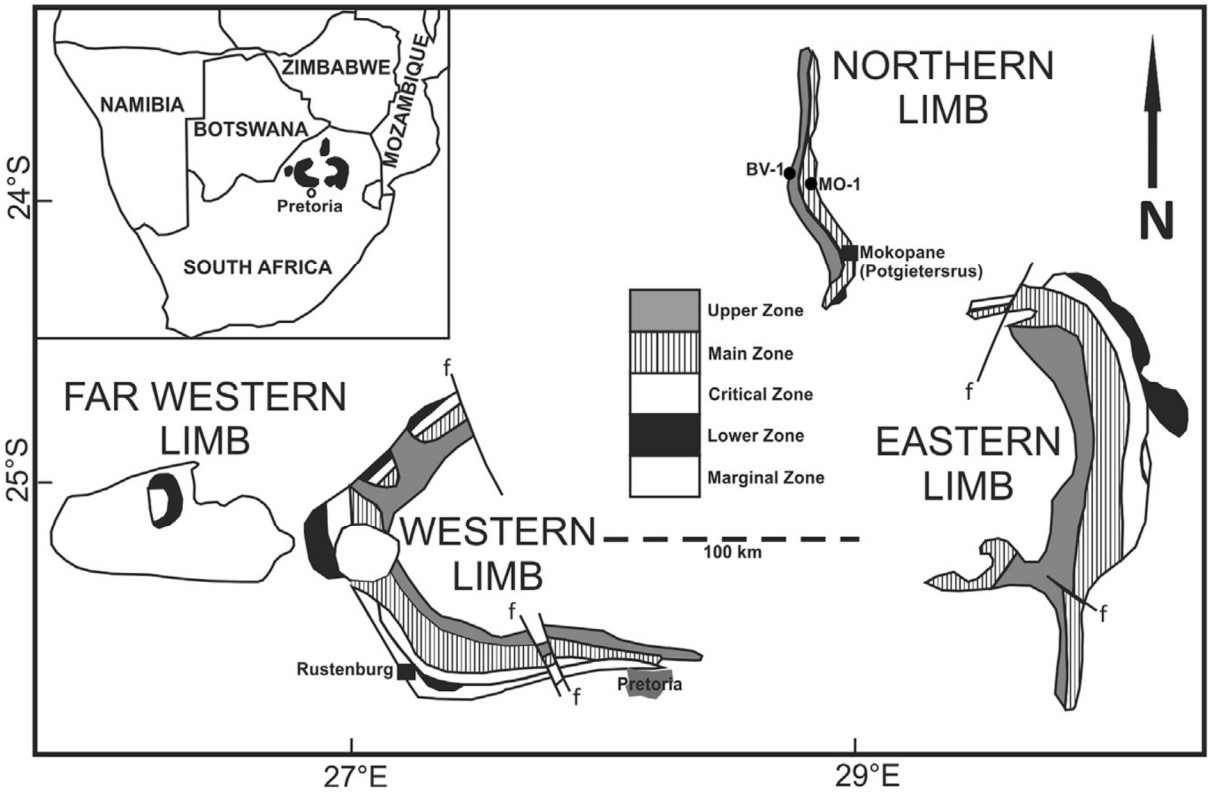

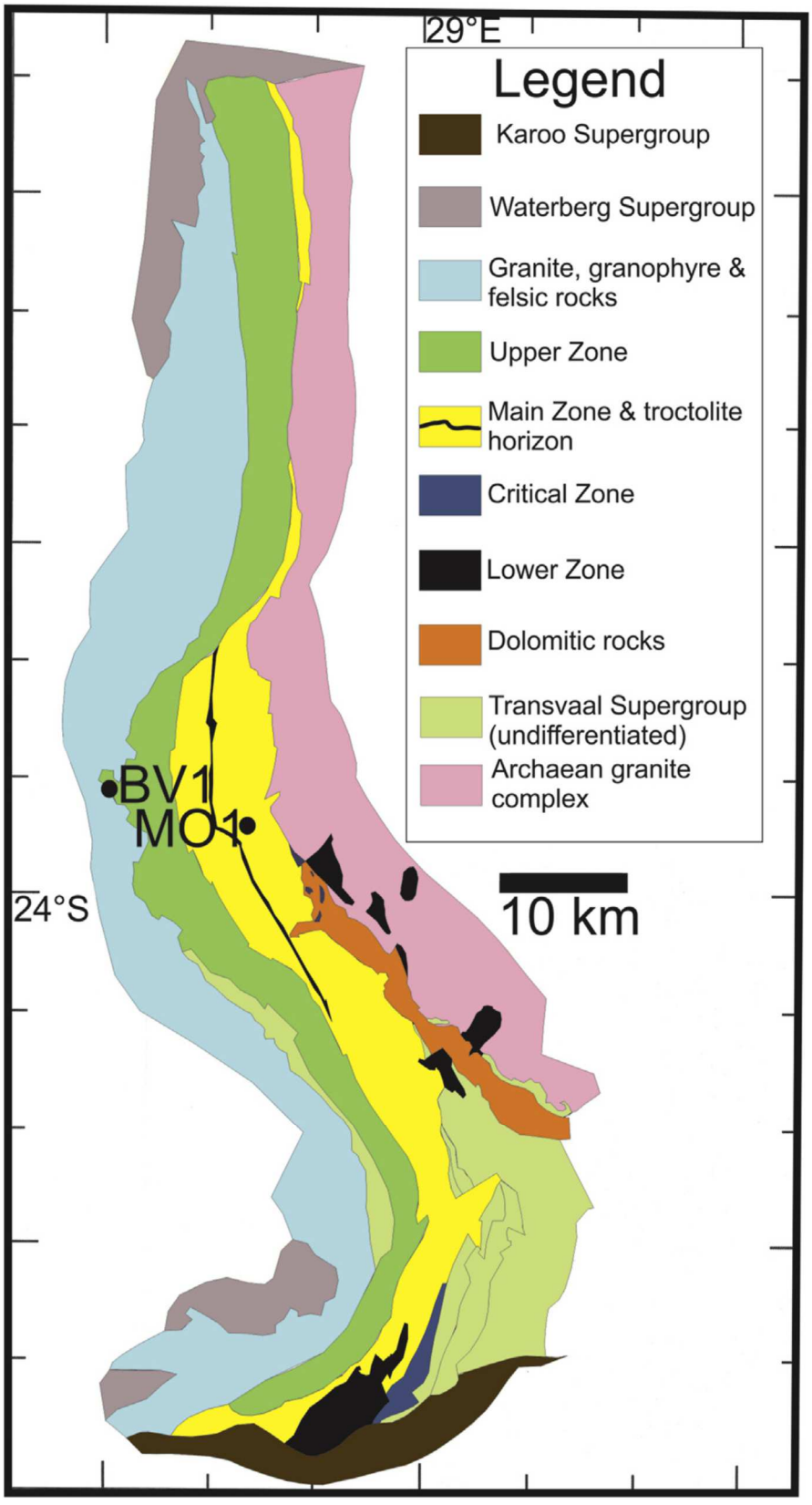
29°E
Legend
Karoo Supergroup
Waterberg Supergroup
Granite, granophyre & felsic rocks
Upper Zone
Main Zone & troctolite horizon
Critical Zone
Lower Zone
Dolomitic rocks
Transvaal Supergroup (undifferentiated)
Archaean granite complex
BV1
MO1
24°S
10 km

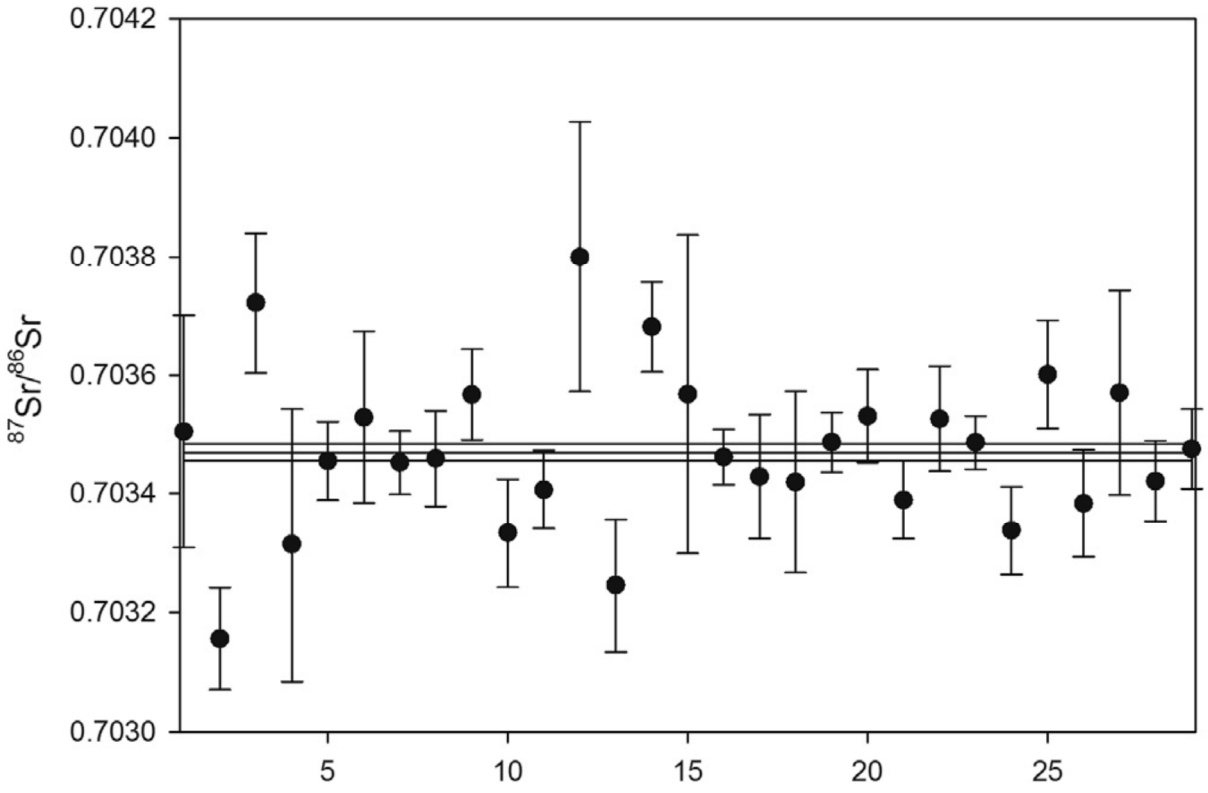
0.7042
0.7040
0.7038
0.7036
0.7034
0.7032
0.7030
$^{87}Sr/^{86}Sr$
5
10
15
20
25

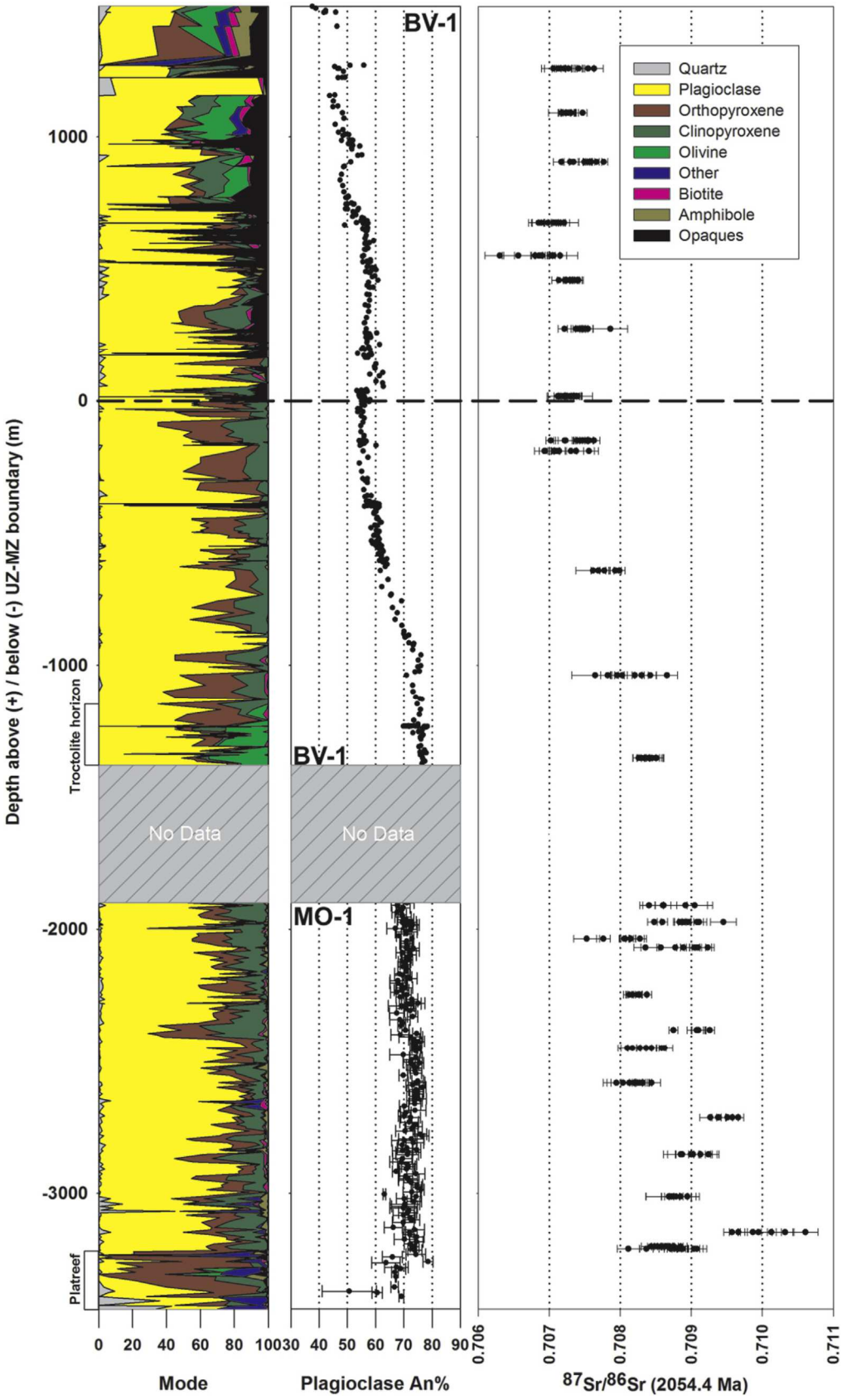
BV-1
BV-1
MO-1
No Data
No Data
Quartz
Plagioclase
Orthopyroxene
Clinopyroxene
Olivine
Other
Biotite
Amphibole
Opaques
Depth above (+) / below (-) UZ-MZ boundary (m)
1000
0
-1000
-2000
-3000
Troctolite horizon
Platreef
0 20 40 60 80 100
Mode
30 40 50 60 70 80 90
Plagioclase An%
0.706 0.707 0.708 0.709 0.710 0.711
87Sr/86Sr (2054.4 Ma)